Human melanocytic nevi result from impaired senescence due to activated Wnt signaling

Jeffrey Scott Pawlikowski

Submitted in fulfilment of the requirements for the Degree of Doctor of Philosophy

Institute for Cancer Sciences
CRUK Beatson Labs
University of Glasgow
September 2012

Abstract

Melanocytes within benign human nevi are the paradigm for tumor suppressive senescent cells in a pre-malignant neoplasm. These cells typically contain mutations in either the BRAF or NRAS oncogene and express markers of senescence, including $p16^{INK4A}$ [1-4]. However, a nevus can contain 10s to 100s of thousands of clonal melanocytes and approximately 25% of melanomas are thought to arise in association with a pre-existing nevus [5-9]. Neither observation is indicative of fail-safe senescence-associated proliferation arrest and tumor suppression. I set out to better understand the status of nevus melanocytes. Proliferation-promoting Wnt target genes, such as Cyclin D1 and c-Myc, were repressed in oncogene-induced senescent melanocytes *in vitro*, and repression of Wnt signaling in these cells induced a senescent-like state. In contrast, Cyclin D1 and c-Myc were expressed in many melanocytes of human benign nevi. Specifically, activated Wnt signaling in nevi correlated inversely with nevus maturation, an established dermatopathological parameter linked to clinical benignancy [10,11]. Single cell analyses of lone interfollicular epidermal melanocytes and nevus melanocytes in tissue showed that expression of proliferation-promoting Wnt targets correlates with prior proliferative expansion of $p16^{INK4A}$-expressing nevus melanocytes. In a mouse model, activation of Wnt signaling delayed, but did not bypass, senescence of oncogene-expressing melanocytes, leading to massive accumulation of proliferation-arrested, $p16^{INK4A}$-positive, non-malignant melanocytes. I conclude that clonal hyperproliferation of oncogene-expressing melanocytes to form a nevus is facilitated by transient delay of senescence due to activated Wnt signaling. The observation that activation of Wnt signaling correlates inversely with nevus maturation, an indicator of lower malignant potential, supports the notion that persistent destabilization of senescence by Wnt signaling contributes to the malignant potential of nevi.

Table of contents

List of Tables

List of Figures

Acknowledgements

Every student has one or two teachers whose wisdom influences him or her far outside the boundaries of a classroom. Mr Steve Miller and Mr Ray Edwards taught me science in school, but more importantly, prepared me for life as a scientist and a man. I will forever be indebted for the education they have given me and deeply thank them for it. This thesis would not be presented to you without them paving its way.

It is hard to believe that I have been in the Adams lab for six years. Peter has been a terrific mentor over the years and is always available to provide help. His knowledge is remarkable and I thank him for supporting me in the lab. I first joined the lab when it was located at Fox Chase Cancer Center in Philadelphia, USA. Here I met key collaborators for this thesis, most importantly Dr Hong Wu, a skilled dermatopathologist whose discussions led to many key findings. Although it is every student's nightmare to be relocated in the middle of his or her PhD, I was excited to travel to Scotland and now thank Peter for giving me the opportunity. The lab quickly grew into a large group of friendly, talented, and hard-working scientists and I thank them all for the added help over the years.

I would like to thank my mother and father for providing guidance and a wonderful childhood where I was always pushed to strive for the best, in my studies as well as the rest of my daily endeavours.

Most importantly, I would like to thank my wife Lyndsay who has been there for me through it all over the past four years. The time spent working towards my PhD was stressful at times but together we have made it the best four years of my life. With our first baby on the way I cannot wait to see what our future holds as a family.

Thank you to the University of Glasgow and Cancer Research UK (CRUK) for funding my work as it would not have been possible without it.

Publications arising from this work and other collaborations

Kennedy, A.L., Morton, J.P., Manoharan, I., Nelson, D.M., Jamieson, N.B., Pawlikowski, J., McBryan, T., Doyle, B., McKay, C., Oien, K.A., Enders, G.H., Zhang, R., Sansom, O.J., and Adams, P.D. (2011). Activation of the PIK3CA/AKT Pathway Suppresses Senescence Induced by an Activated RAS Oncogene to Promote Tumorigenesis. Molecular Cell *42*, 36–49.

Moyes, L.H., McEwan, H., Radulescu, S., Pawlikowski, J., Lamm, C.G., Nixon, C., Sansom, O.J., Going, J.J., Fullarton, G.M., and Adams, P.D. (2012). Activation of Wnt Signaling promotes development of dysplasia in Barrett's Oesophagus. The Journal of Pathology. *1*, 99-112.

Sawicka, M., Pawlikowski, J., Wilson, S., Ferdinando, D., Wu, H., Adams, P.D., Gunn, D.A., and Parish, W. (2012). The Specificity and Patterns of Staining in Human Cells and Tissues of p16INK4a Antibodies Demonstrate Variant Antigen Binding. PloS One. *Accepted*.

Ivanov, A., Pawlikowski, J., Manoharan, I., Rai, T.S., Nelson, D.M., Shah, P., Wu, H., Berger, S.L., and Adams, P.D. (2012). Lysosome-mediated processing of chromatin in senescence. *Submitted*.

Pawlikowski, J., McBryan, T., King, A., Maier, A.B., Blyth, K., Wu, H., and Adams, P.D. (2012). Human melanocytic nevi result from impaired senescence due to activated Wnt signaling. *In Preparation*.

Declaration

I declare that all of the work in this thesis was performed personally. No part of this work has been submitted for consideration as part of any other degree or award.

Abbreviations

3'-UTR	3’ untranslated region
5'-UTR	5’ untranslated region
APC	adenomatous polyposis coli
ARF	alternate reading frame protein
BCC	basal cell carcinoma
BH-FDR	Benjamini and Hochberg false discovery rate
BrdU	5-bromo-2'-deoxyuridine
BSA	bovine serum albumin
CDK	cyclin dependent kinase
CK1	casein kinase 1
DAB	3,3’-diaminobenzidine
DAPI	4’6-diamidino-2-phenylindole
DDR	DNA damage response
DKK1	dickkopf 1
DMEM	Dubelcco's modified eagle medium
DNA	deoxyribonucleic acid
dnTCF	dominant negative TCF
Dsh	Dishevelled
ECM	extra-cellular matrix
ES	enrichment score
FFPE	formalin-fixed-paraffin-embedded
Fzd	Frizzled
GAP	GTPase-activating protein
γH2Ax	phosphorylated histone H2AX
GO	gene ontology
GSEA	gene set enrichment analysis
GSK3	glycogen synthase kinase
H&E	haematoxylin and eosin
HMGA	high-mobility group A proteins
HMGS	human melanocyte growth supplement
HP1	heterochromatin protein 1
hTERT	human telomerase reverse transcriptase
IF	immunofluorescence
IHC	immunohistochemistry
IL2	interleukin-2
IL6	interleukin-6
IL8	interleukin-8
MAPK	mitogen activated protein kinase
MC1R	melanocortin 1 receptor
MDM2	mouse double minute 2
MEF	mouse embryonic fibroblast
miRNA	micro ribonucleic acid
MITF	microphthalmia-associated transcription factor
MOI	multiplicity of infection
mRNA	messenger ribonucleic acid

NES	normalized enrichment score
NF-kappaB	nuclear factor-kappaB
NK	natural killer
OIS	oncogene induced senescence
ORF	open reading frame
PanIN	pancreatic intraductal neoplasia
PAX3	paired box gene 3
PBS	phosphate buffered saline
PBT	PBS+BSA+Tween 20
PC	principal component
PcG	polycomb group complex
PCR	polymerase chain reaction
PD	passage doubling
PDGF	platelet derived growth factor
PEI	polyethylenimine
PIN	prostatic intraepithelial neoplasia
PML	promyelocytic leukemia
PTEN	phosphate and tensin homologue
qRT-PCR	quantitative real time polymerase chain reaction
RAS GEF	RAS guaninine-nucleotide exchange factor
RGP	radial growth phase
RIN	RNA integrity number
RNA	ribonucleic acid
RNAseq	RNA sequencing
ROS	reactive oxygen species
rRNA	ribosomal RNA
RS	replicative senescence
SA beta-gal	senescence associated beta-galactosidase
SAHF	senescence associated heterochromatin foci
SASP	senescence associated secretory phenotype
SB	Laemmli sample buffer
SCC	squamous cell carcinoma
SIRT1	sirtuin 1
SMS	senescence messaging secretome
TYR	tyrosinase
TYRP1	tyrosinase-related protein-1
TYRP2	dopachrome tautomerase
VGP	vertical growth phase
WT	wild type

1 Introduction

1.1 Cellular Senescence

Leonard Hayflick first described senescence in 1965 by showing that primary human fibroblasts undergo a finite number of cell divisions in culture [12,13]. Also known as the "Haylick Limit", senescence is characterized as an irreversible or stable arrest of cellular proliferation. These non-dividing cells were shown to remain viable and did not respond to external mitogenic stimuli. In addition, the growth arrest was specific to primary mammalian cells unlike prior cell cultures that Hayflick explained to be immortal because they were derived from tumorous tissue [14]. It was also noted that in order for a cell to escape senescence they must assume properties of cancerous cells. Hayflick marvellously hypothesized that the finite lifetime of cell strains *in vitro* may be an expression of aging at a cellular level. Since these original hypotheses, further details have been elucidated about cellular senescence. These initial findings would lay the groundwork for hallmark findings in cancer biology, cell biology, and aging.

Senescence is a multi-faceted cellular state. In the nearly fifty years since Hayflick first hypothesized about a role of senescence in tumor suppression and aging, the definition of senescence has become much clearer. Senescent cells are not quiescent or terminally differentiated cells. It is not a form of cell death as senescent cells can survive long periods of time, even decades, without proliferating. Senescence regulates many distinct and complex processes, some of which even have opposing effects; namely, tumor suppression, tumor promotion, aging, and normal tissue repair. In order to understand the roles of senescence properly the molecular biology of the process must first be further elucidated, notably the triggers, effectors, and markers of senescence.

1.1.1 Triggers of senescence

1.1.1.1 Short telomeres

Senescence is induced by numerous stimuli. One such trigger limiting the growth of human cells in culture is the shortening of DNA at the ends of chromosomes (telomeres) [15,16]. Comprised of repetitive stretches of DNA and their associated proteins that cap the ends of linear chromosomes, telomeres function to protect against DNA degradation [17]. Telomeres are gradually shortened 50-200 base pairs each time a cell's DNA is replicated due to the inability of DNA polymerases to move bidirectionally and prime a new DNA strand (also known as the "end-replication problem") [18-21]. The enzyme telomerase is able to reinstate lost DNA but its expression is only present in a small subset of cells, meaning that most proliferating cells' DNA shortens with age. Some human primary fibroblast strains (e.g. BJ) can be immortalized by transfection of the catalytic subunit of telomerase, hTERT [22,23]. The shortening of telomeres is a "biological clock" that acts as a replication counter to eventually induce senescence [18]. Mechanistically, the growth arrest is a consequence of uncapped telomeres which are initiated by destabilized telomeric loops in shortened telomeres [24]. Senescence induced in response to critically shortened telomeres is termed replicative senescence (RS).

1.1.1.2 DNA damage and other molecular stresses

Senescence can also be induced by severe DNA damage, especially when it causes double strand breaks [25]. Many agents such as some chemotherapeutic drugs promote double strand DNA breaks and thereby induce senescence in normal cells. Importantly, some of these drugs can also induce senescence in certain tumor cells, pointing to a role for senescence in therapy [26]. Other treatments that induce senescence alter the overall organization of DNA rather than its primary structure. For instance, histone deacetylase inhibitors modify chromatin towards a more decondensed state in order to induce senescence

[27,28]. This alteration in chromatin organization is paradoxical, with more condensed chromatin (heterochromatin) being more predominant in the senescent state [29]. Further understanding of how senescence can be triggered by both heterochromatin disruption and by processes that are associated with its formation is of importance as histone deacetylase inhibitors are being investigated for treating certain cancers [30].

Many external stimuli can also induce senescence. Such mechanisms include radiation, oxidative stress (cell culture in ambient oxygen which is hyperphysiological)[31-33] and inappropriate substrata (growing to confluence in culture). The various external stressors that are independently able to induce senescence may also have a cumulative gradual effect on cell autonomous triggers. For example, extrinsic stresses such as oxidative stress may affect intrinsic factors, such as DNA damage accumulation and shortening of telomeres, demonstrating the complexity of the senescence response to various stressors.

1.1.1.3 Oncogenes

The most interesting trigger of senescence in regards to this study is oncogene-induced senescence (OIS). Oncogenes are mutant versions of normal genes involved in cell growth and have the potential to transform cells in conjunction with additional mutations. OIS involves activation of oncogenes or inactivation of tumor suppressors and induces senescence due to the presence of high mitogenic signals and DNA damage [34-37]. This uncontrolled increase in signaling initiates senescence through the misfiring and collapse of replication forks [38-40]. The idea that the OIS response is due to the presence of high mitogenic signals is supported by the finding that mouse cells cultured in serum free medium (to reduce the mitogenic pressure of serum) are resistant to OIS [41]. Additionally, some murine cells do not undergo RS in serum free conditions, outlining the importance of excessive mitogenic stimulation required for senescence [42,43]. Even though OIS does not involve telomere shortening, many oncogenes induce a strong DNA damage response (DDR) due to the DNA damage that is caused by

aberrant DNA replication. The DDR serves to initiate and maintain the senescence response.

OIS was first noticed when an oncogenic form of RAS, a cytoplasmic transducer of mitogenic signals, was expressed in normal human fibroblasts [34]. The RAS protein family are cytoplasmic transducers of mitogenic signals and contains three members, H-, K- and N-RAS. RAS is activated downstream of many growth factors such as platelet derived growth factor (PDGF), epidermal growth factor (EGF), as well as various adhesion molecules [44-46]. Additional downstream effectors can be triggered upon activation of RAS by RAS guaninine-nucleotide exchange factors (RAS GEFs) to allow for the exchange of bound GDP to GTP [47]. Among these are members of the mitogen activated protein kinase (MAPK) pathway such as RAF, MEK, and BRAF that have also been shown to induce senescence when overexpressed or expressed in an activated oncogenic form [2,35-37]. Through the effects of these targets and others, RAS is able to control cell proliferation, growth and survival upon its activation. RAS signaling is counteracted by RAS GTPase-activating proteins (GAPs), which coverts active RAS (RAS-GTP) to its inactive form (RAS-GDP). Specific point mutations of RAS, most commonly found at residue G12 in the P-loop and the catalytic residue Q61, may lead to the inability of RAS GAPs to convert RAS-GTP to inactive RAS-GDP and it is these activated forms that have been shown to induce senescence [48-50].

1.1.2 Effectors of senescence

1.1.2.1 Tumor suppressors and their mediators

As there are many different triggers of senescence, it is of no surprise that various signaling pathways are involved in the establishment and maintenance of a senescent cell. As outlined in Figure 1.1, there are multiple pathways at the heart of the senescence program. The central pathways involved include the $p16^{INK4A}$/pRB and p53 tumor suppressor pathways and their activators, oncogene

signaling (MAPK/ERK pathway) and DNA damage signaling. These pathways are heavily intertwined, but they can also independently halt cell-cycle progression. To make matters even more complex, these pathways are often found to be species, cell type, or context dependent as key components of the senescence network are continually uncovered.

As briefly mentioned in the context of senescence triggers, the DNA damage response is important in initiating and maintaining senescence in response to shortened telomeres, activated oncogenes, and some forms of DNA damage such as oxidative stress. In order to achieve and maintain the senescence response, DNA damage activates a signaling cascade involving the protein kinases ATM and ATR as well as the phosphorylation of histone H2A.X that causes the formation of DNA damage foci around the presented DNA damage. Activation of the downstream kinases Chk1 and Chk2 follows, and eventually p53 activation is triggered. Additional activation of p53 is facilitated through the activation of alternate-reading-frame protein (ARF), which inhibits a facilitator of p53 degradation, E3 ubiquitin–protein ligase (MDM2) [51]. Activation of p53 drives senescence through one of it many targets, CDKN1a, which codes for the Cyclin/CDK2 (or CDK1) inhibitor p21 [52]. Cyclin-dependent kinases (CDKs) are regulators of the cell cycle and through binding a regulatory cyclin protein have the ability to promote cell cycle progression. p21 can directly arrest cell division through inhibition of CDK1/2, and so reinforce the cell cycle arrest through activation of the pRB tumor suppressor pathway. This is accomplished, in turn, as p21 inhibits CDK2 that in turn inhibits pRB. The inhibition of pRB prevents activation of the transcription factor E2F that is required to transcribe genes needed for proliferation. Thus, p21 activates pRB and inhibits expression of E2F target genes.

Stimulation of pRB is also facilitated independently of p53 through activation of the tumor suppressor $p16^{INK4A}$, an inhibitor of the CyclinD/CDK4 (or CDK6) kinase. Inhibition of CDK4 or CDK6 prevents phosphorylation of pRB and progression through the cell cycle. The DDR can also engage the $p16^{INK4A}$/pRB pathway, but this usually occurs after the activation of the p53 pathway.

Activated oncogenes induce the activation of $p16^{INK4A}$ through the MAPK/ERK pathway. This pathway is comprised of a chain of proteins (RAS-RAF-MEK-ERK) that communicate, starting at a surface membrane receptor and ending as a nuclear signal. Downstream targets of the MAPK/ERK signaling pathway, such as ETS transcription factors, are able to induce $p16^{INK4A}$ expression. The activity of ETS is counteracted by ID proteins, which as expected, are down regulated in senescent cells. In addition, several other studies have proposed a role for p38MAP kinases (p38MAPK) in senescence-associated up regulation of $p16^{INK4A}$ [53-55]. Similar to $p16^{INK4A}$, p38MAPK is triggered by many stressors itself and is one of the major members in the family of mitogen activated protein kinases (MAPKs) [54,56]. While the mechanism by which p38MAPK activates $p16^{INK4A}$ is not clear, it is conceivable that it might be through the action of a group of transcriptional repressor complexes known as polycomb group complexes (PcGs). Several studies have shown PcGs as direct regulators of the CDKN2A gene, which codes for $p16^{INK4A}$ and ARF. Therefore, through reduced expression of an INK4a repressor, $p16^{INK4A}$ expression may be induced. More specifically, a target of p38MAPK, MAPKAPK3, has been reported to phosphorylate PcG proteins and relieve repression of CDKN2A [57].

In an effort to better understand the components controlling cellular senescence many groups have experimentally eliminated the main components of the pathways mentioned above. When the expression of key proteins was decreased – namely p53, p21, or DDR proteins such as ATM or CHK2 – senescence was prevented and in some cases (such as in the presence of low $p16^{INK4A}$ or an oncogene) the senescence growth arrest could be reversed [16,39,52,58-60]. Ultimately, most cells senesce due to the employment of the $p16^{INK4A}$/pRB and/or p53 tumor suppressor pathways, yet some forms of senescence appear to be independent of these pathways [61].

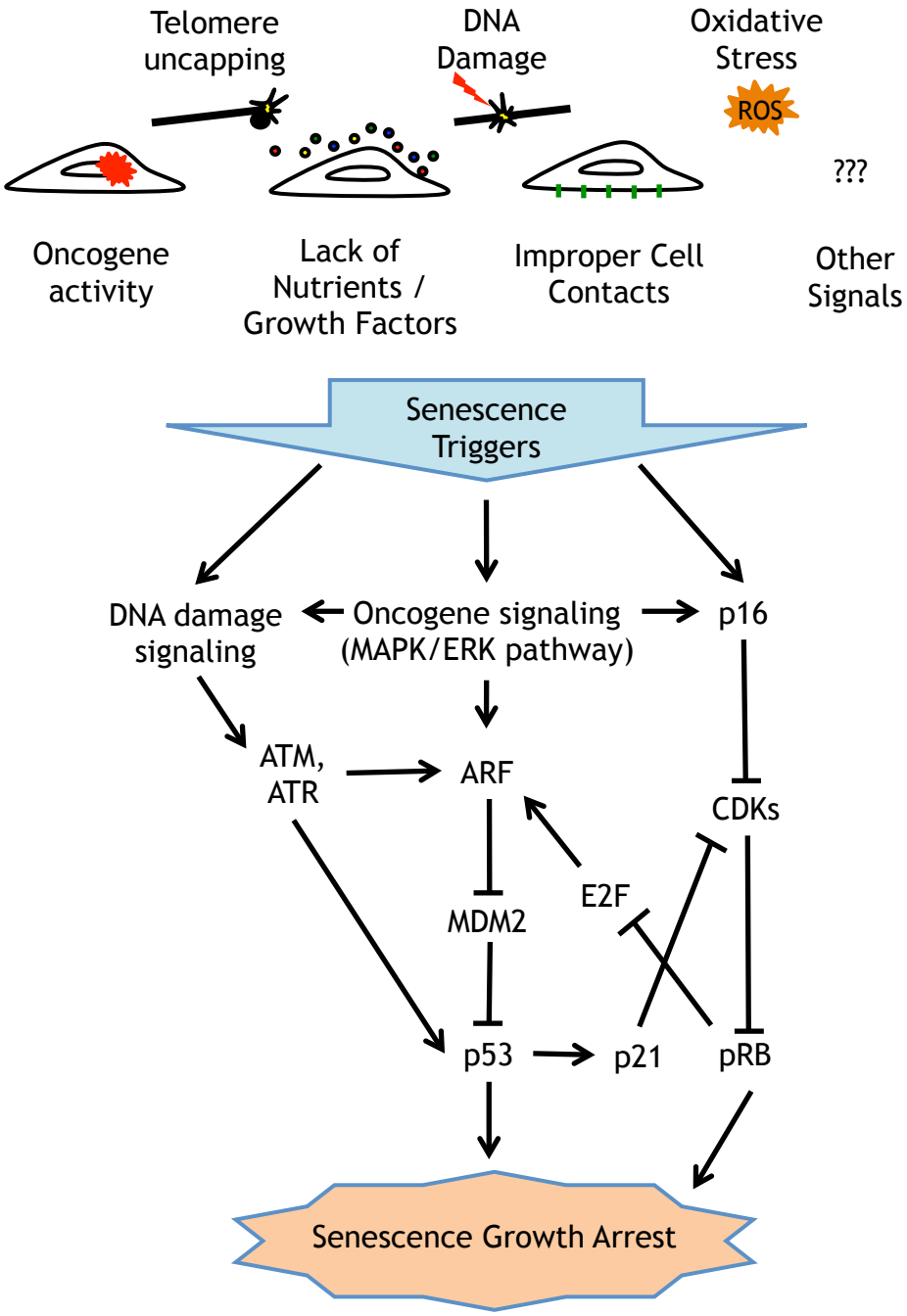

Figure 1.1 Triggers, signals, and effectors of senescence
Senescence triggers exist in many forms including telomere uncapping (as a result of shortened telomeres), DNA damage, oxidative stress, and activated oncogenes among others. These triggers then engage the p53 and/or the $p16^{INK4A}$/pRB effectors of senescence through the activation of signaling pathways such as DNA damage and oncogene signaling. p53 expression is able to reinforce the senescence growth arrest by inducing the expression of the CDK inhibitor, p21. By suppressing CDK activity, phosphorylation of pRB is repressed to avoid inactivation. $p16^{INK4A}$ is another CDK inhibitor that prevents pRB phosphorylation and inactivation. pRB is able to reinforce the senescence growth arrest by suppressing the transcription factor E2F. Aside from stimulating the expression of genes required for cell-cycle progression, E2F can stimulate a growth arrest by inducing ARF expression and in doing so engaging the p53 pathway by inhibiting a negative regulator of the pathway, MDM2. Note that not all proteins involved in cellular senescence are shown.

1.1.2.2 Regulation of senescence by chromatin

One of the first investigations looking into the effectors of senescence did not focus at the genomic level but rather at what molecular characteristics influence the transcriptional changes in aged cells [62]. In this analysis thirty years ago, the occurrence of chromatin changes in senescence was noted and their importance was postulated. Over twenty years would pass until the dramatic changes in chromatin distribution would be described [29]. Senescence associated heterochromatin foci (SAHF) are punctate domains of heterochromatin that form in many cell types in response to a large-scale chromosome condensation. While the alteration of chromatin structure during senescence does seem to be a conserved trait among all species even as dissimilar as yeast, the formation of SAHF in response to senescence is specific to some human cells [63,64]. SAHF have been proposed to silence genes that are required for proliferation, such as Cyclin A, in order to reinforce the cell cycle arrest [29].

Interestingly, the two master regulators of senescence, $p16^{INK4A}$/pRB and p53 pathways have both been implicated in the formation of SAHF. Initially, the $p16^{INK4A}$/pRB pathway was the only pathway implicated as it was found that the knockdown of $p16^{INK4A}$ or pRB significantly suppresses SAHF formation after the introduction of an activated oncogene, yet the cells still arrested and still exhibited other markers characteristic for senescence. Similar to growth arrest, once established, SAHF no longer require $p16^{INK4A}$ or pRB for maintenance [29,65]. Further analysis has also shown that the p53 is implicated in the formation of SAHF [66].

Upon the onset of senescence SAHF quickly develop during which time there are transient interactions among histone chaperone proteins including those of the HUCA complex – HIRA, UBN1, CABIN1, and ASF1a [67,68]. This family of proteins has been shown to have many roles including the formation of heterochromatin in yeast, flies, and plants [69-73]. Members of this complex also act independent of

each other in such processes as aiding in the control of posttranslational histone modification [74-76].

Once formed, SAHF contain individual portions of single condensed chromosomes [77]. Each focus contains modifications and associated proteins characteristic of transcriptionally silent heterochromatin, such as methylated lysine 9 of histone 3 (H3K9Me), heterochromatin protein 1 (HP1), the histone H2A variant macroH2A and the high-mobility group A (HMGA) proteins [29,68,77-79]. Outside of SAHF, macroH2A proteins have a known role in gene silencing [80]. This protein is a transcriptionally repressive variant of histone H2A and is a marker of the inactive X chromosome (Xi) in female mammals [81]. It still remains to be understood exactly how macroH2A contributes to the senescence phenotype. Interestingly, macroH2A contains a unique domain that sets it apart from all other histones. The function of this domain is not fully understood, but it is able to bind to NAD metabolites (such as poly-ADP-ribose bound to chromatin), hinting at a role in cell metabolism and a possible link to cell senescence working through the chromatin structure [82]. Markers of transcriptionally active euchromatin are excluded from SAHF, such as acetylated lysine 9 of histone 3 (H3K9Ac) and methylated lysine 4 of histone 3 (H3K4Me) [29,77].

1.1.2.3 MicroRNAs

MicroRNAs (miRNAs) are a large family of small noncoding (~22nt) endogenous RNAs conserved among animals, plants, and viruses, and function to regulate gene expression through interfering with translation or induction of target mRNA degradation [83-86]. Specifically, miRNAs suppress protein expression at the posttranscriptional level by binding to the 3' untranslated region (3'-UTR) of messenger RNA (mRNA), resulting in reduced translation or degradation. Alternatively, some miRNAs bind to the 5' untranslated region (5'-UTR) or open reading frame (ORF) of target mRNAs or even function to activate gene expression rather than inhibiting it [87-89]. miRNAs regulate many diverse target regulatory networks, thanks in part to the fact that a single miRNA can regulate multiple mRNAs and many miRNAs can cooperatively control a single mRNA

target [90]. One of the many target regulatory networks being heavily investigated as a target of miRNAs is the senescence pathway.

The differential expression of many miRNAs in senescent cells when compared to primary cells indicates a role for miRNAs in senescence [91]. Members within the miR-34 family of miRNAs have been shown to be directly regulated by a master regulator of senescence, p53 [92]. Gene promoters in the miR-34 contain p53 binding sites and are also able to increase the activity of p53 by reducing expression of sirtuin 1 (SIRT1). SIRT1 functions though deacetylating p53 in a NAD^+-dependent manner and thereby decreases p53-mediated transcriptional activation, resulting in the reduced expression of downstream proteins such as p21. Therefore, upon miR-34a expression SIRT1 levels are repressed, leading to an increase in p53 acetylation and activity to promote the senescence response [93,94]. Illustrating the complexity and diversity of miRNAs, miR-34a has also been implicated as a strong inducer of senescence in a p53 independent manner during OIS [95]. Countless other miRNAs have been shown to regulate key effector pathways of senescence; no doubt the full extent of their roles in senescence has yet to be revealed [96].

1.1.2.4 Autophagy

Autophagy is a lysosomal degradation pathway that degrades damaged or unnecessary cellular components and recycles them into the cytosol. Usually considered a pro-survival response for protecting cells under stress, research has uncovered roles of autophagy in biological processes as diverse as development, differentiation, immunity, aging and cell death [97]. Evidence also points to a link between cellular senescence and autophagy. Initial research in linking these two cellular process found that autophagy is decreased in senescent cells [98]. In line with this, the impairment of autophagy has recently been shown to induce premature senescence in human fibroblasts through the activation of p53 due to the build up of reactive oxygen species (ROS) from dysfunctional mitochondria [99]. However, other studies found autophagy to be increased in oncogene induced senescent cells based on the finding that many autophagy specific genes

(ATG genes) are upregulated upon senescence and the presence of autophagic vacuoles [100]. Activation of autophagy in senescence seems to be dependent on repression of PI3K-AKT-mTOR pathway, which when inactivated promotes senescence through several effectors including pRB and p53 [100,101]. Furthermore, inhibition of autophagy has been shown to delay the oncogene-induced senescence phenotype, suggesting that autophagy facilitates the senescence process [100].

For a cell to become senescent there are many drastic changes that a cell must undergo, such as dramatic changes in chromatin structure. In addition and discussed in more depth below, a senescent cell also typically secretes a diverse mix of growth and regulatory factors. In order for a senescent cell to provide these signals to its surrounding environment a large amount of protein synthesis is required, which depends on raw materials. As autophagy has been found to be required for efficient expression of at least two hallmark secreted molecules of senescent cells, IL-6 and IL-8, it is conceivable that autophagy serves to provide a senescent cell the required building blocks needed for a functional senescence response [100].

1.1.3 Phenotypes of senescence

1.1.3.1 Common markers of senescence

It is important to understand that there is no single marker of senescence that can be used by itself to identify a cell as senescent. When identifying cells as senescent one must use a combination of senescence markers before making such a conclusion. For instance, a traditional place to start when identifying a cell as senescent is by confirmation of cell cycle exit. Common ways of examining cell cycle arrest include a loss in proliferation genes, Ki67 or Cyclin A, as well as a decrease in the incorporation of the synthetic thymidine analog bromodeoxyuridine (BrdU). Other characteristic morphological traits of senescent cells include a large, flattened morphology and the presence of

lysosomal vacuole compartments that can be stained with beta-galactosidase [102]. Senescence associated beta-galactosidase (SA beta-gal) staining is the most common marker of senescence used both *in vitro* and *in vivo*, but as referred earlier, it must be used in combination with other markers of senescence for a correct identification of senescence. Underlining the importance of using multiple markers of senescence, contact-inhibited or serum starved cells in tissue culture, as well as proliferating dysplastic epithelium in the gastrointestical tract, have been found positive for SA beta-gal but not found to be otherwise senescent [103-105].

As noted earlier, there are many changes to chromatin structure, notably the formation of SAHF. SAHF can be identified *in vitro* by immunofluorescence analysis and staining with 4'-6'-daiamidino-2-phenylindole (DAPI) [29]. There are many other markers that are associated with senescence but also overlap other signaling pathways and cell cycle states. Many markers of the DDR response are often used as markers of senescence such as nuclear foci of phosphorylated histone H2AX (γH2AX) and their co-localization with DNA repair and DNA damage checkpoint factors such as 53BP1 [106]. One of the earliest markers of senescence, before the formation of SAHF, a flattened morphology, or presence of SA beta-gal, is the translocation of the chromatin regulator HIRA into a subnuclear organelle, called the promyelocytic leukemia (PML) nuclear body [68]. PML bodies are proposed sites of assembly for macromolecular regulatory complexes and protein modification and serve additional roles in tumor suppression and senescence [107-109]. Additional markers commonly used as indicators for senescence include the cell cycle inhibitors $p16^{INK4A}$, $p15^{INK4b}$, p21, and p53 [110-116]. The p53 induced gene, DCR2 and the transcription factor, DEC1 have also been shown to be increased during senescence but their functional involvement in senescence remains unknown [116].

1.1.3.2 The senescence associated secretome

In addition to the repression of proliferation genes, senescent cells often down-regulate extracellular matrix proteins and up-regulate matrix degrading enzymes as well as secrete inflammatory cytokines and other immune modulators [117,118].

Collectively known as the senescence associated secretory phenotype (SASP), these genes were originally identified as markers of senescence rather than active participants in the establishment and maintenance of senescence [119]. This powerful mode of cellular interaction that a senescent cell has with its surrounding environment has also been given the name "senescence-messaging secretome" (SMS) to underscore the importance of the communicative functions in the senescence response [120].

Regulation of the SASP is likely to be multi-dimensional as the group of genes are multi-faceted and control varying areas of a cell's inflammatory response. Nonetheless, recent work has pointed towards the nuclear factor-κB (NF-κB) as the master regulator of SASP as it regulates the expression of more genes than pRB and p53 combined. In addition, NF-κB suppression caused escape from immune recognition and cooperated with the inactivation of p53 to bypass senescence [121]. Furthermore, autocrine signaling through SASP members IL-6 and IL-8 is essential for cells to enter senescence as well reinforcing the cell growth arrest [122,123]. In some cases contributors to the SMS (and therefore SASP) can stimulate the innate immune system to trigger tumor clearance [124].

Many members of the SASP phenotype are able to influence the microenvironment of a cell, some of which, such as pro-inflammatory cytokines, have pro-oncogenic effects in certain conditions. This is in line with proliferation rates, migration, and invasion of premalignant cells being enhanced when they are grown in co-culture with senescent cells or their conditioned media [125,126]. As the SASP is important to the understanding of this thesis, its will be further discussed in the chapters outlining the functions and pathologies of senescence.

1.1.4 Functions of senescence

In the 50 years since senescence was first described, the physiological functions of cellular senescence have been slow to be elucidated. However, it is

becoming apparent that the functions of senescence are diverse and impinge on fundamental biological processes.

1.1.4.1 Tumor suppression

To form a tumor, cancer cells typically must acquire an unrestrained growth potential, a trait that is suppressed by senescence[127]. Underlining the critical role of senescence in tumor suppression, many of the same triggers that initiate cell transformation are equally able to elicit a senescence response. Two dominant tumor suppressor pathways are at the heart of the senescence program are the p53 and the pRB/p16^{INK4A} pathways [15,35,58,115,128-134]. Most if not all cancers have mutations in these pathways bypassing their ability to induce senescence.

It was only within the last decade that scepticism that cellular senescence was merely an artifact of *in vitro* cell culture shock has diminished [135]. During this time period many independent groups have found that cells undergo senescence in premalignant tissues while aspects of senescence are absent from their malignant state [2,115,116]. Analysis on human and murine tissue showed senescent tumor cells in lung adenomas, pancreatic intraductal neoplasia (PanIN lesions), prostatic intraepithelial neoplasia (PIN lesions), and melanocytic nevi, all of which are known premalignant tissues. Studies also showed that senescence was abolished in the equivalent malignant state, lung adenocarcinomas, pancreatic ductal adenocarcinomas, prostate adenocarcinomas, and melanomas, respectively [1,115,116]. Specifically in mouse models, tumor suppressor genes such as PTEN or oncogenes such as NRAS have been altered to induce senescence and resulted in the development of pre-malignant lesions without signs of apoptosis [114,115]. Upon inactivation of senescence through deletion of senescence modulators such as p53 or chromatin modulators, full-blown malignancy occurred. Of particular interest for this study is the premalignant, and presumed senescent state, of melanoma – nevi. Senescence has also been observed in melanocytic nevi in mice with BRAFV600E expressed specifically in their melanocytes [136]. Appropriately, the vast majority of benign human nevi

have also been found to have a BRAFV600E mutation [3]. In sum, several lines of evidence from human tissues and mouse models strongly support the idea that senescence is a potent tumor suppression mechanism.

1.1.4.2 Tissue repair

When one thinks of the process of wound repair the first thing that likely comes to mind is the healing of a cut in ones skin. In order for this healing process to occur, three main tasks must progress in harmony. This includes attracting immune cells to clear pathogens to initiate inflammation, stimulation of growth factors to allow new tissue formation (fibrosis), and tissue remodelling to down regulate many of the previous drastic changes [137]. These three linked phases of tissue repair occur in numerous types of wound healing, besides physical wounds, such as chronic viral infections, chemical damage, and even nutrient depravation. Recent studies have revealed a role for senescence and the SASP in control of the wound healing response.

To analyze the role of senescence during tissue repair, a mouse model of liver damage has been employed [138]. Upon the induction of liver damage through chemical treatment, hepatic stellate cells proliferate and secrete extra-cellular matrix (ECM) resulting in the formation of a fibrotic scar. These cells soon senesce and display a SASP resulting in the down regulating of ECM components and the increased expression of MMPs, which can also degrade ECM proteins. In addition, senescent hepatic cells secrete chemokines to attract natural killer (NK) cells that will ultimately clear the excess of hepatic stellate cells. Therefore, the presence of senescence during liver healing acts to resolve fibrosis once the healing has taken place in order to allow the restoration of normal tissue function. The study also showed that when hepatic stellate cells are compromised for their ability to undergo senescence severe fibrosis entails after acute liver injury, pinpointing the importance of senescence in facilitating a portion of the wound healing response.

More recently another mouse model has been developed for analysing the role of senescence in wound healing [139]. In this model excisional cutaneous wounds were created using a small punch biopsy. The ECM protein CCN1 had previously been shown to have a role in wound healing and is important for cell migration, differentiation, and survival [140]. After wounding of a wild type mouse, the healing tissue was found to contain senescent fibroblasts, while after wounding of a mouse with a mutant CCN1, wounds became much more fibrotic. This fibrosis could even be reversed after the application of topical CCN1 as it was able to induce senescence and promote secretion of MMPs to resolve the fibrotic tissue. Therefore, cellular senescence allows for a functional wound healing response thanks in part to the SASP.

1.1.5 Pathologies of senescence

1.1.5.1 Aging

Senescent cells have been shown to increase with age in a variety of mammalian tissues [102,141-145]. Specifically, a rise in biological features and molecular markers of senescence such as SA beta-gal, shortened telomeres, and DNA damage signals, as well as increased activity in effectors of senescence such as p38MAPkinase, $p16^{INK4A}$, and HIRA have all been associated with aged tissue [19,102,142,146-149]. In line with a link between senescence and aging, the accumulation of senescent cells is also related to age associated tissue pathologies such as osteoarthritis, atherosclerosis, and live cirrhosis [150-152]. Experimentally, inactivation of pro-senescence pathways such as $p16^{INK4A}$ in a prematurely aged mouse model is able to prolong cell renewal and transgenic expression of hTERT extends longevity in cancer-resistant mice [153-157]. Conversely, elevation of another tumor suppression pathway, p53, in a murine model was able to shorten life span and showed signs of premature aging such as loss of fertility, osteoporosis, reduced hair growth, dermal thinning, and

retarded wound healing [158,159]. Cells from these mice also underwent rapid senescence when grown in culture, pinpointing a strong correlation between excessive cellular senescence and premature aging phenotypes [158]. More recently, it has been uncovered that the removal of senescent cells can prevent or delay the generation of age-related phenotypes demonstrating that the clearance of senescent cells or blocking their effects many represent a tool in treating or delaying age-related diseases [160].

The process of aging was originally hypothesized to be simply due to the accumulation of mutations [161]. Soon after in 1957 Williams proposed a theory to explain how something apparently detrimental can be positively selected for in evolution [162]. This theory is known as antagonistic pleiotropy and stipulates that a biological process can be both beneficial and deleterious, depending on the age of the organism. Specifically, a subset of the genes responsible for the negative effects are selected for because they can confer a reproductive advantage early in life while conferring harmful effects in aged individuals. The foundation for the theory of antagonistic pleiotropy rests on the fact that most organisms evolve in environments that are full of fatal extrinsic hazards, a so-called "survival of the fittest". Such extrinsic hazards include predation, disease, and starvation and under these conditions the presence of aged individuals is rare, therefore minimizing the selection against processes that promote disabilities later in life. In other words, age-associated phenotypes are not under the control of natural selection and therefore processes that promote fitness in young individuals can be detrimental in aged organisms [162,163]. According to this view, senescence is beneficial in young organisms through its ability to promote tumor suppression, but has detrimental effects on old organisms.

A possible mechanism for how cellular senescence can lead to aging phenotypes is through the depletion of important stem cell and other progenitor cell pools. For example, studies on neurons, melanocytes, and pancreatic islet cells have demonstrated an age-associated decline in the presence as well as proliferation of undifferentiated stem and/or progenitor cells [153,155,164]. However, the renewal capacity and number of hematopoietic stem cells do not decline but

rather increase with age, although their function is altered [165,166]. As referred to earlier, senescent cells can also impair tissue function through the action of secreted molecules, namely components of the SASP [167]. Damage imparted by certain members of the SASP can contribute to altered tissue function, homeostasis, and cell renewal capacity – all factors important in aging. For example, one family of secreted molecules, the MMPs, have been shown to contribute towards the degradation of cartilage, tendon, and bone during age related pathologies such as osteoarthritis and rheumatoid arthritis [168]. In sum, current research has pointed towards the contribution of senescence in tissue and organismal aging as being multi-faceted. Senescence regulates aging by influencing stem and progenitor cell proliferation and renewal as well as the more encompassing role imposed by the secretome.

1.1.5.2 Tumor promotion

As one of the hallmark roles of senescence is tumor suppression, it is odd to think that senescence is also able to aid in tumors. However, the antagonistic pleiotropy theory also explains how senescence is able to function as a tumor promotion mechanism as according to the proposed theory, while senescence is initially beneficial to an organism, it becomes detrimental in aged individuals. The mechanism of how senescence promotes cancer appears to be due to the ability of senescent cells being able to fuel the cells around them. Through this nonautonomous mechanism, defined earlier as the SASP, senescent cells secrete a large amount of cytokines and chemokines into their surrounding environment [167]. Also, by further stimulating the immune system many secreted factors such as IL-6, IL-8, VEGF, and the MMPs are able to induce proliferation and/or invasion of the surrounding cells [169-174]. As there is an increase of senescent cells with age, persistent amounts of secreted factors may accumulate, possibly stimulating the formation of a tumor. It is possible that a larger, chronic amount of SASP signaling promotes the pro-tumorigenic effects while lower amounts of SASP promote its tumor suppressive effects. Whatever the main contribution of SASP might be, either pro- or anti- tumorigenic, it seems to be clearly context dependent.

1.1.6 Differences among species

The mouse (*Mus musculus*) is regarded as one of the best, if not the best, model organism used in the laboratory for studying the molecular counterparts of a human. The mouse and human genomes are approximately the same size and contain nearly the same number of genes. Most human genes have mouse counterparts that are closely related in function, and mutations that often cause a disease in humans sometimes do the same in mice. The genetic makeup of a mouse can be altered to make a transgenic mouse and as they are easily bred, the production of large cohorts can be done in a rather timely manner. All of these traits as well as others make the mouse an ideal model system and it is of no surprise that it has been used heavily for the understanding of senescence. However, it is important to recognize that there are significant differences between senescence in mouse and human cells.

Starting with the triggers of senescence, one of the major differences between a mouse and human is the length of the telomeres. Mouse fibroblast telomeres are approximately eight times the length of human fibroblast telomeres (40kb in mouse, 5kb in human) [175]. Also, in contrast to human cells, most somatic mouse cells express telomerase [176]. In human, telomerase is only present, with the exception of malignancies, in germ line cells and some stem cells and lymphocytes during clonal expansion. Therefore, the "end replication problem" discussed previously as an initiator of senescence is less of a problem in mouse cells than human cells as demonstrated by the fact that mouse cells do not typically undergo senescence due to shortened telomeres unless they have been genetically altered to have mutations in genes that affect telomere length. Most strikingly, primary mouse embryonic fibroblasts (MEFs) are immortal when cultured in physiological (2-3%) oxygen [32].

Other critical differences between mice and humans in respect to senescence involve the effector pathways. Senescence in MEFs can be bypassed by inhibiting either the function of pRB (together with related proteins, p107 and

p130) or p53 separately, while in human cells inactivation of both pRB and p53 pathways is required to abrogate senescence [34,177-179]. This is due to the fact that in human cells the pRB pathway can be activated independently of p53 through the upregulation of $p16^{INK4A}$ whereas in MEFs $p16^{INK4A}$ is not a critical regulator of senescence [180,181]. Nonetheless, both the pRB and p53 tumor suppressor pathways are important in mouse and human cellular senescence. It appears that additional anti-proliferative pathways are employed in human cells to lead towards a stronger cell cycle arrest.

Mouse cells also differ in the way that p53 is activated for the induction of senescence. In mice, the p19ARF protein is important for the stabilization of p53 activity through inhibition of mouse double minute 2 (MDM2), an ubiquitin ligase for p53 [182]. The human homolog of p19ARF is p14ARF (referred to as ARF previously), which responds differently to OIS than its mouse counterpart. The human protein p14ARF is not upregulated upon OIS whereas the expression of p19ARF mouse protein is increased [183]. Human cells subjected to OIS still increase in expression of many other tumor suppressor genes, such as $p16^{INK4A}$ and p21, without drastic changes in ARF levels [183]. These findings indicate a lesser role for the ARF locus in human senescence as compared to mouse senescence.

Aside from differences in tumor suppressor pathways, dissimilarities exist in the chromatin structure of senescent mouse and human cells. Recent work has shown that mouse cells do not form robust punctate SAHF as human cells do in response to an activated oncogene or shortened telomeres [63]. Consistent with this, changes in the regulation of HIRA (a chromatin modulator) were absent between proliferating and senescent mouse cells [63].

All the differences existing between mouse and human cells in regard to senescence and outlined above may explain how human cells have a firmer control on cellular senescence. In line with this, human cells are much less prone to transformation than mouse cells and mice get cancer after 2-3 years of life whereas in humans it is usually much later [184,185].

1.2 Melanoma and its precursors

1.2.1 Architecture of the skin

1.2.1.1 The human skin

The skin is the largest organ of the body, accounting for roughly 15% of the total body weight in adult humans. Its roles include distinguishing, separating, as well as protecting an individual from its surroundings. As overviewed in Figure 1.2, these vital responsibilities of human skin are possible due to an elaborate structure that is separated into three layers, including the epidermis, dermis, and hypodermis. While these three layers of the skin are present all throughout an individual, there are regional differences such as skin thickness, epidermal appendages (such as hair follicles and sweat glands), and even the molecular signaling of certain cell types within the skin. These regional differences define many characteristics of an individual, covering a human with hair in all areas except for their palms and soles as well as enabling individuals to absorb water through the skin of their mouth while creating a vital barrier in all other areas.

The uppermost portion of the skin, the epidermis, functions mainly in protection and homeostasis. The epidermis is a stratified epithelium that is continuously renewing itself. While it does not contain blood vessels, it is comprised of mainly three types of cells, keratinocytes, melanocytes, and Langerhans' cells. Keratinocytes make up the vast majority of the cells in the epidermis, contributing about 90-95% of the total cells [5]. The epidermis is further composed of continuous layers, each with a specialized role and morphology of keratinocyte. The bottom layer of the epidermis, the basal layer, is where epidermal keratinocytes originate as it contains stem cells and cycling keratinocytes that express proliferation antigens such as Ki67 and label with BrdU. From here, the daughter keratinocytes migrate upwards towards the skin

surface while undergoing keratinization. Keratinization involves both biochemical and morphological changes of keratinocytes as the cells convert and migrate into a horny (cornified) material at the surface of the skin [186,187]. Such changes involve the flattening and high compaction of cells nearer to the skin surface as well as the production of keratin, a fibrous protein that largely makes up the cytoskeleton. Depending on the location of the keratinocytes, different keratins contribute to varying phenotypes, such as shedding of keratinocytes or even the production of a nail. The process of producing a daughter cell keratinocyte, its migration upward, and its subsequent shedding from the cornified material takes roughly 30 days.

Keratinocytes also aid in the production of a distinct border between the epidermis and the dermis, the basement membrane. In cooperation with fibroblasts in the dermis, keratinocytes within the basal layer of the epidermis secrete a number of extracellular matrix components (such as collagen and lamins) that subsequently form the basement membrane [188]. The basement membrane acts to anchor the epidermis to its underlying dermis. Among the keratinocytes of the basal layer sitting adjacent to the basement membrane are specialized cells called melanocytes. These cells are regularly distributed along the basement membrane at a ratio of one melanocyte per four to ten basal keratinocytes. Their density varies regionally with the maximum density on genital skin, and least density in the abdominal skin [189,190]. Melanocytes are especially important for protecting from UV damage as they mediate the tanning response. As melanocytes are a key component of the studies making up this thesis, further details of their characteristics and their ensuing roles will follow in subsequent sections.

The final main cell type located in the epidermis is the Langerhans cell. These mobile, dendritic, antigen-presenting cells are most prominent in the middle portion of the epidermis known as the stratum spinosum or malpighian layer. Originating from CD34+ haemopoietic precursors of bone marrow, Langerhans cells protect the skin from exogenous agents by taking up and processing the foreign antigen followed by presenting it to naive T-cells [191]. The dendritic nature of Langerhans cells enables them to extend between adjacent

keratinocytes and monitor a large surrounding area within the epidermis even though they only make up 3-6% of all cells in the epidermis. In addition to keratinocytes, melanocytes and Langerhans cells, the normal human epidermis contains a low percentage of Merkel cells and lymphocytes. Merkel cells function as mechanosensory cells and enable the sense of light touch [192]. The lymphocytes present in the epidermis are found mainly in the basal layer and serve predominantly as a T-memory/effector cells to aide in cell-mediated immunity [193].

Located within the epidermis and extending downwards into the dermis and hypodermis are epidermal appendages, namely, sweat glands and hair follicles. Sweat glands are tubular exocrine glands that play a vital role in thermoregulation, consisting of a secretory coil and an excretory duct. Hair follicles, also known as pilosebaceous follicles, vary in size and morphology, and undergo cyclical growth proceeding through three distinct phases (anagen, catagen, telogen) of uneven duration. During these phases the morphology of a hair follicle varies dramatically in order for the production or growth of hair to proceed. The hair follicle is comprised of many segments; the upper portion within the epidermis varies little with time morphologically and is made up of an epithelial sheath that extends down to the hair bulb and around the hair shaft. Lower down the follicle extends the opening for the sebaceous duct. The sebaceous glands excrete an oily material called sebum that acts to lubricate and waterproof the skin and hair. The ensuing section of the hair follicle is the bulge region, where arrector pili muscles insert into hair follicles allowing it to stand upright and thus increase the thermal barrier. Also located within the hair bulge are multipotent stem cells that can develop into epithelial cells and melanocytes [194-197]. Interestingly, it has been observed that age-related hair greying is associated with defective self-maintenance of these melanocyte stem cells and their gradual loss over time [164]. The hair follicle then extends down to the hair bulb (papilla), a terminal bell-like extremity containing a collection of epithelial cells that are responsible for hair growth, and melanocytes that give the hair pigmentation. The epithelial cells responsible for hair growth are one of the most proliferative groups of cells, explaining why radio- and chemotherapy are often associated with hair loss.

As mentioned earlier, the basement membrane acts as a barrier between the epidermis and dermis. It also plays a fundamental role in regulating the exchange of metabolic products between the epidermis and dermis as well as support for cell migration during a wound healing response. To allow for better adhesion between the two surfaces the surface area is increased by the formation of alternating upward projections (dermal papillae) and descending depressions (rete ridges). The attached dermis subsequently provides supportive, compressible, and elastic connective tissue to protect the epidermis and all of its extending appendages. Fibroblasts are the primary cells that make up the dermis and work to produce ECM (primarily collagen) and the necessary glycoproteins and proteoglycans necessary to interact with them. The ECM allows for the mechanical resistance of the skin and accounts for more than 98% of the dermis. As in the epidermis, some Langerhans cells are also present in the upper portion of the dermis as well as dermal dendrocytes, which perform functions of macrophages or antigen-presenting cells. Deeper within the dermis is another immune cell, the mast cell. These cells function in wound healing as well as pathogen defense and are characteristically nearby to vasculature within the dermis. The vasculature within the skin is abundant in all areas except for the epidermis and is involved with supplying the skin with nutrients, wound healing, thermoregulation, and immune reactions.

The deepest layer of the human skin is the hypodermis (also known as subcutaneous tissue). This fatty tissue serves to insulate, act as a nutritional store, and protect the underlying muscle or connective tissue from mechanical injuries. The hypodermis is made up primarily of adipocytes and contains larger blood vessels and nerves than those found in the dermis.

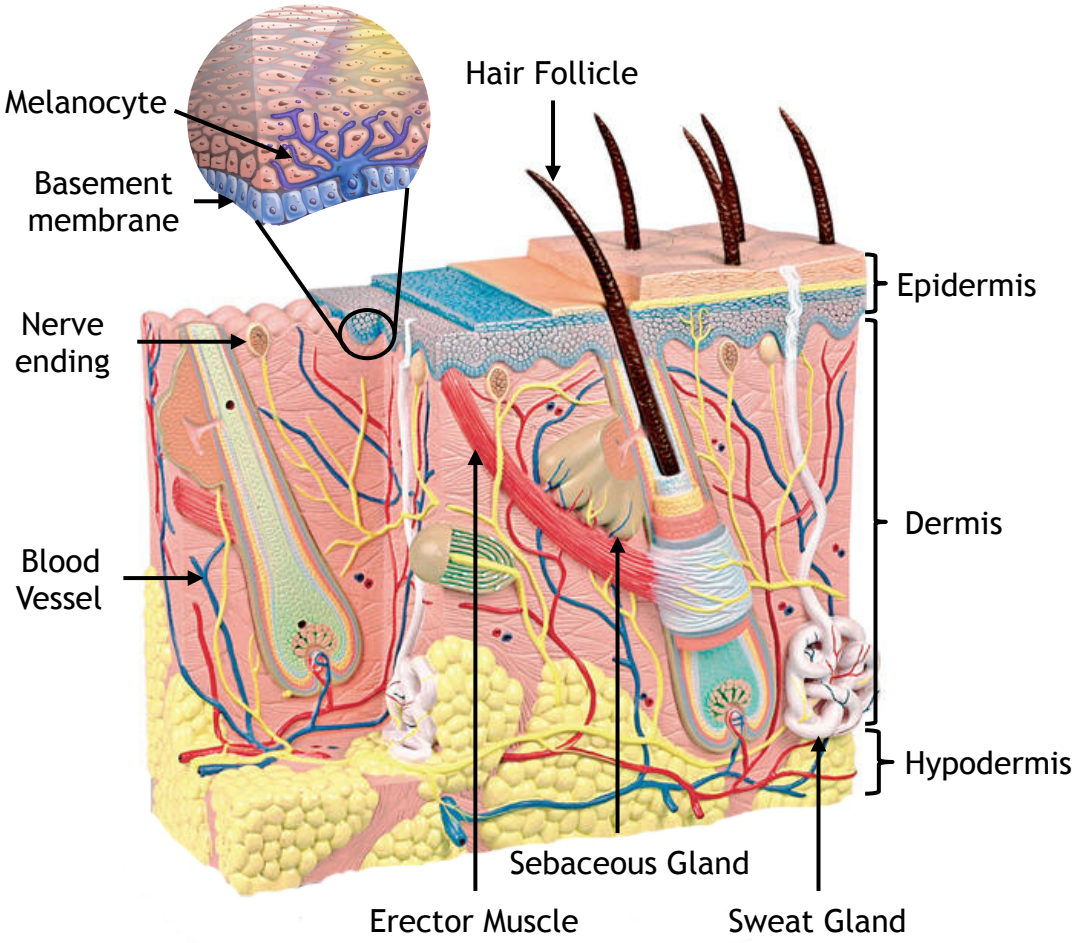

Figure 1.2 Morphology of normal human skin
Refer to text for a more detailed overview of the human skin. Briefly, the human skin is composed of three layers, the epidermis, dermis, and hypodermis. Melanocytes are located along the basement membrane and in the bulb of the hair follicle (not shown). Melanocytes within the basal layer of the epidermis make contact with many surrounding keratinocytes to allow transfer of melanin. The dermis is made up of many epidermal appendages, blood vessels, and nerves. Figure adapted from http://www.research.uky.edu/odyssey/summer08/tan.html and http://www.inds.co.uk/anatomy/skin.htm.

1.2.1.2 The mouse skin

The basic structure of human and mouse skin are quiet similar except for differences in size [198]. However, some differences exist in the presence or absence of a few cutaneous structures. Such examples include the preputial and clitoral glands and the tail exclusively in mice, while only humans have apocrine sweat glands. The mouse skin is composed of four distinct tissue types: from top to bottom, epidermis, dermis, hypodermis, and panniculus carnosus (not present in humans).

At birth, the mouse epidermis is relatively thick but quickly thins within a few weeks as the hair coat begins to grow. In addition to a thinner epidermis in mice compared to human skin, melanocytes are absent in the murine interfollicular epidermis. Any skin color in a normal mouse is usually patchy and only produced in the mid-to late growing stage of the hair cycle (anagen). Melanocytes are normally restricted to hair follicles and nevi are absent from wild type mice. Similar to human skin, mouse epidermal and dermal cells form a basement membrane to serve as a barrier between the two sections. The dermis of the mouse is much thinner than the human dermis but shows very few anatomical differences otherwise. Whereas the human dermis thins with age, the dermis of a mouse remains constant throughout aging. Vascularization also differs within the dermis, as the human dermis is heavily vascularized to allow for thermoregulation whereas the mouse dermis is poorly vascularized and the predominant capillary networks are associated with the hair bulbs [198]. The lack of dermal vascularization in mice may also be an evolutionarily conserved trait to minimize the severity of injury that may occur from predation.

As in the human skin, the hypodermis lies beneath the dermis in the mouse skin and is composed of adipocytes. The hypodermis in mice also contains an additional type of fat known as brown fat which functions to generate body heat, as mice cannot shiver. The thickness of the hypodermal fat layer also changes dramatically with the seasons and as hair follicles move through their growth cycles [198].

In addition to the absence of interfollicular epidermal melanocytes, another difference between a mouse and human skin is the presence of an extensive panniculus carnosus muscle in mice. This skeletal muscle marks the boundary between the skin and the underlying connective tissue and muscle. This relatively thin muscle remains the same thickness throughout the life of a mouse and allows a mouse to move its skin. In humans the platysma muscle of the neck and face are described as one of the very few muscles that has well-defined features of the panniculus carnosus, as it enables facial expressions [198].

1.2.2 The melanocyte

1.2.2.1 Melanocyte development

Melanocytes are pigment cells found primarily in the epidermis and hair bulbs of the skin (cutaneous melanocytes) but may also be found in other areas such as the eye or inner ear (extracutaneous melanocytes) [199]. Of particular interest for this thesis are the epidermal melanocytes that contribute to photoreception and thermoregulation by packaging the pigment melanin into specialized organelles (melanosomes) and delivering them to adjacent keratinocytes. Melanocytes are derived from neural crest cells, a migratory multipotent population that are also able to give rise to neurons, smooth muscle cells, glial cells, medullary secretory cells, bone cells and cartilage cells. Neural crest cells arise uniformly at the dorso-lateral edge of the closing neural folds of the vertebrate embryo neuraxis. Neural crest cells are specifically located between the non-neural ectoderm and the neural plate, also referred to as the neural plate border. Undifferentiated precursors of melanocytes, melanoblasts, are derived from migrating neural crest cells in embryonic skin. Melanoblasts have been shown to migrate dorsolaterally between the dermomyotome and the overlying ectoderm and then ventrally through the developing dermis to the final destination in the basal layer of the epidermis and hair follicles [200-205]. A specific and timely induction of melanoblast differentiation occurs that is regulated by many factors. Included

in these factors are the signaling molecules of the Wnt family of proteins [206-209]. Discussed in more detail later, Wnt are a family of glycoproteins that activate a variety of important roles in embryonic development, cell differentiation, and cell polarity generation. Within melanoblasts, the activation of Wnt signaling is able to induce the transcription of microphthalmia-associated transcription factor (MITF), the master transcriptional regulator of the melanocyte lineage. The activation of MITF subsequently stimulates the differentiation of melanoblasts into melanocytes though the transcriptional induction of melanogenic enzymes: tyrosinase (TYR), tyrosinase-related protein-1 (TYRP1), and dopachrome tautomerase (TYRP2) [210]. Fully differentiated melanocytes are present by birth and characterized by pigmentation and the presence of well-developed dendrites [211].

New evidence has also shown that melanocytes have the ability to populate the skin without developmental dermal migration [212]. Neural crest cells have also been shown to migrate along a ventral pathway to contribute in forming the glia and neurons of the peripheral nervous system. Rather surprisingly, the growing nerves can act as a stem/progenitor niche containing Schwann cell precursors from which a large number of melanocytes arise. In a similar manner to melanoblast differentiation, the Schwann cell precursors rely on MITF for further differentiation into melanocytes. Therefore, even though melanocytes may develop from distinct modes, commonalities in cellular signaling determine the fate of melanocyte differentiation.

1.2.2.2 Pigmentation

Melanocytes are highly dendritic cells enabling a single melanocyte to be in contact with between 30 and 40 surrounding keratinocytes at any given time to form the "epidermal-melanin unit" [213,214]. The interaction between melanocytes and adjacent keratinocytes is mediated and strengthened through many anchoring junction proteins such as E-cadherin, desmoglein, and connexins [215]. The direct contact enables the uninterrupted transfer of molecules between cells to allow processes such as proliferation and biochemical signaling.

One key role made possible by the contact between melanocytes and keratinocytes is the tanning response. In response to UV radiation, melanocytes produce melanin within specified organelles called melanosomes. These organelles are then transferred from melanocytes to neighboring keratinocytes (most likely through the pinching off of a melanocyte dendrite tip by adjacent keratinocytes), where they form an umbrella-like cap over the nucleus to protect against harmful UV rays [216,217].

Melanin is present in two variations in humans: eumelanin, being dark in color, and phaeomelanin, being yellow or red. The presence or absence of either melanin gives the skin and hair their characteristic coloring [218,219]. The principal ingredient for the synthesis of all melanins is the amino acid tyrosine, with cysteine also being required for the production of phaeomelanin. As previously mentioned briefly, the action of the enzymes TYR, TYRP1, and TYRP2 are vital for melanogenesis and are all transcribed by MITF [220]. Failings in melanin synthesis cause defects in pigmentation as it has been displayed that organisms lacking MITF activity are albino and humans with Waardenburg syndrome type 2 exhibit heterochromia of the iris and deafness due to a mutation in MITF [221].

MITF is central to melanocyte viability and function as it is able to control both melanocyte survival through transcription of genes like BCL2 (an apoptosis regulator) as well as melanin synthesis through genes like TYR. UV-induced pigmentation (sun tanning) requires induction of MITF through an extensive signaling cascade. Upon UV induction, pro-opiomelanocortin (POMC) is processed in a p53 dependent manner (predominantly in keratinocytes) into various bioactive peptides including adrenocortocotropins (ACTH), melanotropins (alpha-, beta-, gamma-MSH), lipotropins, and endorphins [222,223]. Interestingly, the endorphins produced by the UV induced POMC cleavage may contribute towards a sun-seeking behaviour, making it “addictive” [222]. Other POMC derivatives such as alpha-MSH and ACTH are important determinants for constitutive pigmentation and the cutaneous response to UV [224-226]. The release of these biomolecules from keratinocytes in response to UV has a paracrine effect on melanocytes that is mediated by the melanocortin 1 receptor (MC1R) and upon activation a further signaling cascade mediated by cAMP is initiated

resulting in the activation of MITF to allow for proliferation of melanocytes and the production of melanin. The melanin is then packaged into melanosomes and transferred to keratinocytes to protect against further UV radiation. Defects in MC1R or POMC result in reduced melanin production and a red-hair phenotype [227].

1.2.3 The nevus

The term "nevus" may refer to a variety of neoplastic skin lesions but most commonly denotes a melanocytic nevus, more commonly known as a mole. For the purpose of this manuscript the term "nevus" (nevi plural) will always refer to a melanocytic nevus. A nevus is a benign neoplastic proliferation of melanocytes, leading to a localized lesion that is usually less than 5mm in diameter. Nevi vary drastically in appearance, as they can be present in both pigmented and nonpigmented forms as well as flattened or raised, dome-like forms. Melanocytic nevi are pathologically identified by the presence of nevus cells arranged at least partially in clusters or "nests". Nesting can occur along the dermal-epidermal junction (junctional nevus), within the dermis (dermal nevus), or in both areas simultaneously (compound nevus). Other defining characteristics of nevus melanocytes, distinguishing them from solitary epidermal melanocytes, are that nevus melanocytes have a tendency to be more rounded than dendritic in cell shape, have a larger size, and tend to retain their pigment rather than transfer it to neighbouring keratinocytes [228,229]. The vast majority of nevi are acquired nevi, meaning they are formed after birth, but nevi are also capable of forming prior to birth (in utero) in which they are classified congenital nevi. In addition, acquired nevi can be classified further as common or atypical as well as into well-defined variant groups such as halo nevi, blue nevi, and Spitz nevi.

1.2.3.1 The life history of a nevus

The life history of a nevus is still poorly understood but their presence has shown to be influenced many factors such as race, environmental factors, and age. While there are no differences in the presence of nevi between sexes, Caucasians do have greater numbers of nevi than darker skinned ethnicities such as Asians or Blacks [230] [231]. In line with this, a greater prevalence of nevi is associated with fairer skinned Caucasians [232].

The first mention of the term "nevus" was in 1896 by Paul Gerson Unna, a dermatopathologist from Hamburg, Germany. He also originated the term "Abtrofung" (dropping off) in reference to the descent of cells from the epidermis into the dermis, at which point he named them "nevus cells" [233]. These cells were originally incorrectly classified as keratinocytes as they resembled epithelial cells of the epidermis. Although additional initial findings have since been found incorrect, this historic work did lay the foundation for further theories of nevogenesis.

The life history of a nevus also points towards nevi being clonal hyperproliferations (originating from a single cell) [9,234]. Acquired nevi are not present at birth but start appearing throughout childhood and adolescence, reaching a peak in the third decade of life [230]. Nevi then disappear with age and are largely absent in aged individuals [230,235]. In addition, the evolution and involution of nevi correlates with their histological appearance, from junctional to compound to intradermal nevi. For instance, junctional proliferation of nevus cells is present in nevi biopsied from children, but decreases with age. In contrast, intradermal nevi are rare in children, and their proportion increases with age, as does the incidence of fibrosis, metaplasia, and neuroid changes. This end point of differentiation is therefore likely to be a later stage in a nevus life history and not an alternative source of origin for intradermal nevi, as previous theories speculated.

Other theories have speculated alternative mechanisms regarding the origin of nevi. According to Masson's theory of dual origin, the nevus cells in the upper dermis develop from epidermal melanocytes, while the nevus cells in the lower dermis develop from Schwann cells supplied by nerves in the surrounding area

[236]. The fact that both melanocytes and Schwann cells are neural crest derived supports this idea, however the theory has been largely ruled out due to advancements in the identification of melanocytes. For instance, electron microscopic examination of neuroid structures in nevi showed that they contain melanosomes, a trait specific to melanocytes [237]. In addition, melanocyte specific markers such as Melan A and tyrosinase are positive in nevi but usually absent in neural cells and neuralfibromas [238]. However, as Schwann cell precursors have been shown to act as a cellular origin for melanocytes, Mason's theory of dual origin cannot be definitively ruled out [212]. Nonetheless, the majority of dermatologists, pathologists and further supportive evidence agree that a nevus likely develops from a single melanocyte.

Another source of prior debate in the field of nevus development is the relationship between epidermal melanocytes and the cells of a nevus (nevocytes). Some researchers believe that these two types of cells have a different embryologic genesis, with nevocytes differentiating from nevoblasts [239]. However, this hypothesis has been largely rejected due to the fact that nevoblasts have yet to be identified *in* vivo and characteristics of nevus cells and epidermal melanocytes are one and the same [240]. For instance, electron microscopy has shown that many of the structures of epidermal melanocytes are present in nevus cells as well [229]. Cultured nevus cells have also been shown to be highly dendritic, a key characteristic of epidermal melanocytes. It would appear that the morphological features particularly associated with nevus cells are due to secondary adjustments of the cells to their new environment. Even though the histogenesis of a nevus is still not fully resolved, it can be said that nevus cells are benign neoplastic variants of melanocytes (differing from Schwann cells). Consequently, the nesting pattern of a nevus may be due to a response to the local microenvironment, a functionally altered state, or even injury.

1.2.3.2 The nevus as a model for senescence

In order to create a defined nevus, the melanocytes within it must stop proliferating at a certain stage. The growth of a nevus is most obviously regulated by $p16^{INK4A}$ as humans with germline mutations in this gene harbor an increased presence of nevi and a higher risk of development into a melanoma [241]. Further initial support for nevi being senescent comes from a variety of additional observations. Melanocytes from nevi grown *in vitro* have limited lifespans when compared to melanocytes from the epidermis and have properties of senescent melanocytes such as large, stellate, well-pigmented and/or binucleate cells [242-244]. In addition, telomerase activity is largely absent in nevi, while it is present in states of melanocytic proliferations such as dysplastic nevi (atypical nevi that may resemble melanoma) and melanomas [245,246].

It wasn't until the groups of Dorothy Bennett and Daniel Peeper published two elegant papers on the subject that concrete evidence was obtained to show that nevus melanocytes are senescent [1,2]. In order to demonstrate that nevus melanocytes are senescent, the authors showed that nevi express elevated levels of $p16^{INK4A}$, display increased SA beta-gal activity, and show a lack of Ki67 staining. These findings were also the opposite in melanoma that alternatively displayed loss of $p16^{INK4A}$ expression and SA beta-Gal staining and a gain in Ki67 staining. Arguing against a role for replicative senescence they also found that telomere length in nevi was equivalent to cells from normal skin and longer than in melanoma cells. Most significantly, these papers showed that nevus senescence arises specifically through OIS as activation of the BRAF oncogene *in vitro* displayed many of the same senescence associated markers as a nevus *in vivo*.

The activated, oncogenic form of BRAF has been found to be predominant in melanoma, as roughly 60-80% of melanomas contain the BRAFV600E mutation [247]. Remarkably, this same mutation was also found present in nevi and even at a similar frequency as in the malignant state [3]. Additionally, in many cases where the BRAF oncogene is not activated, an equivalent oncogene such as NRAS is [248-251]. As inferred from other cell types, these mutations are functionally very similar as both activate the MAPK intracellular signaling pathway, and in doing so

promoting cell proliferation and inhibit apoptosis. Upon the activation of an oncogene it has been reported that there is an initial moderate stimulation of proliferation, but in primary cells it is thought that the growth-inhibitory response ultimately overrules any mitogenic signaling to enforce senescence. In support of the activation of oncogenes contributing to nevus formation, zebrafish expressing a mutant BRAF transgene specifically in melanocytes develop nevus-like lesions. Upon the loss of p53 these growths proceed to form melanomas [252]. Similarly, in a mouse model when mutant BRAF was expressed in melanocytes, benign lesions reminiscent of nevi were formed. These lesions remain stable for several months to more than a year and importantly express several senescence markers. It is also important to realize that nevi are not present in either zebrafish or mice normally; therefore being able to cause the formation of a benign neoplastic growth that is phenotypically similar to human nevi by only activating a single oncogene is quite remarkable.

Interestingly, human benign nevi rarely express detectable p53 or p21, indicating that their type of senescence relies most heavily on $p16^{INK4A}$ activation or an additional unidentified tumor suppressor [1]. In line with these findings, some reports show that $p16^{INK4A}$ is not mandatory for OIS *in vivo*, as nevus formation was unimpaired when mice were crossed onto a $p16^{INK4A}$-deficient background, although reduced latency and increased melanoma penetrance was observed [136,253].

1.2.4 Melanoma

Melanoma (cancer of melanocytic origin) is the least common, yet most deadly of the three types of skin cancer. The other two types of skin cancer, squamous cell carcinoma (SCC) and basal cell carcinoma (BCC) account for 89% of all skin cancer incidents yet less than 20% of skin cancer related deaths in the UK [254,255]. Melanoma is the most serious form of skin cancer as progression towards metastasis occurs rather quickly, is often undetectable, and can affect fairly young individuals. For instance, around half of all people who die from malignant melanoma are under the age of 70 while almost 9 out of 10 non-

melanoma skin cancer deaths are in people aged 65 and over [255]. Unfortunately the incidence of melanoma has doubled in the past 20 years as sun-seeking behaviour has become more common, in the absence of necessary precautions (using sunblock). In addition to ultraviolet radiation and sun sensitivity, risk factors for melanoma include: a family history of melanoma, multiple benign or atypical nevi, a previous melanoma, and immunosuppression. Even with advancements in melanoma prognosis and therapy, mortality rates continue to raise at nearly the same rate as its incidence, emphasizing the importance in continued research into diagnosing and treating melanoma as well as an increased public understanding of melanoma so that certain risks factors can be minimized or avoided.

1.2.4.1 Induction of melanoma

The vast majority of melanomas are thought to begin as intraepidermal or intraepithelial melanocytic proliferations, as most metastatic melanomas have identifiable components from this region. It is estimated that roughly 20% of all melanomas arise from a pre-existing nevus but such estimates are difficult to measure [5-9]. A classic model for the clinical progression of melanoma is often represented using the Clark model as adapted in Figure 1.3 [256]. This model heavily oversimplifies melanoma progression as many melanomas do not strictly follow this progression, with some melanomas skipping steps in the progression of a malignant disease. However, the Clark model of melanoma progression does serve as a valuable tool for understanding histological changes and their relation to genetic alterations that may take place in the progression from normal melanocytes to a melanoma.

According to this model the first change that takes place towards the progression of a melanoma is the formation of a nevus. Proliferation of a solitary melanocyte can be activated in part through mutations in the MAPK/ERK signaling pathway (BRAF or NRAS) but this proliferation is limited due to OIS, therefore rarely allowing further progression towards a melanoma. The next step towards a melanoma may then involve the development of cytologic atypia in

dysplastic nevi that arises from a new lesion or a pre-existing benign nevus. The melanocytes vary in degree of atypia and the proportion of cells with nuclear atypia. Traits associated with atypical melanocytes include enlarged nuclei (and their nucleoli) with varying shapes and chromatin patterns. Irregular nuclear contours and the thickening of nuclear membranes are also characteristic during this time of altered cell growth, DNA repair, and susceptibility to cell death.

In order for such drastic changes to occur it is obvious that the proliferation arrest induced by senescence must be overcome. One of the main routes to override senescence in melanoma lies through inactivation of tumor suppressor genes. For example, in 25-40% of cases with familial melanoma, a genetic defect inactivates CDKN2A that encodes the tumor suppressor genes $p16^{INK4A}$ and p19 (ARF). It has also been demonstrated that within dysplastic nevi there is a frequent loss of heterozygosity at the CDKN2A locus in the addition to occasional mutations [257]. Dysplastic nevi stain for $p16^{INK4A}$ at a lesser rate and in a more patchy pattern than benign nevi, suggesting that dysplastic nevi may have escaped $p16^{INK4A}$-dependent senescence [1]. With molecular changes allowing the override of senescence, a lesion is able to progress to melanoma *in situ*. During this *in situ* stage there is lateral growth that is confined to the epidermis, therefore termed radial growth phase (RGP). Once melanocytes have reached this phase of progression, neoplastic melanocytes have been found to be immortal which can be achieved through activation of human telomerase reverse transcriptase (hTERT). It is reported that more than 90% of human cancers express hTERT and the rest are able to extend their telomeres through an abnormal mechanism called alternative lengthening of telomeres (ALT). Not surprisingly, benign nevi have little or no telomerase activity while the majority of melanomas have substantial telomerase activity [245,246].

The transition from RGP to vertical growth phase (VGP) involves expansion through the basement membrane into the dermis and subcutaneous tissue and is a key indicator of the metastatic potential and clinical outcome. Consistent with this, there are many changes in growth factor dependence during melanoma progression, especially between RGP and VGP. For instance, RGP melanoma cells are dependent on multiple growth factors for proliferation, are

incapable of anchorage-dependent growth and are not tumorigenic in immunodeficient mice. Mutations that repress apoptosis are also an important aspect enabling growth factor independent proliferation in VGP cells. Such mutations include that of the tumor suppressor phosphatase and tensin homologue (PTEN) leading to its inactivation. PTEN is a phosphatase that degrades the phosphoinositide and AKT activator, PIP3 [258]. More recently, loss of PTEN has also been shown to bypass senescence in melanoma [259]. Following malignant transformation, melanoma cells become self-sufficient from growth factors, a feature which may influence their metastasis to other organs [260-263].

Melanoma can metastasize through lymphatic channels, by direct extravascular migratory spread, or hematogenously, therefore being able to appear at any site in the body. Metastases are more frequently found in the skin, lymph nodes, and subcutaneous tissue than visceral organs. Skin metastases occur in roughly 50% of melanoma patients located proximal to lymphatic drainage areas or at a remote location. The most common site for melanoma metastases is lymph nodes as approximately 70% of melanoma patients develop metastases at this location [264].

In summary, melanoma progression is associated with deregulated signaling pathways in transformed melanocytes. The pathways altered may include, but are not limited to, MAPK/ERK activation, CDKN2A inactivation, hTERT activation, and PTEN inactivation. Apart from the activation of MAPK/ERK signaling initiating an initial melanocytic proliferation, the stage at which these mentioned pathways are altered is somewhat variable during melanonomagenesis. As melanomas are so diverse, it is of little surprise that their formation is as equally multidimensional.

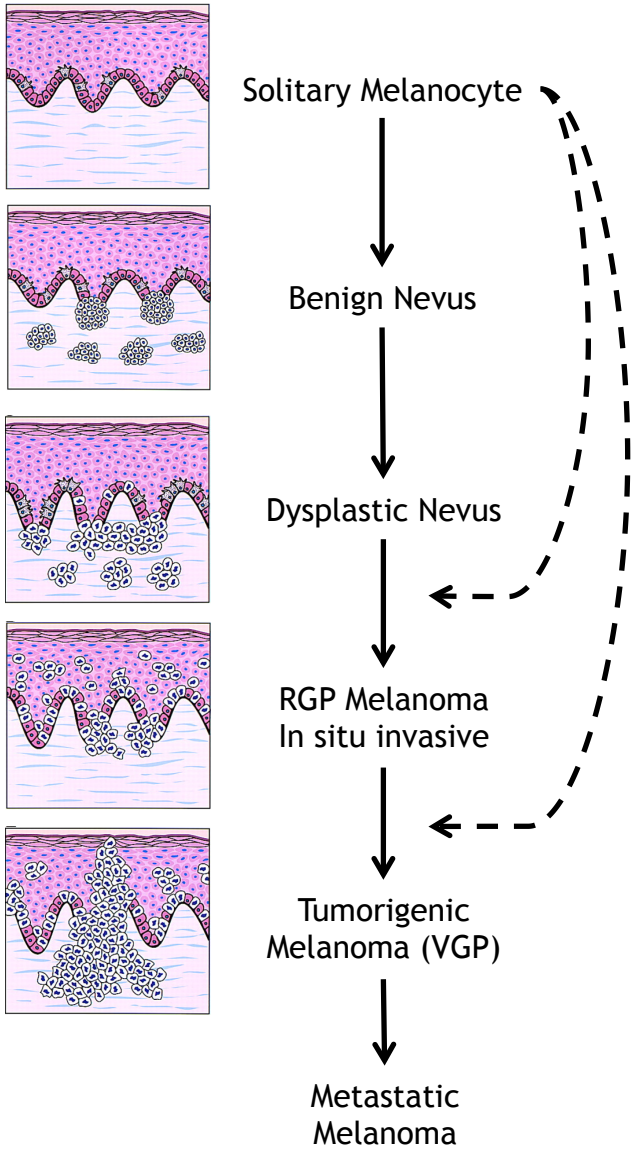

Figure 1.3 The histological progression of melanoma
Melanoma progression consists of various stages. In normal skin there is a uniform distribution of melanocytes sitting along the basement membrane (white cells). Melanoma can arise from nevi, which contain nests of melanocytes. Some nevi contain atypical melanocytes and become dysplastic. Radial growth phase (RGP) is considered the primary malignant stage and is characterized by a pagetoid spread of melanocytes upwards. The vertical growth phase (VGP) has increased malignant potential, as the melanoma is able to pass through the basement membrane to enter the vasculature. Figure adapted from Chin et.al.,1998 [265].

1.2.4.2 Melanoma therapies

The identification of mutant BRAF as a driver of melanoma progression was a major turning point in the development of therapeutics for melanoma. Before this point and as recently as 2010 there were only two Food and Drug Administration (FDA) approved therapies for the treatment of metastatic melanoma. The alkylating agent dacarbazine was approved for treatment in 1975 and established a new standard of treatment even though it resulted in only a partial response with median survival ranging 5 to 11 months and an overall 1-year survival rate of 27% [266]. In 1992 the FDA approved the use of interleukin-2 (IL2). Similar to previous therapies, IL2 was only effective in a small number of patients (6%) and as this immunotherapy approach was required to be used at high-doses, any response was associated with high levels of toxicity [267]. It wasn't until 2011 when two new agents, the anti-CTLA4 antibody ipilimumab and the BRAF inhibitor vemurafenib, displayed a survival benefit in randomized phase III clinical trials [268,269]. Ipilimumab proved that immunotherapy is efficacious in a subset of melanomas while vemurafenib was shown to be nearly ten times more effective than dacarbazine in a randomized phase III trial [270,271].

As BRAF is mutated in roughly 70% of all melanomas it makes an ideal therapeutic target [3,247]. Vemurafenib was FDA approved in late 2011 as the first ever "mutation-specific" therapy for melanoma and proved to be the most successful treatment to date as drug trials showed response rates of more than 50% in metastatic melanoma patients with a BRAFV600E mutation [271]. Although these results were very promising, this is not the whole story. Almost all patients given vemurafenib soon acquire resistance and most diseases ultimately continue progression [272]. As this was initially found to be such an encouraging therapy, many different research groups quickly performed research into the mechanism of resistance in an attempt to develop a combination therapy to fight resistance. Melanoma cells did not typically acquire secondary BRAF mutations following BRAF inhibitor treatment. Yet, there are many different mechanisms of resistance, and there are even reports of different mechanisms

occurring in the same lesion [273]. Potential resistance mechanisms include BRAF truncations, NRAS mutations, and MEK mutations [273-276]. These mechanisms are able to over compensate for the inhibition of BRAF, leading towards resistance. With these findings and continued research, the understanding of how a complex set of mutations act within a melanoma and how to successfully treat them is continuing to move forward. As a result of the rapidly evolving knowledge in the field it is hoped that melanoma will become a more manageable disease instead of the rather deadly disease it is today.

1.3 Wnt signaling

1.3.1 Wnt signaling pathway

In 1982, it was found that activation of the Wnt1 gene, originally name INT-1, resulted from the integration of a mouse mammary tumor virus proviral DNA in virally induced breast tumors and was a key event in development of the tumor [277]. Prior research in Drosophila had already identified a homolog of INT-1, called *Wingless*, which was found to control segment polarity during fly larval development. Since then Wnt signaling has found to have key roles in all phyla of the animal kingdom [278-280].

The Wnt family of proteins is a highly conserved group of 19 signaling molecules that are able to regulate many distinct pathways. Wnt-regulated pathways are organized into two major categories, canonical and non-canonical signaling. The canonical Wnt signaling pathway controls gene expression programs that regulate cell fate and morphogenesis and is often deregulated in cancer and other degenerative diseases. In this pathway, overviewed in Figure 1.4, the secreted Wnt ligands bind to Frizzled (Fzd) and LRP5/6 co-receptors to induce beta-catenin stabilization and entry into the nucleus to activate the transcription of target genes of the LEF/TCF transcription factor family. The non-canonical pathways are more numerous but most known for regulation of

cell polarity through stimulation of cytoskeleton reorganization and the mobilization of calcium. Crucially, canonical-Wnt signaling is dependent on beta-catenin for signal transduction, whereas non-canonical Wnt signaling is not. Depending on the specific Wnt ligand involved, either the canonical or non-canonical Wnt pathway may be activated [281]. The primary Wnt receptors, the Fzd proteins, are seven-pass transmembrane receptors that use an extracellular cysteine-rich domain to bind Wnt ligands [282]. There are 10 different Fzd proteins, each of which has the ability to bind to Wnt ligands at their cysteine-rich domain. The co-receptor and transmembrane protein LRP is also required for proper Wnt signaling.

The stabilization of beta-catenin is the hallmark of canonical Wnt signaling. In the absence of Wnt ligands, the levels of beta-catenin are regulated by a multiprotein destruction complex composed of adenomatous polyposis coli (APC), Axin, Casein Kinase 1 (CK1), and Glycogen Synthase Kinase 3 (GSK3) (Figure 1.4, left). Within the destruction complex, CK1 and GSK3 function to phosphorylate beta-catenin, leading to its ubiquitination and subsequent proteasomal degradation [283]. When Wnt ligands are present, they interact with the Fzd membrane receptor to induce the association of Axin with phosphorylated LRP [284,285] (Figure 1.4, right). The binding of a Wnt ligand to the receptor complex has also been shown to recruit binding of the cytoplasmic phosphoprotein Dishevelled (Dsh) to Fzd [286]. Once Dsh is activated through phosphorylation by specific kinases, it is able to release beta-catenin from the destruction complex to inhibit phosphorylation of beta-catenin, so allowing its accumulation. Cytoplasmic levels of beta-catenin accumulate leading to nuclear translocation and resulting transcriptional activation.

Many of the specifics into how beta-catenin is transported into the nucleus of a cell are still not determined but recent findings suggest a role for microtubules and active transport [287]. Nonetheless, in the absence of activated Wnt signaling beta-catenin is absent from the nucleus and TCF/LEF transcription factors complex with Groucho to repress Wnt target genes (Figure 1.4, left). In the presence of nuclear beta-catenin Groucho, beta-catenin converts TCF/LEF into a transcriptional activator (Figure 1.4, right). Three other proteins important for

the transcription of Wnt target genes are BCL9, Pygopos, and CBP. Many target genes for the canonical Wnt signaling pathway have been identified in both development and tumorigenesis [288]. Examples of such target genes include MITF, c-Myc, Cyclin D1, PPARdelta, MMP7, and the transcription factors AP-1, c-jun and fra1 [289-294]. Whereas most Wnt target genes are cell type specific, an exception lies with the target gene Axin2, which also acts as a negative feedback regulator [295]. Similar to its ortholog Axin, Axin2 is thought to negatively regulate Wnt signaling by promoting the phosphorylation and consequent degradation of beta-catenin through the action of GSK3. In sum, Wnt signaling is regulated in many ways to enable control of pathway duration or intensity, facilitating its many different roles in cells and tissues.

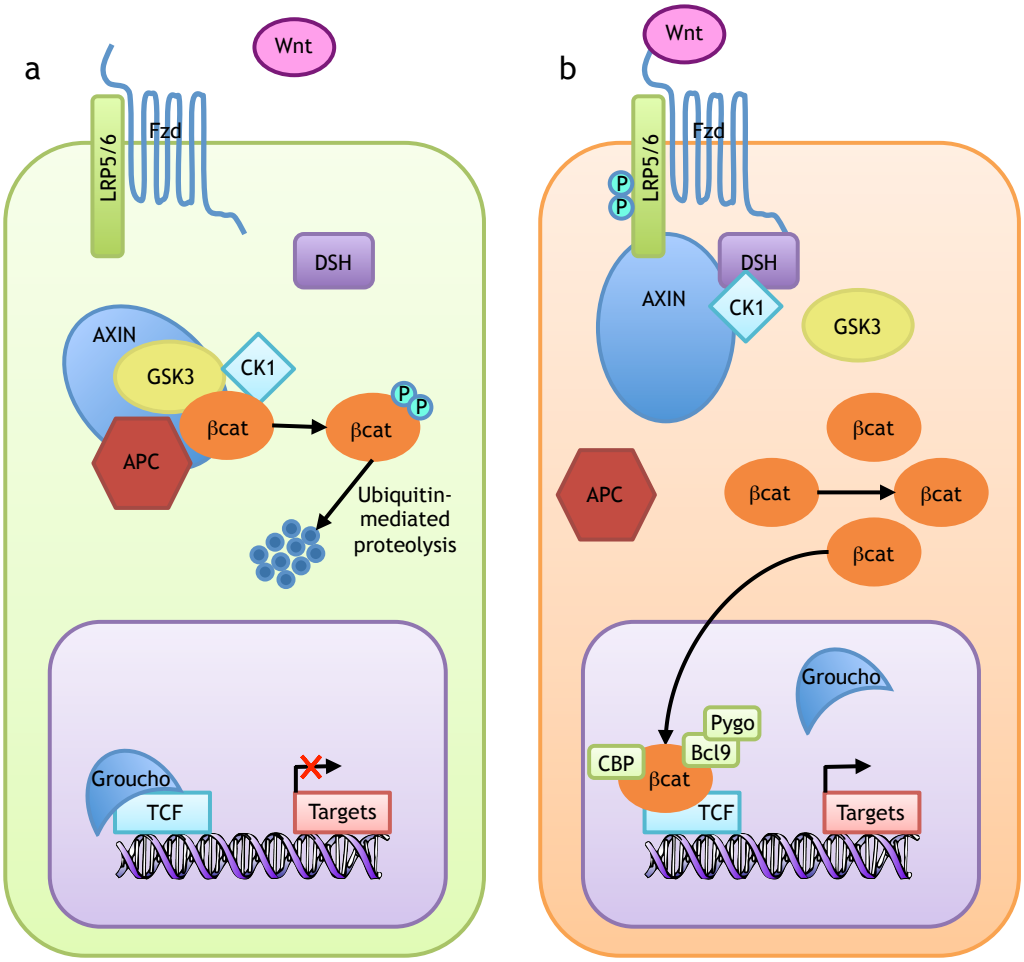

Figure 1.4 The Wnt signaling pathway
(a) In the absence of Wnt, the destruction complex binds and phosphorylates beta-catenin. Phosphorylated beta-catenin is then released by the destruction complex and subsequently ubiquitinated and degraded by the proteasome. In the absence of nuclear beta-catenin TCF occupies and represses its target genes, aided by the transcription repressor Groucho. (b) In the presence of Wnt, Axin becomes associated with phosphorylated LRP and the destruction complex falls apart, stabilizing beta-catenin. Cytoplasmic beta-catenin accumulates and then translocate to the nucleus where it replaces Groucho from TCF and recruits transcriptional coactivators such as CBP, Pygopos, and Bcl9 to allow for the expression of downstream targets such as Cyclin D1, MITF, and Myc.

1.3.2 The role of Wnt signaling

1.3.2.1 Wnt signaling in melanocyte development

Among its numerous other roles, the Wnt signaling pathway has been found to be essential for melanocytes [207,296-299]. As discussed in section 1.2.2.1, melanocytes arise from neural crest cells that migrate from the lateral edge of the neural plate to give rise to many cell types including melanocytes. The decision as to which cell type to differentiate into has been found to be largely dependent on Wnt signaling [296]. During neural crest induction a specific subset of Wnt family members are expressed in spatiotemporal patterns. Specifically, Wnt-1 and Wnt-3a both play critical roles in the development of the neural crest. In addition, these two Wnt ligands also promote the development of neural crest cells specifically into pigment cells, whereas in the absence of Wnt-1 and Wnt-3a neural crest cells favor a neuronal or glial cell fate [207,296]. Independently, Wnt-1 signals to melanoblasts in a paracrine manner to increase melanocyte numbers. Additional Wnt ligands such as Wnt-6 and Wnt-8 are required for the induction and expansion of the neural crest [300]. Besides an obvious role in the development of melanocytes, studies have revealed that Wnt signaling has a critical role in determination of epidermal stem cell fate. Therefore, Wnt signaling controls the regulation of every major cell type in the adult skin and is critical for skin development, maintenance, repair, and regeneration.

In humans, melanoblasts reach their final destination within the epidermis and differentiate into melanocytes both within hair follicles and along the basal layer of the epidermis. To establish this population of cells, Wnt signaling has been found to regulate melanoblast proliferation through regulation of beta-catenin [301]. The isolated melanocytes located along the basal layer of the epidermis interact heavily with surrounding keratinocytes and many of these interactions are influenced by Wnt signaling. For instance, palmoplantar areas (palms and soles) of the epidermis are thickened and hypopigmented due to regulation of the downstream target and negative regulator of Wnt signaling

Dickkopf1 (DKK1) [302]. DKK1 suppresses melanocyte function and growth through the inhibition of beta-catenin, which regulates cellular proliferation and MITF, ultimately regulating pigmentation, as previously noted. Further roles of Wnt signaling in the skin include within hair follicles; Wnt signaling has been shown to influence hair follicle development, the entry of follicle cells into the active growth phase, and even the regeneration of hair follicles after wounding [303-306]. Highlighting the role of Wnt signaling in hair follicle functioning, aberrant activation of this pathway is present in a majority of pilomatrixomas (benign skin tumors derived from the hair matrix) [307].

Of the many downstream targets of canonical Wnt signaling, one of the most important to melanocytes is the melanocyte specific micropthalmia factor (MITF-M) [293]. MITF consists of many different isoforms (-A, -B, -C, -H, -M) each differing in their amino-terminus and expression patterns. Once activated within melanocytes, MITF is able to contribute to many different downstream pathways among which are pigment target and antigens such as TYR, melan-A, and gp100 [308]. During melanogenesis many genes differentially regulate the MITF promoter, including the transcription factor paired box gene 3 (PAX3). PAX3 activates MITF expression to initiate a mitogenic cascade, while simultaneously acting to prevent terminal differentiation by competing with the functionality of MITF in the production of TRP2. Upon the presence of canonical Wnt signaling, PAX3 mediated repression of MITF is relieved and final differentiation can proceed [309]. Therefore, PAX3-expressing melanoblasts located within the hair follicle reside in an undifferentiated state until the presence of beta-catenin relieves the repression, allowing for the development of a melanocyte. Furthermore, Wnts have been shown to be vital in the development of epidermal melanocytes as they are one of only three factors required for the differentiation of a human embryonic stem cell into a fully differentiated melanocyte [310].

As MITF has many numerous key roles, its regulation is controlled at many varying levels. As mentioned earlier, MITF is influenced by DKK expression as it has been shown that fibroblasts secreting DKK can inhibit melanin production in neighboring melanocytes [311]. Non-canonical Wnt signaling, specifically via Wnt-

5a can also inhibit melanogenic antigens transcribed by MITF [312]. Supporting evidence shows that Wnt-5a signaling can antagonize the actions of canonical Wnt ligands Wnt-1 and Wnt-3a [313,314].

1.3.2.2 Wnt signaling in melanoma

Activation of both the canonical and non-canonical Wnt signaling pathways is required for melanoma. As mentioned, these two pathways mutually oppose each other. Once the melanocytes have become transformed, Wnt-5a levels increase to inhibit canonical Wnt signaling through down regulation of beta-catenin resulting in the promotion of metastasis [315]. Strong expression of Wnt-5a in melanoma has also been associated with poor outcome [316]. Remarkably, nevi have also been shown to express high levels of Wnt-5a and downstream targets of canonical Wnt signaling [317-319]. The significance of canonical and non-canonical Wnt signaling in nevi is unclear. The role of Wnt-5a in nevi is likely to be different from its function in melanoma cells, as Wnt-5a's functions are very context dependent, even acting as a tumor suppressor in many cancers [320-322]. This thesis will address the significance of canonical Wnt signaling in nevi.

Studies have shown deregulated Wnt signaling in many diseases and cancer models [323,324]. Notably, nearly all colorectal carcinomas harbour inactivating mutations in the APC tumor suppressor that results in the inability for the formation of the Wnt destruction complex that is required to prime beta-catenin for proteasomal degradation [325]. Hence, nuclear beta-catenin levels are increased (most prominently at the invasive front in colon cancer) [326]. Unlike colon cancer, where the primary mechanism of Wnt signaling activation is through mutation within the pathway, it has been found that mutations leading to constitutive canonical Wnt signaling within melanoma are uncommon [327,328]. Nonetheless, almost one-third of primary human melanoma specimens display accumulation of nuclear beta-catenin in the absence of any detectable mutations [327-329]. As a result, it is hypothesized that the activation of canonical Wnt signaling is driven by the methylation or mutation of APC, overexpression of

the proto-oncoprotein SKI, or the increased presence of Wnt ligands, presented either by neighboring cells or tumor cells themselves [260,330].

One way in which beta-catenin has been shown to influence the initiation of melanoma is through bypassing senescence [331]. Previous work in fibroblasts has shown that during the onset of both OIS and RS the presence of the canonical Wnt ligand Wnt-2 decreases causing a reduction in Wnt signaling as indicated by an increase in GSK3 activity and a decrease in transcriptionally active beta-catenin [332]. The ability for canonical Wnt signaling to antagonize OIS is in line with the role of OIS in tumor suppression and Wnt-signaling in tumour promotion. In agreement with Wnt signaling being able to suppress senescence in relation to melanoma, activated beta-catenin has been found to suppress senescence in melanocytes harbouring an activated RAS oncogene by repressing $p16^{INK4A}$ transcription [331].

Another way in which Wnt signaling influences melanoma is through transcription of its target genes. One such gene that is directly regulated by canonical Wnt signaling is the POU protein BRN2 (also known as POU3F2) [333]. BRN2 was originally identified in neuronal cells where it functions in the development of the central nervous system but is also expressed at low levels in melanocytes as they are similarly derived from neural crest cells [334]. Studies have shown that BRN2 is overexpressed in melanoma cell lines and also able to induce proliferation and invasion in cells of the melanocyte lineage [333,335]. In addition to being up regulated by beta–catenin, expression of BRN2 is strongly up regulated by MAP kinase signaling and, specifically, downstream of BRAF [333,336].

MITF is also an important Wnt target in melanoma. As MITF and its downstream targets play a central role in regulation of the differentiation, growth, and survival of cells of the melanocytic lineage, changes in the expression levels of MITF can greatly alter cellular characteristics such as proliferation. Fittingly, MITF has been shown to potentially act as a dominant oncogene as it is amplified or mutated in roughly 20% of metastatic melanomas [308,337,338]. The gain-of-function mutation occurs within an area that in post-translationally modified by the addition of a small ubiquitin-like-modifier SUMO [339]. Upon mutation,

sumoylation is inhibited resulting in an increase in MITF transcriptional activity [339,340]. As many of MITF targets are pivotal for cell growth and proliferation such changes can result in a more viable cell. For instance, the anti-apoptotic factor Bcl2 is a target of MITF, causing an increase in MITF to be anti-apoptotic as would be favoured for the development and spread of a melanoma [341]. Therefore, as the expression of MITF has a central role in the determination of the metastatic phenotype, it is often used as a diagnostic tool for melanoma [342,343].

Thus far it has been discussed that Wnt signaling may promote melanoma among many ways such as its ability to abrogate melanocyte senescence or induce downstream targets. Other lines of evidence suggest that the situation is more complicated. Studies suggest that canonical Wnt signaling antagonizes proliferation and metastasis of advanced melanoma, and patient survival is improved in those cases with elevated canonical Wnt signaling [344,345]. Consequently, there is a large amount of conflicting data regarding the status and role of Wnt signaling in melanoma. In sum, the role of Wnt signaling in melanoma and the relationship between Wnt signaling, senescence and nevi is not defined.

2 Materials & Methods

2.1 Materials

2.1.1 Reagents and solutions

Reagent/Solution	Details	Source
3,3-Diaminobenzidine (DAB)		DAKO
Ampicilin		Sigma
Bromodeoxyuridine (BrdU)		Sigma
DAPI		
DNA ladders		Invitrogen
DNA loading dye		
DNase1		Invitrogen
DTT		Sigma
Dubelcco's Modified Eagle Medium (DMEM)		Gibco
ECL Western Blotting Substrate		Pierce
Ethanol		
Ethidium Bromide		Sigma
Foetal Bovine Serum		
Formaldehyde, 10%		
Glutaraldehyde		Sigma
Goat Serum		
Hematoxylin		Vector
Human Melanocyte Growth Supplement (HMGS)		Invitrogen
Hydrogen Peroxide		Sigma
L-Glutamine (200mM)		Gibco
Laemmli Sample Buffer (SB)	63mM TrisHCl, 10% Glycerol, 2% SDS, 0.0025% Bromophenol Blue, pH6.8	
Max Factor Nail Varnish		Nailfinity
Medium 254		Invitrogen
Methanol		Fisher
Non-fat dried Milk		Marvel
Optimem	with glutmax	Invitrogen
Paraformaldehyde		Sigma

PBS/EDTA (PE)	PBS+1mM EDTA	Beatson Institute Central Services
PBST	PBS + 0.5% Tween20	
PBT	PBS + 1%BSA + 0.5% Tween20	
Penicillin-Streptomycin		Gibco
Phosphate Buffered Saline (PBS)	170mM NaCl, 3.3mM KCL, 1.8mM Na2HPO4, 10.6mM H2PO4	Beatson Institute Central Services
Polybrene		Millipore
Polyethylenimine (PEI, 10mM)		Sigma
prolong gold antifade mounting media		Invitrogen
Protein Assay Dye Reagent Concentrate	5x Bradford Reagent	Bio-Rad
Puromycin		Millipore
Running Buffer		Beatson Institute Central Services
SB + DTT	0.1M DTT	
SDS (10%)		Beatson Institute Central Services
Target retrieval solution, pH6		DAKO
Target retrieval solution, pH9		DAKO
TBST	TBS + 0.1% Tween-20	Beatson Institute Central Services
Transfer Buffer	50mM Tris, 40mM glycine, 0.04% SDS, 20% methanol	Beatson Institute Central Services
Tris Buffered Saline (TBS)	10mM Tris-HCl, pH7.4, 150mM NaCl	Beatson Institute Central Services
Tris-acetate-EDTA (TAE)	40mM Tris, 0.1% glacial acetic acid, 1mM EDTA	Beatson Institute Central Services
Tris-EDTA (TE)	10mM Tris-HCl, pH 8.0, 1mM EDTA	Beatson Institute Central Services
TritonX		Sigma
Trypsin		Invitrogen
Trypsin Neutralizer		Invitrogen
VectaMount Mounting Medium		Vector
X-gal		Sigma
Xylene		Fisher
Agarose	Electrophoresis grade	Melford

Table 2.1 Reagents and solutions

2.1.2 Antibodies and dyes

Antigen	Details	Dilution	Source
53BP1	rabbit	1:100 (IF)	Cell Signaling (4937)
Alexafluor 594 goat	rabbit IF secondary	1:500 (IF)	Invitrogen (A11012)
Alexafluor 594 goat	mouse IF secondary	1:500 (IF)	Invitrogen (A11001)
beta-actin	mouse	1:5000 (WB)	Sigma (a1978)
beta-catenin (clone 14/beta-catenin)	mouse	1:125 (IHC)	BD Transduction (610154)
beta-catenin (9562)	rabbit	1:1500 (IHC)	Cell Signaling (9562)
beta-catenin (clone beta-catenin 1)	mouse	1:50 (IHC)	DAKO (M3539)
BRAF	mouse	1:200 (WB)	Santa Cruz (sc5284)
BrdU	mouse	1:40 (IF)	DAKO (M0744)
cMYC	mouse	1:500 (IHC)	Santa Cruz (sc40)
CyclinA	rabbit	1:200 (WB)	Santa Cruz (sc751)
CyclinD1	rabbit	1:100 (IHC/IF)	DAKO (M3642)
DEC1		(WB)	Novus (NB100-1800)
EnVision+System HRP labelled polymer	mouse	neat (IHC)	DAKO (K4001)
EnVision+System HRP labelled polymer	rabbit	neat (IHC)	DAKO (K4003)
Histone H2A	rabbit	1:500 (IHC)	Abcam (ab132923)
Histone H2B	rabbit	1:500 (IHC)	Abcam (ab1790)
Histone H3	mouse	1:500 (IHC)	Cell Signaling (3680)
IgG control	mouse	1:2000 (IHC)	Vector (I-2000)
IgG control	rabbit	1:5000 (IHC)	Vector (I-1000)
IgG, HRP-linked	rabbit WB secondary	1:2000 (WB)	GE Healthcare (NA934)
IgG, HRP-linked	mouse WB secondary	1:2000 (WB)	DAKO (P0447)
Ki67	rabbit	1:1000 (IHC)	Vector (VP-K-451)
Ki67	mouse	1:100 (IF)	Thermo (MA1-90584)
LaminB1	rabbit	1:1000 (IHC)	Abcam (ab16048)
Melan A	mouse	1:50 (IHC/IF)	DAKO (M7196)
p16INK4A (E6H4)	mouse	neat (IHC/IF)	MTMlabs (9511)

p16INK4A (F12)	mouse	1:1000 (IHC/IF)	Santa Cruz (sc-1661)
p16INK4A (JC8)	mouse	1:100 (IHC)	Santa Cruz (sc-56330)
p16INK4A (G175-405)	mouse	1:200 (IHC)	BD (551153)
p16INK4A (2D9A12)	mouse	1:400 (IHC)	Abcam (ab54210)
p16INK4A (M-156)	rabbit	1:200 (IHC)	Santa Cruz (sc-1207)
Phospho-RB (Ser807/811)	rabbit	1:1000 (WB)	Cell Signaling (9308)
RB (4H1)	mouse	1:2000 (WB)	Cell Signaling (9309)
S100	rabbit	1:400 (IHC/IF)	DAKO (X0311)

Table 2.2 Antibodies and dyes

2.1.3 Enzymes and kits

Kit/Enzyme	Supplier
DNA 1000 Kit	Agilent
ECL Western Blotting Substrate	Pierce
Omniscript RT Kit	Qiagen
Qiashredder Columns	Qiagen
Quant-iT RNA Assay Kit	Invitrogen
QuantiTect Probe PCR Kit	Qiagen
RNA 600 Nano Kit	Agilent
Rnase-free Dnase	Qiagen
RNeasy Mini Kit	Qiagen
TruSeq RNA Sample Preparation Kit	Illumina

Table 2.3 Enzymes and kits

2.1.4 Plasmids

Name	Description	Source
psPAX2	Packaging Plasmid	Addgene
pLP/VSVG	Packaging Plasmid	Invitrogen
HIV-CS-CG-$BRAF^{V600E}$-puro	Activated BRAF	Peeper Lab
HIV-CS-CG-puro	Empty Vector	Peeper Lab
EF1alpha-dnhTCF4/SV40-PuroR	dnTCF	Addgene
EF1alpha-SV40-PuroR	Empty Vector	Addgene

Table 2.4 Plasmids

2.2 Methods

2.2.1 Cell culture

2.2.1.1 Cell lines used

Name	**Type**	**Source**	**Product Number**
HEMn-LP	Human epidermal melanocytes	Invitrogen	C-002-5C
HEK293T/17	Highly transfectable human kidney	ATCC	CRL-11268
A2058	Human Melanoma	ATCC	CRL-11147
SK-MEL-28	Human Melanoma	ATCC	HTB-72
C32	Human Melanoma	ATCC	CRL-1585
Malme-3M	Human Melanoma	ATCC	HTB-64
WM-266-4	Human Melanoma	ATCC	CRL-1676

SK-MEL-5	Human Melanoma	ATCC	HTB-70
A375	Human Melanoma	ATCC	CRL-1619

Table 2.5 Cell lines used

2.2.1.2 Cell maintenance

Human epidermal melanocytes were cultivated in medium 254 supplemented with HMGS plus 10 units/ml penicillin and 10 ug/ml streptomycin, at 37°C, in a humidified atmosphere containing 5% CO_2. HEK293T cells and all melanoma cell lines mentioned were grown in DMEM media supplemented with 10% (v/v) FBS, 2mM L-glutamine plus 10 units/ml penicillin and 10 ug/ml streptomycin, at 37°C, in a humidified atmosphere containing 5% CO_2.

For passaging cells, medium was removed by aspiration, the cells rinsed with PBS, then detached with 10% trypsin/PE solution. Once cells became detached the trypsin was quenched with trypsin neutralizer and the cells were pelleted by centrifugation. Cells were then re-suspended in culture media and subsequently transferred into appropriate tissue culture flasks. Note that the "age" of human epidermal melanocytes was carefully recorded, as they are primary cells and will senesce with continued growth *in vitro*. The age of cells is recorded by noting passage doubling (PD). For example, sub-culturing through a 1:2 split represents 1 PD while sub-culturing through a 1:4 split represents 2 PD.

For long-term storage, medium was removed from the cells by aspiration, the cells rinsed with PBS, then detached with 10% trypsin/PE solution. Once cells became detached the trypsin was quenched with trypsin neutralizer and the cells were pelleted by centrifugation. They were then re-suspended in 10% DMSO in FBS, placed in cryotubes and frozen at -80°C over night and then transferred to liquid nitrogen tanks for long-termed storage.

2.2.2 DNA Manipulation

2.2.2.1 Diagnostic restriction digest

Diagnostic restriction digests were performed in order to confirm the identity of plasmids used in subsequent sections. Typically, 0.5 micrograms of purified plasmid DNA was incubated with 1 total unit of enzyme(s) in the presence of a supplied buffer and water for 1 hour at 37°C. Samples were then analyzed using agarose gel electrophoresis.

2.2.2.2 Agarose gel electrophoresis

DNA electrophoresis was carried out on an agarose gel composed of a specific percent electrophoresis grade agarose (depending on size of DNA being analyzed, usually between 0.8% and 1.2% w/v) dissolved in TAE buffer. Prior to solidification of the gel, the intercalator ethidium bromide was added at a final concentration of 0.5 micrograms per milliliter. A proper amount of 10x DNA loading dye was added to each DNA sample to result in a final 1x solution. Samples were then loaded onto the gel alongside a suitable DNA ladder. The gel was then run at 100 volts until the DNA had migrated a suitable distance. DNA samples were then visualized using UV transillumination.

2.2.3 Lentiviral mediated gene transfer

2.2.3.1 Production of lentivirus

HEK293T were seeded one day prior to transfection in a T175 flask at 15x10^6 cells with 25 milliliters media. Cells were 80-90% confluent at time of transfection. Into 5 milliliters of Optimem the following plasmid constructs were added and filter sterilized though a 0.22 micron filter: 32.5 micrograms packaging plasmid psPAX2, 17.5 micrograms envelope plasmid pLP/VSVG, and 50

micrograms of vector construct of interest. In another vial 1 microliter of 10mM polyethylenimine was added to 5 milliliters of optimem and filtered through a 0.22 micron filter. Both mixtures were then combined and incubated for 20 minutes at room temperature. The 293T packaging cells were then washed with prewarmed optimem and the 10 milliliter optimem/DNA/PEI mix was added to the cells. Cells were incubated to allow for transfection for 4 hours at 37°C, 5% CO2. The media was then removed and replaced with 30 milliliters of fresh DMEM + 10% FBS and incubated at 37°C, 5% CO2. After 48 hours the supernatant was removed, filtered through a 0.45um filter, and placed in a 50 milliliter falcon tube. The supernatant was subsequently stored at 4°C until required. 30 milliliters of fresh DMEM + 10% FBS was again placed onto the cells and incubated for an additional 24 hours at 37°C, 5% CO2. At this time point (72 hours after transfection) the supernatant was collected as before. Both batches of virus supernatant were then concentrated in an untracentrifuge (Optima L-90K Ultracentrifuge and the SW28 9E473 rotor) by spinning cells at 70000 xg at 4°C for 2 hours. The supernatant was then decanted and 100x less PBS than was originally concentrated was placed on the virus pellet to dissolve it. This was then placed on a rocker at 4°C for 4 hours to dissolve the pellet before further manual resuspension and making aliquots. The concentrated virus was then stored at -80°C.

2.2.3.2 Lentivirus quantitation and infection

Cells were plated at a known concentration in a 6 well dish and left to attached to the surface overnight. Media was then removed and 0.5 milliliter of media containing polybrene at a final concentration of 8 micrograms per milliliter was added to each well. Lentivirus was then added using serial dilutions in order to determine the Multiplicity Of Infection (MOI), starting with an overdose likely to be toxic to the cells and ending with a very dilute concentration that will not infect the cells. A high dose is usually 20 microliters of concentrated virus and the lowest dose tested would usually be 0.1 microliters of concentrated virus per 0.5 milliliters media. Virus was added to cells for 6 hours to allow infection. Virus containing media was then removed, cells were washed once with PBS, and

2 milliliters of normal media was added to each well. Twenty-four hours later the virus-infected cells were selected for with 1 micrograms per milliliter puromycin. Three days after the addition of drug the MOI was calculated by counting the number of successfully infected cells (puromycin resistant) divided by the number of total cells present in an uninfected group of cells. This MOI value was then used for subsequent lentiviral infections so that the optimal amount of virus is added to a known amount of cells resulting in the highest amount of infection with the smallest amount of stress.

2.2.4 Protein expression in cultured cells

2.2.4.1 Cell lysis for protein

Whole cell lysates were taken using hot Laemmli sample buffer (SB, + 0.1M DTT). Roughly 200 microliters were used per 60 millimeter tissue culture dish and cells were scrapped with the hot samples buffer, placed into an eppendorf tube, vortexed briefly, and heated for an additional 5 minutes at 100°C. Further mechanical disruption and homogenization of the lysate was done by repeated suction through a 25-gauge needle. Whole cell protein lysates were then stored at -80°C.

2.2.4.2 Protein quantification

Protein concentration of cell lysates was determined using the Bio-Rad Protein Assay (Bradford Assay). This assay uses Coomassie blue dye, which changes color in response to various concentrations of protein. In order to determine concentrations of lysates a 1 microgram per milliliter BSA stock was used as a standard to use as a reference for the unknown lysate concentration. 700 microliters of 1x Protein Assay Dye Reagent was added to each ependorf tube. Three tubes are used as references that contain a known concentration of 0.5 microgram per milliliter and 1 microgram per milliliter BSA as well as a blank containing no BSA. To each standard 1 microliter of SB was added, as SB is able to alter the ability for the dye to change color as well as SB being present in all the lysate samples. For each sample, 1 microliter was added to the 700

microliters of Protein Assay Dye Reagent. After a 5 minute incubation in the dark at room temperature, samples were transferred into cuvettes and analyzed on a spectrophotometer set at 595nm. Values were recorder for each standard and sample and samples concentrations were calculated in reference to the standards.

2.2.4.3 SDS-PAGE

SDS-poly-acrylamide (SDS-PAGE) gels were produced at varying percentages acrylamide in order to sufficiently resolve protein samples. Protein samples were equalised with 1xSB so that all samples were 40 micrograms of equal volume. Samples were then boiled for 5 minutes, quenched quickly of ice, centrifuged, and loaded onto gels. Protein ladders were also loaded for reference. Gels were the run at 125 volts in running buffer until sufficient resolution had occurred using either Bio-Rad's Mini-Protean Tetra electrophoresis system or Thermo Scientific's Owls P10DS Dual Gel System, depending on the size of the gel run. Membranes were then used for western blotting to allow for detection of specific proteins.

2.2.4.4 Western blotting

Whole cell lysates resolved on SDS-PAGE gels were transferred onto a PVDF membrane in blotting buffer for 1 hour at 100 milliamps. Prior to transfer PVDF membranes were activated using methanol. After transfer, blots were allowed to fully dry. Blots were subsequently soaked in methanol, and then blocked in TBS+5% milk for one hour. Please note that this step as well as all following steps required constant agitation through rocking of the membrane (at room temperature) to ensure proper even distribution of all solutions. Blots were then quickly rinsed with TBS+2%BSA+5% normal goat serum and incubated with a primary antibody for one hour in the same solution. Samples were then washed 3 times for 10 minutes each with TBST before incubation with an appropriate HRP-conjugated secondary antibody for one hour in TBST+5% milk. Details of all

antibodies used are included in Table 2.2. Blots were then washed with TBST 3 times for 10 minutes each and visualised by chemiluminescence using Pierce ECL Western Blotting Substrate. Visualization was enabled by autoradiography using Fuji Super RX medial X-ray film and a Kodak X-Omat 480 RA X-Ray processor.

2.2.4.5 General immunofluorescence

Cells were cultured on glass coverslips for at least 12 hours to allow for adherence. Cells were then washed with PBS twice and fixed with 4% paraformaldehyde for 10 minutes at room temperature. The coverslips were then washed twice with PBS followed by permeablization with PBS + 0.2% Triton X-100 for 2 minutes and washing again twice with PBS. Samples were then blocked using PBS + 3%BSA + 1% goat serum for 1 hour at room temperature. Primary antibodies were diluted into PBS + 3% BSA + 1% goat serum and administered by inverting coverslips onto a 200 microliter drop of antibody for 1 hour at room temperature. Coverslips were then transferred back into the dish and washed 3 times with PBS + Triton X-100. Presuming both an anti-mouse and anti-rabbit primary were used, the secondary antibodies alexafluor 594 goat anti-rabbit and alexafluor 488 goat anti-mouse were both diluted into PBS + 3% BSA + 1% goat serum and placed onto coverslips for one hour in the dark at room temperature. Details of all antibodies used are included in Table 2.2. Samples were washed with PBS three times and treated with DAPI (0.1ug/ml in PBS) in the dark for five minutes and washed with PBS three times. Samples were then preserved by applying roughly 75 microliters of Prolong gold antifade reagent mounting media, placing a coverslip on the specimen, and sealing with nail varnish.

2.2.4.6 Immunofluorescence of BrdU

Cells were grown on coverslips and incubated with BrdU at 10uM final concentration in normal growth media for a suitable period of time to allow incorporation. Overnight (16h) was suitable for proliferating melanocytes. Once

labelled with BrdU, media was removed and coverslips were washed with PBS twice. Cells were then fixed for ten minutes with 4% paraformaldehyde at room temperature followed by washing three times with PBS. TritonX (0.5% in PBS) was used to permeabilize the cells for 3 minutes and then the cells were again washed twice with PBS. DNA was subsequently fragmented with 5 units per 200 microliters of DNase1 for 15 minutes. The reaction was then quenched with 20mM EDTA for 5 minutes. Coverslips were washed three times with PBS+ 0.1% BSA. Anti-BrdU primary antibody was applied to samples in PBT for 1 hour at room temperature. Coverslips were then washed twice with PBS before incubating the samples in alexafluor 594 secondary in PBS+3% BSA+ 1% goat serum for 1 hour in the dark. Coverslips were washed twice with PBS then incubated with DAPI (0.5ug/ml in PBS) and lastly washed again with PBS 3 times. Samples were then preserved by applying roughly 75 microliters of Prolong gold antifade reagent mounting media, placing a coverslip on the specimen, and sealing with nail varnish.

2.2.5 Senescence associated beta-galactosidase assay

In subdued light, 1 mg/ml X-gal solution (5-bromo-4-chloro-3-indolyl-â-galactopyranoside, Sigma-Aldrich Co), 0.12 mM K3Fe(CN)6, 0.12 mM K4Fe(CN)6 and 1mM MgCl2 in PBS, pH 7.0, was prepared. Cells were washed in PBS (pH 7.2) and fixed with fresh 0.5% glutaraldehyde in PBS for 5 minutes at room temperature. Cells were washed again with PBS then the cells were stained with X-gal solution (pH 7.0) for 24 h at 37°C. The pH is modified from Dimri *et al.* because growing melanocytes also often stain at pH 6.0 [1,102]. Cells were viewed in water and photographed.

2.2.6 Gene expression analysis and validation

2.2.6.1 Total RNA isolation and quality control

Total RNA isolation was completed using the RNeasy Mini Kit according to manufacturers recommendations. Briefly, cells were lysed on ice into RLT buffer supplemented with beta-mercaptoethanol. Cell lysates were homogenised by mechanical disruption via centrifugation with Qiashredder columns. Residual genomic DNA was removed on-column via DNaseI digestion. RNA was then further purified through wash steps and eluted into water. Collected RNA was then stored at -80°C until needed.

Isolated RNA was subsequently analyzed quantitatively on a Qubit fluorometer using the Quant-iT RNA Assay kit and qualitatively on a bioanalyzer using the RNA 6000 Nano kit according to manufacturers recommendations.

2.2.6.2 Microarray data analysis

Total RNA samples were generated as described above in triplicate. Biotinylated cRNA was subsequently hybridized to GeneChip human genome U133 Plus 2.0 by the Paterson Institute Microarray Service (CRUK). For analysis Affymetrix raw data files (.CEL) for each GeneChip were imported into R and analyzed using the Bioconductor (www.bioconductor.org) packages. The GC Robust Multi-array Average (GCRMA) method was used to background correct and normalize all samples. T-tests were used to determine differential expression based on the log-normalized values produced by the GCRMA method. Differentially expressed genes were defined as those for which the change between Empty Vector and BRAF exceeding 1.5 fold (or less than -1.5 fold) and where the BH-FDR adjusted P-value was less than 0.05. Subsets of genes from the array were visualized using heatmap.2 from the Gplots2 package.

2.2.6.3 RNAseq sample preparation

Sample preparation for RNA sequencing was completed using the TruSeq RNA sample preparation kit according to manufacturers specifications. Briefly, 4 micrograms of high quality total RNA was isolated as described above. mRNA was then purified, fragmented, and reverse transcribed to produce cDNA. Any remaining RNA was then removed and a replacement strand of cDNA was formed to produced double-stranded (ds) cDNA. Upon further purification and end repair to convert overhangs to blunt ends, the 3' ends of each nucleotide were adenylated to prevent the strands from ligating to one another during the subsequent steps. Indexing adapters were then ligated to the ends of ds cDNA, preparing them for hybridization onto a flow cell. PCR was then used to selectively enrich for DNA fragments that have adapter molecules on both ends as well as to amplify the amount of DNA in the library. PCR cycles were minimized (12 cycles) to avoid skewing representation within the library. Libraries were then validated using the Agilent DNA 1000 Kit in conjunction with a bioanalyzer. Libraries were later sequenced using the Illumina GAIIX sequencer at the Beatson Institute.

2.2.6.4 RNAseq analysis

For analysis, RNAseq paired end reads are aligned to the human genome (hg18) using a splicing aware aligner (tophat). Reference splice junctions are provided by a reference transcriptome (Ensembl build 54) and novel splicing junctions are determined by detecting reads that span exons that are not in the reference annotation. Aligned reads are processed to assemble transcript isoforms and abundance is estimated using the maximum likelihood estimate function (cuffdiff) from which differential expression and splicing can be derived.

2.2.6.5 cDNA synthesis

First-strand cDNA synthesis was completed using Omniscript reverse transcription kit according to manufacturers specifications. Briefly, roughly 500 nanograms of high quality RNA was incubated with reaction cocktail and

incubated for 60 minutes at 37°C. This reaction cocktail contained all necessary components for reverse transcription of RNA into cDNA, including: dNTPs (5mM each), oligo-dT primer (10mM), RNAse inhibitor (10U/microliter), Omniscript reverse transcriptase, buffer, and water. The resulting cDNA was then stored at -20°C.

2.2.6.6 qRT-PCR

Following the conversion of RNA into cDNA, gene expression was examined using quantitative real time PCR (qRT-PCR). qRT-PCR was completed using the QuantiTect Probe PCR Kit according to manufacturers specifications. This reaction uses the polymerase HotStarTaq DNA polymerase in conjunction with TaqMan dual-labeled probes in order to achieve high specificity and sensitivity in PCR. Briefly, roughly 20 nanograms of cDNA were used as a template and a final primer concentration of 0.5 micromolar for each primer and probe concentration of 0.25 micromolar was found suitable for each reaction. Upon the addition of the supplied QuantiTect Probe PCR Master Mix the reaction was placed in a thermocycler. An initial step of 95°C for 15 minutes was required for activation of HotStarTaq DNA polymerase. Gene amplification followed with a 2-step cycle, denaturation for 15 seconds at 94°C and a combined annealing/extension step for 60 seconds at 60°C. Following each cycle fluorescence data was collected by the thermocycler to allow for signal quantitation. The program was allowed to continue for 40 cycles by which time all the specific signals would be sufficiently amplified.

2.2.6.7 Primers for qRT-PCR

The following primers and probes listed below were used in conjunction with the qRT-PCR method listed above. The TaqMan double-quenched probe (5'FAM/ZEN/3'ABkFQ) with two quenchers, ZEN and ABkFQ, and the FAM reporter were developed following the manufacture instructions (IDT, Integrated DNA Technologies, Skokie, IL, USA). All sequences are oriented 5' to 3'.

CYCLIND1 Probe--/56-FAM/TGGTGAACA/Zen/AGCTCAAGTGGAA CCT/3IABkFQ/
CYCLIND1 Primer 1--TCTGGCATTTTGGAGAGGAAG
CYCLIND1 Primer 2--CATCTACACCGACAACTCCATC

MITF Probe--/56-FAM/CAGACCCAC/Zen/CTCGAAAACCCCA/3IABkFQ/
MITF Primer 1--GCTTGCTGTATGTGGTACTTG
MITF Primer 2--TCAGACACCAGCCATAAACG

MYC Probe--/56-FAM/CCCCTCAAC/Zen/GTTAGCTTCACCAACA/3IABkFQ/
MYC Primer 1--AGTAGAAATACGGCTGCACC
MYC Primer 2--TTCGGGTAGTGGAAAACCAG

GAPDH Probe--/56-FAM/AAGGTCGGA/ZEN/GTCAACGGATTTGGTC/3IABkFQ/
GAPDH Primer 1--ACATCGCTCAGACACCATG
GAPDH Primer 2--TGTAGTTGAGGTCAATGAAGGG

2.2.7 Protein expression analysis in tissue samples

2.2.7.1 Haematoxylin and eosin stain

For every sample processed a corresponding haematoxylin and eosin (H&E) stain was completed to allow for general histological morphology examination. The haematoxylin stains nuclei blue while the eosin stains the cytoplasm of the tissue constituents various shades of red or pink. All H&E staining was completed by the Beatson Institute's histology service according to a standardized operating procedure. Briefly, samples were dewaxed and hydrated by washing with xylene for five minutes followed by washing with decreasing concentrations of industrial methylated spirits (IMS, 100% 1 minute then 70% 1 minute). Samples were then rinsed with water and placed into Gills

Haematoxylin solution for 7 minutes. Samples were again washed with water followed by dipping into 1% acid alcohol 10 times before again washing with water. Samples were then allowed to blue by placing into Scotts water for 2 minutes. Samples were then washed again with water before being transferred into Putts Eosin for 4 minutes. After a brief rinse with water samples were dehydrated by placing into 70% IMS and 100% IMS (x2) for 15 seconds each followed by immersion into xylene 3 times for 30 seconds each. Samples were then preserved by applying 75 microliters of VectaMount Mounting Medium and placing a coverslip on the specimen.

2.2.7.2 Immunohistochemistry

Human specimens were supplied as FFPE samples on glass slides. Sections were dewaxed by heating at 60°C for 10 minutes followed by immersion into xylene twice for five minutes each. Samples were then rehydrated through graded ethanol concentrations (twice 100% ethanol for five minutes, once 95% ethanol for two minutes, and once 70% ethanol for two minutes) followed by water for an additional two minutes. Antigen retrieval was done by immersing samples for ten minutes into 98-100°C target retrieval solution, pH6 or 9 depending on antibody specifications. This was done in a coplin jar preheated in a boiling water bath and by diluting the 10x stock retrieval solution to 1x in water. Slides were allowed to cool at room temperature for 30 minutes before being washed with water three times for five minutes. Any endogenous peroxidases within the sample were then quenched in a 2% hydrogen peroxidase in methanol solution. Samples were again washed three times with water before blocking proteins with PBT for one hour. Specimens were then circled with a hydrophobic barrier in order to reduce the amount of liquid required to cover the sample. Primary antibody was diluted in PBT and 100-500 microliters was applied to each sample depending on size of specimen. Samples were subsequently washed three times for five minutes each in PBST. Depending on the species of primary antibody used either mouse or rabbit EnVision+ System- HRP Labelled Polymer was applied to each specimen for 1h followed by washing with TBST three times for five minutes each. Details of all antibodies used are included in Table 2.2.

Staining was visualized by applying DAB until the signal had reached proper intensity (between 30 seconds and 10 minutes). Samples were briefly rinsed with water followed by counterstaining with Hematoxylin for one-and-a-half minutes followed by rinsing briefly with water. Specimens were "blued" by submersing in Scott's water for one minute followed by dehydration through increasing ethanol concentrations (tap water for 2 minutes, once 70% for 2 minutes, once 95% for 2 minutes, twice 100% for 2 minutes, and twice xylene for 2 minutes). Samples were then preserved by applying 75 microliters of VectaMount Mounting Medium and placing a coverslip on the specimen.

2.2.7.3 Fluorescent based immunohistochemistry

Tissue samples subjected to fluorescent based immunohistochemistry were subjected to dehydration, antigen retrieval, protein blocking, and primary antibody exposure as described above. Samples were washed three times for five minutes each in PBST after primary antibody incubation. Depending on the species of primary antibody used either mouse or rabbit Alexafluor 594 diluted in PBST was applied. For co-immunofluorescence primary antibodies of different species were used with the relevant fluorophore conjugated secondary antibody. Secondary antibodies were allowed to hybridize for 30 minutes followed by washing with PBST three times for five minutes each. Details of all antibodies used are included in Table 2.2. Specimens were then treated with DAPI (1ug/ml) diluted in PBST followed by washing with water twice for five minutes each. Samples were then preserved by applying roughly 75 microliters of Prolong gold antifade reagent mounting media, placing a coverslip on the specimen, and sealing with nail varnish.

2.2.8 Mouse Work

2.2.8.1 Home office project and personal licensing

All animal work was reviewed prior to completion and approved in project and personal licenses issued by the UK Home Office.

2.2.8.2 Generation of colonies

TyrNRAS mice and APCfl.fl mice were mated to TyrCre mice [346-348]. Progeny from these crosses were then interbred to obtain TyrCreAPCfl.fl/TyrNRAS and were maintained on a C57B6 background. Animals were kept in conventional animal facilities and monitored frequently, and experiments were carried out in compliance with UK Home Office guidelines.

2.2.8.3 Genotyping of mice

Routine mouse genotyping of animals was completed by Transnetyx genotyping services by PCR analysis on ear tissue biopsies taken during weaning (6 weeks of age).

2.2.8.4 Tissue isolation and processing

Mice were euthanized either by rising concentrations of CO_2 or cervical dislocation and relevant tissues quickly dissected. Fixed tissues were then processed by Beatson Institute histology service. Once tissues were received by the histology service, they went through trimming, processing, embedding and orientation, and microtomy. Briefly, collected tissue was trimmed if required to an appropriate size to allow adequate processing. The samples were then placed into a designated processing cassette and stored in either 10% Neutral Buffered Formaldehyde (NBF) or 70% ethanol until subsequent processing. The tissue was then processed using a Thermo Finnesse. During this process the tissue was dehydrated using increasing concentrations of ethanol (70%, 90%, 95%, 100% x3) and then washed with xylene three times to remove any alcohol. Molten paraffin wax was then pumped into the chamber to absorb any residual

xylene and allowing for proper embedding in the next step. Tissues were then orientated with respect to the view of interest and embedded into molten paraffin wax. This was done by placing the processed tissue into a heated metal mould containing molten paraffin wax. The product was then transferred to a cold plate (-5°C), allowing the molten wax to solidify. Samples could then be removed from the mould and tissue blocks were stored indefinitely at room temperature.

If sections were required on glass slides for analysis via such methods as immunohistochemistry, the tissue blocks were placed into a microtome block holder and trimmed to allow exposure of the full face of the tissue. Once trimmed the blocks were cooled on a cold plate to harden the blocks and make sectioning easier. Sections were then routinely cut at 4 micrometers, floated onto a 50°C heated water bath, and picked up onto a glass slide. Slides containing tissue sections were then baked at 60°C for a minimum of 1 hour to allow for proper fixation of the tissue to the glass slide. Samples were then stored at 4°C until further analyses were performed.

3 Characterization of BRAFV600E induced senescence in melanocytes

3.1 Introduction

The senescent phenotype is influenced by many factors, such as the magnitude of the inducing oncogenic activity, the specific oncogene or tumor suppressor that is mutated, and the cell type hosting the senescence response. For instance, oncogenic KRAS expression in fibroblasts does not induce senescence *in vitro* when expressed at normal levels and shows little activation in its downstream effectors ERK and AKT [349]. *In vivo* studies have also looked at the influence of varying levels of activated oncogenes in senescence [350]. When the expression of the activated form of HRAS (G12V) was titrated in a mouse, only high overexpression led to the formation of low-grade tumors containing cells positive for senescent markers. Within mice expressing moderate levels of HRAS tumors were absent as were any signs of senescence.

The first oncogene shown to trigger senescence was a tumor-derived allele of HRAS [34]. Since then, many other activated oncogenes, such as BRAF and MEK, and inactivated tumor suppressors have been found to initiate senescence. As RAS signaling occurs through the MAPK cascade, it was originally presumed that activated forms of BRAF and MEK would also produce similar phenotypes to RAS. Early studies supported this idea [35]. However, more recent studies have highlighted differences. Even physiological levels of BRAFV600E are sufficient to trigger senescence in fibroblasts *in vitro,* while as mentioned above, hyperphysiological levels of an activated RAS oncogene are needed for a similar response [2].

Apart from the specific oncogene and magnitude of its activity, mechanisms of senescence induction also greatly differ between cell types. For example, it has been reported that mouse fibroblasts deficient in one copy of $p16^{INK4A}$ are able to senesce normally while mouse melanocytes heterozygous for the same

deletion show an impaired senescence response [242,351]. In human melanocytes, $p16^{INK4A}$ is expressed in some melanocytes within a nevus, displaying a mosaic expression pattern when stained for. This pattern does not correlate with the homogeneous presence of SA beta-gal in nevi [1,2]. In addition, the inactivation of $p16^{INK4A}$ does not bypass senescence and nevus formation in a mouse model, suggesting that there are multiple pathways and mechanisms involved in the senescence of melanocytes and in order to truly understand its manner one must study the process in the appropriate cell type [136].

To better understand the senescence of primary human melanocytes, I compared gene expression of primary human melanocytes containing an activated BRAFV600E oncogene with normal primary human melanocytes. The activated oncogene BRAFV600E was used as it has previously been shown to initiate senescence in melanocytes, as well as due to its common presence in benign human nevi [1-3]. Genome wide expression analysis was done using both microarray and RNA sequencing (RNAseq). In addition, multiple melanoma cell lines were also analyzed by the later method to gain a better understanding of the expression program of senescent melanocytes versus melanoma cells.

3.2 Results

3.2.1 Expression of BRAFV600E in human primary melanocytes

In order to better understand senescence of primary human melanocytes the activated oncogene BRAFV600E was expressed in primary human melanocytes [3]. Initial attempts at transfecting melanocytes using retroviruses were unsuccessful. This effect seemed cell specific however as fibroblasts (IMR90s) could be easily infected with the same virus preparation. Although there are some reports using retroviruses to transfect melanocytes, successful integration of many retroviruses into the host's genome has been shown to require mitosis [1,352,353]. As primary human melanocytes proliferate at a rather slow speed (doubling time of roughly 4 days) compared to many other cell types, it was decided that a new mode of gene transfer must be used, one that enables transfection into non-dividing and slowly dividing cells. Lentiviruses infect both

dividing and non-dividing cells and have also previously been shown to successfully transfect melanocytes [2,354]. Dr. Daniel Peeper (NKI) kindly donated the lentiviruses HIV-CS-CG-BRAFE600-puro and its equivalent empty vector, HIV-CS-CG-puro, which he had used to induce senescence in melanocytes (Figure 3.1a) [2]. Subsequent confirmation of the plasmids was done to confirm their identity before further studies were completed (Figure 3.1b). Upon confirmation, lentivirus was produced from the plasmids and placed onto melanocytes to allow gene transfer. The resulting cells were successfully transfected as confirmed through puromycin resistance and increased expression of BRAF (Figure 3.2).

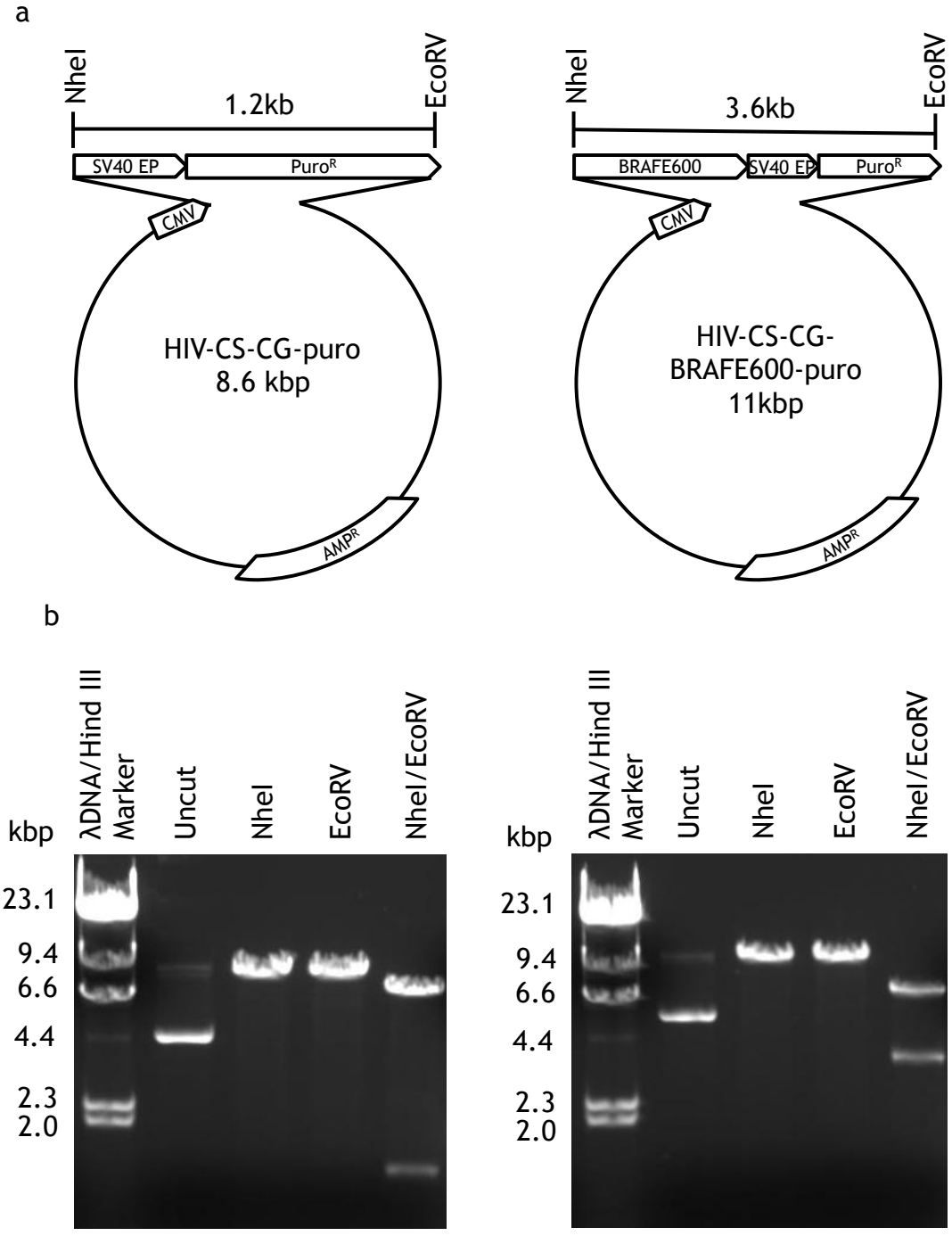

Figure 3.1 Diagnostic digest of BRAFV600E and empty vector plasmids.
(a) Maps of plasmids used for lentiviral mediated gene transfer. (b) Diagnostic digests were completed to confirm plasmid identity and resolved on an agarose gel using electrophoresis, HIV-CS-CG-puro left, HIV-CS-CG-BRAFE600-puro right. Both plasmids were cut with the restriction enzymes NheI and EcoRV separately as well as simultaneously (both restriction enzymes cut each plasmid once). Diagnostic digest of HIV-CS-CG-puro with NheI and EcoRV separately linearized the plasmid and bands resolved at approximately 8.6kbp while simultaneous digestion resolved bands at approximately 1.2 and 7.4kbp. Diagnostic digest of HIV-CS-CG-BRAFE600-puro with NheI and EcoRV separately linearized the plasmid and bands resolved at approximately 11kbp while simultaneous digestion resolved bands at approximately 3.6 and 7.4kbp.

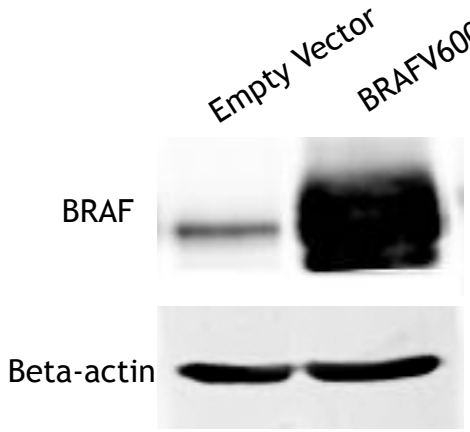

Figure 3.2 Expression of BRAFV600E in human primary melanocytes.
Representative western blot of BRAFV600E infected primary human melanocytes. Endogenous BRAF levels could be detected in melanocytes infected with an empty vector virus but at a drastically lower level compared to BRAFV600E infected melanocytes. Equal amounts of whole cell lysates were loaded onto a polyacrylamide gel and beta-actin was used as a loading control.

3.2.2 Confirmation of senescence upon BRAFV600E expression

Previous reports of lentivirus mediated gene transfer of BRAFV600E into primary melanocytes have shown that short-term exposure (3-7 days) of the activated oncogene results in enhanced melanocyte proliferation [2]. This period is then followed by the induction of senescence, with many markers of senescence present at 14 days post induction. Therefore, for the purpose of this study all analysis of BRAFV600E expression melanocytes were done 14 days post-infection. At this time point, BRAFV600E-expressing cells displayed a somewhat flattened morphology and the presence of SA beta-gal in comparison to both uninfected and control empty vector-infected cells (Figure 3.3). Other senescence markers included markers of cell cycle exit, such as repression of Cyclin A and BrdU incorporation, reduced levels of total RB and its phosphorylation, as well as the expression of DEC1 and the appearance of SAHF (Figure 3.4-3.6).

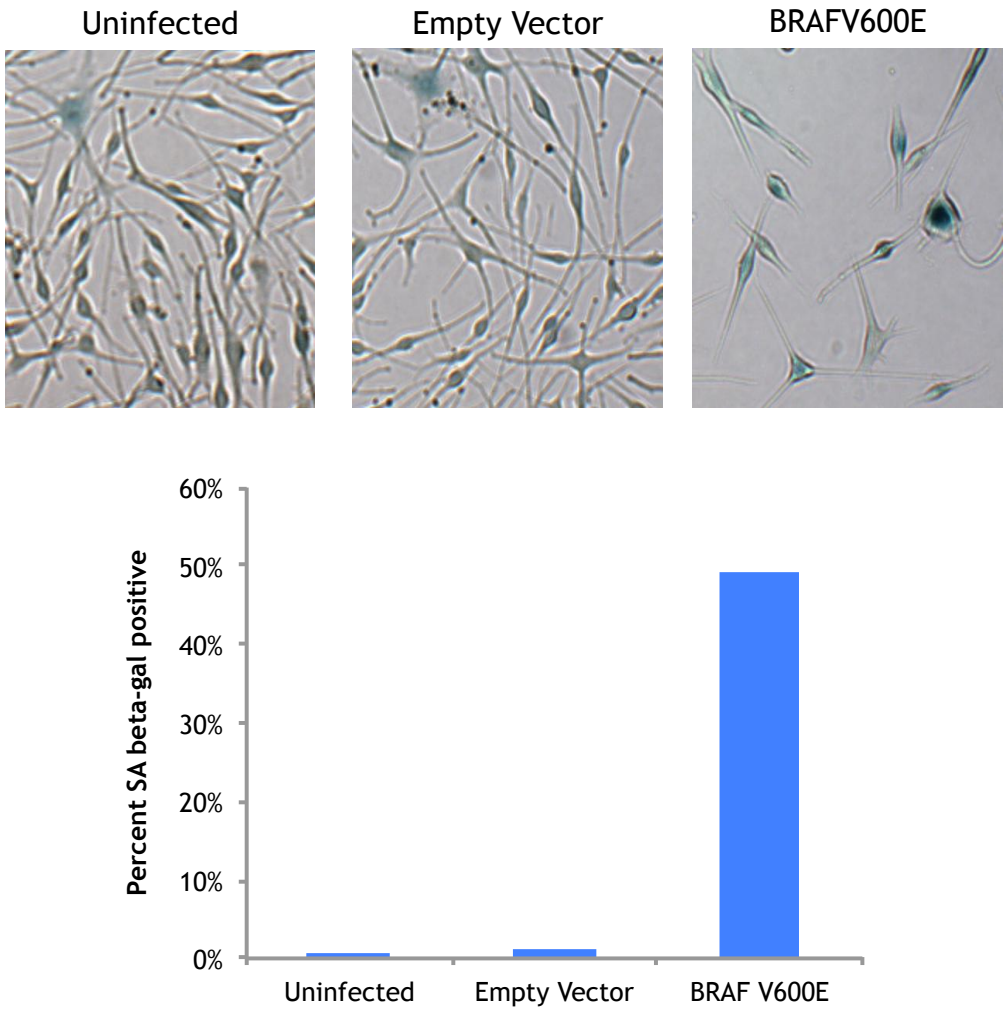

Figure 3.3 BRAFV600E-induced melanocytes stain wih SA beta-gal.
14 days post infection, BRAFV600E-infected melanocytes were stained for senescence associated beta-galactosidase (SA beta-gal) using empty vector infected and uninfected as controls. Analysis of cellular morphology was also noted and consistent with previous findings as BRAFV600E-infected melanocytes became slightly broadened, although not as drastically as when induced with certain other activated oncogenes [355].

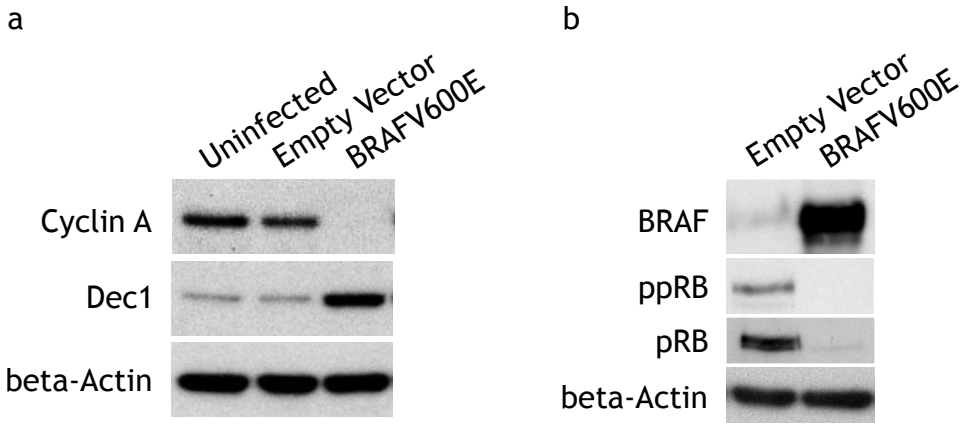

Figure 3.4 Expression of senescence markers upon induction of BRAFV600E.
The expression of many proteins associated with senescence was observed by western blot analysis. (a) Expression of the S phase cyclin, Cyclin A, is down regulated upon BRAFV600E induced senescence. The p53 target DEC1 has been shown to promote senescence and is up regulated in BRAF-induced senescence [356]. (b) Upon BRAFV600E-induced senescence, total RB is reduced and also found in its hypophosphylated state, being active and inhibiting cell cycle progression[357].

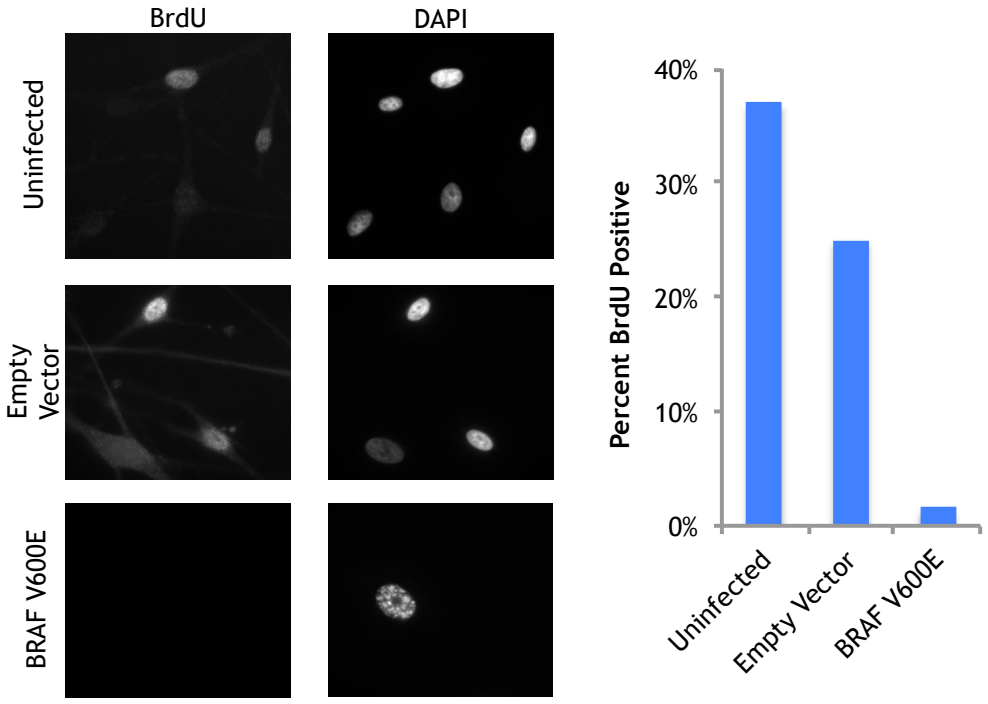

Figure 3.5 BRAFV600E-induced melanocytes do not incorporate BrdU.
Bromodeoxyuridine (BrdU) is a synthetic thymidine analogue that it is incorporated during S-phase of the cell cycle. Upon BRAFV600E expression in melanocytes BrdU incorporation was drastically reduced, signifying a decrease in cell proliferation.

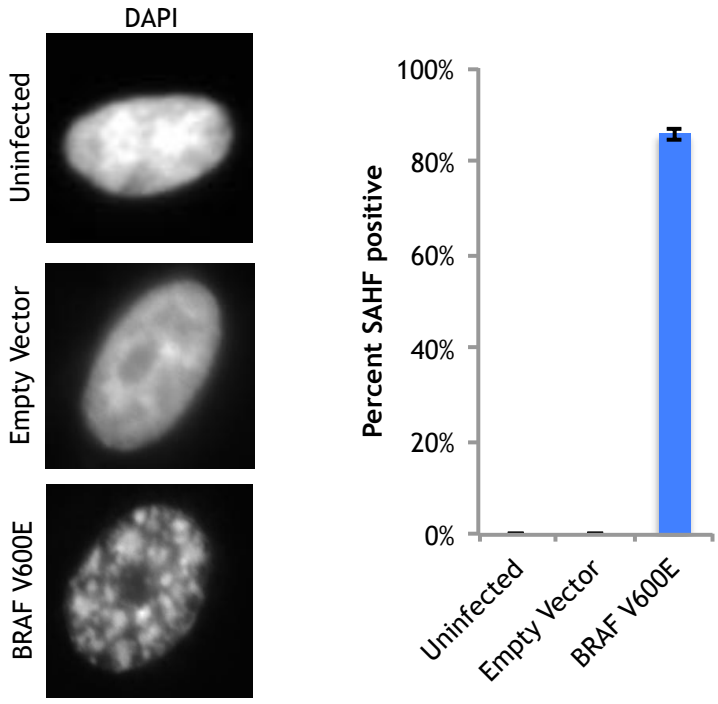

Figure 3.6 BRAFV600E-induced melanocytes display SAHF.
4',6-diamidino-2-phenylindole (DAPI) is a fluorescent marker for DNA. The nucleus of a proliferating cell routinely stains uniformly with DAPI as their chromatin is present in a relaxed, euchromatic state. Upon senescence, DNA becomes more compact and is rearranged into senescence associated heterochromatic foci (SAHF). SAHF were excusive to BRAFV600E-induced melanocytes where it was present in the vast majority of nuclei.

3.2.3 Microarray-based expression analysis of BRAFV600E expressing human primary melanocytes

In order to better understand senescence of primary human melanocytes, BRAFV600E-expressing, empty vector-infected, and uninfected melanocytes were profiled by a gene expression microarray. RNA was harvested 14 days post-infection in biological triplicates for each condition of melanocyte. The RNA was then analyzed qualitatively using a bioanalyzer and was found to be of high quality (Figure 3.7). The Agilent 2100 Bioanalyzer enables quantitation and quality control of RNA. The overall quality of the RNA is summarized by providing an RNA Integrity Number (RIN) [358]. RIN values range from 1 being the worst to 10 being the best, with good quality RNA used for analysis ideally displaying a RIN higher than 8. In addition, a histogram is provided by the bioanalyzer that displays the size distribution of the RNA species, usually showing two bands in high quality RNA, comprising the 28S and 18S ribosomal RNA (rRNA) species (Figure 3.7). Once the integrity of the RNA was confirmed, the RNA was further processed by the CR-UK Microarray Facility in preparation for microarray hybridization on the GeneChip Human genome U133 Plus2 Array, to allow for expression analysis by over 47000 probesets.

Before subsequent analysis of microarray data, it was important to remove sources of variation between arrays of non-biological origin, also known as normalization. Through operation of the open source software Bioconductor, the GC Robust Multi-array Analysis (GCRMA) method was used by Dr. Tony McBryan to background correct and normalize all samples [359]. T-tests were then used to determine differential expression based on the log-normalized values produced by the GCRMA method.

Principal component analyses were done on the samples to determine the consistency between replicate samples. Principal component analysis functions to reduce the dimensionality of the data while retaining most of the variation in the data set. This mathematical algorithm accomplishes this reduction by identifying directions (principal components) along which there is maximal variation in the data. Therefore, by using only a few components, each sample

can be represented by a relatively few numbers instead of by values for thousands of variables. As seen in Figure 3.8, experimental triplicates clustered well when graphed according to the two maximal principal components, confirming that replicates of the same infection are most similar to one another compared to different infections. As displayed in the principal component analysis (Figure 3.8) the component showing the most variation, principal component 1 (PC1), separated the uninfected and empty vector-infected samples from the BRAFV600E-infected samples. The second most variable component, principal component 2 (PC2), was then able to separate empty vector-infected and uninfected samples. As seen in Figure 3.9 there are minimal significant changes associated with virus infection. Therefore, when BRAF-infected samples are compared to empty-vector infected samples, nearly all significant changes are also observed in BRAF-infected samples compared to uninfected samples.

Following confirmation of sample clustering, log-normalized values were ranked according to fold change between empty vector and BRAFV600E-expressing samples and differentially expressed genes were defined as those with a change exceeding 1.5 fold and Benjamini and Hochberg False Discovery Rate (BH-FDR) adjusted P-value of less than 0.05. These analyses returned 4370 and 5215 probes that were up and down regulated, respectively.

Having identified melanocyte genes whose expression was regulated by the presence of BRAFV600E, key pathways were identified that were altered upon its expression. Consistent with previous studies in other cell types, Gene Set Enrichment Analysis (GSEA) showed that the most up regulated gene sets were those involved in extracellular and inflammatory signaling, collectively known as the SASP [167]. Specifically, up regulation of many genes in the Gene Ontology (GO) group “Inflammatory Response” and documented SASP genes were noted upon BRAFV600E-induced senescence [167] (Figure 3.10-3.11, Supplementary List 1 and 2). Alternatively, the most down regulated GO groups included chromosome and cell cycle related gene sets (Figure, 3.12). Hierarchical clustering of a previously selected set of genes linked to cell proliferation confirmed global

repression of proliferation-associated genes, as would be expected during a senescence response (Figure 3.13, Supplementary List 3) [360].

a

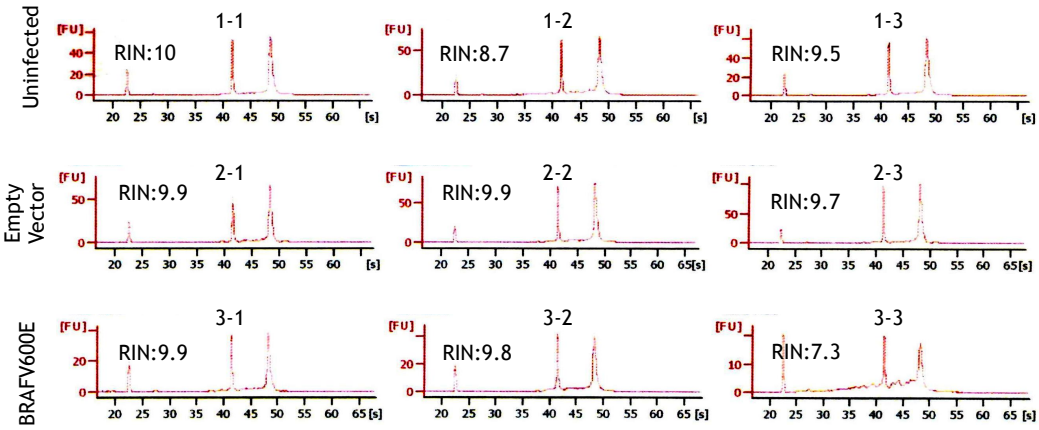

b

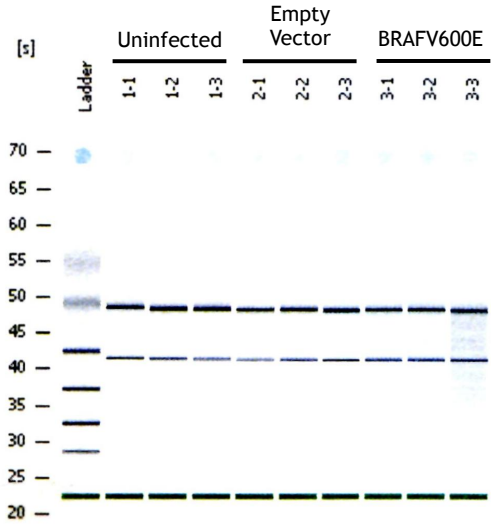

Figure 3.7 Analysis of the purity and integrity of the RNA samples used for microarray analysis.

RNA was harvested from uninfected, empty vector infected, and BRAFV600E-infected melanocytes and analyzed using an Agilent Bioanalyzer. (a) Electrophoretic scans from the Agilent Bioanalyzer show that high quality RNA was obtained. The first small peak is a loading dye used to standardize the runs. The other peaks that resolved at roughly 43 and 49 seconds are the 18S and 28S small and large subunit of the ribosome, respectively, which make up the vast majority of total RNA samples. Crisp 18S and 28S rRNA bands are indicative of intact RNA. The Agilent Bioanalyzer also calculated RNA integrity values. In (b) the same information is conveyed as in (a) but in a form reminiscent of an agarose gel, making comparison among samples easier.

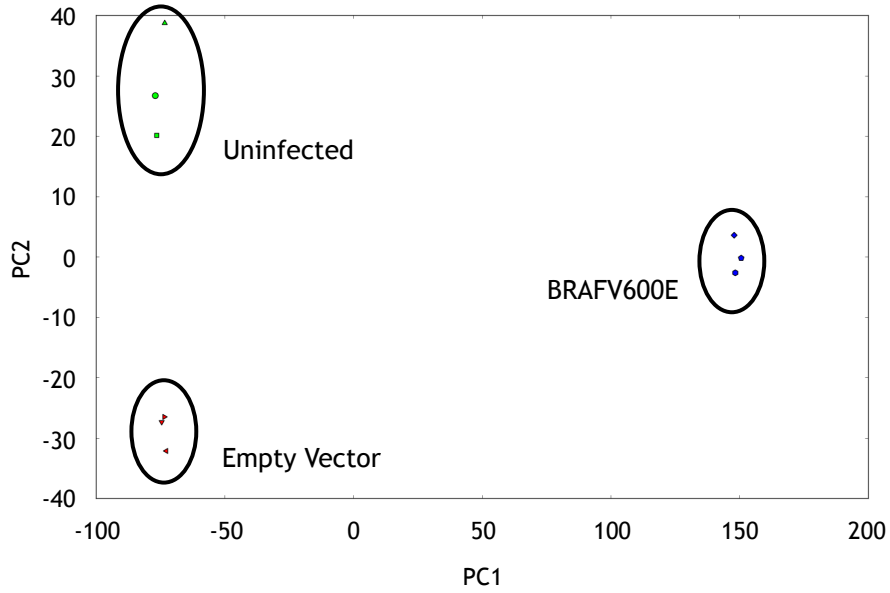

Figure 3.8 Principal component analysis of microarray samples.
Principal component analysis was done on raw sample data to reduce the dimensionality of the data while retaining the most variation in the data set. Analyses separated the three sample groups while the triplicates clustered well, revealing that samples contained little variation between replicates. Principal component 1 (PC1) was only able to distinguishing BRAV600E-infected melanocytes from the other control cells, signifying that the vast majority of data collected was due to changes occurring upon BRAFV600E induction.

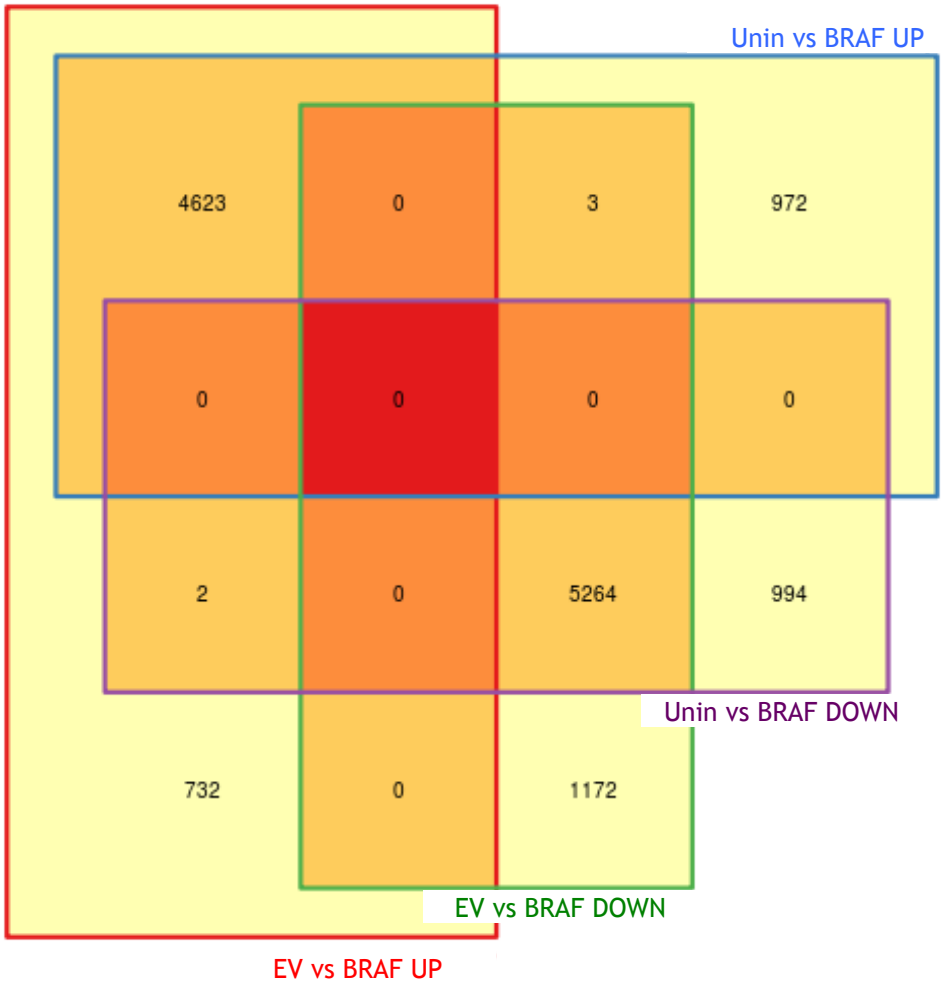

Figure 3.9 Overview of changed probes in microarray.
Changes were only considered significant if they exceeded 1.5 fold change and had a Benjamini and Hochberg False Discovery Rate (BH-FDR) adjusted P-value of less than 0.05. Outlined in the 4 set unweighted square Venn diagram above, it can be seen that the uninfected and empty vector expression profiles were very similar, with only 5 probes showing a change in a different direction (interferon induced transmembrane protein 1, interferon induced transmembrane protein 1, ---, protocadherin 20, solute carrier family 6 member 17). In total, 9892 probes were found to be changing in both control (EV and unin) versus BRAFV600E-infected conditions (up in both 4623, down in both 5264, same direction 9887, different direction 5).

a

Up regulated

Gene Set	Number of Genes	ES	NES	FDR p-val
1 INFLAMMATORY RESPONSE	121	0.71	2.18	< 0.001
2 GROWTH FACTOR ACTIVITY	51	0.80	2.15	< 0.001
3 EXTRACELLULAR SPACE	234	0.64	2.12	< 0.001
4 GENERATION OF A SIGNAL INVOLVED IN CELL CELL SIGNALING	27	0.88	2.11	< 0.001
5 EXTRACELLULAR REGION	425	0.61	2.11	< 0.001
6 EXTRACELLULAR REGION PART	321	0.62	2.10	< 0.001
7 RESPONSE TO EXTERNAL STIMULUS	295	0.61	2.07	< 0.001
8 RESPONSE TO WOUNDING	180	0.64	2.07	< 0.001
9 DEFENSE RESPONSE	250	0.61	2.03	< 0.001
10 CELL CELL SIGNALING	394	0.58	1.99	0.001
11 HORMONE SECRETION	17	0.90	1.97	0.001
12 SECRETION	161	0.82	1.94	0.002

b

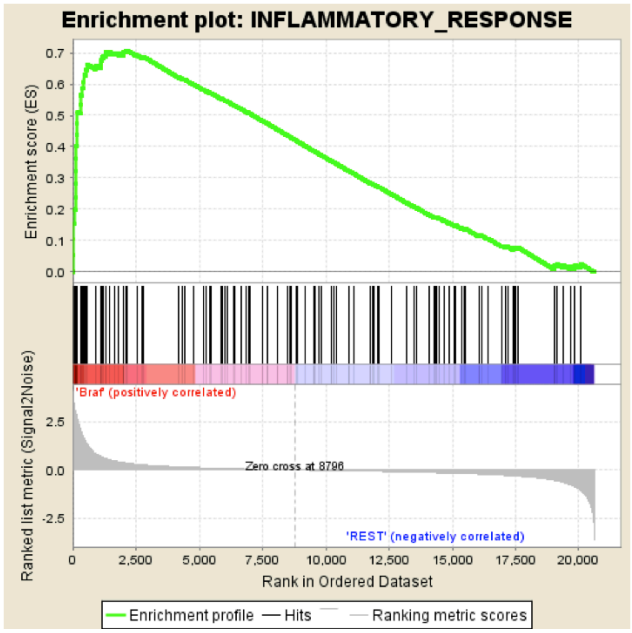

Figure 3.10 Most up regulated gene sets from microarray analysis.
Gene set enrichment analysis (GSEA) was used to interpret gene expression data. (a) The most up regulated gene sets (upon BRAFV600E infection) were those related to the inflammatory response, extracellular signaling and secretion. Enrichment scores (ES) reflect the degree to which a gene set is overrepresented at the extreme top or bottom of the ranked microarray data. Each ES was normalized to account for size of the set, yielding a normalized enrichment score (NES). A positive ES and NES value correlates with gene sets that are up regulated in BRAFV600E data sets compared to empty vector and uninfected gene expression sets. (b) Enrichment plot for inflammatory response showed that the vast majority of genes within the set are up regulated as they are clustered to the left side, where BRAFV600E gene expression data is located.

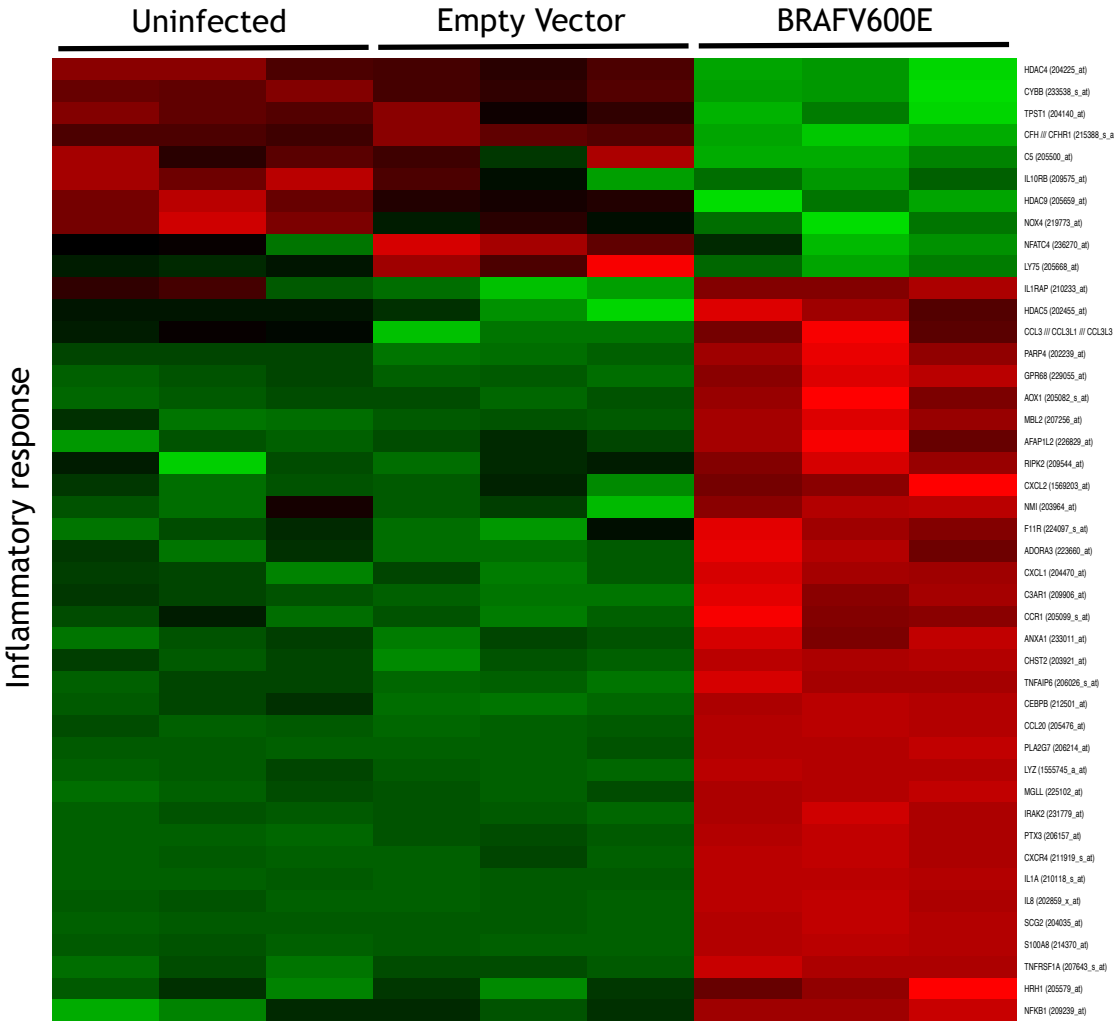

Figure 3.11 The inflammatory response is up regulated upon BRAFV600E-induced senescence.
Microarray heat map representation of the changed genes (Fold changes > 1.5, BH-FDR < 0.05) within the gene ontology (GO) term inflammatory response, the most up regulated gene set from GSEA analysis. Up regulated genes red, down regulated genes green.

a

Down regulated

Gene Set	Number of Genes	ES	NES	FDR p-val
1 CHROMOSOME	115	-0.65	-2.16	< 0.001
2 SPINDLE	39	-0.78	-2.14	< 0.001
3 CHROMOSOMAL PART	89	-0.66	-2.09	< 0.001
4 M PHASE OF MITOTIC CELL CYCLE	79	-0.66	-2.09	< 0.001
5 CHROMOSOME PERICENTRIC REGION	27	-0.80	-2.07	< 0.001
6 MICROTUBULE CYTOSKELETON	143	-0.59	-2.03	< 0.001
7 CELL DIVISION	20	-0.84	-2.03	< 0.001
8 CYTOKINESIS	18	-0.86	-2.02	< 0.001
9 MITOSIS	76	-0.65	-2.02	< 0.001
10 CELL CYCLE PROCESS	181	-0.56	-2.00	< 0.001
11 M PHASE	106	-0.60	-1.97	0.001
12 CHROMOSOME SEGREGATION	28	-0.77	-1.96	0.001

b

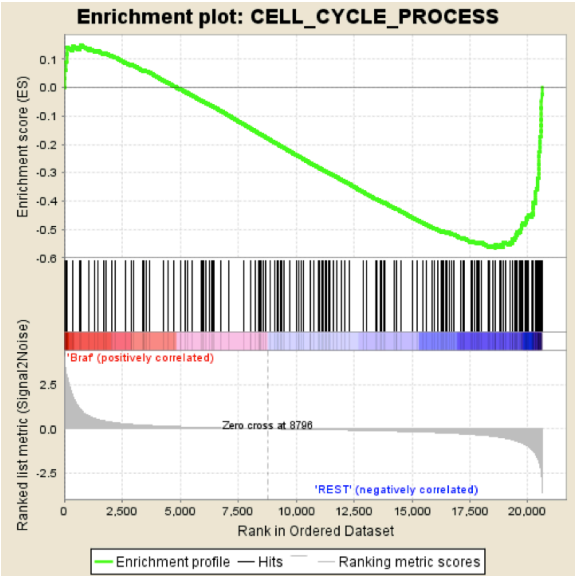

Figure 3.12 Most down regulated gene sets from microarray analysis.
Gene set enrichment analysis (GSEA) was used to interpret gene expression data. (a) The most down regulated gene sets (upon BRAFV600E infection) were those related to the cell cycle. Enrichment scores (ES) reflect the degree to which a gene set is overrepresented at the extreme top or bottom of the ranked microarray data. Each ES was normalized to account for size of the set, yielding a normalized enrichment score (NES). A negative ES and NES value correlates with gene sets that are down regulated in BRAFV600E data sets compared to empty vector and uninfected gene expression data. (b) Enrichment plot for cell cycle process shows that the vast majority of genes within the set are down regulated as they are clustered to the right side where uninfected and empty vector gene expression data is located. There is also enrichment to the left side where the inhibitors of the cell cycle are located, such as p21, p15, and p16.

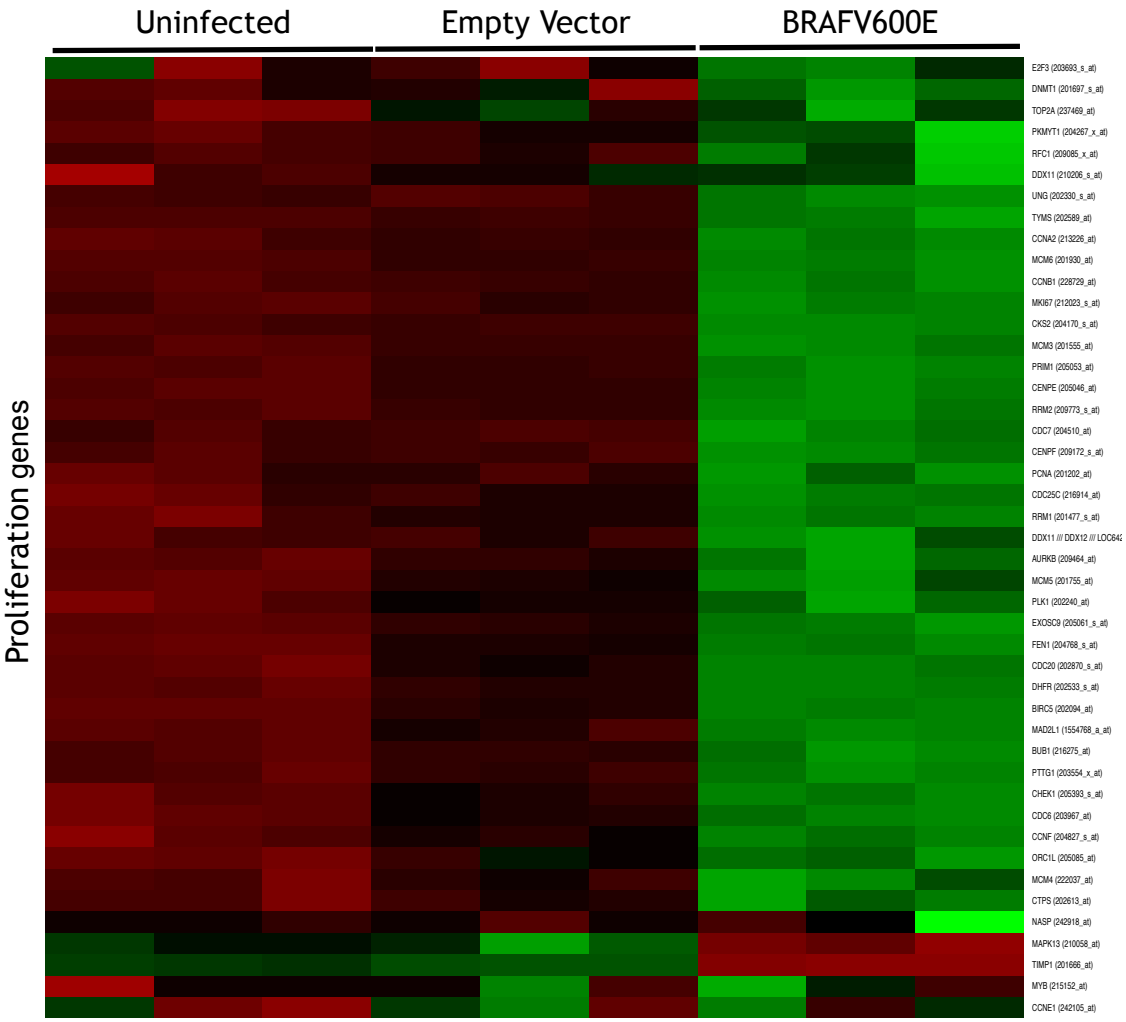

Figure 3.13 Proliferation genes are down regulated upon BRAFV600E-induced senescence. Microarray heat map representation of all proliferation genes extracted from Whitfield, M. L., George, L. K., Grant, G. D. & Perou, C. M. Common markers of proliferation. *Nature Reviews Cancer* **6**, 99-106, (2006). Up regulated genes red, down regulated genes green.

3.2.4 RNAseq-based expression analysis of BRAFV600E expressing human primary melanocytes and melanoma cell lines

I wanted to compare the expression profile of senescent melanocytes to melanoma cells to assess the relationship between oncogene-induced senescence and cell transformation. Therefore, uninfected and BRAFV600E-infected melanocytes, 7 human melanoma cell lines, each harbouring an activated BRAFV600E or NRASQ61K oncogene, were analyzed through RNAseq (Table 3.1). I chose to sequence RNA from uninfected cells rather than empty vector infected cells, because the expression programme of uninfected and empty vector infected cells was very similar and the 7 melanoma cell lines are uninfected. As shown in Figure 3.14 high quality RNA was used for preparation of cDNA libraries. Sequencing libraries were prepared using Illumina's TruSeq RNA sample preparation and sequenced on an Illumina GAIIx by 36bp paired end sequencing, as this has been shown to perform well in subsequent data analysis [361].

Once sequenced, RNAseq paired end reads were aligned to the human genome (hg18) for analysis. Globally there was a strong correlation between fold changes observed by microarray and RNAseq data (Figure 3.15) (underscoring the validity of comparing BRAFV600E-infected melanocytes with either uninfected or empty vector-infected melanocytes). Analysis of selected genes in BRAFV600E-infected and uninfected melanocyte RNAseq data confirmed repression of proliferation genes such as CCNA2 (Cyclin A) and CENPA, as well as the activation of growth-arrest genes such as CDKN2A ($p16^{INK4A}$) and CDKN2B ($p15^{INK4b}$) (Figure 3.16).

Both proliferation arrest and the SASP have been suggested to contribute to senescence-mediated tumor suppression [167]. Therefore, I asked whether malignant melanomas typically over-ride proliferation arrest and the SASP, as judged by these gene signatures. Analysis of RNAseq expression data from BRAFV600E-infected and uninfected melanocytes compared to melanoma cell lines showed that all of the proliferation-promoting genes that were repressed in senescence were expressed in melanoma cell lines (Figure 3.17). In contrast,

many of the inflammatory response and SASP genes up regulated in senescence were also expressed in the melanoma cell lines (Figures 3.18 and 3.19). Specific documented SASP genes that expressed in senescence and melanoma included IGFBP3, IL8, CCL20, CXCL2, and IL1beta [167]. Based on these results, I conclude that primary human melanocytes expressing BRAFV600E *in vitro* undergo proliferation arrest and express the SASP. Reactivation of cell proliferation, but not suppression of the SASP, is tightly linked to evasion of senescence and progression to melanoma.

Cell Line	BRAF/NRAS Mutation
C32	BRAFV600E
A2058	BRAFV600E
A375	BRAFV600E
MalMe3M	BRAFV600E
SKMEL28	BRAFV600E
WM2664	BRAFV600E
SKMEL5	NRASQ61K

Table 3.1 Melanoma cell lines used for RNA sequencing.

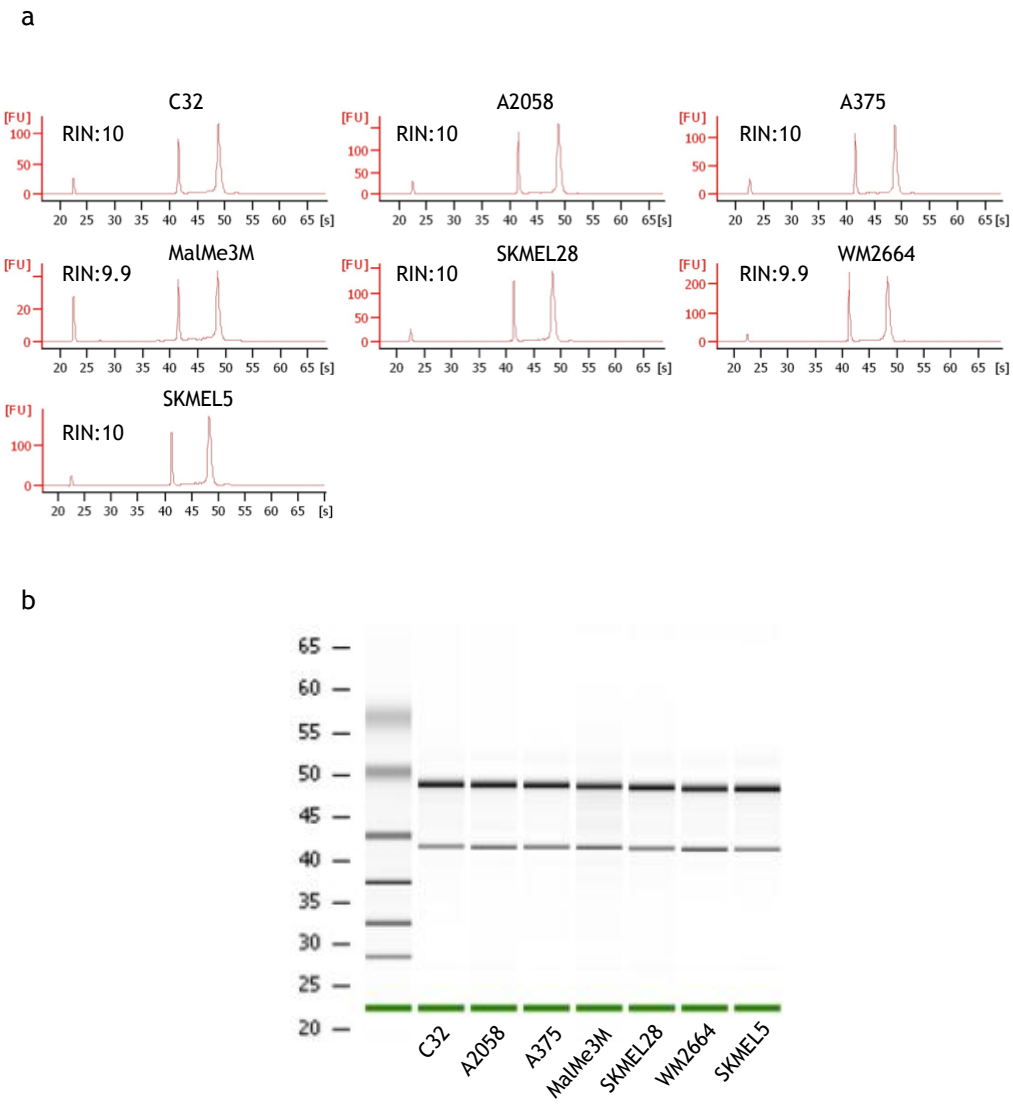

Figure 3.14 Analysis of the purity and integrity of the RNA samples used for RNA sequencing analysis.
RNA was harvested from 7 melanoma cell lines and analyzed using an Agilent Bioanalyzer. (a) Electrophoretic scans from the Agilent Bioanalyzer show that high quality RNA was obtained. The first small peak is a loading dye used to standardize the runs. The other peaks that resolved at roughly 43 and 49 seconds are the 18S and 28S small and large subunit of the ribosome, respectively, which make up the vast majority of total RNA samples. Crisp 18S and 28S rRNA bands are indicative of intact RNA. The Agilent Bioanalyzer also calculated RNA integrity (RIN) values. In (b) the same information is conveyed as in (a) but in a form reminiscent of an agarose gel, making comparison among samples easier.

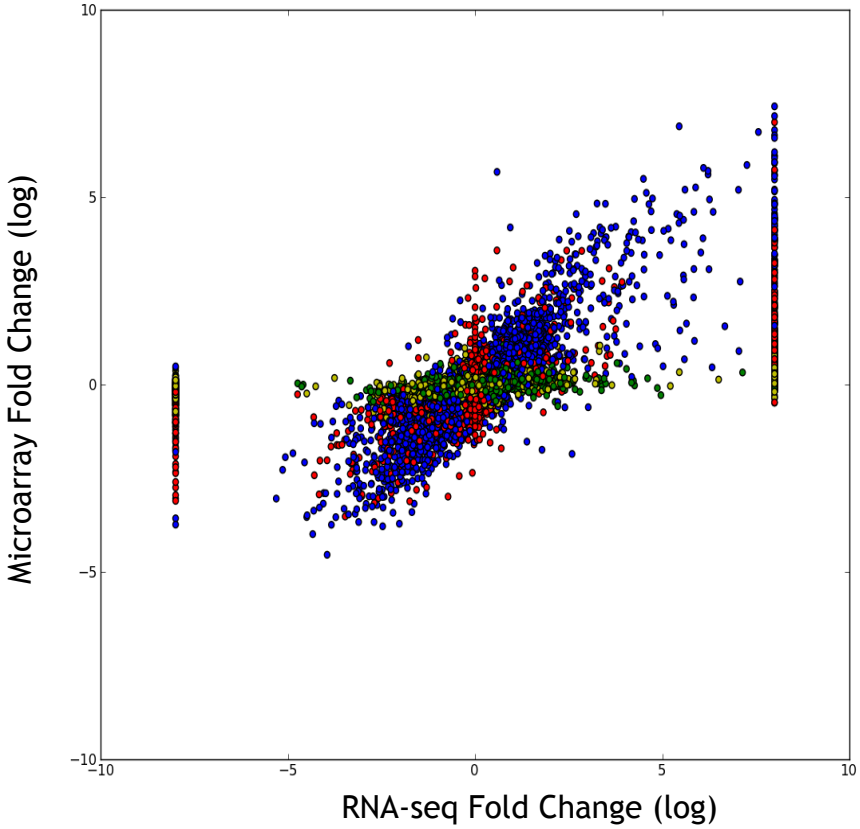

Figure 3.15 Changes found in RNAseq largely correlate with those found in microarray. Correlative analysis of microarray and RNAseq. Blue, significant in both. Green, significant by RNAseq only. Red, significant by microarray only. Yellow, not significant by either. Fold changes are shown to be correlative as changes that were found to be significant based on both analyses (blue) formed a line at a 45 degree angle.

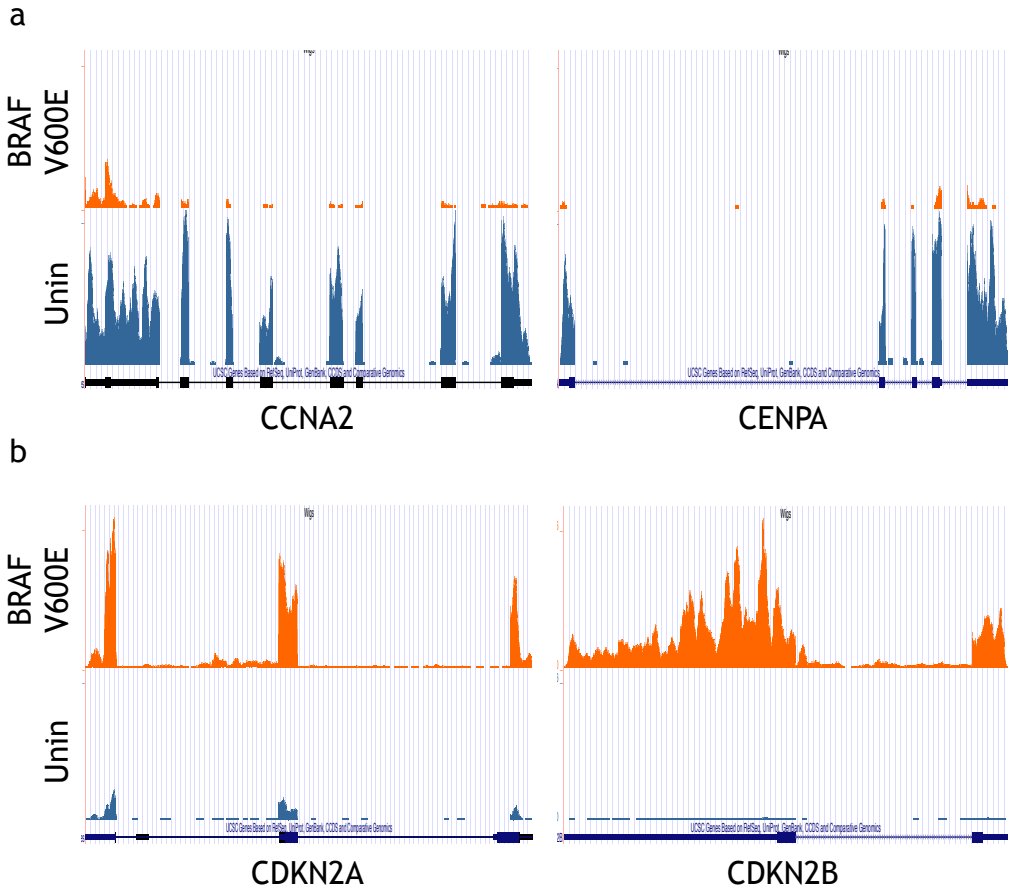

Figure 3.16 Representative RNAseq data.
Aligned RNAseq traces at indicated genes were visualized using the UCSC genome browser. Findings made by comparing (a) proliferation and (b) tumor suppressor genes in uninfected and BRAFV600E-induced melanocytes were consistent with those found in the microarray (either unin vs. BRAFV600E or EV vs. BRAFV600E (not shown)).

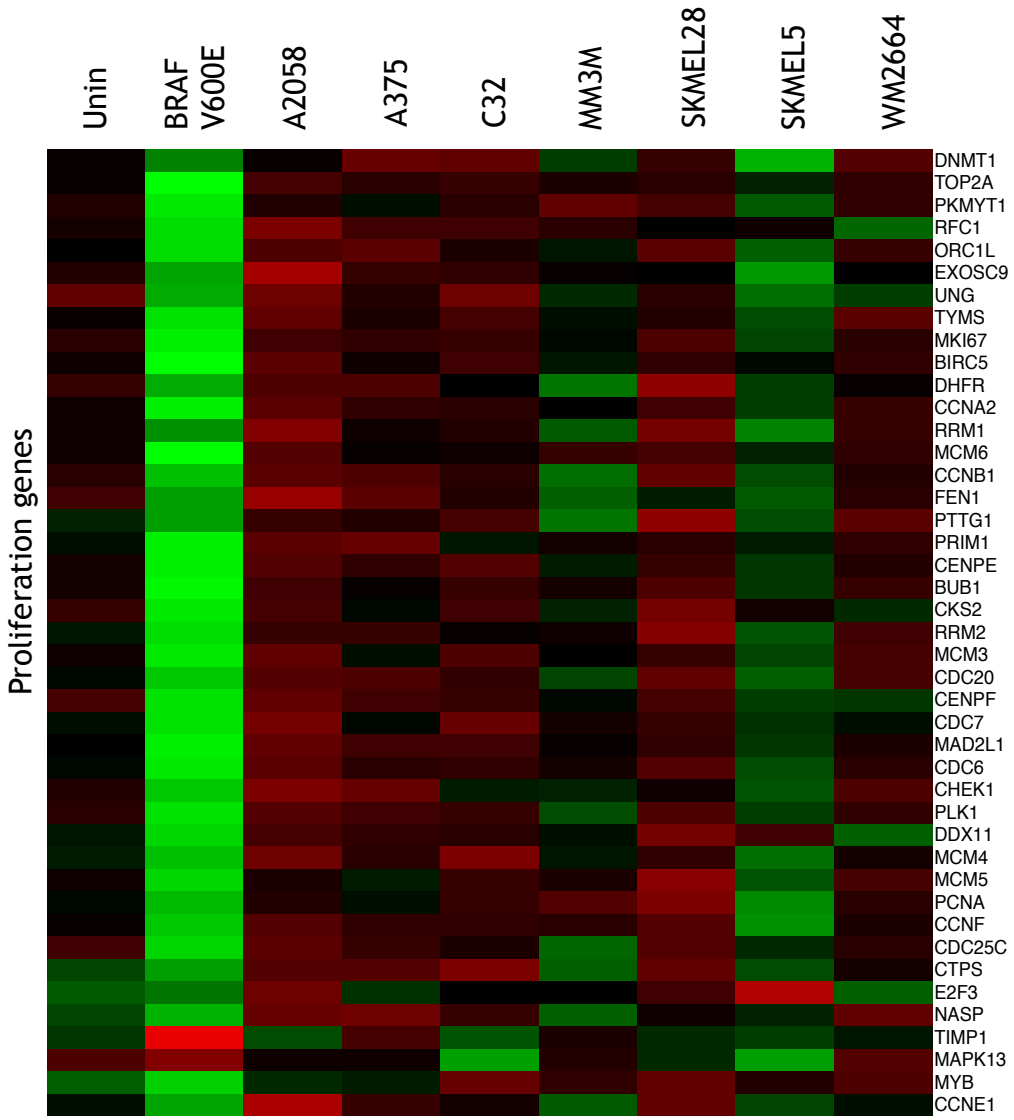

Figure 3.17 Proliferation genes repressed upon senescence are expressed in melanoma cell lines.
RNAseq heat map representation of all proliferation genes extracted from Whitfield, M. L., George, L. K., Grant, G. D. & Perou, C. M. Common markers of proliferation. *Nature Reviews Cancer* **6**, 99-106, (2006). Up regulated genes red, down regulated genes green.

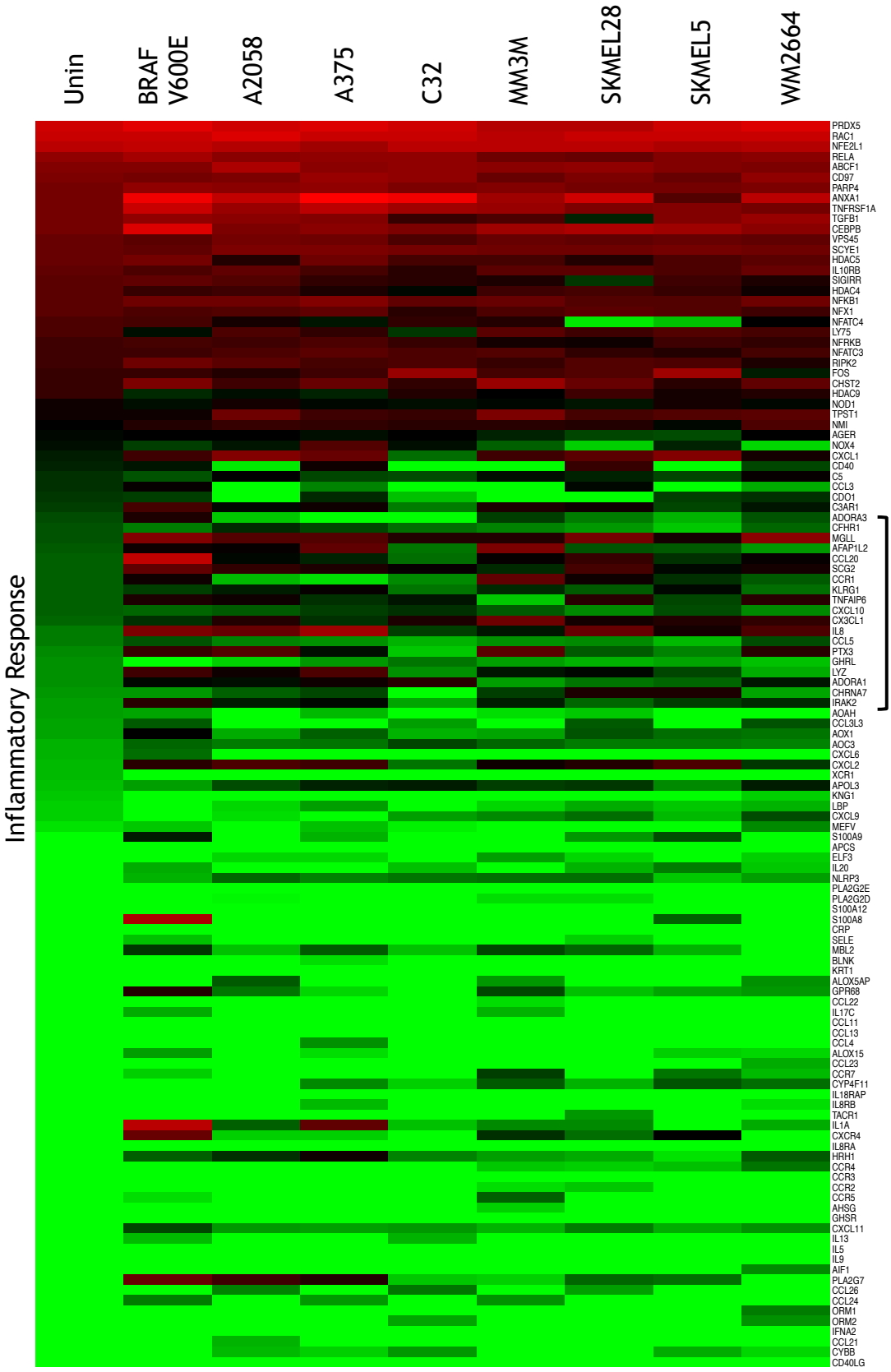

Figure 3.18 Some inflamatory genes upregulated during senescence are also expressed in melanoma cells lines.
RNAseq heat map representation of all genes within the gene ontology (GO) term inflammatory response, the most up regulated gene set from GSEA analysis. Bracketed area contains genes that are up regulated upon BRAFV600E-induced senescence and also expressed in melanoma cell lines. Up regulated genes red, down regulated genes green.

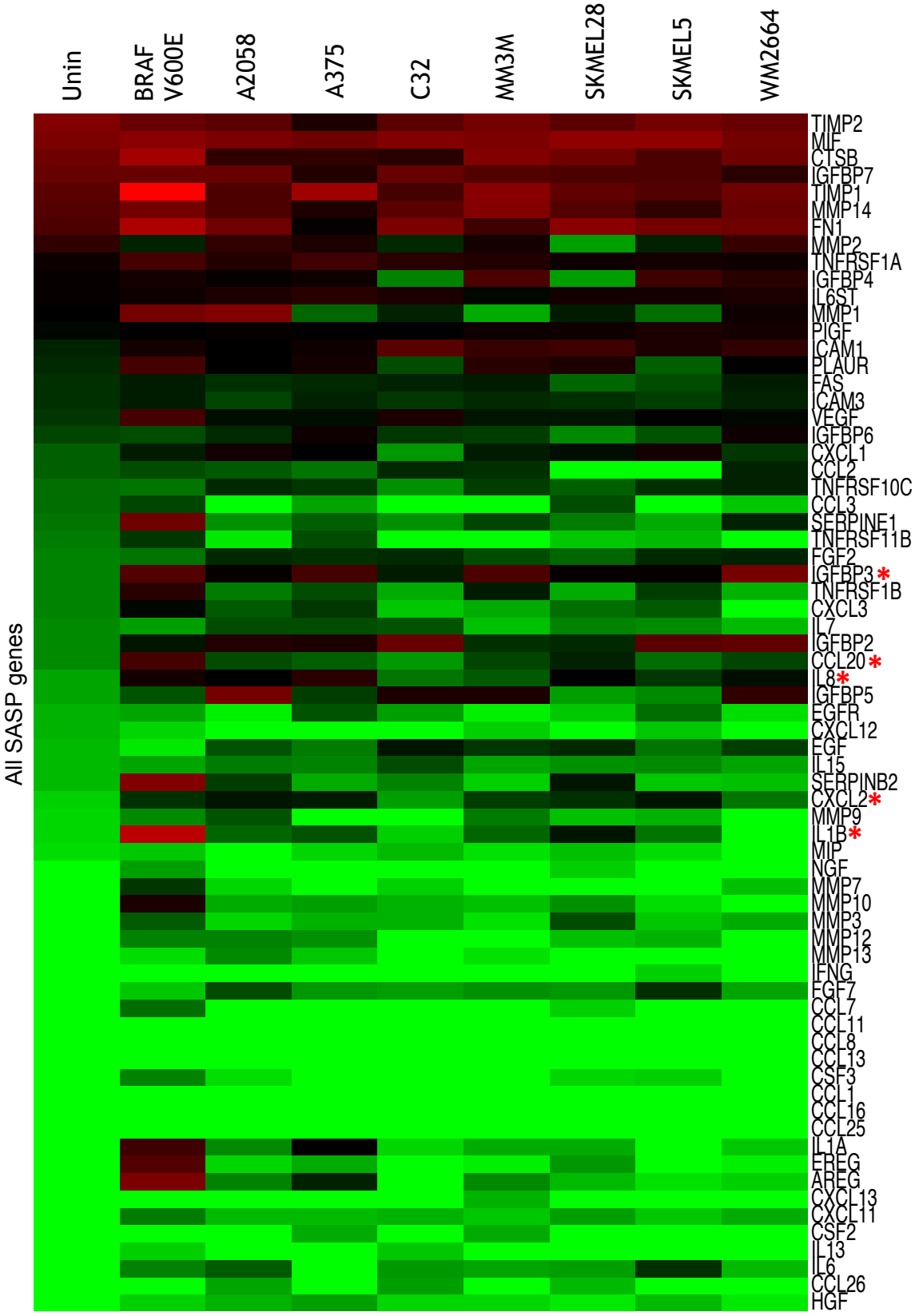

Figure 3.19 Some SASP genes upregulated during senescence are conserved in melanoma cells lines.

RNAseq heat map representation of all genes SASP genes. Gene list derived from Coppé, et al, *Annual review of pathology*, (2010)[167]. Some genes that are up regulated upon BRAFV600E-induced senescence are also expressed in melanoma cell lines. Up regulated genes red, down regulated genes green. Red asterisks indicate key genes that show increased expression in senescent cells and melanoma cell lines compared to uninfected melanocytes.

3.3 Discussion

While many previous studies have examined the global gene expression program of senescence, when I initiated this study there was no such report in melanocytes made senescent by a BRAFV600E oncogene [116,117,123]. In agreement with previous reports looking at the influence of BRAFV600E expression in melanocytes, the activated oncogene BRAFV600E was able to induce senescence in melanocytes, based on specific cell and molecular assays [1,2]. Specifically, a flattened morphology, cell cycle exit, expression of DEC1, appearance of SAHF, and expression of SA beta-gal confirmed senescence. Extending this, a gene expression signature could be assigned to BRAFV600E-induced senescence in melanocytes. GSEA revealed that one of the most down regulated gene set was "cell cycle process" linked to a reduced expression of nearly all examined proliferation genes, while the most up regulated gene sets involved extracellular and inflammatory signaling, collectively known as the SASP. Moreover, through further genome wide comparisons with 7 different melanoma cell lines, the expression of many SASP genes was also observed in these transformed lines, suggesting that the revival of cellular proliferation, but not suppression of the SASP, is associated with evasion of senescence and progression to melanoma. In other words, evasion of senescence and progression to melanoma presumably requires reactivation of cell proliferation, but does not appear to require complete suppression of the SASP.

In fact, while proliferation arrest is likely always tumor suppressive, the effects of the SASP appear to be multi-faceted and are able to deliver a number of different outcomes. SASP signaling is able to inhibit carcinogenesis through contributing towards a senescence arrest or by supplying alarm signals and tissue repair. Alternatively, SASP signaling may also induce carcinogenesis through chronic and persistent inflammation. In support of the carcinogenic influence of SASP, many factors secreted by senescent cells have been shown to promote tumor development *in vivo* as well as tumorigenic-associated phenotypes *in vitro* such as proliferation and invasiveness [125,126,171,362-366]. For example, melanoma tumor cells have been shown to express high levels of the SASP protein CXCR-2

as compared to normal melanocytes, which has been proposed to allow amplification of the SASP network through the binding of additional chemokines such as GROalpha and IL8 [122,367]. These ligands are also preferentially expressed in melanoma cell lines compared to melanocytes and have important roles in melanocyte transformation and melanoma cell proliferation, among others [368,369]. Thus, the senescent microenvironment may stimulate the proliferation of pre-malignant cells within a nevus to allow for the progression of a melanoma. Alternatively, expression of the SASP in cells that have escaped senescence by other means, such as genetic inactivation of PTEN or $p16^{INK4A}$, might continue to promote neoplastic development.

From results thus far, I concluded that primary human melanocytes expressing BRAFV600E *in vitro* undergo proliferation arrest and express the SASP. In addition, the reactivation of cell proliferation, but not suppression of the SASP, was found tightly linked to the evasion of senescence and progression to melanoma. One of the outstanding issues remaining to be investigated is the specific influence of the SASP as a whole, or certain components making up the SASP, on senescence and the progression of melanoma. Although some of these aspects will be investigated in later chapters of my research, I suspect that the results in this chapter will also provide a valuable tool for many other important insights. Ultimately, the analyses described in this chapter may aid in understanding other aspects of melanoma progression, such as the identification of novel melanoma tumor suppressors, a potential role of the immune system during the escape of senescence and tumor progression, or even the identification of a drugable target required for melanoma progression.

4 Selective repression of proliferation-promoting Wnt target genes is linked to senescence

4.1 Introduction

In the previous chapter I described how senescence is induced upon BRAFV600E-induction in melanocytes as judged, among other characteristics, by a proliferation arrest and the expression of SASP. In view of the importance of senescence as a tumor suppressor in melanoma, the poorly defined role of Wnt signaling in melanoma progression, and previous data from the Adams and Larue labs suggesting that Wnt signaling can bypass senescence, I set out to analyze more closely the role of Wnt signaling in OIS of melanocytes [1,2,331,332].

4.2 Results

4.2.1 Identification of altered Wnt signaling in BRAFV600E-induced melanocyte senescence

When analysis of the gene expression data was performed specifically on Wnt target genes, clear changes were apparent. However, whether the pathway as a whole is activated or inhibited during senescence is unclear, as there are both increases and decreases in expression of direct Wnt target genes in senescence (Figure 4.1, Supplementary List 4).

Interestingly, when proliferation-promoting Wnt target genes, such as Cyclin D1 and c-Myc were specifically looked at, many appeared to be repressed (Figure 4.2). Expression of MITF was also repressed in senescent melanocytes (Figure 4.2). MITF has been reported to have both positive and negative effects on melanocyte proliferation, yet it is often amplified or a target of gain-of-function mutation in melanomas, suggesting that its proliferation-promoting effects can be dominant [337,370,371]. Western blot analysis and qRT-PCR were used to further

confirm the repression of proliferation-promoting Wnt target genes (Figure 4.2). These results show that Wnt signaling is altered upon BRAFV600E-induced senescence and suggest that the repression of key proliferation promoting Wnt target genes may have a role in BRAFV600E-induced senescence in melanocytes.

Upon further analysis of the SASP genes altered upon BRAFV600E-induced senescence, I observed that many SASP or SASP-like genes are, in fact, Wnt target genes. Such genes that were identified as players in both Wnt signaling and the SASP include FGF family members, FST (a TGFbeta regulator), MMP7, and VEGF (Table 4.3) [167]. As these genes are expressed during BRAFV600E-induced senescence and in melanoma cell lines these genes may play a role in the progression of melanoma.

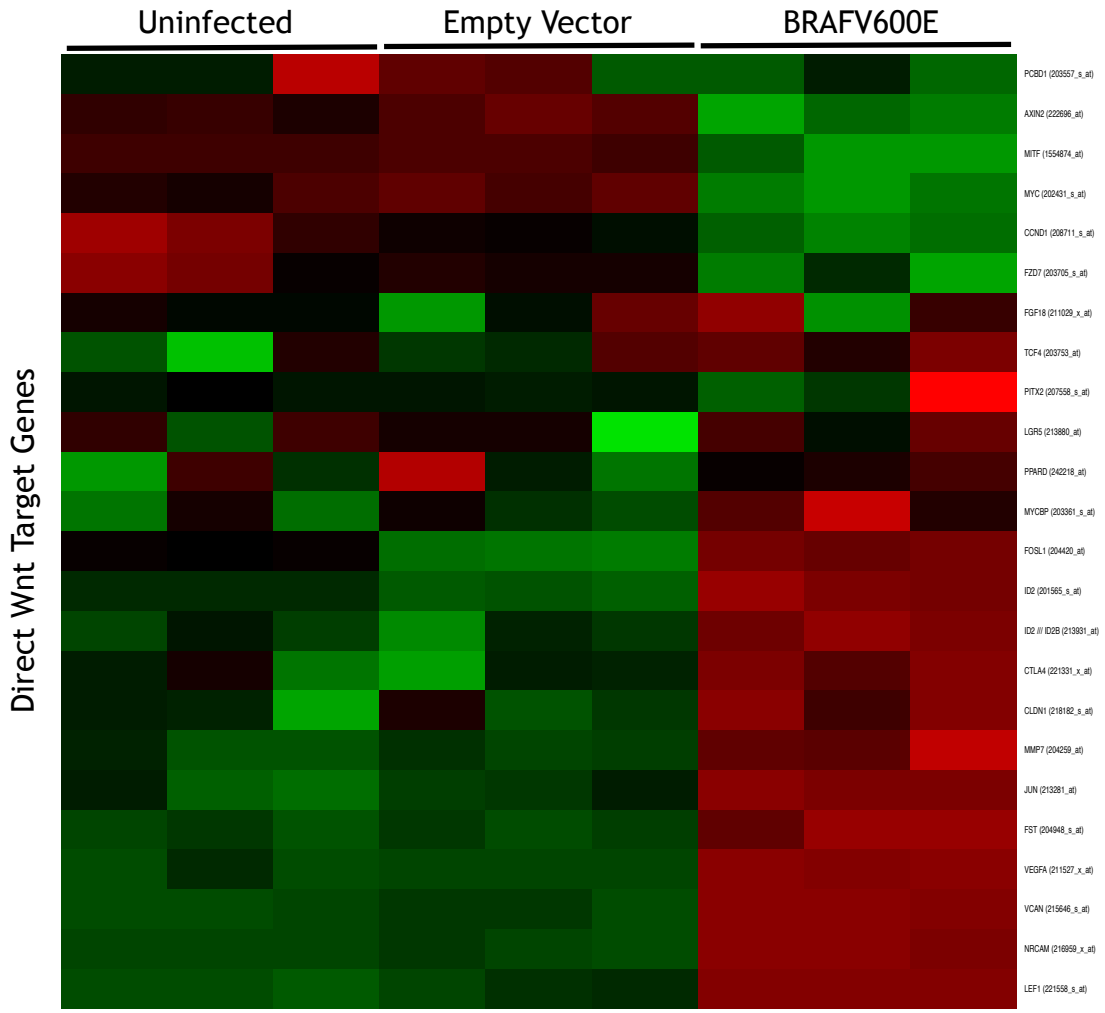

Figure 4.1 Wnt signaling is altered upon BRAFV600E-induced senescence in melanocytes. Microarray heat map representation of direct Wnt target genes. Gene list derived from http://www.stanford.edu/group/nusselab/cgi-bin/wnt/target_genes and further confirmed through primary literature indicating the transcription factor TCF/LEF is bound to the gene promoter. It is unclear whether Wnt signaling is activated or inhibited upon BRAFV600E-induced senescence in melanocytes as direct Wnt target genes are both up and down regulated.

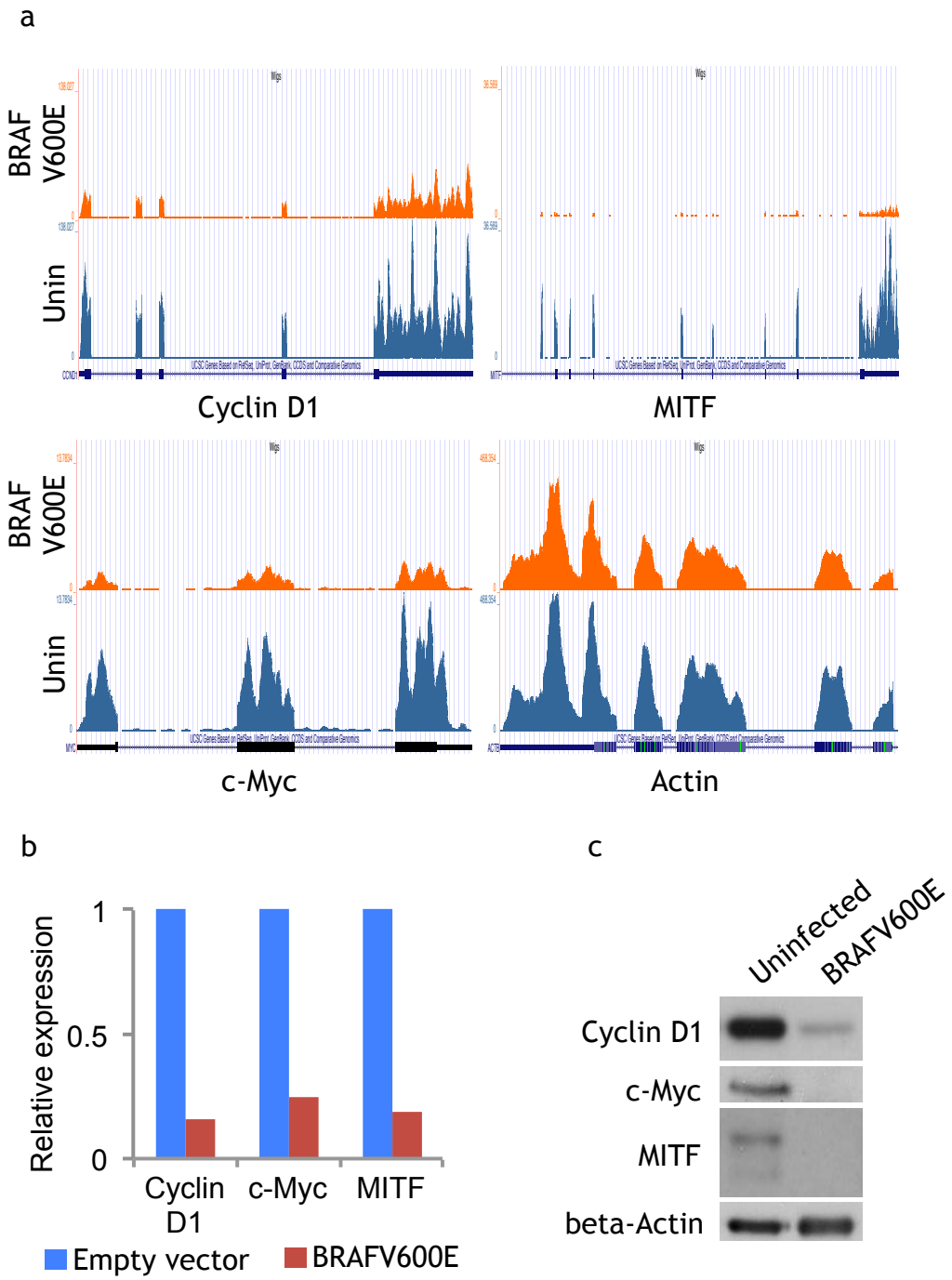

Figure 4.2 Proliferation-promoting Wnt target genes are down regulated during BRAFV600E-induced senescence in melanocytes.
(a) Aligned RNAseq traces of key proliferation-promoting Wnt target genes were visualized using the UCSC genome browser. Housekeeping genes such as actin were confirmed to be at equal levels. (b) Confirmation of (a) using qRT-PCR. Samples were all normalized to GAPDH. (c) Protein levels were also confirmed via western blot analysis.

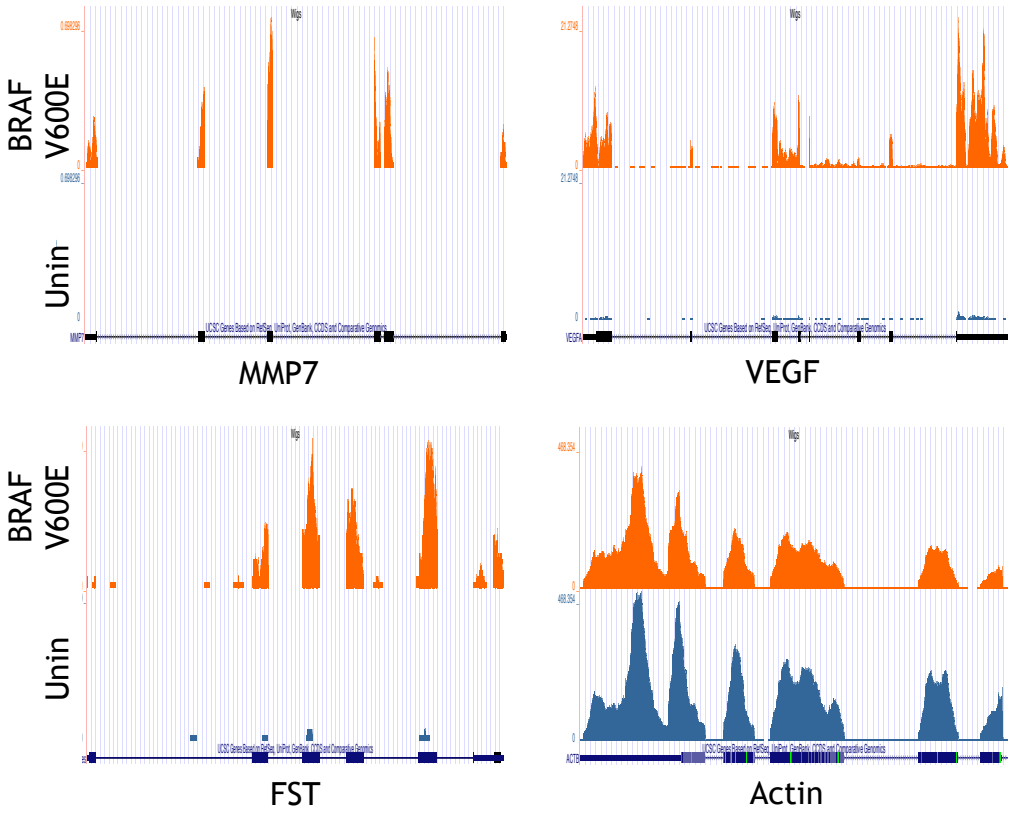

Figure 4.3 Certain SASP genes that are up regulated during senescence are Wnt target genes. RNAseq traces of Wnt target genes that also have a role in SASP were visualized using the UCSC genome browser. Housekeeping genes such as actin were confirmed to be at equal levels.

4.2.2 Inhibition of Wnt signaling in melanocytes

To determine the consequence of inhibition of Wnt signaling in melanocytes, Wnt signaling was inhibited using an inhibitor of Wnt-mediated transcription, dominant negative TCF-4 (dnTCF) [372]. dnTCF was introduced into melanocytes via lentiviral mediated transfection and its expression verified by western blot analysis (Figure 4.4). This amino-terminally deleted TCF-4 binds Wnt target genes nonproductively due to its inability to bind to beta-catenin. As expected, upon expression of dnTCF, the transcription of downstream Wnt targets was inhibited (Figure 4.5). Upon the inhibition of Wnt signaling, cellular proliferation was greatly diminished, as judged by a loss in the expression of Cyclin A as well as decreased incorporation of BrdU (Figure 4.6 and 4.7). These findings are largely in line with studies in colorectal cancer cells where expression of dnTCF also induced a growth arrest, as judged by a robust G1 arrest via FACS analysis and a decrease in colony size in colony-forming assays [291,373]. Importantly, cell viability was found to not alter after the expression of dnTCF in these same studies. Moreover, I showed here that melanocytes expressing a dnTCF display a flattened morphology and express SA beta-gal, two hallmarks of senescence (Figure 4.8). Together, these results are consistent with the idea that repression of proliferation-promoting Wnt target genes in senescent melanocytes enforces the senescent phenotype.

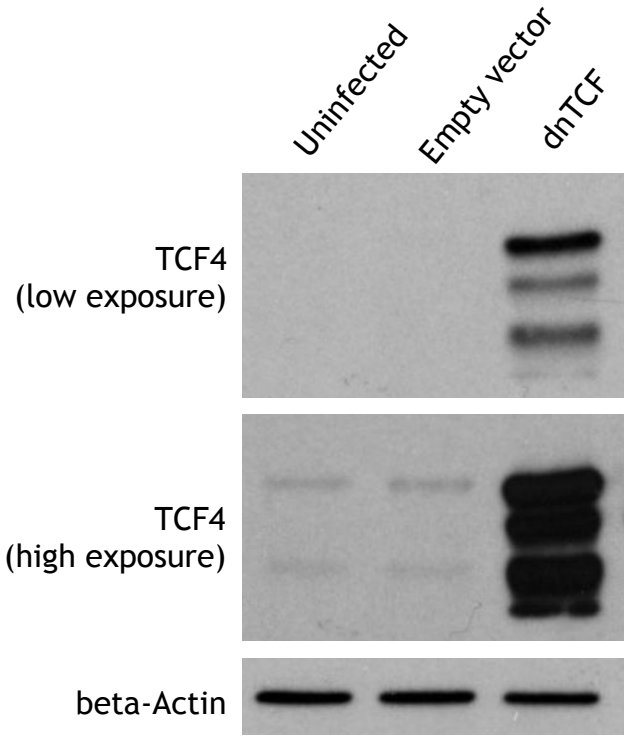

Figure 4.4 Expression of dnTCF in human primary melanocytes.
Representative western blot of dominant-negative TCF (dnTCF) infected primary human melanocytes. Endogenous TCF levels could be detected in empty vector infected and uninfected melanocytes but at a drastically lower level compared to dnTCF transfected melanocytes (see high exposure). Equal amounts (μg) of whole cell lysates were loaded onto a polyacrylamide gel and beta-actin was used as a loading control.

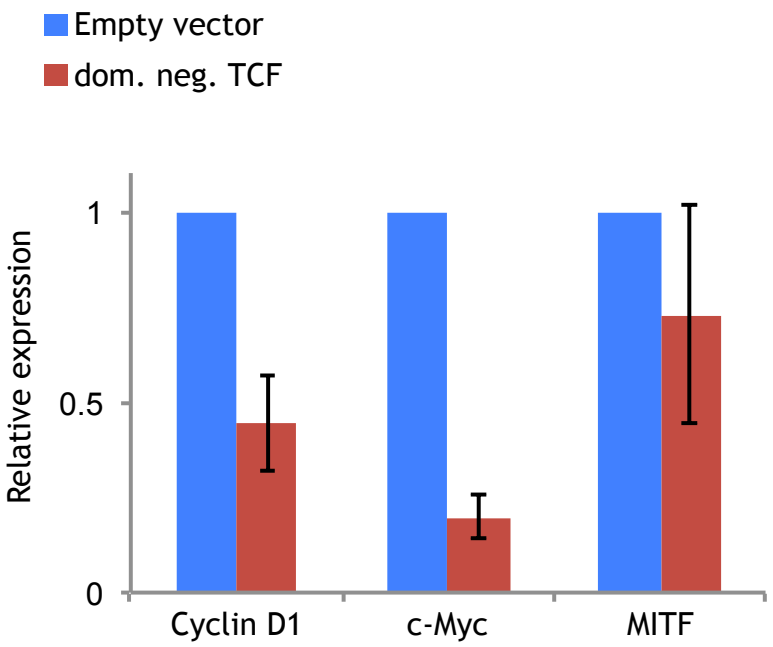

Figure 4.5 dnTCF inhibits Wnt signaling.
RNA was harvested from melanocytes 7 days post infection with dominant negative TCF (dnTCF) and empty vector infected melanocytes. Gene expression was analyzed using qRT-PCR. Expression levels of proliferation promoting Wnt target genes were examined, all of which were down regulated upon. Expression levels were normalized to GAPDH.

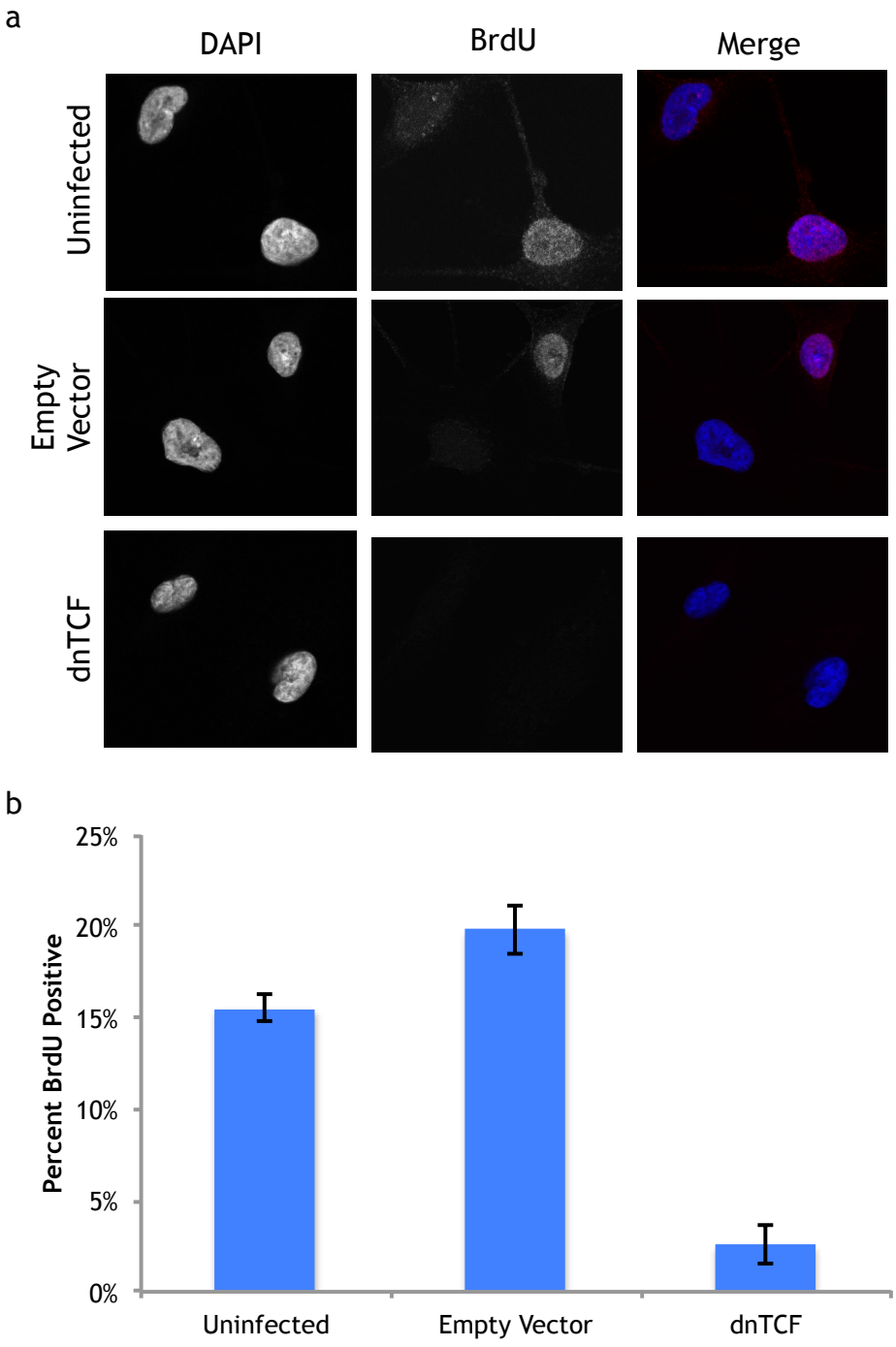

Figure 4.6 Incorporation of BrdU is decreased upon inhibition of Wnt signaling
Seven days post infection with dnTCF, cells were analyzed for proliferation by measuring BrdU incorporation. Uninfected and empty vector transfected melanocytes were used as controls. Inhibition of Wnt signaling through the use of a dnTCF caused a reduction in proliferation as judged by a decrease in BrdU incorporation. (a) Representative immunofluoresenece images for BrdU staining and (b) quantitation of biological triplicates.

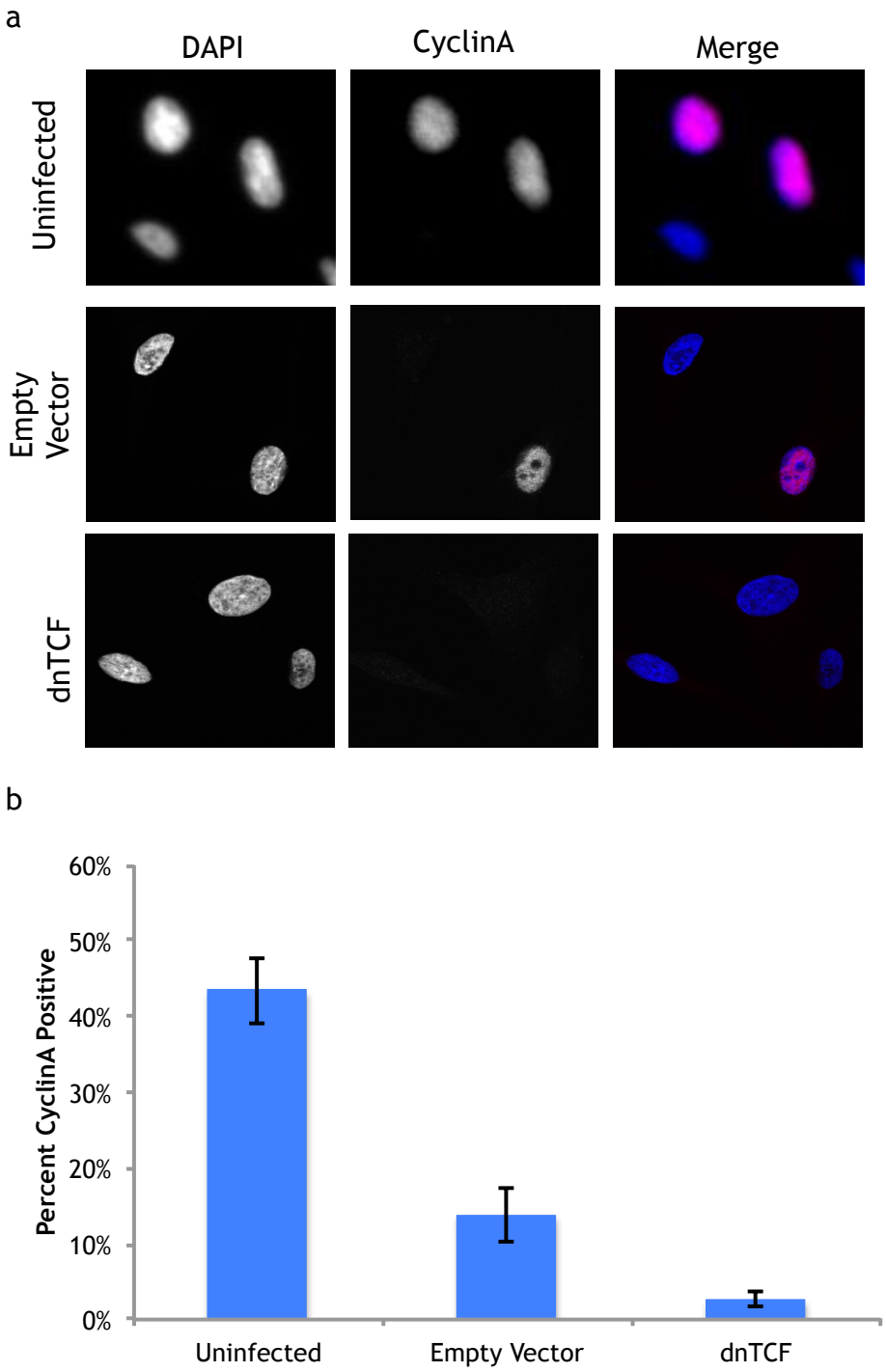

Figure 4.7 Expression of Cyclin A is decreased upon inhibition of Wnt signaling
Seven days post infection with dnTCF, cells were analyzed for proliferation by expression of Cyclin A. Uninfected and empty vector transfected melanocytes were used as controls. Inhibition of Wnt signaling through the use of a dnTCF caused a reduction in proliferation as judged by a decrease in expression of Cyclin A. (a) Representative immunofluoresenece images for Cyclin A and (b) quantitation of biological triplicates.

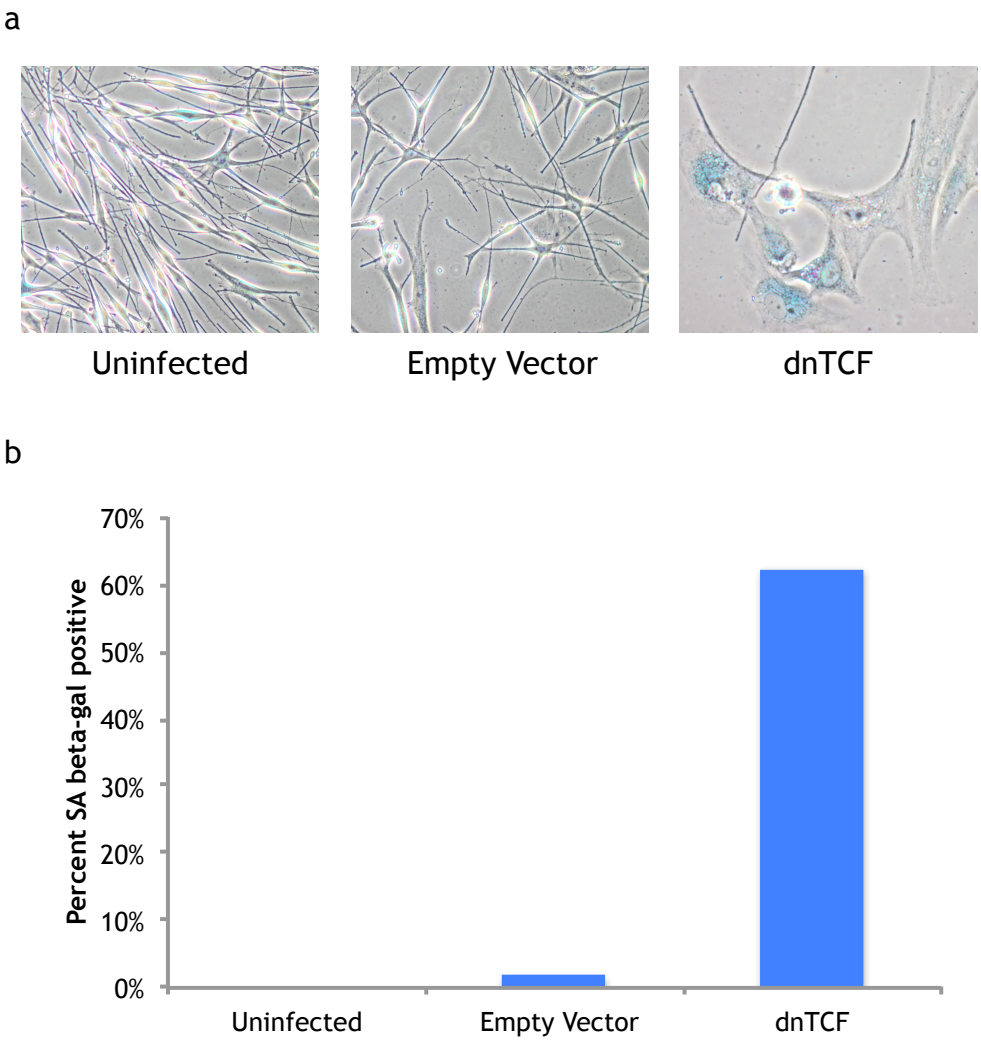

Figure 4.8 Expression of SA beta-gal upon inhibition of Wnt signaling
Seven days post infection with dnTCF, cells were analyzed for the presence of senescence associated beta-galactosiade (SA beta-gal) activity. Uninfected and empty vector transfected melanocytes were used as controls. Inhibition of Wnt signaling through the use of a dnTCF caused cells to broaden and flatten, a common feature of cells *in vitro*. Melanocytes transfected with dnTCF also stained positive for SA beta-gal. (a) Representative bright field images and (b) quantitation.

4.3 Discussion

Analysis of my gene expression data suggests a complex role for Wnt signaling in the regulation of senescence-associated proliferation arrest and the SASP. Results gathered in this chapter, suggest that repression of proliferation-promoting Wnt targets genes has a dominant role in enforcing the senescence associated proliferation response. Key proliferation promoting Wnt target genes that were down regulated upon BRAFV600E-induced senescence, including Cyclin D1, c-Myc, and MITF, and ectopic repression of Wnt signalling induced a senescence-like state. On the other hand, many other Wnt targets remain active in senescence, either due to activation by a non-Wnt pathway, or because Wnt remains active in senescent melanocytes. Interestingly, a number of these expressed Wnt targets include SASP genes, suggesting that activation of Wnt signaling in senescent melanocytes might promote the SASP. This is in line with previous reports showing a complex role for Wnt signaling in the regulation of senescence-associated proliferation arrest [344].

These surprising results can offer one explanation for the conflicting data regarding Wnt signaling in melanoma (see Introduction). Activation of Wnt signaling in melanoma might be expected to activate the tumor suppressive features of the SASP, but also promote cell proliferation. The picture is further complicated by the fact that the SASP can also have tumor promoting roles in some contexts [167]. Thus, whether Wnt signaling is tumor suppressive or promoting will be highly context dependent. Indeed, this appears to be the case for Wnt signaling in melanoma as many there are conflicting reports showing Wnt signaling can be both tumorigenic and tumor suppressive in melanoma [297,344,345].

5 Wnt signaling and other molecular markers of heterogeneity in human melanocytes

5.1 Introduction

According to the prevailing view of nevogenesis, nevi form due to a clonal hyperproliferation of melanocytes harbouring activated BRAF or NRAS oncogenes [9,234]. The hyperproliferation is ultimately arrested and the progression towards melanoma is avoided due to OIS of melanocytes [1,2]. While this hypothesis has been pivotal in the field of senescence and has established human nevi as the paradigm of OIS, it does not adequately reflect many key aspects of nevus biology and their relationship to melanoma.

First, nevi are surprisingly large, containing 10s or 100s of thousands of cells, all derived from clonal hyperproliferation of a single oncogene-expressing melanocyte; this is not intuitively indicative of an efficient senescence-associated proliferation arrest [3,9].

Second, nevi typically develop *in utero* (congenital nevi) or are acquired in childhood and adolescence, but rarely form in adulthood [374]. Therefore, the number of nevi an individual possesses does not correlate with the presumed mutational load in tissue.

Third, roughly 20% of human melanomas are thought to arise from a pre-existing nevus, which is not consistent with a failsafe mechanism of senescence-associated tumor suppression [5-9].

Fourth, nevi exhibit increasing "maturation" in the deeper portions of the lesion. Maturation is an established dermatopathogical parameter used diagnostically and prognostically in the clinical setting and is an indicator of lower malignant potential as it is largely absent it advanced disease [10,11]. As shown in Figure 5.1, maturation is characterized by melanocytes in the deeper,

more mature, portion of a nevus typically being smaller and more spindle shaped compared to the upper, less mature portion. Specifically, the superficial portion of compound and intradermal nevi usually contain cohesive nests of pigmented, round to polygonal cells containing eosinphilic cytoplasm, uniform nuclei, delicate nuclear membranes, and uniform nucleoli. These nevus cells in the upper dermis are commonly classified as type A cells [11,236]. Within the middle of a nevus, melanocytes are often present in smaller nests and cords of type B cells and morphologically often take on more of a lymphoid than epithelial resemblance. For instance, cells often display a decreased amount of cytoplasm, lack melanin, and show a smaller, slightly more hyperchromatic nuclei. The deepest portion of a nevus may contain type C cells that resemble fibroblasts or Schwann cells because they are usually elongated and possess a spindle-shaped nucleus [5].

Maturation is associated with enhanced proliferation arrest, and the upper and least mature portion of a nevus has been shown to, albeit rarely, contain mitotic cells, further questioning nevi as a model of canonical oncogene-induced senescence [375,376]. Although mitoses within nevi have been reported across a range of donor ages, they have been reported at increased frequency during childhood and pregnancy [377,378]. Nonetheless, this upper and less mature portion of a nevus can still be considered to be in a senescent-like state, based on widespread expression of $p16^{INK4A}$ and SA beta-gal [1,2]. In sum, while the cellular and molecular basis of nevus maturation is poorly understood, this phenotypic heterogeneity does not sit well with the simple model of nevi resulting from straightforward oncogene-induced senescence as it demonstrates clear differences within the lesion.

Finally, one of the most widely used biomarkers of senescence in nevi is $p16^{INK4A}$. Nonetheless, $p16^{INK4A}$ staining in nevi is not straightforward and is hard to explain. In fact, $p16^{INK4A}$ expression in nevi is mosaic in nature. To date, there has been no clear answer for why only certain cells within a nevus stain positive for $p16^{INK4A}$. Therefore, even the most well characterized tumor suppressor in

nevi is not fully understood, highlighting the importance for an enhanced understanding of nevus biology.

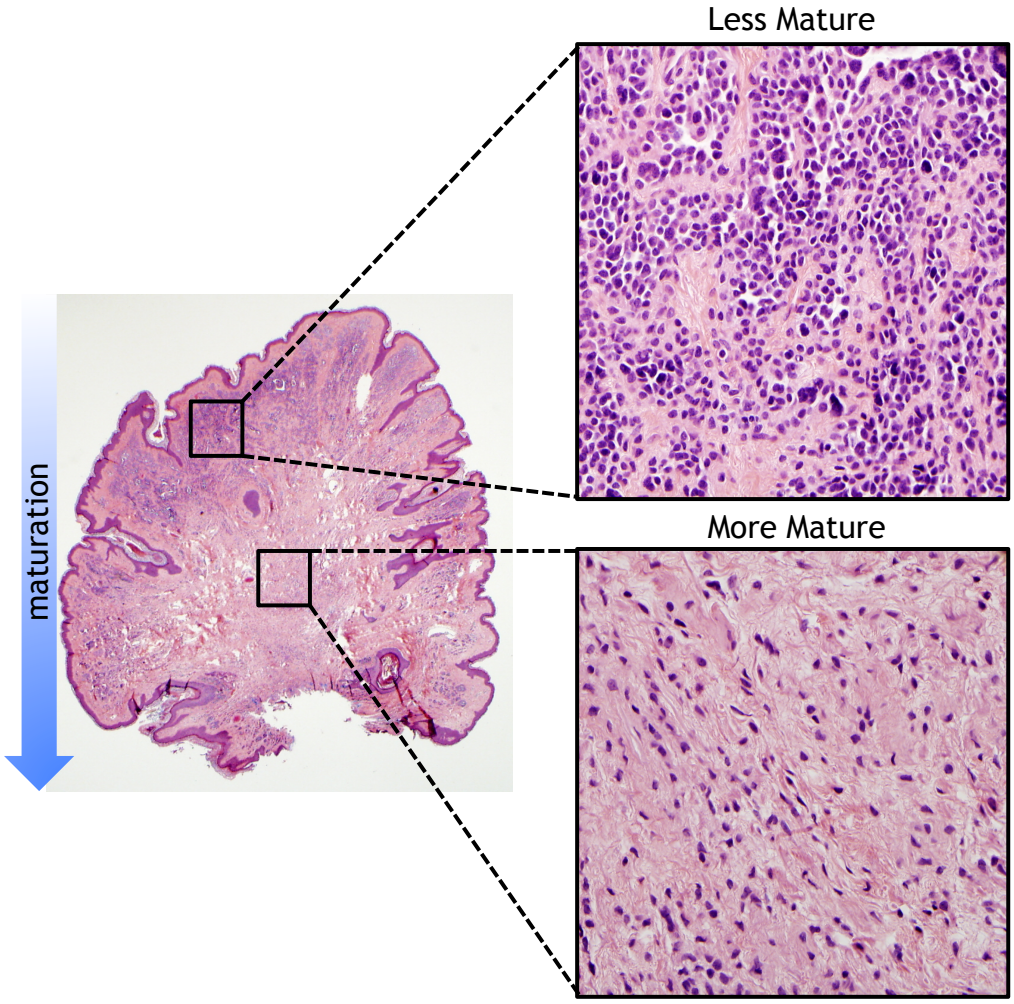

Figure 5.1 Nevus Maturation
Maturation is a common trait seen in benign nevi. H&E staining of a nevus reveals that melanocytes within the upper, less mature, portion of the nevus are more rounded while melanocytes within the deep, more mature, portion of the nevus are smaller and more spindle shaped. See text for more information.

5.2 Results

5.2.1 Human benign nevi show many characteristics of senescence

In order to gain a better understanding of nevus senescence, many markers of senescence were studied. Some of these analyses such as the presence of $p16^{INK4A}$ and lack of Ki67 staining have previously been published and subsequently verified here (Figure 5.2-5.6) [1,2]. Other biomarkers of senescence that have been reported to be lacking in nevi such as p21 and p53 were also confirmed for their absence (Figure 5.7) [1,2,379]. Finally, additional biomarkers and characteristics of senescence that have not yet been used in the analysis of nevus senescence were also studied, such as the expression of Lamin B1 and core histones (Figures 5.8-5.11).

Ki67 is an indicator of proliferation and its expression is strictly associated with cellular proliferation [380]. Upon analysis of Ki67 in human nevi it can be seen that cells within the nevus stain negative, while there are clearly a few proliferating keratinocytes present within the epidermis that serve as internal positive controls (Figure 5.2). Note that the presence of melanocytes is marked by either Melan A or S100 here as it is for the remainder of this thesis.

Further confirmation of senescence-associated staining was performed with $p16^{INK4A}$. There are a vast number of antibodies that bind to $p16^{INK4A}$ as the protein is widely used for cancer diagnosis and research. For an antibody to be used in a diagnostic kit it must be fully validated to ensure its specificity and sensitivity to the target is correct. Unfortunately many antibodies that are routinely used for research are not tested as vigorously. Of the many $p16^{INK4A}$ antibodies on the market, only one has been rigorously tested in human samples to a high enough degree to be used in a diagnostic kit, clone E6H4, and it is now used to diagnose cervical cancer [381]. Recently, additional $p16^{INK4A}$ antibodies have been meticulously tested for their specificity and sensitivity, validating the $p16^{INK4A}$ clone JC8 antibody, while exposing that caution is needed when working with the commonly used $p16^{INK4A}$ antibody clone F-12, at least in human samples

[382]. As clearly seen in Figure 5.3 and 5.4, $p16^{INK4A}$ clone E6H4 stains the bulk of a nevus, albeit heterogeneously. The expression of $p16^{INK4A}$ was not preferential in any particular region of the nevus. In order to further validate this antibody and confirm the expression of $p16^{INK4A}$, I tested 5 additional antibodies. As seen in Figures 5.5 and 5.6, a similar staining pattern was seen in 3 out of 6 antibodies tested. Specifically, $p16^{INK4A}$ clones E6H4, JC8, and G175-405 all showed sensitivity, specificity, and reproducibility. Slight variations in staining patterns did exist between nevi, with some nevi showing a more cytoplasmic stain and others predominantly nuclear. Staining patterns in both the nucleus and cytoplasm are consistent with prior findings showing $p16^{INK4A}$ expression in the cytoplasm as well as nucleus of the cell [383]. As the mosaic staining pattern of $p16^{INK4A}$ was present with all the antibodies that successfully stained the nevus tissue it is likely that the complexity of the staining is not an artifact due to staining methodology or antibody specificity.

Due to the expression of $p16^{INK4A}$ being mosaic in nevi, additional tumor suppression mechanisms may act in cooperation to ensure senescence within all melanocytes of a nevus. To examine this I looked into the staining patterns of other tumor suppressors such as p21 and p53. In agreement with previous studies, I found an absence in the expression of p21 and p53 in nevus tissue (Figure 5.7) [1,2]. Unfortunately, as there was no positive control for these analyses, absence of these proteins cannot be concluded definitively.

As senescent cells often show changes in nuclear morphology, such as enlarged and irregular nuclei and chromatin reorganization, recent work has looked into changes that occur to the nuclear lamina during senescence. Composed of lamins, the nuclear lamina is located between the inner nuclear membrane and the peripheral chromatin and is involved in many nuclear activities of the cell including DNA replication, cell cycle regulation, and nuclear and chromatin organization [384]. With regards to senescence, lamin B1 has been shown to be absent from senescent cells whose proliferation arrest has been initiated from DNA damage, replicative exhaustion, or oncogene expression [385,386]. I was interested to known whether lamin B1 is repressed in senescent nevus melanocytes *in vivo*. Remarkably, I confirmed that senescent nevus melanocytes

in vivo are deficient in lamin B1, compared to non-senescent epidermal keratinocytes (Figure 5.8). Therefore I have identified a further maker of senescence in nevi, specifically, the down regulation of lamin B1.

One of the most recent characteristics found associated with senescence is the gradual loss of histones. Histones, together with DNA in nucleosomes, are the basic building blocks of eukaryotic chromatin. Previous studies showed that senescent yeast and fibroblasts *in vitro* contain reduced amounts of histone and/or regions of the genome that are depleted of histones [64,387,388]. A hallmark of cellular senescence is the rearrangement of chromatin, and loss of histones is proposed to contribute to this feature of senescence. As this finding has only been reported *in vitro* I was interested to see if this characteristic could be replicated *in vivo*. Therefore, I stained benign human nevi to detect histones. As expected, all epidermal keratinocytes overlaying the nevus stained strongly and uniformly for nuclear core histones, H2A, H2B and H3 (Figure 5.9). In line with previous findings *in vitro*, a considerable proportion of Melan A-positive nevus melanocytes stained weakly for these core histones. Importantly, I observed that the proportion of weakly staining nuclei increased in the deeper portion of the nevus, away from the skin surface (Figures 5.10 and 5.11). As discussed above, the deeper portion of a benign nevus is recognized as being more mature [10,11]. These results imply that melancoytes within human nevi contain reduced levels of nuclear histones and, in contrast to $p16^{INK4A}$, this correlates of cellular senescence, proliferation arrest, as well as clinical benignancy.

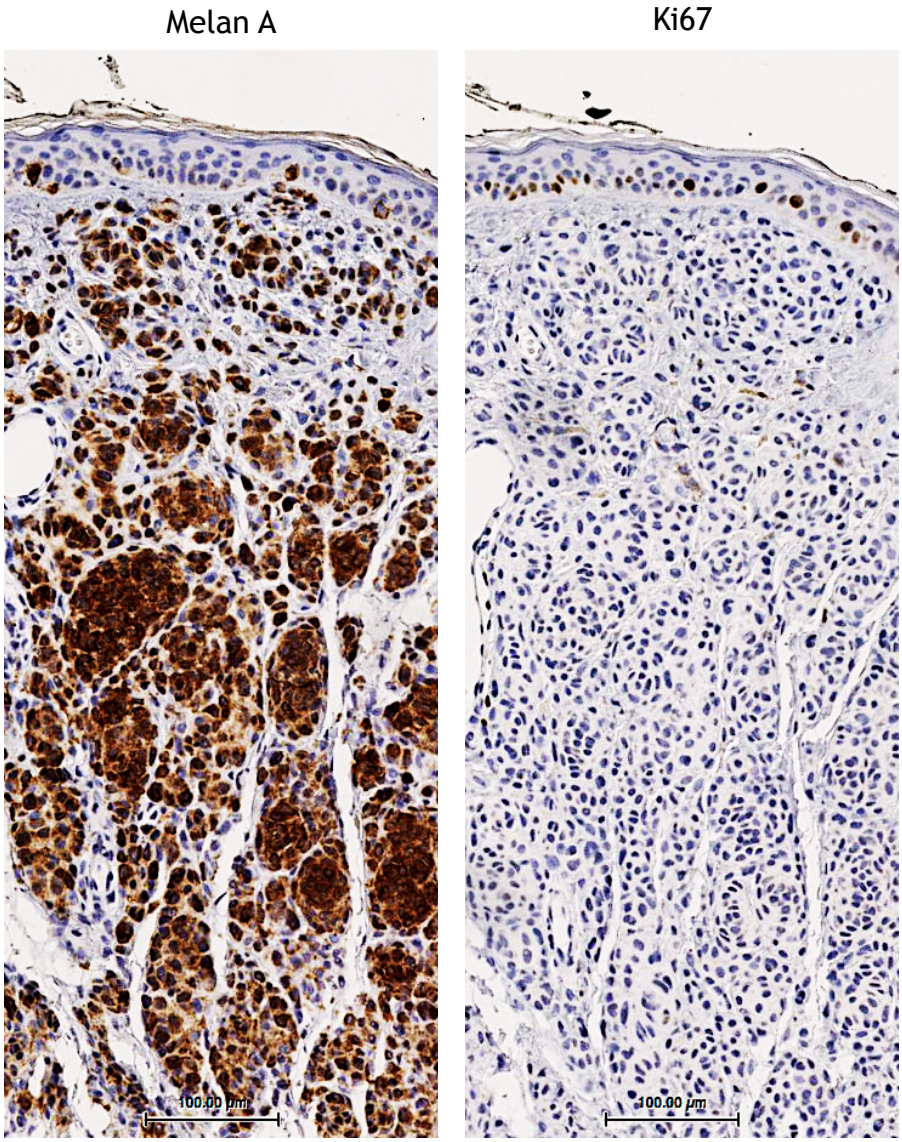

Figure 5.2 Nevus melanocytes are Ki67 negative
Immunohistochemistry of benign human nevi using the proliferation marker Ki67. Melan A was used to properly identify melanocytes in concordant sections. Note the absence of Ki67 in nevus melanocytes while the expression of Ki67 in proliferating epidermal keratinocytes served as an internal positive control. Expression is marked by brown staining using DAB while all nuclei were stained blue using hematoxylin.

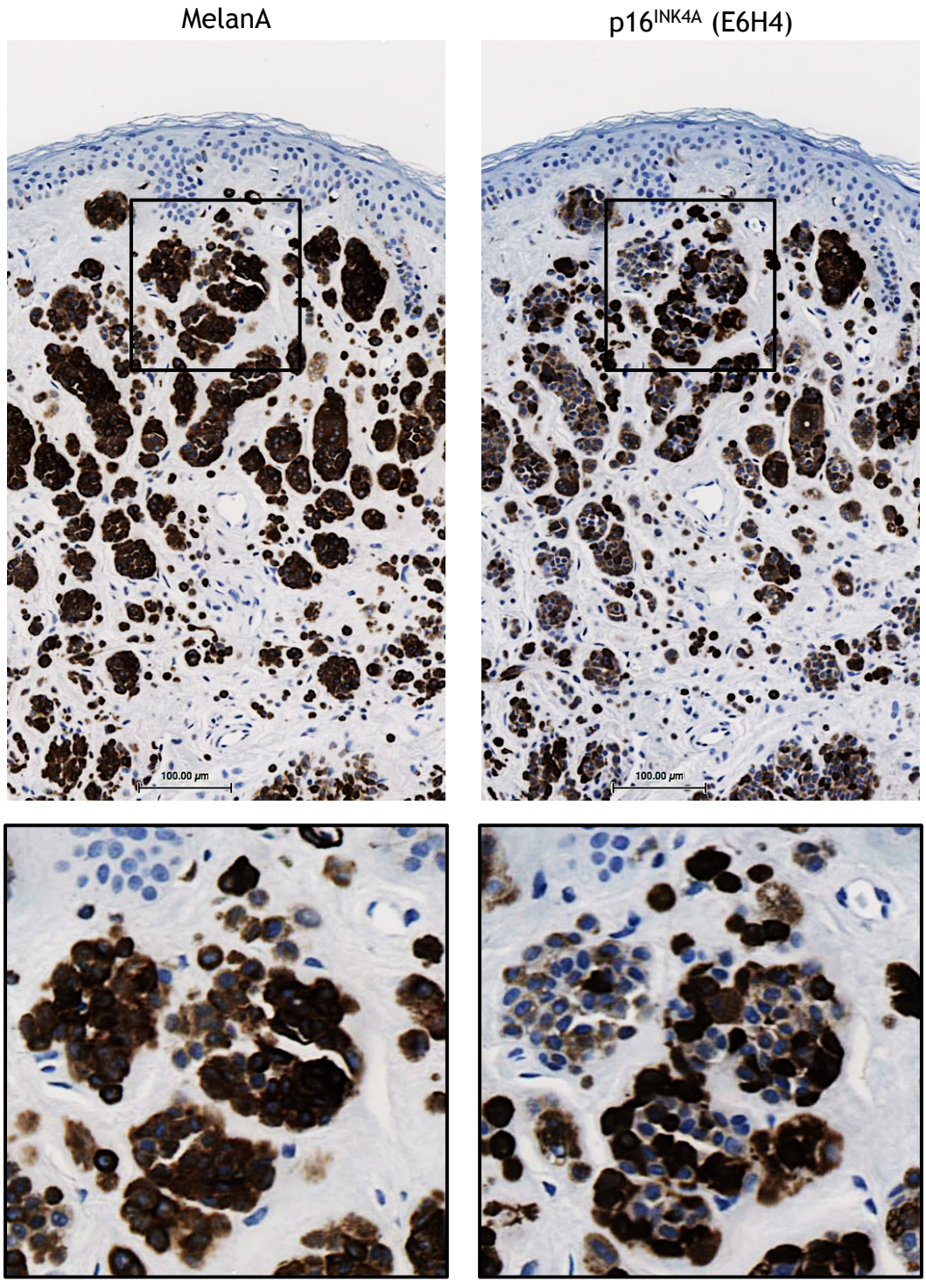

Figure 5.3 Benign human nevi stain positive for p16^{INK4A} via IHC.
Immunohistochemistry of benign human nevi using the validated p16^{INK4A} antibody clone E6H4. Melan A was used to properly identify melanocytes in concordant sections. Note that not all nevus melanocytes expressed p16INK4A as it displayed a mosaic pattern.

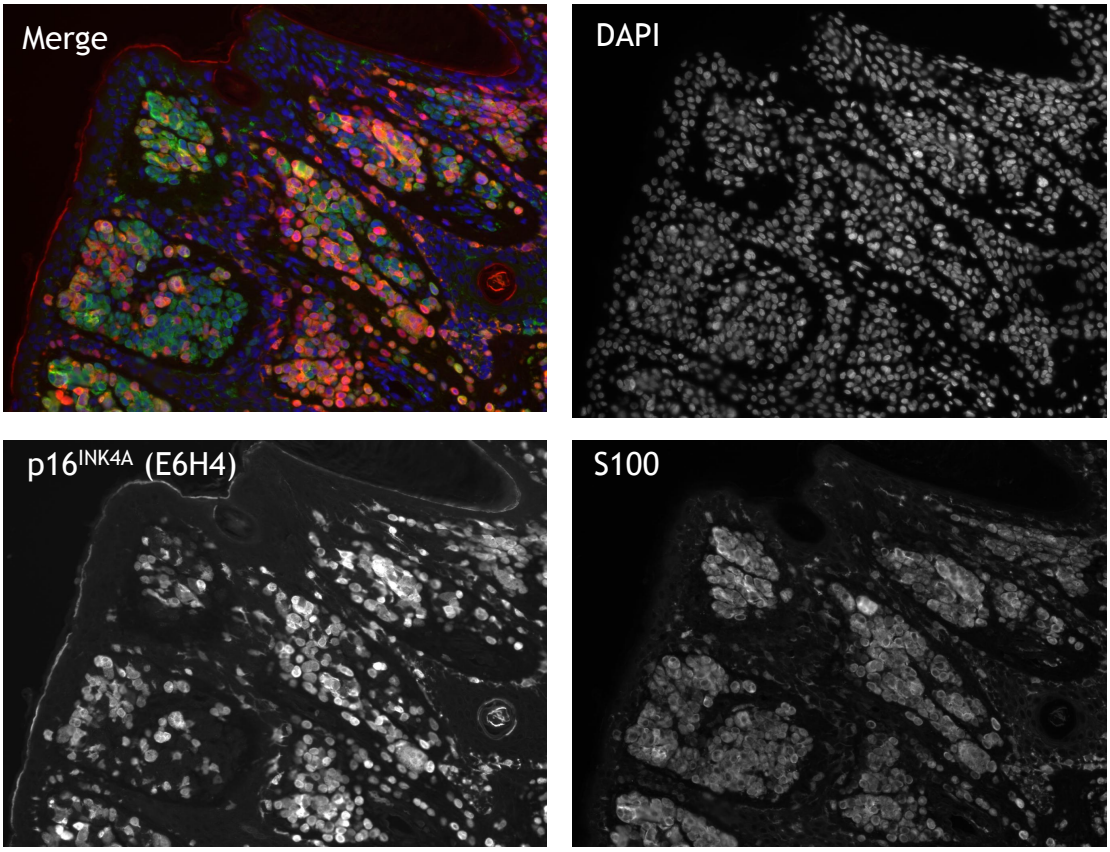

Figure 5.4 Benign human nevi stain positive for p16^{INK4A} via IF.
Immunofluorescence of benign human nevi using the validated p16^{INK4A} antibody clone E6H4. DAPI was used to stain all nuclei while S100 was used to identify melanocytes. Note that not all nevus melanocytes expressed p16^{INK4A} as it displayed a mosaic pattern.

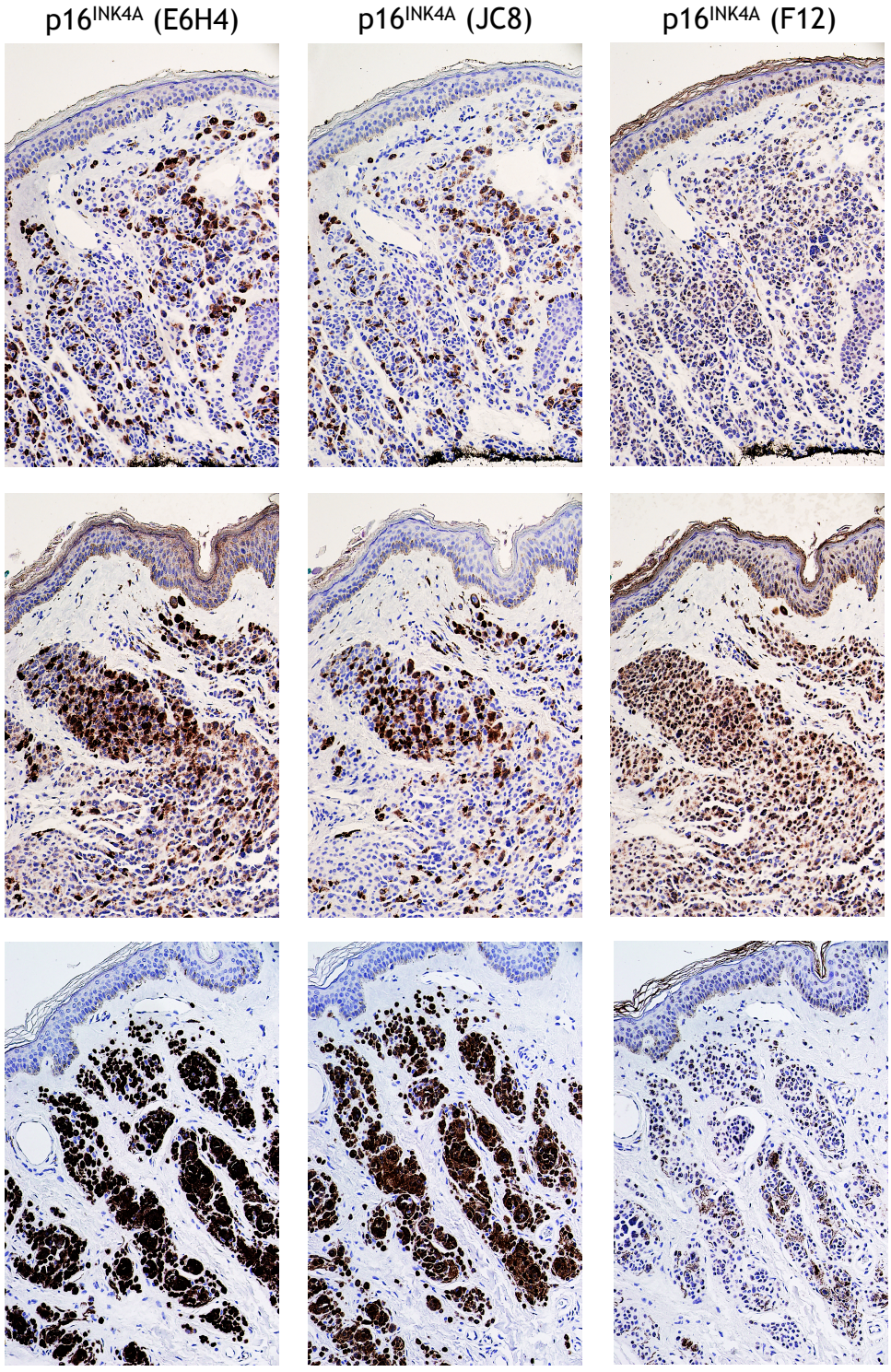

Figure 5.5 Validation of p16^{INK4A} staining in benign human nevi.
Benign nevi were stained with multiple p16^{INK4A} antibodies to further validate expression. Shown are 3 different nevi stained with 3 different p16^{INK4A} antibodies. The p16^{INK4A} antibody clone E6H4 was used as a positive control while p16^{INK4A} antibody clones JC8 and F12 were examined for specificity in concordant sections. Clone JC8 appeared to be specific while clone F12 staining was suboptimal as many some nevi appeared to have nonspecific staining (middle right) and others did not show any staining (bottom right).

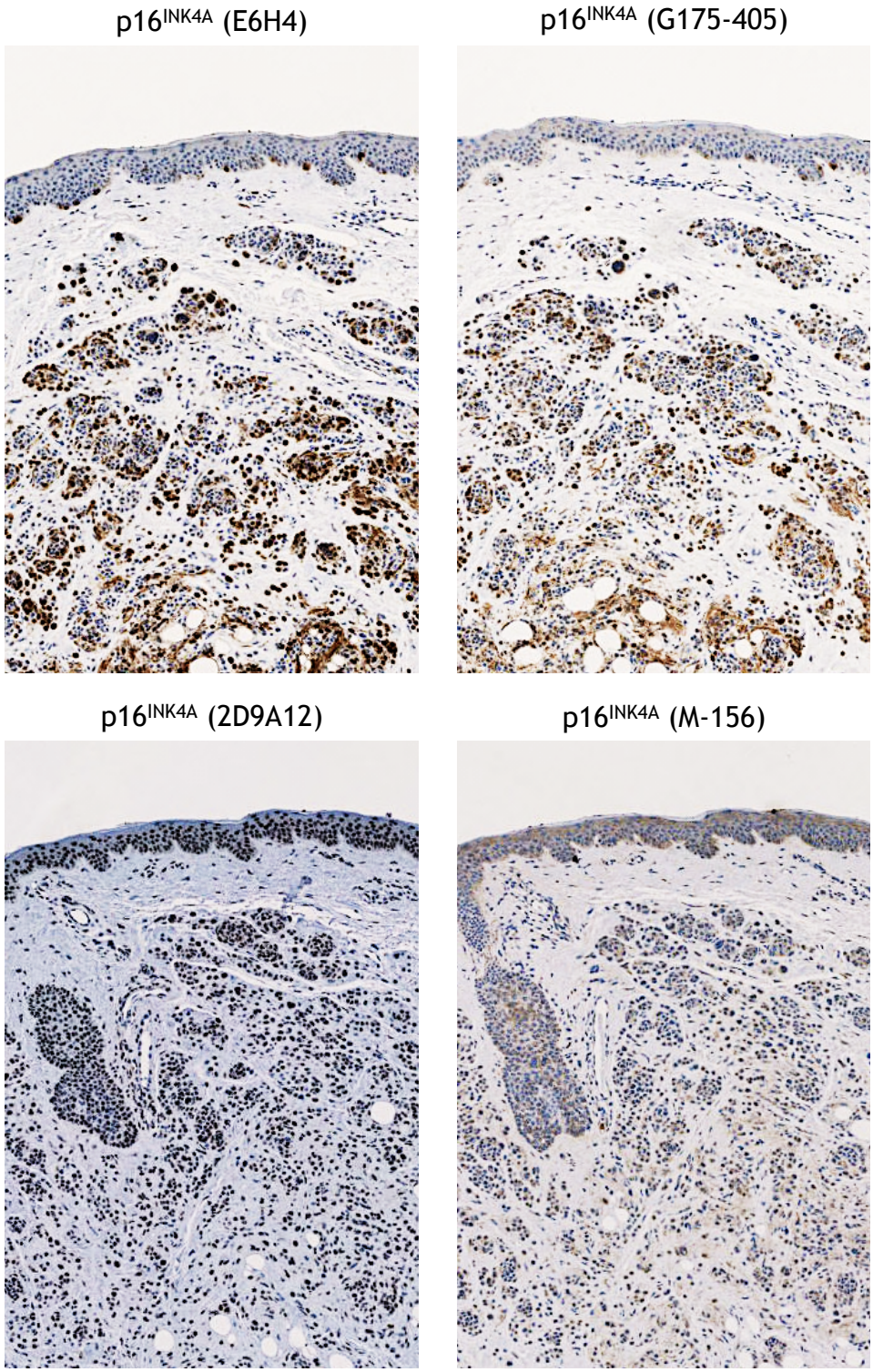

Figure 5.6 Validation of p16^{INK4A} staining in benign human nevi.
Benign nevi were stained with multiple p16I^{NK4A} antibodies to further validate expression. The p16^{INK4A} antibody clone E6H4 was used as a positive control while p16^{INK4A} antibody clones G175-405, 2D9A12, and M-156 were examined for specificity. Clone G175-405 appeared to be specific as it closely mirrored the staining of clone E6H4. Clone 2D9A12 staining was suboptimal as many proliferating epidermal cells stained positive. Clone M-156 was also suboptimal as no specific stain was noticed.

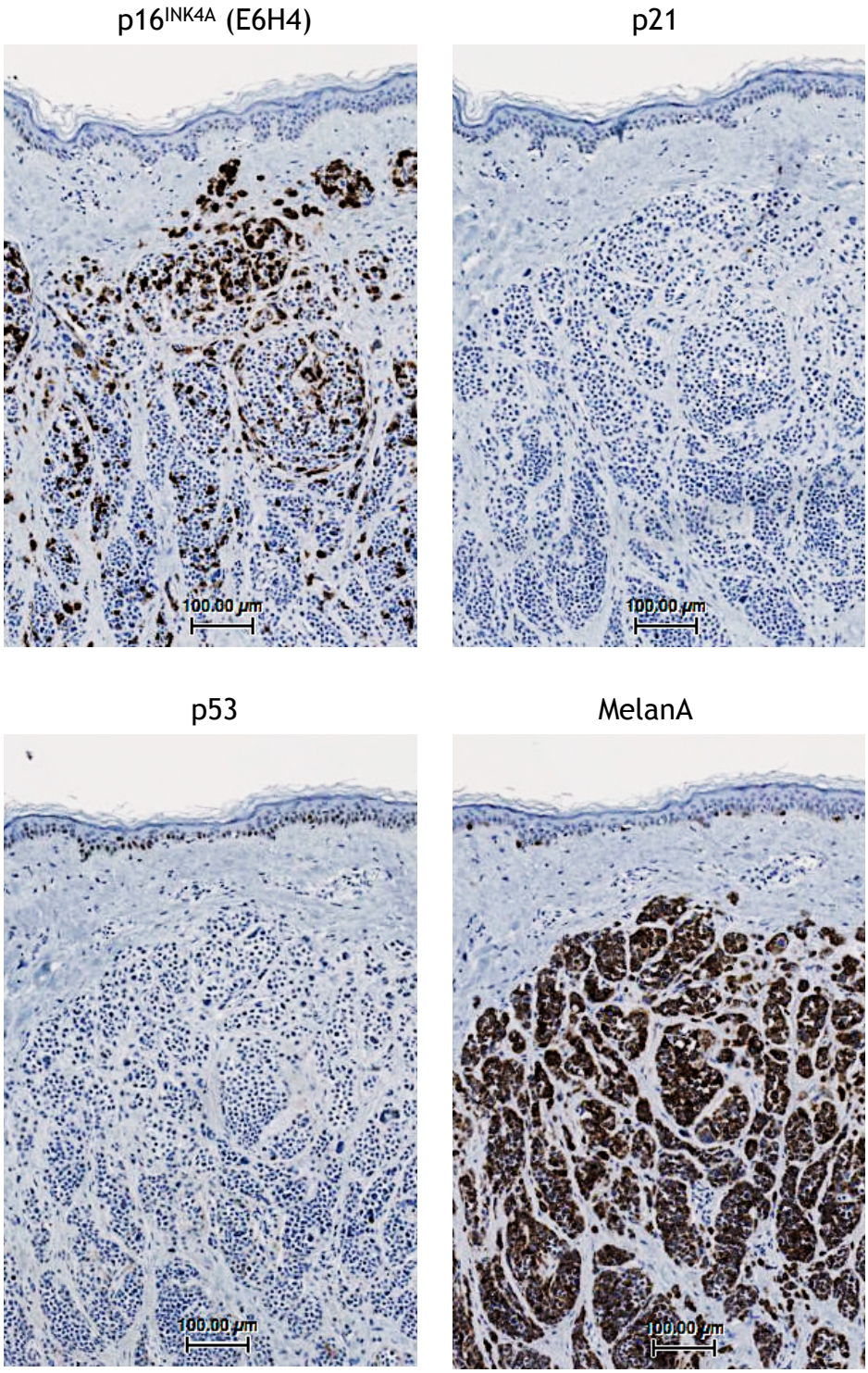

Figure 5.7 Expression of p21 and p53 is not apparent in benign human nevi.
Benign nevi were stained with the tumor suppressor proteins $p16^{INK4A}$, p21, and p53. The $p16^{INK4A}$ antibody clone E6H4 was used as a positive control while Melan A was used to identify melanocytes in near concordant sections. Expression of p21 and p53 was not evident in any nevi examined, with representative images shown.

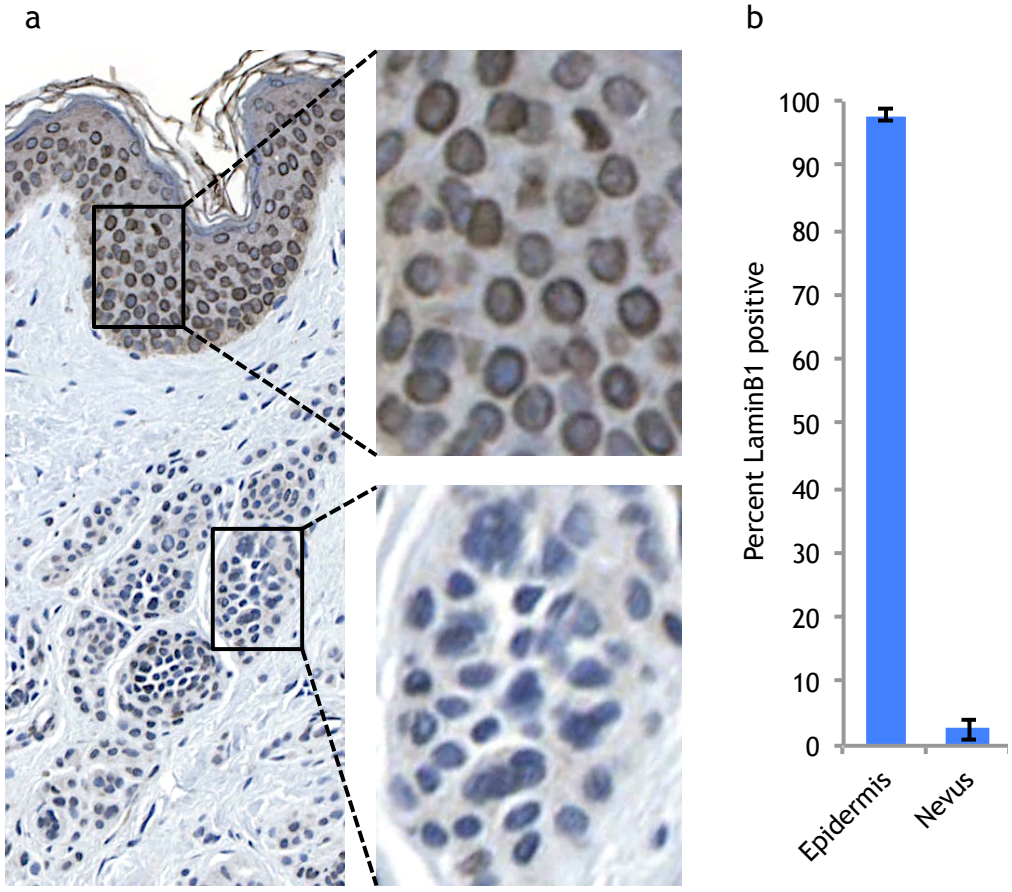

Figure 5.8 Expression of LaminB1 is down regulated in nevus melanocytes.
Expression of the nuclear envelope protein LaminB1 was examined in benign human nevi using IHC. (a) Expression was observed in epidermal cells that are thought to be non-senescent while expression was down regulated in nevus melanocytes. (b) Quantitation of LaminB1 expression in eight different nevi.

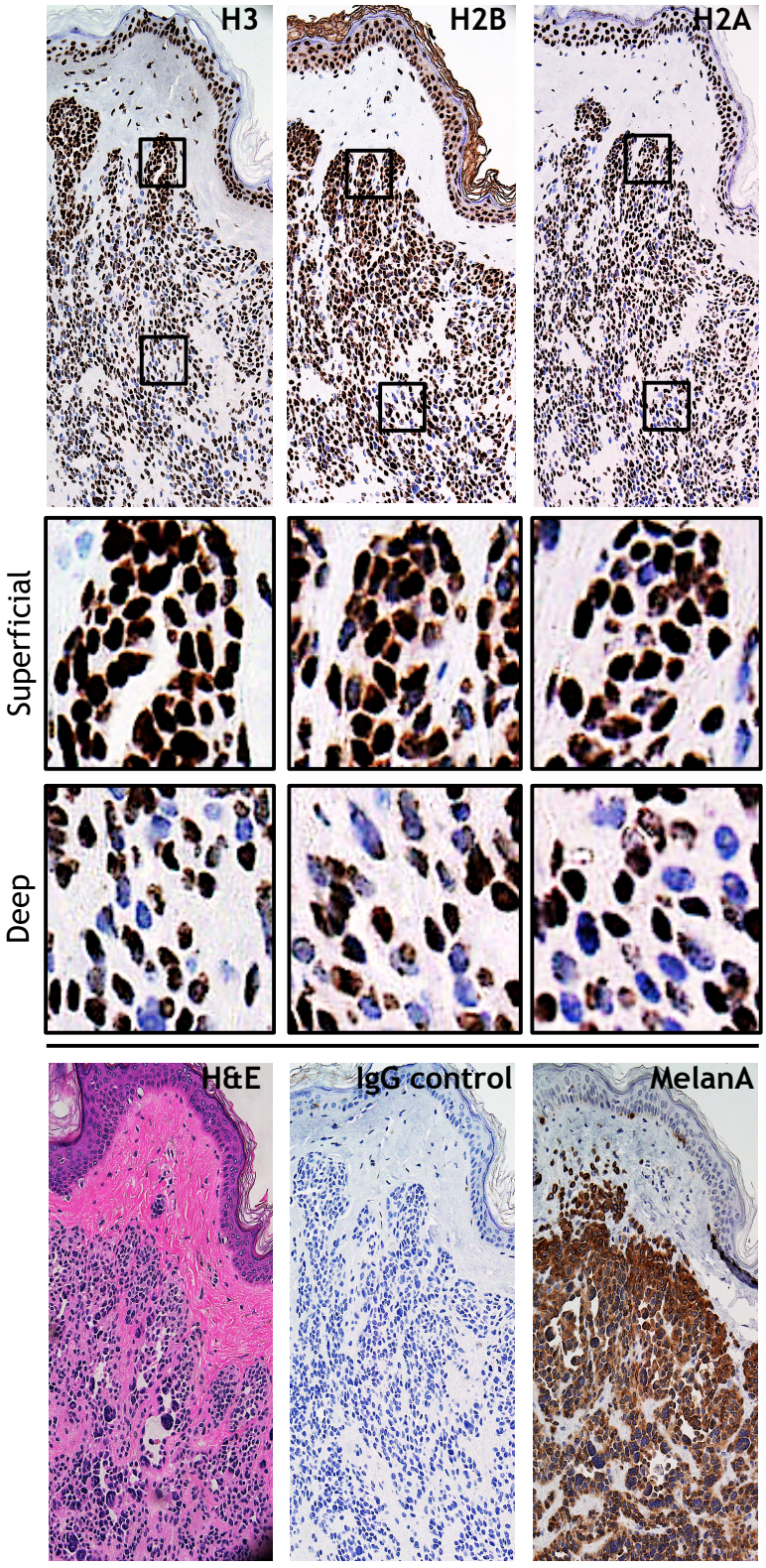

Figure 5.9 Expression of histones correlates inversely with nevus maturation.
The expression of many core histones (H3, H2A and H2B) was examined for their presence in nevi using IHC. Representative images show that staining was most prominent in the epidermis and superficial areas of the nevus while deeper within the more mature portion of the nevus not all cells stained positive for histones. Also shown are H&E staining to show general morphology, IgG control, and Melan A to show melanocytes.

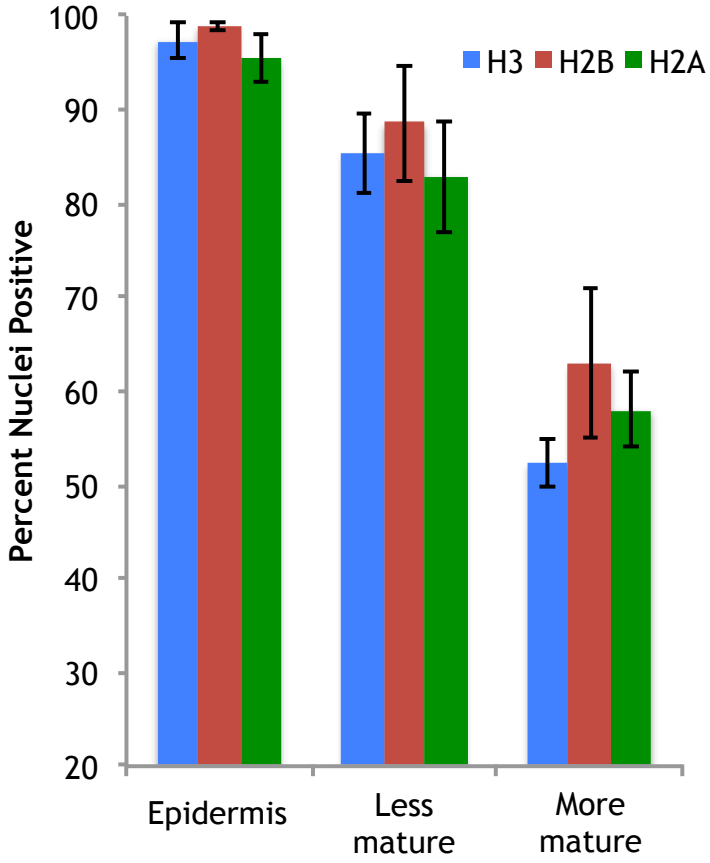

Figure 5.10 Expression of histones correlates inversely with nevus maturation.
The expression of core histones (H3, H2A and H2B) shown in Figure 5.9 was quantitatively measured. Six different nevi were stained and their positivity was calculated in different regions within each nevus.

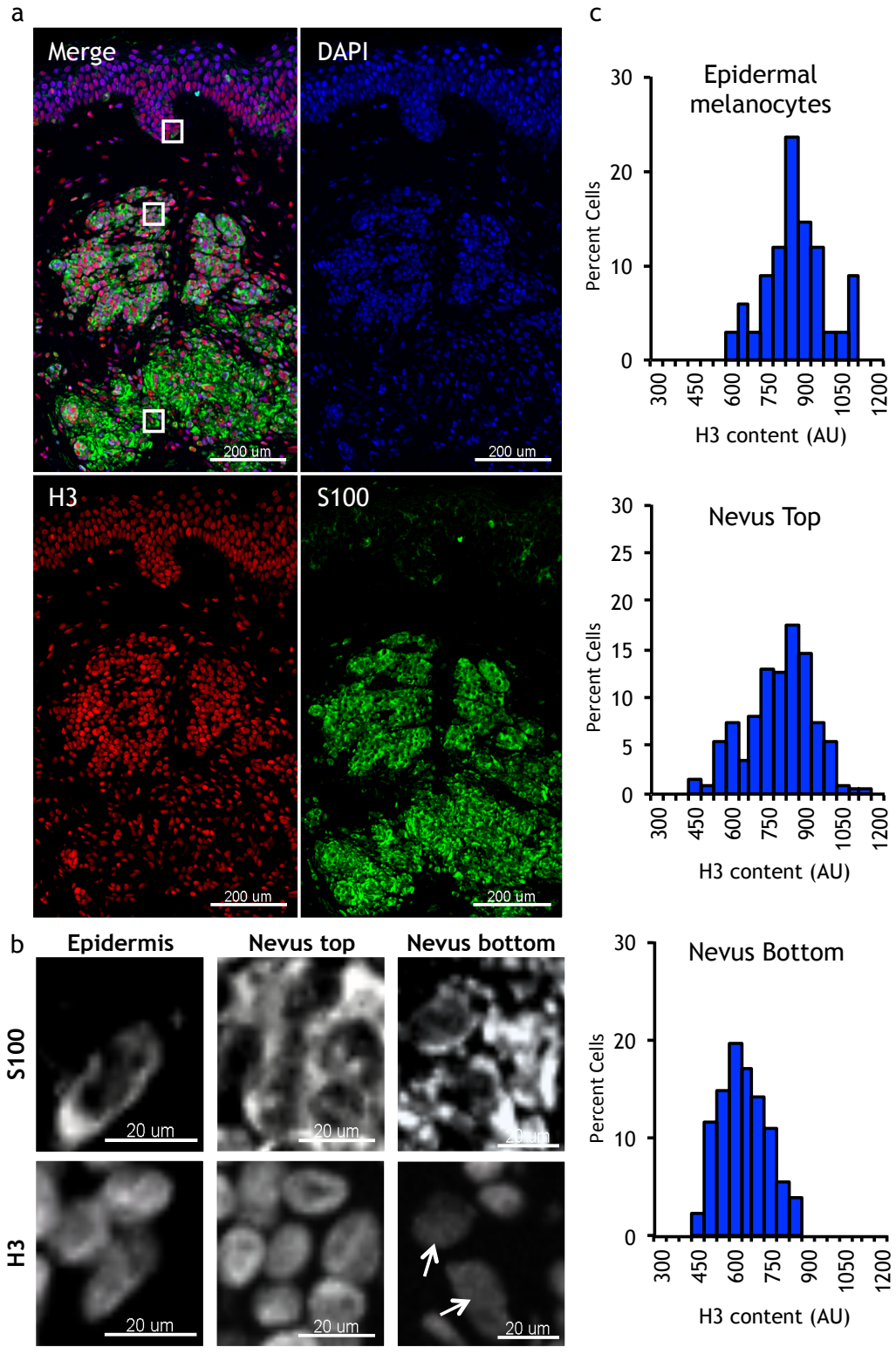

Figure 5.11 Intensity of histone expression correlates with nevus maturation.
Representative image of a benign nevus stained for histone H3 using immunofluorescence. DAPI was used to stain all nuclei while S100 was used to identify melanocytes. Boxed areas in (a) merge image shown in (b) at higher magnification images. Note that H3 staining intensity is reduced towards the more mature nevus bottom (arrowed nuclei). (c) Quantitation of H3 staining intensity in different areas of the nevus and epidermal melanocytes.

5.2.2 Wnt signaling is activated inversely to maturation in benign human nevi

Given the tight link between evasion of the senescence-associated proliferation arrest and melanoma (Chapter 3), and the role for repression of Wnt signaling in driving the senescence-associated proliferation arrest (Chapter 4), I was surprised by previous reports suggesting that human benign nevi express proliferation-promoting Wnt targets, such as Cyclin D1, c-Myc and MITF [317-319]. To confirm this finding I initially optimized the staining for beta-catenin using 3 separate antibodies in human colorectal carcinoma tissue, as this malignancy is known to often contain hyperactivation of Wnt signaling [325] (Figure 5.12). Upon confirmation of nuclear beta-catenin in colon cancer tissue, the same methodology was used on nevus tissue and I confirmed that many melanocytic nests of human benign nevi exhibited expression of nuclear beta-catenin (Figures 5.13). All nevi stained showed nuclear expression of beta-catenin (28 out of 28). In order to analyze the presence of downstream targets of nuclear Wnt signaling in the same cells as beta-catenin, adjacent sections of nevi were stained. As a melanocyte is roughly 7 micrometers in length and sections are routinely cut of 4 micrometer thickness, a single melanocyte is usually present in 2 adjacent sections. As shown in Figure 5.14, many of the same cells located within a nest of a nevus stain positive for beta-catenin, Cyclin D1, and/or c-Myc. The vast majority of nevi stained positive for Cyclin D1 and c-Myc (27 out of 28 and 6 out of 8, respectively).

Interestingly, localization of activated Wnt signaling was linked to nevus maturation [10,11]. Expression of nuclear beta-catenin, c-Myc and Cyclin D1 was more marked in the upper, less mature portion of the nevus (Figures 5.13b, 5.15). Together, these data indicate that incomplete maturation of nevus melanocytes correlates with failure to repress expression of proliferation-promoting Wnt targets, genes whose repression are likely drivers of senescence-associated proliferation arrest. Hence, incomplete maturation is likely to reflect an impaired or flawed senescence program.

From the results above it can be gathered that the deeper, more mature portion of the nevus may perhaps be classified as more senescent than the upper portion of the nevus, even though this portion stains similar for other markers of senescence such as $p16^{INK4A}$ and SA beta-gal.

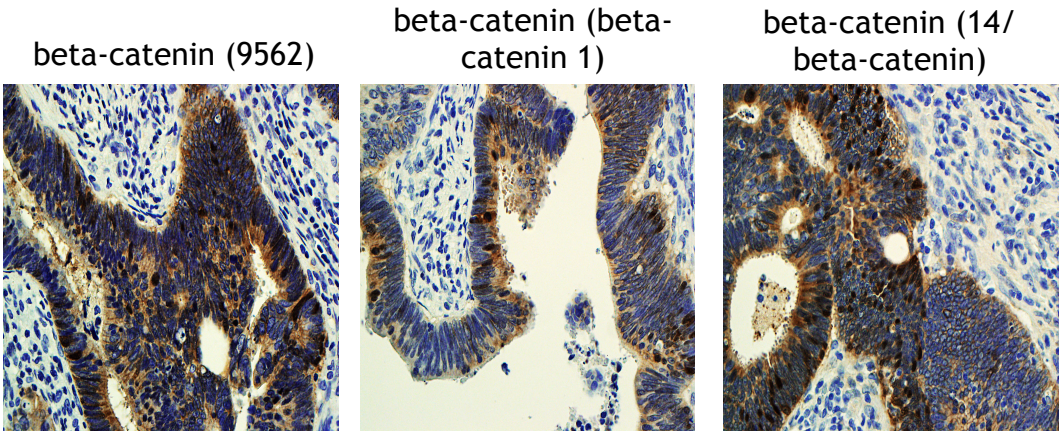

Figure 5.12 Validation of beta-catenin IHC in colon cancer tissue.
Beta-catenin IHC was optimized on colon cancer tissue to shown activation of the Wnt signaling pathway (nuclear and cytoplasmic stain) [389]. All three beta-catenin antibodies (clone 9562, beta-catenin 1, and 14/beta-catenin) showed clear positivity as indicated by nuclear and cytoplasmic staining of many cells located within the tumor tissue.

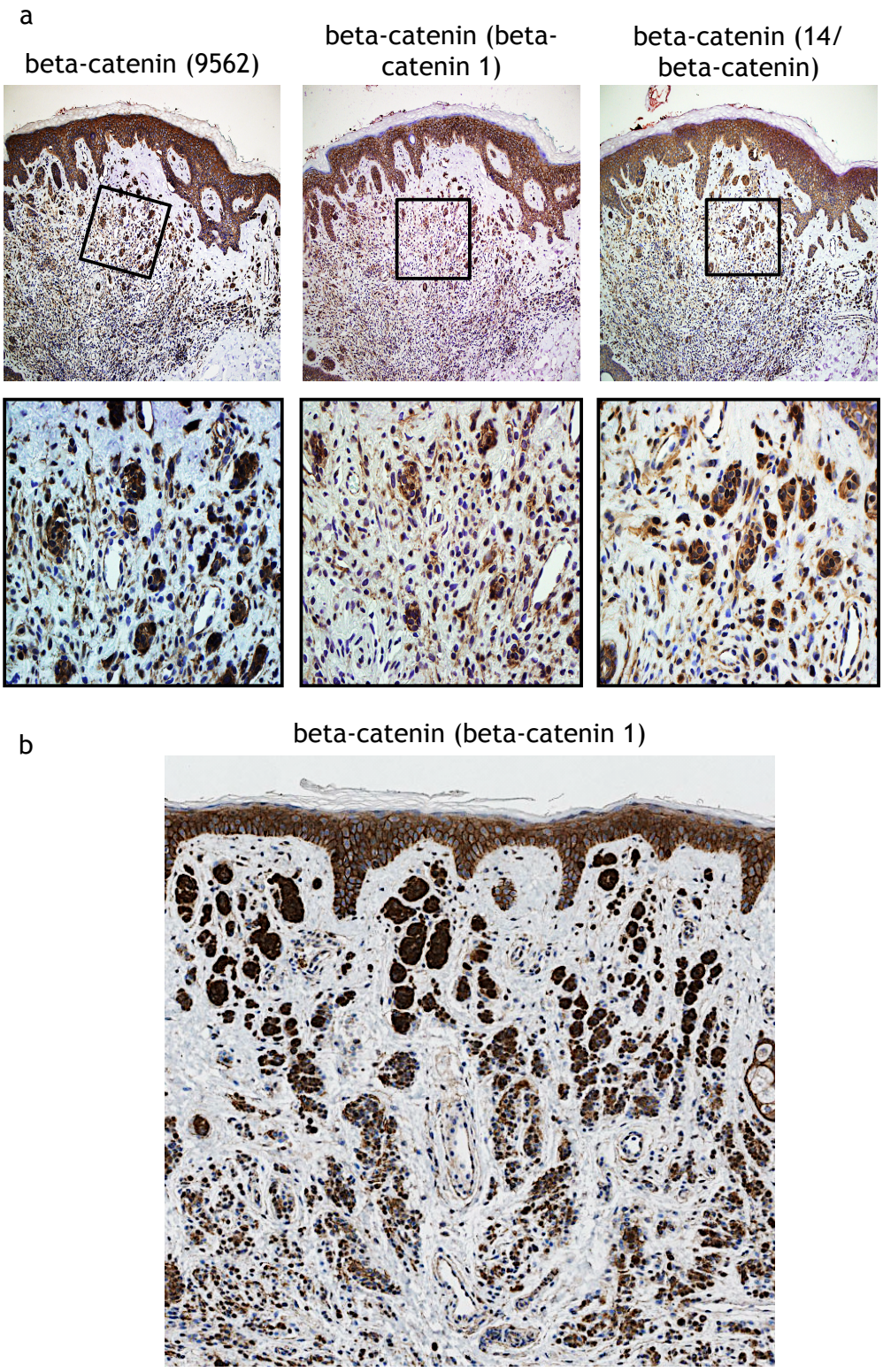

Figure 5.13 Benign nevi display nuclear beta-catenin staining.
Benign human nevi were stained for beta-catenin using IHC. (a) Three different antibodies were used to detect expression (clone 9562, beta-catenin 1, and 14/beta-catenin), using the same conditions as in previous optimization on human colon cancer tissue. Representative images of beta-catenin expression are shown with all three antibodies showing comparable staining. (b) beta-catenin clone beta-catenin 1 was used for all subsequent stainings. Note that beta-catenin also localizes to cell-cell junctions (a marker of inactive Wnt signaling) as is especially evident in the epidermis.

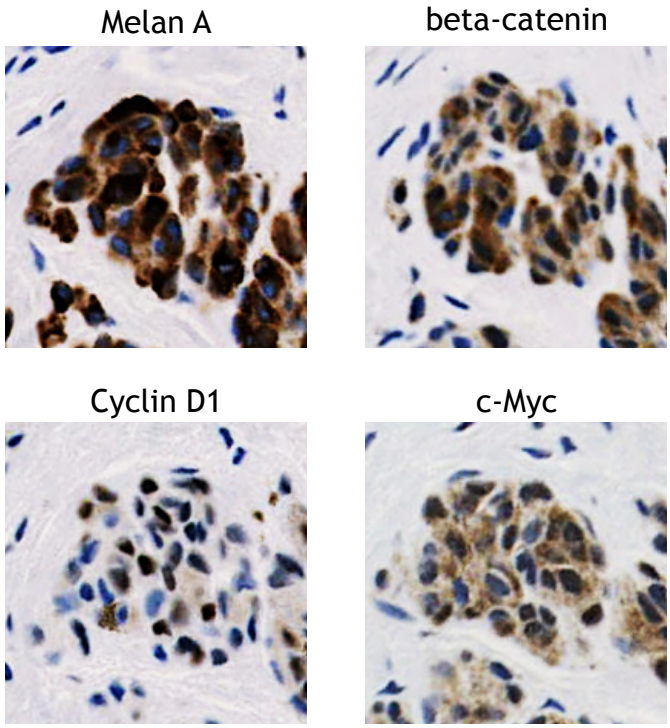

Figure 5.14 Nevus melanocytes express proliferation-promoting Wnt target genes.
Representative images of a melanocytic nest within a benign nevus stained for beta-catenin and proliferating-promoting Wnt target genes. Melan A was used to distinguish melanocytes. Images shown were taken from serial sections.

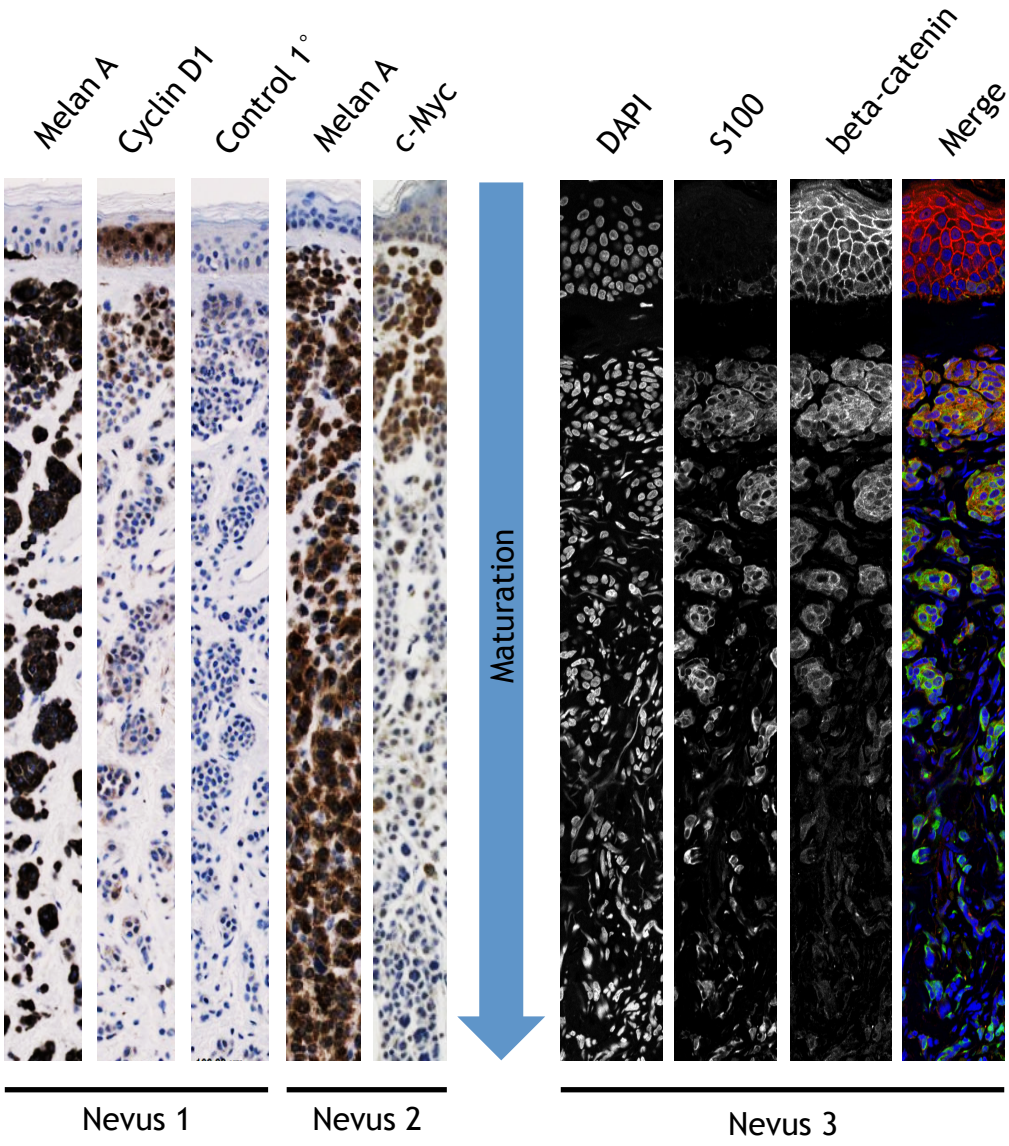

Figure 5.15 Proliferation-promoting Wnt target genes stain inversely to nevus maturation. Nevi were stained with beta-catenin and the Wnt target genes Cyclin D1 and c-Myc using IHC and IF. Melan A and S100 were used to identify melanocytes. An irrelevant primary antibody was used as a control. Serial sections were used within each nevus analysis where appropriate.

5.2.3 Some isolated epidermal melanocytes are apparently senescent and negative for Wnt signaling

The relationship between melanocytes within a nevus and solitary melanocytes along the basal layer of the epidermis has long been of interest as a nevus is thought to arise from clonal hyperproliferation of a single solitary melanocyte [9,234]. Also known as nevomelanocytes, melanocytes located within a nevus differ from melanocytes found interfollicularly within the epidermis in three substantial ways [390]. First, nevus melanocytes tend to have rounded bodies rather then the dendritic morphology associated with lone melanocytes in the basal layer. Second, the nevus cells retain their pigment rather than transferring it to surrounding keratinocytes [228]. Third, nevus melanocytes cluster in nests, in contrary to solitary melanocytes, which spread uniformly along the basement membrane. It is presumed that many signaling pathways are altered upon the formation of a nevus to allow for these morphological disparities. Yet, some changes that were once believed to be hallmark characteristics of nevi have now been re-examined in isolated melanocytes. These differences between nevus melanocytes and epidermal melanocytes have reinforced the notion that the latter are senescent, together with the assumption that the former are not senescent. However, in the course of this thesis, I made observations that question the prevailing view.

As shown in Figure 5.16 I was able to identify $p16^{INK4A}$ positive solitary cells along the basement membrane as melanocytes, based on staining with both S100 and Melan A. Closer analysis of isolated, epidermal $p16^{INK4A}$-positive melanocytes showed that, in contrast to nevus melanocytes, they invariably failed to express Wnt targets, Cyclin D1 and c-Myc (Figures 5.17). This was particularly vivid in epidermal melanocytes overlaying dermal nevus melanocytes - the latter expressed $p16^{INK4A}$ and Cyclin D1, whereas the former expressed only $p16^{INK4A}$ (Figure 5.18). Therefore, this comparison of Wnt signaling expression between two distinct populations of $p16^{INK4A}$-positive melanocytes, lone interfollicular epidermal melanocytes and dermal nevus melanocytes, appears to identify two different modes of senescence.

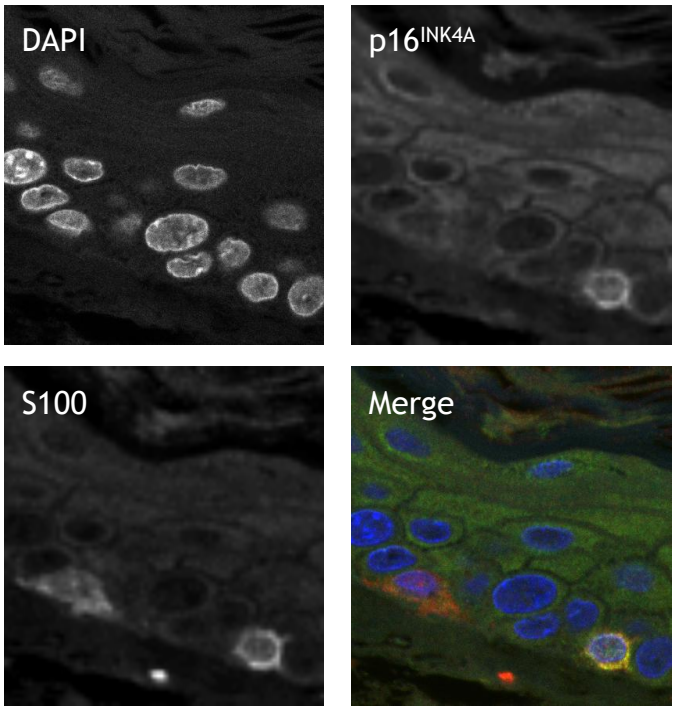

Figure 5.16 Some epidermal melanocytes are p16^{INK4A} positive.
Representative image of normal human skin stained for p16^{INK4A} (clone E6H4) using immunofluorescence. DAPI was used to stain all nuclei while S100 was used to identify melanocytes.

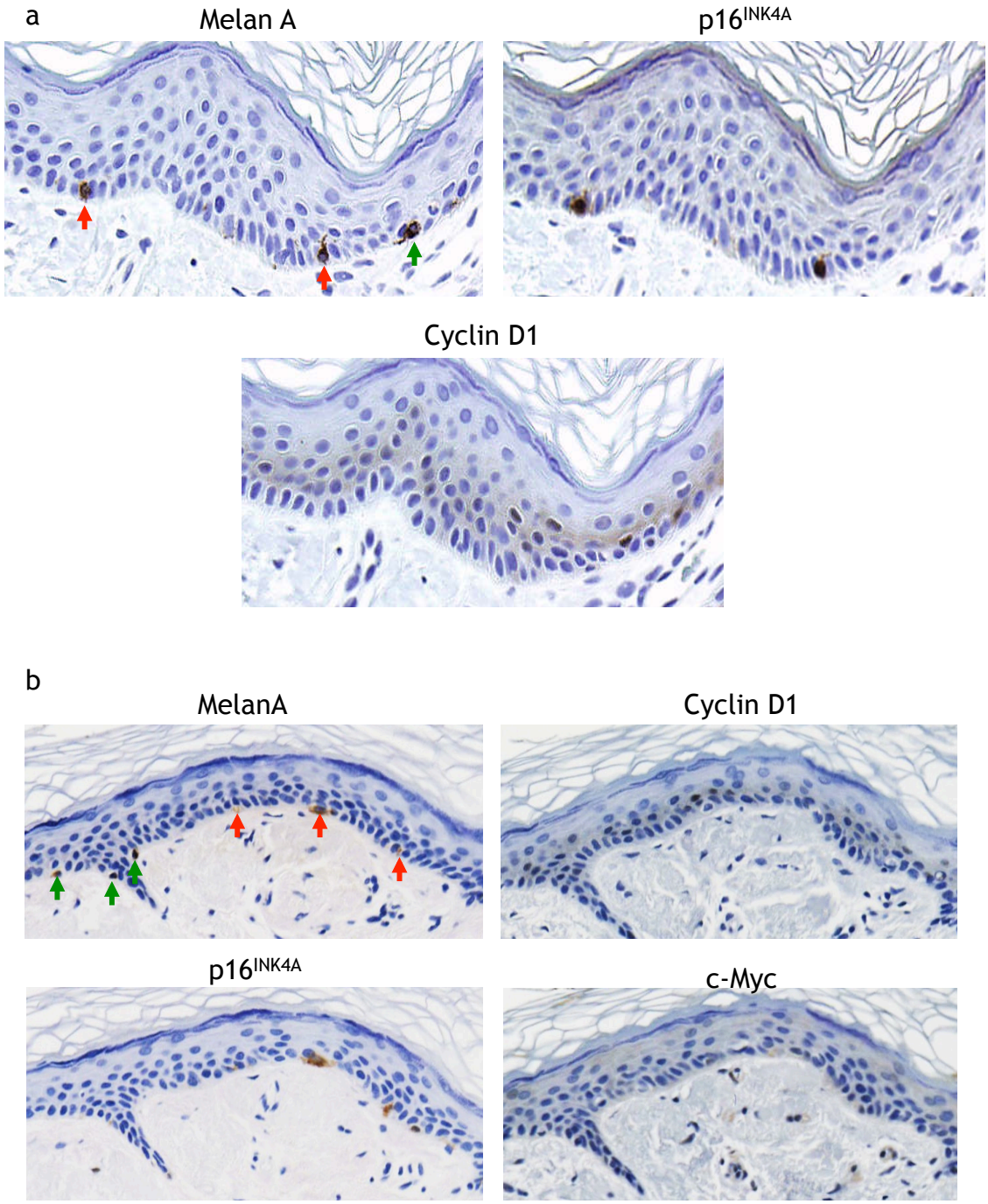

Figure 5.17 p16^{INK4A} positive epidermal melanocytes are not positive for proliferation-promoting Wnt targets.
Representative images of normal human skin stained with p16^{INK4A} and Cyclin D1. Melan A was used to identify melanocytes. (a) Analysis of serial sections showed that all melanocytes stained negatively for Cyclin D1, regardless of whether they stained positive (red arrows) or negative (green arrows) for p16^{INK4A}. Note that Cyclin D1 did faintly stain, as expected, a zone of proliferative cells located in the middle of the epidermis. (b) Same as (a) with the addition of c-Myc lacking expression in p16^{INK4A} positive epidermal melanocytes.

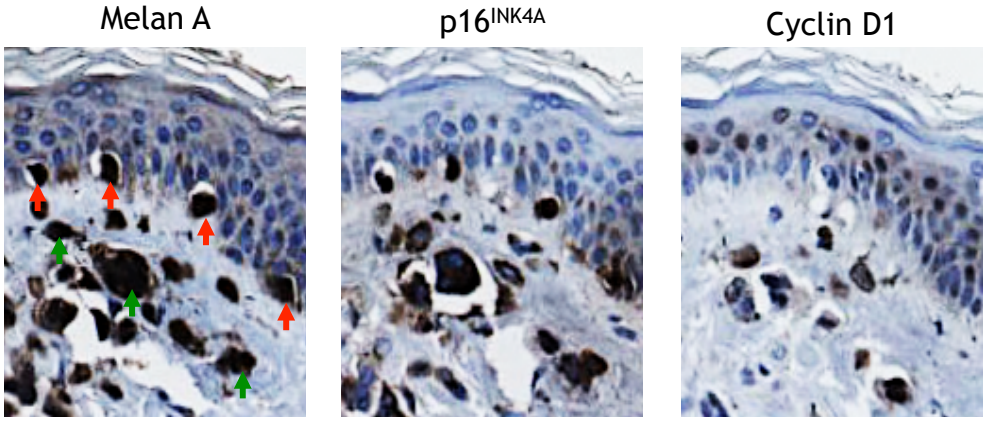

Figure 5.18 Altered expression of a proliferation-promoting Wnt target gene in different melanocytic populations of the skin.
Benign nevi were stained for Cyclin D1, $p16^{INK4A}$ and Melan A. Areas adjacent to the basement membrane were of most interest in order to observe isolated melanocytes as well as nevus melanocytes. In agreement with previous findings, many melanocytes located in nevi and the epidermis stain positive for $p16^{INK4A}$. Also, nevus melanocytes stain positive for Cyclin D1 (green arrows) while epidermal melanocytes do not (red arrows).

5.3 Discussion

In this chapter, I report two major findings:

1. Senescence of human melanocytes is a heterogeneous state. There are multiple cell populations that appear to be in different modes of senescence, based on the absence and presence of specific senescence and proliferation markers and variations in patterns of nesting, morphology, and maturation.
    a. Nevus melanocyte, Wnt positive
    b. Nevus melanocyte, Wnt negative
    c. Epidermal melanocyte, $p16^{INK4A}$ positive, Wnt negative

    To further complicate the picture, nevus melanocytes can also be p16-positive or negative and this does not correlate with activity of Wnt signaling. These data underscore that, despite much work by many labs over recent years, senescence remains a difficult-to-define entity *in vivo*. In fact, these results suggest that there is not a single, uniquely definable senescent state; rather, senescence is a heterogeneous collection of related but distinct states.

2. Activated Wnt signaling correlates inversely with nevus maturation, proliferation arrest and clinical benignancy.

Using histological analysis of benign human nevi and skin samples I have further investigated the role of Wnt signaling in melanocyte senescence. As I previously found that proliferation-promoting Wnt target genes, Cyclin D1 and c-Myc, are down regulated during BRAFV600E-induced senescence in melanocytes, I was surprised to find their expression in benign human nevi. Here I show that the least mature portion of a nevus, that is of highest malignant potential, exhibits activated Wnt signaling and, therefore, perhaps impaired senescence.

Although nevus melanocytes and some solitary melanocytes were both found to be senescent based on expression of $p16^{INK4A}$, their expression of markers of

activated Wnt signaling were quite different. Solitary melanocytes lacked the presence of any markers indicative of activated Wnt signaling while nevus melanocytes were often positive for the same indicators, at least in the least mature portion of the nevus. Based on these data, I suggest that expression of certain proliferation-promoting Wnt target genes contributes to a delay in senescence that allows for oncogene-expressing melanocytes to proliferate and form a nevus before undergoing OIS. When Wnt signaling is absent, the delay in senescence is absent, and the melanocyte remains solitary along the basement membrane.

6 Activation of Wnt signaling promotes proliferative expansion of senescent melanocytes *in vivo*.

6.1 Introduction

In line with the previous results in this thesis I hypothesized that elevated expression of proliferation-promoting Wnt target genes delays the onset of senescence to allow transient hyperproliferation of oncogene-expressing melanocytes to form a nevus. To test this hypothesis, I developed a mouse model system. To date there are many different mouse model systems which use the presence of an activated oncogene (such as RAS or BRAF) specifically in melanocytes to study melanoma biology. Senescence regulators such as $p16^{INK4A}$ and ARF have often been shown to govern the latency and penetrance of melanoma in these models, but little has been studied in these models regarding nevogenesis. In addition, a few of these mouse models have already been used to look at the role of Wnt signaling in melanomagenesis. For instance, elegant work done by Larue and colleagues has found that a stabilized form of beta-catenin in the presence of an NRAS oncogene leads to melanoma with high penetrance and short latency [331]. In a different model, Bosenberg and colleagues have found that stabilized beta-cetenin in melanocytes in the presence of BRAF activation allows for the formation of pigmented tumors with a long latency [391]. In order to better understand the role of Wnt signaling in nevogenesis and to test our hypothesis *in vivo* I generated mice whose melanocytes express an activated oncogene in the presence or absence of activated Wnt signaling.

6.2 Results

6.2.1 Alteration in the pigmentation TyrCreAPCfl.fl/TyrNRAS mice

In order to test the effect of activated Wnt signaling on senescence and its specific role in nevogenesis I made use of three different well-defined mouse models and further bred them to result in the desired genotype. First, mice expressing an activated NRAS (Q61K) oncogene in melanocytes under control of a melanocyte specific tyrosinase promoter (TyrNRAS) were used. Second, a mouse model for activated Wnt signaling was used which functioned by inactivation of APC, a negative regulator of Wnt signaling [348]. Specifically, the inactivation of APC is achieved through the deletion of a portion of APC to introduce of a frameshift mutation. The presence of loxP sites within introns 13 and 14 of the APC gene allow for the partial deletion of the gene and resultant frameshift mutation leading to a non-functioning gene [348]. In order to specifically direct this recombination to melanocytes, a third mouse model was used containing transgenic Cre recombinase under the control of a melanocyte-specific tyrosinase promoter [347]. In the offspring derived from an intercross between these strains carrying the loxP-flanked ("floxed") APC gene and the TyrCre transgene, Cre-loxP site-dependent recombination occurs specifically in melanocytes to inactivate APC. Note that APC remains functional in cells of all other tissues where the Cre transgene is not expressed. Therefore, upon breeding of TyrNRAS and TyrCreAPCfl.fl the resultant progeny was used for analysis, specifically comparing the wildtype, TyrCreAPCfl.fl, TyrNRAS, and TyrCreAPCfl.fl/TyrNRAS mice.

As reported previously, TyrNRAS mice exhibited an excess of S100-positive melanocytes in the dermis and quickly become hyperpigmented, compared to wild type (WT) mice (and also TyrCreAPCfl.fl mice) [346]. Consequently, TyrNRAS mice also showed a darkened coat color and extremities, notably ears, nose, feet and tail (Figure 6.1). Activation of Wnt signaling, by genetic inactivation of APC in TyrCreAPCfl.fl/TyrNRAS mice, exacerbated the NRAS-induced proliferative expansion of S100-positive melanocytes and skin melanization (Figure 6.2). Note that both copies of APC are needed to be floxed in order to observe any marked phenotype, as TyrCreAPCfl.wt/TyrNRAS mice did not display

a noticeably altered phenotype. The increase in melanocyte proliferation specifically in the presence of NRAS and Wnt signaling is present soon after birth and continues into adulthood in TyrCreAPCfl.fl/TyrNRAS mice. To date, no melanomas have been identified in any mice studied although the sacrifice of TyrCreAPCfl.fl/TyrNRAS mice was often required by 150 days of age due to neurological abnormalities such as shakiness and hind leg paralysis. This phenotype is likely associated with proliferation of pre-differentiated melanocytic cells and/or other neural crest derived populations, as the spine and brain of these animals is also pigmented.

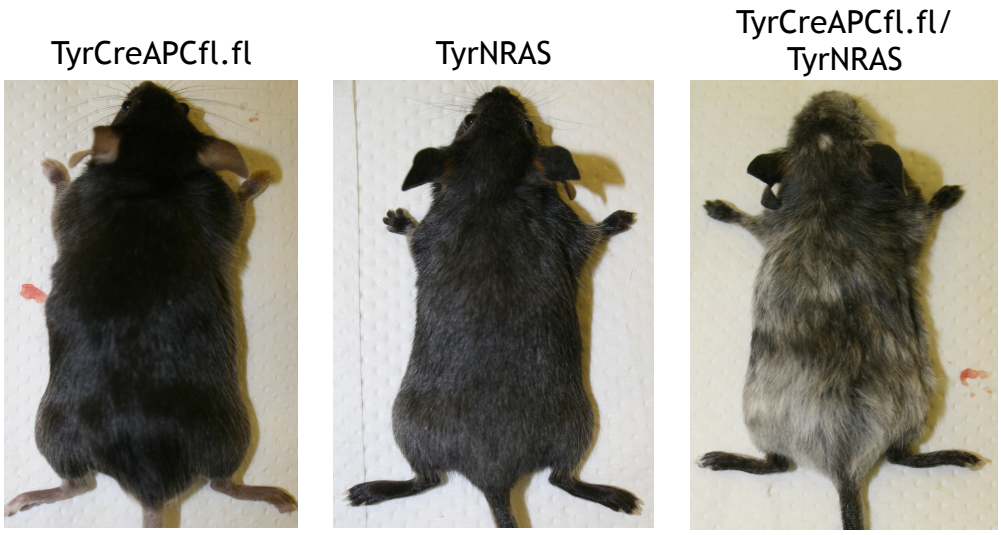

Figure 6.1 Differences in pigmentation are present between mouse genotypes
Representative images of adult TyrCreAPCfl.fl, TyrNRAS, and TyrCreAPCfl.fl/TyrNRAS mice (55-82 days of age shown). TyrCreAPCfl.fl mice show no overt phenotype at this age and seem to closely resemble a wild type (WT) phenotype. Extremities are hyperpigmented in TyrNRAS and TyrCreAPCfl.fl/TyrNRAS mice compared to WT (not shown) and TyrCreAPCfl.fl mice. TyrCreAPCfl.fl/TyrNRAS mice also show a mottled hair pigmentation pattern.

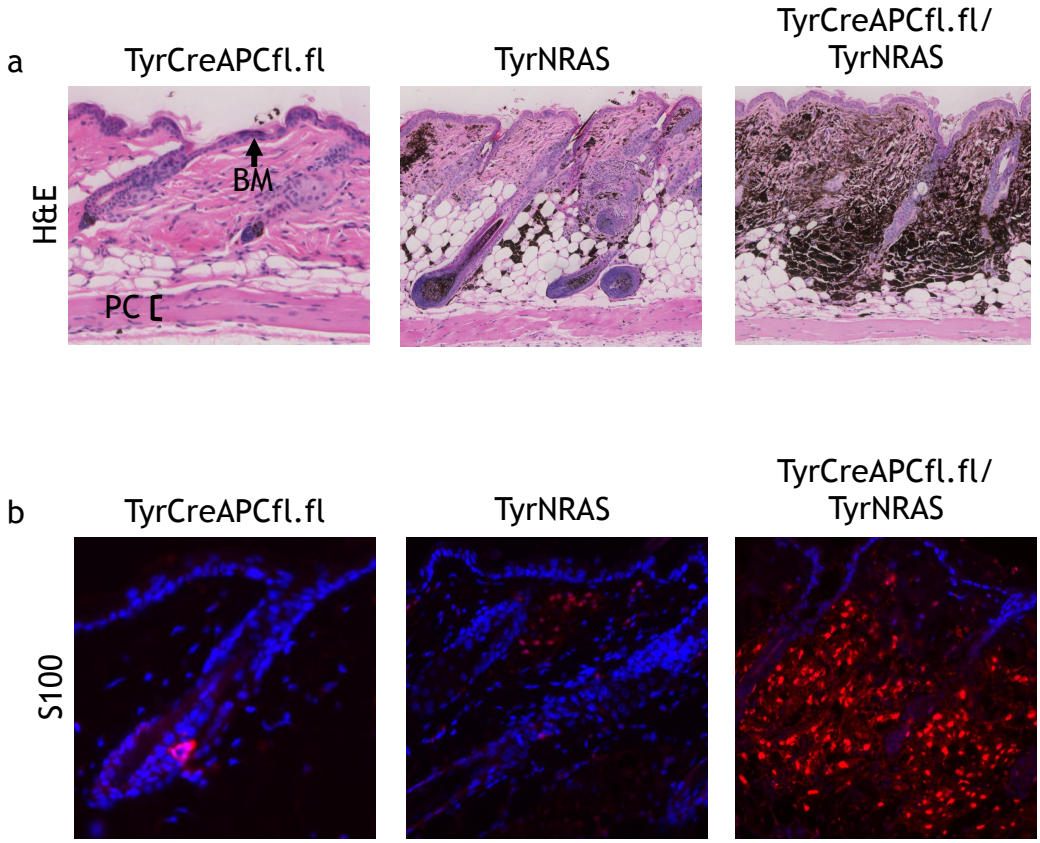

Figure 6.2 Activation of Wnt signaling exacerbates the NRAS dermal hyper-melanocytic phenotype.
(a) H&E staining of the indicated mouse skin shows the presence of melanin (brown) produced by melanocytes. BM, basement membrane; PC, panniculus carnosus. (b) Immunofluorescence also shows a drastic increase in the number of melanocytes (S100 red, DAPI blue). Representative adult mice aged 55-82 days are shown.

6.2.2 Expansion of melanocytes results from a delay in senescence

Upon subsequent histological analysis, the dermal melanocytes of TyrNRAS and TyrCreAPCfl.fl/TyrNRAS mice were found to not be transformed, malignant or invasive. The proliferating melanocytes in young mice (2-7 days) were restricted to the dermal area between the basement membrane and the panniculus carnosus (Figure 6.3). In adult mice, the melanocytes were also restricted to the dermis and showed no signs of anaplasia (de-differentiation) (Figure 6.4). There were no unusual masses or signs of ulceration (Figure 6.4). There was no disruption, invasion, or signs of pressure on the basement membrane and panniculus carnosus (Figure 6.4). These findings are consistent with melanocytes showing an eventual loss of proliferation in both TyrNRAS mice and TyrCre APCfl.fl/TyrNRAS mice. Indicative of this, the percent melanization of the dermis and the number of S100-positive cells in both genotypes eventually reached a plateau (Figure 6.5). Furthermore, while the dermis of young (2-7 days) TyrNRAS and TyrCreAPCfl.fl/TyrNRAS mice contained an excess of Ki67-expressing cells compared to WT mice, in adult (>60 days) mice of both genotypes the Ki67-positive cells were largely depleted (Figure 6.6). Also consistent with a finite proliferative capacity of melanocytic cells in the TyrCreAPCfl.fl/TyrNRAS mice, these mice showed marked hair greying and reduction in melanin in the hair follicles (Figures 6.1 and 6.7). Given that melanocytes of these mice can differentiate normally, based on expression and production of melanin and S100 (Figure 6.8), this can be explained by depletion of pigment producing melanocytes and/or their stem or progenitor cells in the hair follicle, and/or failure of these cells to migrate into or persist in the hair follicle. Either way, the TyrCreAPCfl.fl/TyrNRAS melanocytes do not appear to be immortal *in vivo*. In fact, non-proliferating melanocytes of adult mice of both genotypes were $p16^{INK4A}$-positive (Figure 6.9), indicative of a senescent-like phenotype. Note that for figures of mouse skin immunofluorescence the use of a negative control was used, as shown in Figure 6.10, to confirm the absence of any autofluorescence or background staining due to tissue manipulation.

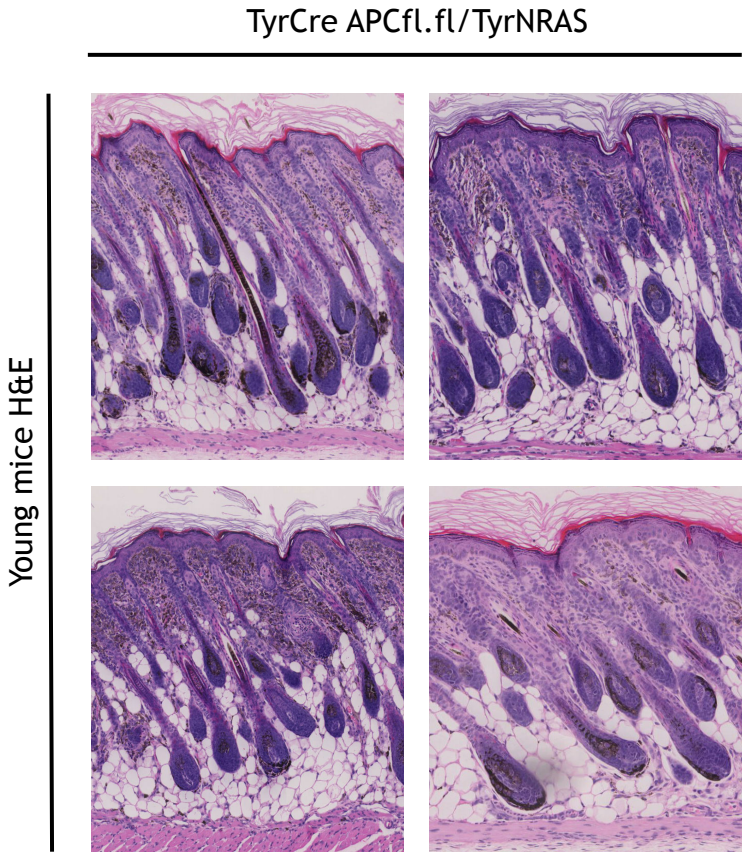

Figure 6.3 Young TyrCreAPCfl.fl/TyrNRAS mice show an increase in melanization
Representative images of 4 young TyrCreAPCfl.fl/TyrNRAS mice (aged 2-7 days). The presence of melanin (brown) between hair follicles can be seen at even a young age and is confined to the dermis, showing no signs of malignancy.

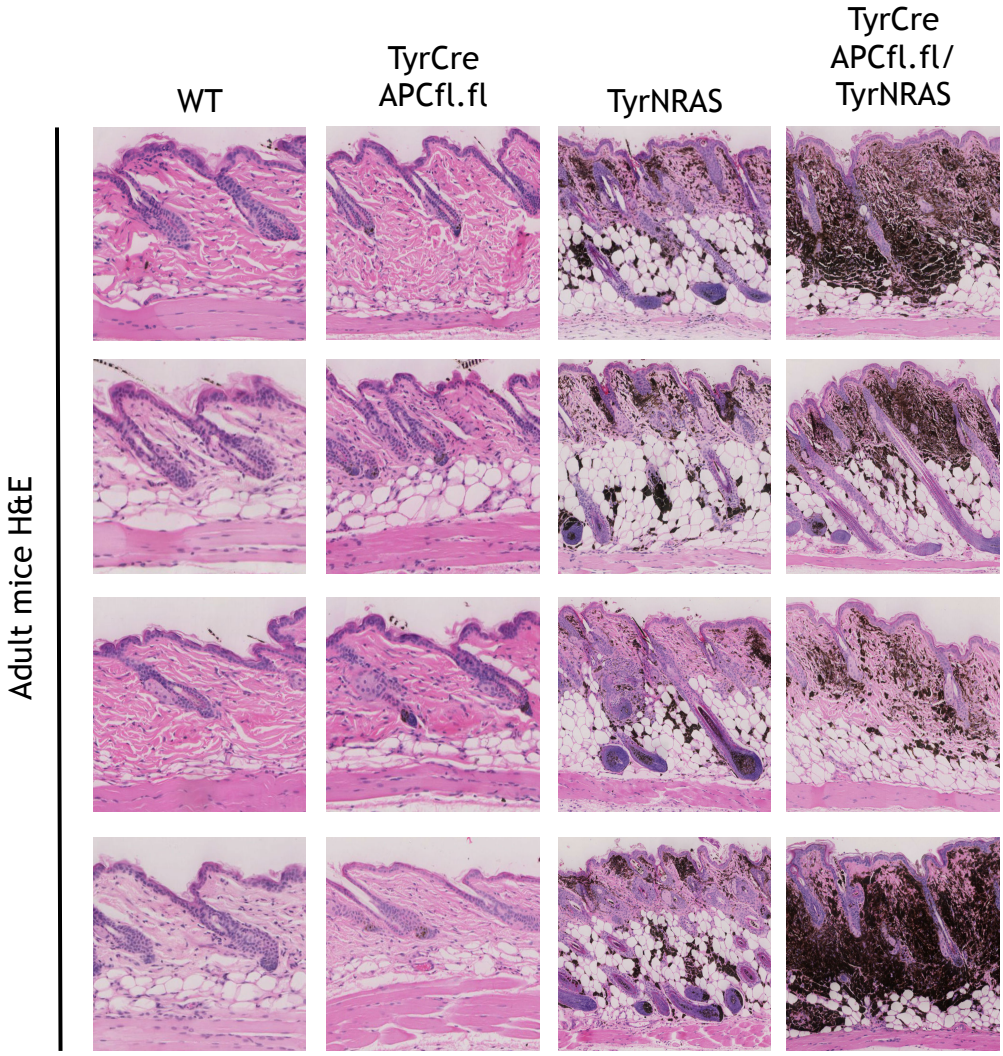

Figure 6.4 Adult H&E sections of all mouse genotypes of interest.
Representative H&E images of 4 adult mice (aged >60 days) for each genotype of interest (WT, TyrCreAPCfl.fl, TyrNRAS, and TyrCreAPCfl.fl/TyrNRAS). The presence of melanin (brown) between hair follicles is confined to the dermis, showing no signs of malignancy.

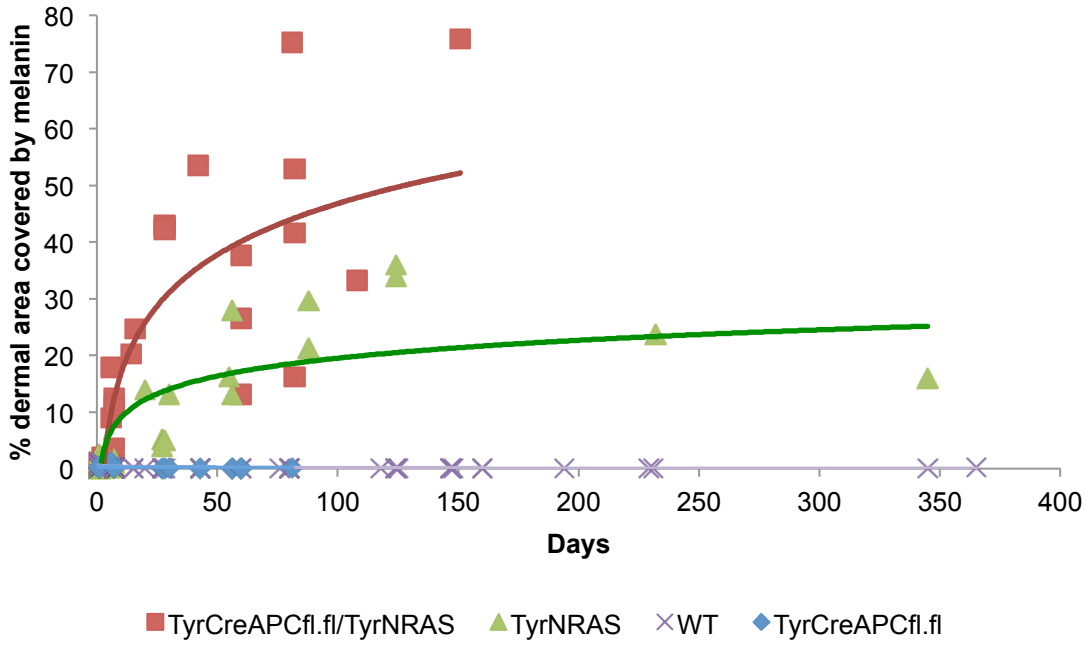

Figure 6.5 Activated Wnt signaling causes an increase in melanocyte proliferation but it is apparently not sustained.
Mice were culled at the indicated points and the amount of dermal melanin present within the skin was measured. Melanin accumulation was used to indicate melanocyte presence as S100 staining was shown to closely mirror the presence of melanin. As WT and TyrCreAPCfl.fl mice did not contain interfollicular melanocytes, melanin was not present in the dermis as indicated by all measured samples lying along the X-axis. TyrNRAS mice became pigmented but melanin accumulation ends soon after birth. TyrCreAPCfl.fl/TyrNRAS mice become more pigmented as the amount of melanin continues to increase into young adulthood before eventually plateauing.

	WT	TyrCreAPCfl.fl	TyrNRAS	TyrCreAPCfl.fl/ TyrNRAS
WT		1	$9.1x10^{-5}$ *	$4.8x10^{-16}$ *
TyrCreAPCfl.fl			$1.5x10^{-2}$ *	$7.8x10^{-10}$ *
TyrNRAS				$9.2x10^{-6}$ *
TyrCreAPCfl.fl/TyrNRAS				

* significant (pairwise comparison p-value < 0.05, bonferroni adjusted)

Analysed factor	Logarithmic R^2
WT	0.484
TyrCreAPCfl.fl	0.144
TyrNRAS	0.682
TyrCreAPCfl.fl/TyrNRAS	0.644

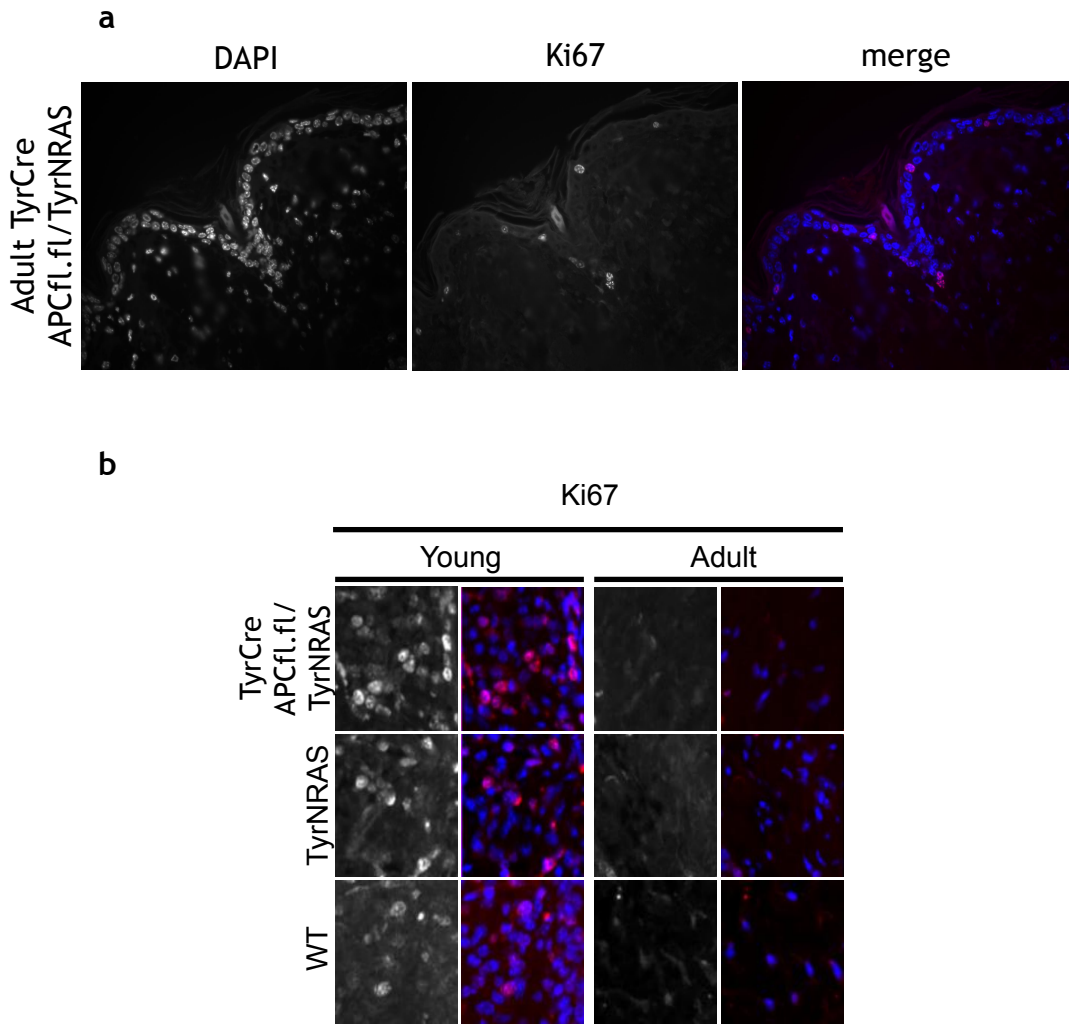

Figure 6.6 Melanocytes in adult TyrCreAPCfl.fl/TyrNRAS mice are not proliferating.
TyrCreAPCfl.fl/TyrNRAS adult skin was stained with Ki67 using IF to observe if melanocytes were proliferating. (a) Representative image showing that dermal cells (melanocytes) do not stain positive for Ki67 while many cells within the epidermis do. (b) Magnified dermal areas of the skin showing Ki67 in indicated genotype in young (2-7 days) and adult (>60 days) mice. Left S100 alone, right S100 (red) merged with DAPI (blue). Note that cell density is drastically decreased in adult mice as indicated by a decrease in DAPI (blue).

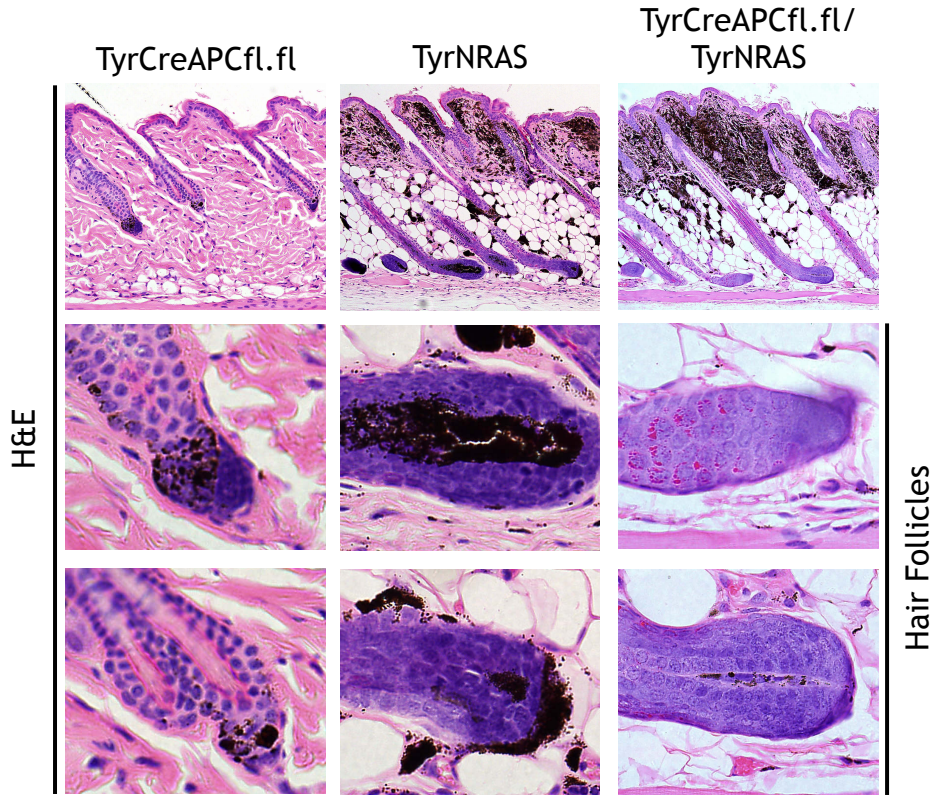

Figure 6.7 Melanin is absent from the hair bulb of TyrCreAPCfl.fl/TyrNRAS mice.
Representative H&E images of adult mice (aged >60 days) for each indicated genotype. Lower images contain magnified hair bulbs present in upper images to better show the presence and absence of melanin (brown/black).

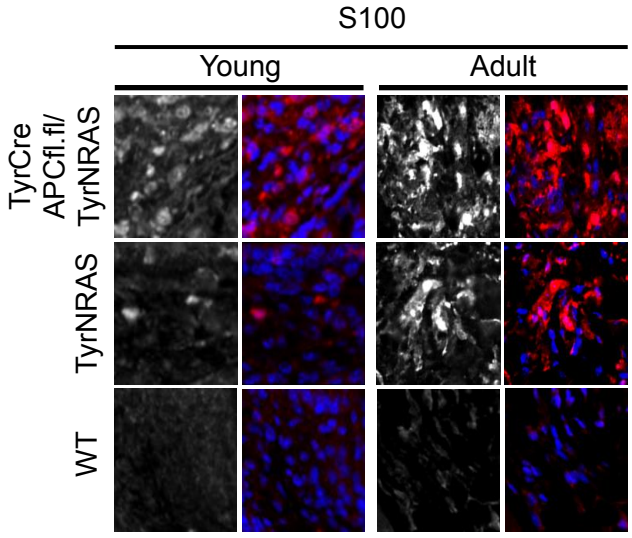

Figure 6.8 TyrCreAPCfl.fl/TyrNRAS mice show a marked increase in melanocytes.
Representative staining for melanocytes using IF for S100 in young (2-7 days) and adult (>60 days) mice of the indicated genotype. Shown are magnified dermal areas of the skin. Left S100 alone, right S100 (red) merged with DAPI (blue).

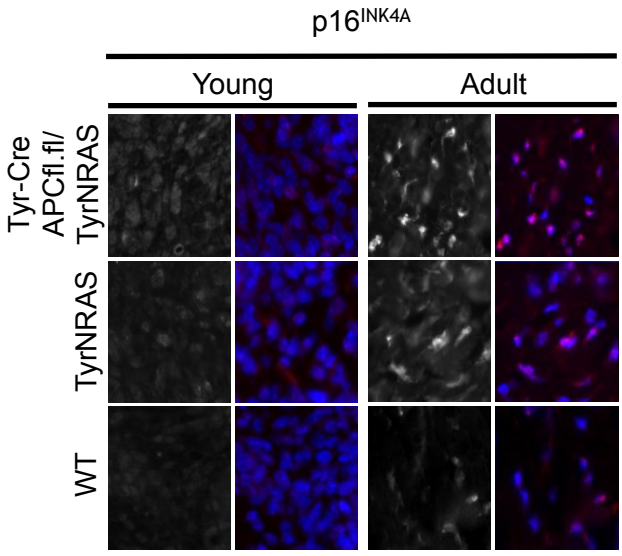

Figure 6.9 Adult mouse melanocytes express the senescence marker p16^{INK4A}
Representative staining for p16^{INK4A} using IF in young (2-7 days) and adult (>60 days) mice of the indicated genotype. The p16^{INK4A} antibody clone F12 was used as it has previously been shown to work in mouse cells by IF [331]. Shown are magnified dermal areas of the skin. Left p16^{INK4A} alone, right p16^{INK4A} (red) merged with DAPI (blue).

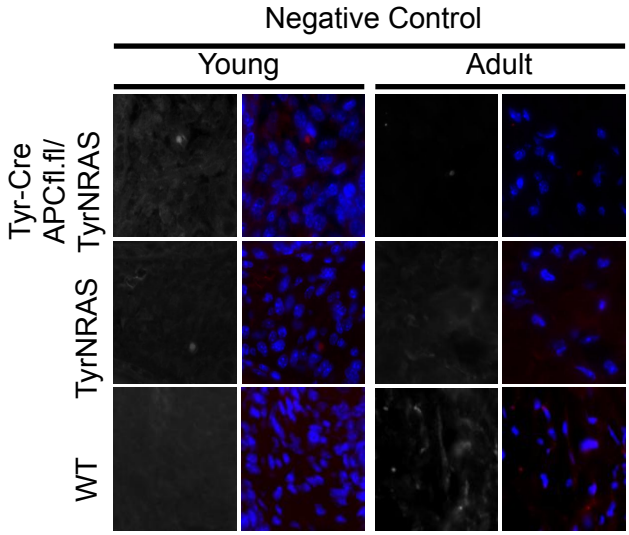

Figure 6.10 Negative control for mouse skin immunofluorescence
Representative staining for control IgG using IF in young (2-7 days) and adult (>60 days) mice of the indicated genotype. Mouse IgG used as control to identify any background staining when using anti-mouse antibodies (such as $p16^{INK4A}$ clone F12). Shown are magnified dermal areas of the skin. Left mouse IgG alone, right mouse IgG (red) merged with DAPI (blue).

6.3 Discussion

Using a murine model I have shown that the activation of Wnt signaling in the presence of an oncogene potentiates oncogene-induced proliferation of melanocytes. However, as the oncogene-expressing melanocytes still become senescent in the presence of Wnt signaling, it is thought that the onset of oncogene-induced senescence is merely delayed in the presence of activated Wnt signaling. This delay allows for an overgrowth of melanocytes resulting in a benign neoplastic melanocytic growth reminiscent of a nevus.

As many human melanomas exhibit activated Wnt signaling, and previous research has shown that a stabilized beta-catenin allele drives escape from NRAS-induced senescence to ultimately melanoma progression, it is thought that our system will also eventually result in a similar fate [327,331]. However, it is important to emphasize that my data indicates that progression likely requires additional genetic and/or epigenetic events – and activation of NRAS and Wnt signaling is not sufficient for melanoma. To date I have not observed melanomas in any of our TyrCreAPCfl.fl/TyrNRAS mice. However, due to debilitating behavioral issues, mice needed to be culled by 150 days of age. This relatively short time is likely insufficient to acquire additional genetic and/or epigenetic alterations that are presumably required to fully escape senescence and progress to melanoma, such as inactivation of PTEN [259,391,392].

When working with this mouse model it needs to be considered how faithfully the inactivation of APC recapitulates the situation of human nevi. In TyrCreAPCfl.fl/TyrNRAS mice, all the melanocytes within a mouse contain an activated oncogene and activated Wnt signaling. Although it has not been analyzed to date, the presence of an activated oncogene is thought to be specific to nevus melanocytes and this thesis shows that Wnt signaling is only present in the upper, least mature portion of a nevus. Therefore the TyrCreAPCfl.fl/TyrNRAS mouse can perhaps be thought of as a giant nevus with traits reminiscent of the upper portion of the nevus. Ideally, the melanocytes within the TyrCreAPCfl.fl/TyrNRAS mice should be stained for markers of active

Wnt signaling to confirm its activation. An additional caveat to this mouse model is that, to my knowledge, human nevi have not been shown to harbor genetic alterations in the Wnt pathway. Instead, activation of Wnt signaling in nevi likely depends on extracellular cues. In time, it should be possible to model this in a mouse. With the aid of additional, better fitting, mouse models a better understanding can be reached regarding the influence of Wnt on nevus formation.

7 Discussion

7.1 Summary

Here I present several lines of evidence to suggest that the formation of nevi results from a transient bypass of senescence due to activated Wnt signaling in melanocytes. Proliferation-promoting Wnt target genes, c-Myc, Cyclin D1 and MITF, were found repressed in senescent melanocytes in culture and upon ectopic repression of Wnt signaling a senescence-like state was triggered in cultured melanocytes. Therefore, repression of proliferation-promoting Wnt targets is linked to senescence of melanocytes. In contrast, nuclear beta-catenin, c-Myc, and Cyclin D1 are expressed in many nevus melanocytes and, compared to lone epidermal $p16^{INK4A}$-positive melanocytes, their expression correlates with a prior hyperproliferation to form a nevus. Lastly, in a mouse model, activation of Wnt signaling delays, but does not bypass, proliferation arrest in oncogenic NRASQ61K-expressing cells, ultimately generating a non-malignant nevus-like hyperproliferation of $p16^{INK4A}$-expressing melanocytes.

According to the current prevailing view, nevi form due to a simple clonal hyperproliferation of oncogene-expressing melanocytes, that are ultimately arrested and prevented from progression to melanoma by oncogene-induced senescence of the melanocytes. While my model is broadly consistent with this model, my model includes the crucial distinction that in the absence of Wnt signaling an activated oncogene fails to generate a nevus. Originally presented in the Introduction of Chapter 5, several paradoxical features of nevi can now be understood according to my revised model of nevogenesis: specifically, that nevi result from a transient delay of oncogene-induced senescence and resultant hyperproliferation of oncogene-expressing melanocytes, driven by activated Wnt signaling.

These paradoxical features are re-stated below:

Paradox 1: Nevi are large, containing 10s or 100s of thousands of cells, all derived from clonal hyperproliferation of a single oncogene-expressing melanocyte [3,9]

Paradox 2: Nevi typically develop *in utero* (congenital nevi) or are acquired in childhood and adolescence, but new nevi rarely form in adulthood [374].

Paradox 3: About 20% of human melanomas are thought to arise from human benign nevi [5-9].

Paradox 4: Nevi exhibit intra-nevus heterogeneity, typically showing increasing unexplained histological "maturation" in the deeper portions of the lesion [374,375].

The first paradox associated with the prevailing model of nevogenesis is that nevi are large, containing 10s or 100s of thousands of cells, all derived from clonal hyperproliferation of a single oncogene-expressing melanocyte. Previous findings have shown that the activation of mitogenic oncogenes such as RAS are able drive proliferation followed by senescence as soon as replication stress or reactive oxygen species reach a critical level to execute a DNA damage checkpoint response [38,39]. Typically, onset of senescence is associated with a brief “proliferative burst”. However, at least *in vitro*, this proliferative response is minimal compared to the roughly 14-17 population doublings needed to generate an average sized nevus. Therefore, the rather large size of a nevus is not consistent with an efficient senescence-associated proliferation arrest. In this thesis, I present evidence that elevated Wnt signals delay senescence to allow the hyperproliferation of oncogene-expressing melanocytes to form a nevus.

A second paradoxical feature associated with the current model of nevogenesis is that nevi typically develop *in utero* (congenital nevi) or are acquired in childhood and adolescence, but new nevi rarely form in adulthood. If nevi result simply from an activated oncogene in a melanocyte, they might be expected to increase in number with age, as the presumed mutational load increases. However, this is generally not the case. Melanoblasts are known to receive and

depend upon Wnt signals for their migration out of the neural crest towards the epidermis as well as their differentiation into mature melanocytes [206-209]. The presence of this Wnt signaling may therefore contribute to senescence delay and explain, in part, why human nevi preferentially grow *in utero* (congenital nevi) or are acquired during childhood and adolescence, but rarely form in adulthood [374,393]. Other factors, such as declining telomere length with age, are also likely to contribute [393]. But, essentially, I propose that nevi are a specific neoplasia whose formation depends on acquisition of an oncogene in a specific developmental context.

The third paradox is that nevi exhibit increasing histological "maturation" in the deeper portions of the lesion. Although maturation is used commonly in the clinic for diagnosis and prognosis, the molecular basis of maturation remains unknown. Yet, the concept of maturation does not sit well with the simple model of nevi resulting from straightforward oncogene-induced clonal hyperproliferation and senescence, and implies a level of homogeneity in the resultant nevus melanocyte population. In this study I show that Wnt signaling is preferentially active in the least mature, more proliferative component of the nevus that appears to be of greater malignant potential [10,11,376]. I propose that variable maturation across a nevus reflects variations in the senescence program, in part due to variations in Wnt signaling.

Lastly, the fourth paradox associated with the current model of nevogensis is that roughly 20% of human melanomas are thought to arise from human benign nevi [5-9]. Although this figure is inherently hard to quantitate, there is a general agreement among clinicians that a significant percentage of melanomas originate in this manner (Dr. Hong Wu, personal communication). This is not consistent with a failsafe mechanism of senescence-associated tumor suppression. According to our model, incomplete maturation associated with activated Wnt signaling is indicative of impaired or flawed senescence and so elevated malignant potential. Moreover, Wnt signaling is activated in some human melanomas and has reported to be a driver of the disease in a mouse model [327,328,331,394]. Therefore, nevi not only reflect impaired senescence but, because they continue to exhibit activated Wnt signaling, they remain

predisposed to malignant melanoma. In essence, I propose that activated Wnt signaling in nevus melanocytes continues to destabilize the senescence program, even after proliferation arrest has been achieved, thus driving malignancy in rare cases.

As with any study, there exist caveats that need to be addressed in my data and unanswered questions. Some of these include:

1. How conclusive is the evidence that repression of proliferation-promoting Wnt target genes drives melanocyte senescence?
2. If proliferation-promoting Wnt targets induce proliferation, why aren't most nevus cells proliferating?
3. How can I better show that Wnt signaling is required for nevus formation?
4. What is the difference between a single $p16^{INK4A}$ positive melanocyte and a nevus melanocyte at the molecular level?

In order to show that the repression of specific proliferation-promoting Wnt targets drives senescence, a more precise method of regulating Wnt signaling will have to be employed than total down regulation of Wnt signaling, as done in Chapter 4. Such methodology may include the use of specific short hairpins to target specific genes of interest, such as c-Myc, Cyclin D1, and MITF. As the hypothesis proposed in this thesis focuses on proliferation-promoting Wnt targets, the use of dnTCF is likely excessive and limits the conclusion that specifically repression of proliferation-promoting Wnt targets drives melanocyte senescence. Nonetheless, as many direct Wnt target genes are still expressed during senescence, it is likely the repression of those Wnt target genes that are repressed during senescence (e.g. key proliferation-promoting genes, c-Myc, MITF, and Cyclin D1) that play the major role in the dnTCF-induced senescen
ce response.

Findings in this thesis have shown that melanocytes within a nevus express proliferation-promoting Wnt target genes. As these genes are known to induce proliferation one would expect many more cells to be proliferating within a nevus. I propose that the activity of tumor suppressor genes, such as $p16^{INK4A}$,

override the effects of proliferation-promoting genes. However, $p16^{INK4A}$ expression is not linked to maturation and Wnt signaling, as would be expected if $p16^{INK4A}$ preferentially acted in areas of higher proliferative potential or enforced stable arrest in those areas of lower proliferative potential. In fact, nevi stain mosaically for $p16^{INK4A}$. It is possible that additional tumor suppressors (such as $p15^{INK4b}$) function within nevi to inhibit the proliferative effects of proliferation-promotion Wnt target genes.

Results in this thesis have shown that nevi contain markers for active Wnt signaling and that upon activation of Wnt signaling, in the presence of an activated oncogene, mouse melanocytes proliferate and then senesce to generate a nevus-like lesion. However, I have not yet directly shown that Wnt signaling is required for nevus formation. One of the most direct methods to test the requirement of Wnt signaling in nevus formation is through administration of a Wnt inhibitor to a mouse that develops nevi. Specifically, Wnt signaling may be blocked in TyrCreER-$BRAF^{+/LSL-V600E}$ mice using an anti-LRP6 antibody [136,395]. These mice use a tamoxifen inducible Cre to trigger expression of activated BRAFV600E from the endogenous BRAF promoter specifically in melanocytes. Upon induction of BRAFV600E, the skin becomes hyperpigmented and approximately 2 months post induction nevi appear harboring senescent melanocytes. Previous findings have shown that antagonistic anti-LRP6 antibodies block Wnt-driven tumor growth *in vivo* [395]. Therefore, according to the findings reported in this thesis, it is anticipated that when Wnt signaling is inhibited in the presence of an activated oncogene in melanocytes, the formation of nevi will be inhibited. This experiment is ongoing.

The findings presented in this thesis focus on the role of Wnt signaling on nevogenesis. As nevi are thought to originate from solitary melanocytes in the epidermis I also examined the status of Wnt signaling in solitary epidermal melanocytes. Surprisingly, I found that these melanocytes are often also $p16^{INK4A}$ positive as they are within a nevus; but unlike nevi epidermal melanocytes never stain positive for markers of activated Wnt signaling. I propose that epidermal melanocytes are senescent as judged by the presence of $p16^{INK4A}$ and remain solitary due to the absence of activated Wnt signaling. A major caveat to this

model is that it is not known if isolated melanocytes contain the BRAFV600E mutation. Although this would be very hard to analyze due to technical reasons, results in this thesis indicate the importance of defining the molecular status of these cells. Regardless, according to this model, epidermal melanocytes only progress to nevi upon an appropriate and well-timed expression of Wnt signaling.

7.2 Final discussion and conclusions

The aim of this PhD was to examine melanocyte senescence as it pertains to one of the most commonly used *in vivo* models of senescence, benign human nevi. Key discoveries of this PhD were made *in vitro*, *in situ*, as well as *in vivo*.

In vitro, evidence was obtained that the repression of the proliferation-promoting Wnt target genes may drive senescence in BRAFV600E transduced senescent melanocytes.

In situ, senescent nevus melanocytes harbour markers of activated Wnt signaling, expressed inversely to maturation, an indicator of lower malignant potential. Also, dermal melanocytes along the basement membrane were found to be in a senescent-like state, as judged by expression of $p16^{INK4A}$ and lack of expression of proliferation-promoting Wnt targets, perhaps explaining why they remain solitary.

In vivo, the activation of Wnt signaling was able to drive hyperproliferation of oncogene-expressing melanocytes, but the proliferation advantage is not continuous as these cells ultimately senesce.

From these findings I propose a revised model that human benign nevi do not reflect a *bona fide* efficient senescence program. Rather, they result from a transient delay of OIS and resultant hyperproliferation of oncogene-expressing melanocytes, driven by activated Wnt signaling. Therefore, nevi harbour activated Wnt signaling that contributes to a partial bypass or impairment of senescence allowing for a proliferative expansion to form a nevus that is already

at an increased risk of progression to cancer. Importantly, the persistence of Wnt signalling in these lesions likely continues to destabilize the senescence program, thereby promoting their progression to cancer in a small minority of cases.

Throughout the time spent doing research for the completion of my PhD I have noticed a clear disconnect between the clinic and basic research science. For instance, aspects such as maturation are routinely used clinically as an indicator of lower malignant potential, yet its molecular basis remains unknown. In addition, according to the research community's current model of nevogenesis, nevi form due to clonal hyperproliferation of oncogene-expressing melanocytes, but are ultimately arrested by OIS. This model sits uneasy with clinical dermatologists and pathologists, as there are many paradoxical features associated with this model. This thesis describes a new model of nevogenesis, which states that nevi result from a transient delay of OIS resulting in a hyperproliferation of oncogene-expressing melanocytes due to Wnt signaling. This new model can clarify many once paradoxical features and thereby shortens the disconnect currently existing between the clinic and research community. I believe that a close relationship between clinicians and basic scientists will lead to many pivotal discoveries and save valuable time in future research that will ultimately lead to new much-needed treatments and cures for such pathologies as melanoma.

8 Appendix

8.1 Supplementary Lists

		Rel to Empty Vector		Rel to Uninfected	
Gene symbol	AffyID	fold change	BH-fdr	fold change	BH-fdr
CXCR4	217028_at	620.0568	0.0003	655.6366	0.0002
PLA2G7	206214_at	307.6582	0.0003	286.8904	0.0002
S100A8	202917_s_at	302.9005	0.0002	296.5189	0.0002
CCL20	205476_at	267.5687	0.0002	223.6915	0.0003
IL1A	210118_s_at	237.8169	0.0001	249.3273	0.0001
S100A8	214370_at	193.8920	0.0002	184.7898	0.0002
IL8	202859_x_at	158.0498	0.0004	145.8184	0.0004
LYZ	213975_s_at	49.7107	0.0003	48.3588	0.0003
PTX3	206157_at	49.6188	0.0004	62.1487	0.0003
IRAK2	231779_at	48.9004	0.0012	49.2873	0.0013
CXCR4	211919_s_at	48.8004	0.0008	56.4106	0.0004
LYZ	1555745_a_at	47.9220	0.0003	40.2809	0.0007
CXCR4	209201_x_at	39.9565	0.0005	41.3716	0.0009
CXCL2	209774_x_at	35.7590	0.0007	33.5355	0.0014
SCG2	204035_at	35.4289	0.0002	35.3762	0.0002
CCR1	205098_at	34.9293	0.0004	15.2854	0.0003
IL8	211506_s_at	23.8834	0.0009	18.9141	0.0014
MGLL	225102_at	18.9092	0.0005	20.7021	0.0011
TNFAIP6	206026_s_at	11.8875	0.0019	9.4500	0.0033
C3AR1	209906_at	8.4412	0.0066	6.2422	0.0108
GPR68	229055_at	6.6490	0.0047	5.9627	0.0063
CEBPB	212501_at	6.2443	0.0003	4.8390	0.0017
ADORA3	223660_at	6.1804	0.0132	5.0488	0.0274
ANXA1	201012_at	6.1476	0.0003	7.1199	0.0002
MGLL	211026_s_at	5.7742	0.0015	6.6443	0.0029
TNFAIP6	206025_s_at	5.0567	0.0063	4.1345	0.0071
AOX1	205083_at	4.7398	0.0153	4.2685	0.0199
CXCL1	204470_at	3.9186	0.0043	3.7274	0.0085
RIPK2	209545_s_at	3.6591	0.0033	4.0558	0.0046
CHST2	203921_at	3.4753	0.0022	3.0326	0.0009
AFAP1L2	226829_at	3.2378	0.0313	4.1021	0.0262
MBL2	207256_at	3.1793	0.0042	3.2404	0.0095
AOX1	205082_s_at	2.9754	0.0200	2.9965	0.0217
TNFRSF1A	207643_s_at	2.8443	0.0009	3.0650	0.0018
ANXA1	233011_at	2.6774	0.0093	2.6148	0.0114
CCL3	205114_s_at	2.6619	0.0332	1.7348	0.1135
HDAC5	229408_at	2.1210	0.1106	1.9897	0.1437
CCR1	205099_s_at	2.1144	0.0173	1.9373	0.0344
PARP4	202239_at	2.0574	0.0061	1.8711	0.0094
NMI	203964_at	2.0351	0.0165	1.7685	0.0333
HDAC5	202455_at	2.0162	0.0486	1.5386	0.0634
F11R	224097_s_at	1.9293	0.0319	1.8773	0.0168
AOC3	204894_s_at	1.8694	0.2107	1.8343	0.2208
IL1RAP	205227_at	1.7825	0.1465	1.7893	0.1004
NFKB1	209239_at	1.7649	0.0047	2.0085	0.0177

HRH1	205579_at	1.7455	0.0473	1.7757	0.0440
CXCL2	1569203_at	1.6225	0.0383	1.6037	0.0330
RIPK2	209544_at	1.5971	0.0210	1.7352	0.0496
IL1RAP	210233_at	1.5872	0.0053	1.2282	0.1636
NFE2L1	200758_s_at	1.5000	0.0124	1.3539	0.0806
GHRL	237647_at	1.4647	0.2766	1.9238	0.1021
F11R	221664_s_at	1.3827	0.0641	1.0240	0.8538
NFATC3	210555_s_at	1.3584	0.1597	1.1678	0.3750
CXCL6	206336_at	1.3347	0.1895	1.2441	0.4253
ADORA1	205481_at	1.3250	0.1023	1.2026	0.2392
LTB4R	236172_at	1.3131	0.0990	1.4042	0.1349
LTB4R	210128_s_at	1.3081	0.1917	1.4417	0.1128
HRH1	205580_s_at	1.2941	0.1585	1.1852	0.2011
CDO1	204154_at	1.2923	0.4999	1.7500	0.2072
RELA	230202_at	1.2729	0.1930	1.1788	0.2445
PTAFR	206278_at	1.2683	0.2444	1.1064	0.4660
HDAC9	1552760_at	1.2603	0.3014	-1.2426	0.5629
NFE2L1	200759_x_at	1.2530	0.0987	1.1255	0.0455
F11R	223000_s_at	1.2476	0.0617	1.2893	0.0654
CXCL2	230101_at	1.2345	0.2113	1.0848	0.4705
IRAK2	1553740_a_at	1.2181	0.1962	1.1023	0.4050
CCR5	206991_s_at	1.2067	0.1734	1.1051	0.5622
FOS	209189_at	1.1696	0.2646	1.1341	0.4951
CX3CL1	823_at	1.1586	0.3598	1.0227	0.9159
CXCL11	210163_at	1.1578	0.2833	1.2260	0.0717
ELF3	229842_at	1.1342	0.5919	1.0109	0.9929
NFATC3	207416_s_at	1.1327	0.4789	1.2389	0.1239
TGFB1	203085_s_at	1.1295	0.2522	-1.1214	0.2837
RELA	201783_s_at	1.1179	0.3019	-1.0004	0.9768
CXCL11	211122_s_at	1.1141	0.4834	1.1994	0.1518
IL17C	224079_at	1.1058	0.3911	1.0391	0.6397
S100A9	203535_at	1.1019	0.2534	-1.0102	0.9188
NFRKB	213028_at	1.0996	0.3721	1.0811	0.2685
ABCF1	200045_at	1.0985	0.4210	1.0685	0.2183
ADORA3	206171_at	1.0973	0.2753	1.1038	0.2398
CCL13	216714_at	1.0871	0.4884	1.0619	0.6186
NFE2L1	214179_s_at	1.0869	0.3999	-1.1044	0.2618
AHSG	204551_s_at	1.0833	0.4728	1.0656	0.3259
PRDX5	222994_at	1.0746	0.2632	1.0532	0.4842
CCL24	221463_at	1.0713	0.5284	-1.1058	0.6150
CCL23	210548_at	1.0688	0.3629	1.0011	0.9778
CCL13	206407_s_at	1.0681	0.2348	-1.0675	0.5791
NLRP3	216015_s_at	1.0640	0.3329	1.0263	0.7049
TGFB1	203084_at	1.0636	0.4280	-1.0679	0.2717
KRT1	205900_at	1.0594	0.6682	-1.0024	0.9565
AGER	217046_s_at	1.0571	0.6938	-1.0186	0.8759
NLRP3	207075_at	1.0570	0.7453	1.0267	0.8992
HDAC9	234393_at	1.0482	0.6671	-1.2724	0.4834
CX3CL1	203687_at	1.0481	0.6968	1.1612	0.1687
GHRL	223862_at	1.0471	0.6782	-1.1729	0.3961
GHSR	221360_s_at	1.0452	0.3946	-1.0771	0.6776
IL13	207844_at	1.0410	0.4712	1.0755	0.3457
APOL3	221087_s_at	1.0410	0.7995	1.0809	0.5987
ALOX15	207328_at	1.0407	0.2473	-1.0269	0.6083
PLA2G2E	221389_at	1.0389	0.8144	-1.1177	0.6047
LBP	211652_s_at	1.0374	0.7175	-1.0838	0.2873
CYBB	217431_x_at	1.0370	0.4951	1.0224	0.5511
NFRKB	206968_s_at	1.0348	0.8457	-1.0642	0.6257
LTB4R	216388_s_at	1.0335	0.5585	-1.0602	0.4984

CCL11	210133_at	1.0267	0.5845	1.0023	0.9757
KLRG1	210288_at	1.0254	0.8651	1.0935	0.4579
CRP	205753_at	1.0252	0.6718	-1.0207	0.6686
CCR2	206978_at	1.0232	0.8700	-1.0224	0.8148
ALOX5AP	204174_at	1.0211	0.9418	1.0389	0.8595
IL18RAP	207072_at	1.0203	0.6458	-1.0423	0.8264
CCL23	210549_s_at	1.0201	0.9061	1.0558	0.6870
ELF3	201510_at	1.0189	0.7409	1.0804	0.4372
ELF3	210827_s_at	1.0179	0.9254	-1.0796	0.6751
NLRP3	216016_at	1.0138	0.8239	1.0296	0.5617
CCR3	208304_at	1.0129	0.9169	-1.0281	0.7647
CCR2	207794_at	1.0116	0.8002	-1.0840	0.5522
NFX1	202584_at	1.0112	0.8743	1.0651	0.2344
KNG1	217512_at	1.0105	0.9534	1.0142	0.9281
IL9	208193_at	1.0102	0.7186	-1.0128	0.9519
IL8RB	207008_at	1.0089	0.9391	1.0626	0.4682
ORM1	205040_at	1.0085	0.9197	-1.0522	0.7530
RELA	209878_s_at	1.0083	0.9127	-1.0106	0.7883
CYP4F11	206153_at	1.0067	0.9268	-1.0351	0.3046
AIF1	215051_x_at	1.0058	0.9646	-1.1321	0.3488
C2 /// CFB	202357_s_at	1.0057	0.9603	-1.0624	0.4753
NFX1	210268_at	1.0044	0.9899	1.1126	0.7570
AIF1	209901_x_at	-1.0010	0.9943	-1.0743	0.4477
CCL5	1555759_a_at	-1.0043	0.9915	1.0703	0.4223
CXCL10	204533_at	-1.0045	0.9602	-1.1255	0.5116
ADORA1	216220_s_at	-1.0053	0.9442	1.0029	0.9931
TACR1	230908_at	-1.0073	0.8200	-1.0675	0.4963
AIF1	213095_x_at	-1.0114	0.9350	1.0707	0.4338
CCR7	206337_at	-1.0130	0.8317	-1.0978	0.2482
NFRKB	237209_s_at	-1.0137	0.9601	-1.0709	0.6214
CD40LG	207892_at	-1.0138	0.8760	-1.0427	0.6609
PLA2G2D	220423_at	-1.0139	0.8694	-1.0307	0.6837
CCL22	207861_at	-1.0154	0.8155	-1.1858	0.0306
ORM1	214465_at	-1.0171	0.8793	-1.1329	0.3814
CCL21	204606_at	-1.0222	0.7721	-1.0779	0.6195
CD97	202910_s_at	-1.0227	0.7391	-1.0353	0.5851
CCL4	204103_at	-1.0229	0.8402	-1.1154	0.6306
XCR1	221468_at	-1.0239	0.6996	-1.1265	0.7177
ORM1	205041_s_at	-1.0254	0.8235	-1.0853	0.4768
NFATC4	205897_at	-1.0275	0.4165	-1.1164	0.2017
NFX1	202585_s_at	-1.0286	0.8435	-1.1036	0.7139
APCS	206350_at	-1.0289	0.8144	1.0193	0.9353
CCL26	223710_at	-1.0301	0.6491	-1.0069	0.7501
IL20	224071_at	-1.0309	0.8317	-1.1374	0.5064
TACR1	208048_at	-1.0319	0.8314	-1.1165	0.4348
NFATC3	210556_at	-1.0330	0.7255	1.0891	0.5317
IL5	207952_at	-1.0334	0.8050	1.0107	0.9801
F11R	222354_at	-1.0338	0.7494	-1.1279	0.4238
PTAFR	211661_x_at	-1.0425	0.4780	1.0017	0.9695
S100A12	205863_at	-1.0459	0.2419	-1.0829	0.2004
HDAC4	1554322_a_at	-1.0459	0.5427	-1.2902	0.0719
NOD1	224190_x_at	-1.0470	0.2413	-1.1843	0.1306
CRP	37020_at	-1.0474	0.4383	-1.0143	0.9339
GPR68	211249_at	-1.0482	0.7809	-1.1387	0.4366
RAC1	208641_s_at	-1.0497	0.1246	-1.1008	0.0470
RAC1	208640_at	-1.0521	0.3138	-1.0926	0.1038
CYBB	203923_s_at	-1.0532	0.8156	1.0885	0.6819
IL8RA	207094_at	-1.0533	0.7112	1.1140	0.1143
GHSR	224554_at	-1.0609	0.5602	-1.0466	0.8127

KNG1	206054_at	-1.0638	0.7162	-1.1263	0.4849
NFX1	1553348_a_at	-1.0681	0.5661	-1.1999	0.2635
SELE	206211_at	-1.0782	0.0592	-1.1479	0.1436
CYBB	203922_s_at	-1.0784	0.3271	1.0425	0.7702
IFNA2	211338_at	-1.0785	0.6028	-1.0388	0.7401
VPS45	207967_at	-1.0824	0.6290	-1.1833	0.3513
PRDX5	1560587_s_at	-1.0853	0.3503	-1.1198	0.2164
AGER	210081_at	-1.0889	0.4702	-1.0122	0.9611
AIF1	207823_s_at	-1.0916	0.2715	-1.1353	0.2838
HDAC9	1552758_at	-1.0916	0.5224	-1.2056	0.1363
LBP	214461_at	-1.0977	0.2294	-1.0418	0.5310
SCYE1	235594_at	-1.0981	0.6380	-1.3140	0.3207
BLNK	207655_s_at	-1.0989	0.5986	-1.0799	0.3387
TACR1	208049_s_at	-1.1005	0.4225	-1.0228	0.7759
AOAH	205639_at	-1.1053	0.1893	-1.3629	0.1639
IRAK2	1553739_at	-1.1076	0.5784	-1.0759	0.4531
SIGIRR	52940_at	-1.1091	0.4604	-1.0581	0.6824
CD40	35150_at	-1.1119	0.2920	-1.1343	0.1139
MEFV	208262_x_at	-1.1153	0.4316	-1.1860	0.2166
TACR1	210637_at	-1.1182	0.4300	1.0374	0.8235
SIGIRR	218921_at	-1.1212	0.2624	-1.3239	0.1479
ADORA2A	205013_s_at	-1.1257	0.3437	-1.2221	0.2238
CD40	205153_s_at	-1.1376	0.0251	-1.3261	0.0798
C2	1554533_at	-1.1431	0.4486	-1.2432	0.1719
AHSG	210929_s_at	-1.1449	0.4767	1.0667	0.5771
IL10RB	209575_at	-1.1494	0.4691	-1.5035	0.0078
NFX1	1553103_at	-1.1511	0.1904	-1.2348	0.2046
C2	203052_at	-1.1548	0.0791	-1.0402	0.2505
CCR4	208376_at	-1.1754	0.0502	-1.0940	0.2752
SCYE1	202541_at	-1.1814	0.0770	-1.2542	0.1820
CXCL9	203915_at	-1.1822	0.1198	-1.1763	0.0741
RAC1	1567457_at	-1.1908	0.1838	-1.3602	0.2987
CHRFAM7A	210123_s_at	-1.1931	0.5063	-1.0677	0.4403
RAC1	1567458_s_at	-1.2005	0.0777	-1.4299	0.1323
NOX4	236843_at	-1.2030	0.3844	-1.3415	0.1489
SCYE1	227605_at	-1.2134	0.0310	-1.3062	0.0829
CCL5	1405_i_at	-1.2515	0.0883	1.1504	0.3261
VPS45	209268_at	-1.2584	0.1269	-1.2144	0.2159
CD40	222292_at	-1.3038	0.1781	-1.1028	0.3930
NFATC4	213345_at	-1.3115	0.0707	-1.1673	0.1766
IL1A	208200_at	-1.3592	0.4520	1.2507	0.2593
SCYE1	202542_s_at	-1.3993	0.0153	-1.4792	0.0060
NOD1	221073_s_at	-1.4645	0.0637	-1.3607	0.0680
CCL5	204655_at	-1.5001	0.0546	-1.1294	0.2191
C5	205500_at	-1.5268	0.1037	-1.6361	0.0195
LY75	205668_at	-1.5420	0.0297	-1.1599	0.0299
HDAC4	204225_at	-1.5762	0.0051	-1.7659	0.0065
HDAC4	228813_at	-1.6223	0.0646	-1.4408	0.0807
NFRKB	237210_at	-1.6249	0.2688	-1.0563	0.6730
NOX4	219773_at	-1.6503	0.0759	-2.7326	0.0216
CD40	215346_at	-1.6660	0.0978	-1.4586	0.1083
NFATC4	236270_at	-2.0413	0.0347	-1.2461	0.3879
CYBB	233538_s_at	-2.0466	0.0072	-2.3424	0.0053
TPST1	204140_at	-2.0508	0.0344	-2.2671	0.0085
HDAC9	205659_at	-2.5564	0.0181	-4.3335	0.0131
CFH	215388_s_at	-10.5450	0.0024	-7.8734	0.0011

Supplementary List 1. GO term Inflammatory Response Genes

		Rel to Empty Vector		Rel to Uninfected	
Gene symbol	AffyID	fold change	BH-fdr	fold change	BH-fdr
IL1B	205067_at	1797.5102	0.0001	2111.7215	0.0001
AREG	205239_at	1603.0853	0.0001	1811.6004	0.0001
IL1B	39402_at	1552.2140	0.0001	1791.6728	0.0001
EREG	205767_at	885.7926	0.0002	1004.3943	0.0001
SERPINB2	204614_at	719.3037	0.0002	861.4145	0.0002
SERPINE1	202628_s_at	534.3540	0.0004	415.7154	0.0001
IGFBP3	210095_s_at	277.2909	0.0001	337.9175	0.0002
MMP10	205680_at	270.2904	0.0001	290.7277	0.0001
CCL20	205476_at	267.5687	0.0002	223.6915	0.0003
IL1A	210118_s_at	237.8169	0.0001	249.3273	0.0001
SERPINE1	202627_s_at	195.4018	0.0006	154.3629	0.0008
IL8	202859_x_at	158.0498	0.0004	145.8184	0.0004
IGFBP3	212143_s_at	118.0244	0.0002	109.2222	0.0002
TNFRSF1B	203508_at	94.4201	0.0001	101.7141	0.0001
CXCL3	207850_at	88.7776	0.0005	77.5205	0.0002
AREG	215564_at	68.6260	0.0004	82.6451	0.0003
FN1	1558199_at	60.9010	0.0007	49.7592	0.0004
MMP1	204475_at	51.0001	0.0007	20.6640	0.0005
PLAUR	210845_s_at	46.6517	0.0001	25.8433	0.0002
FN1	214702_at	44.6955	0.0044	38.0642	0.0045
EREG	1569583_at	40.1969	0.0002	46.1865	0.0002
PLAUR	211924_s_at	39.0223	0.0004	26.2752	0.0001
CXCL2	209774_x_at	35.7590	0.0007	33.5355	0.0014
TIMP1	201666_at	31.6117	0.0002	20.5237	0.0005
PLAUR	214866_at	28.2070	0.0004	17.4992	0.0008
IL8	211506_s_at	23.8834	0.0009	18.9141	0.0014
FN1	214701_s_at	7.5134	0.0004	4.0684	0.0002
TNFRSF11B	204933_s_at	7.2532	0.0026	5.5069	0.0070
ICAM1	202638_s_at	6.6126	0.0016	5.7723	0.0005
CTSB	227961_at	5.6728	0.0011	5.4078	0.0013
CTSB	213274_s_at	5.0788	0.0028	4.1913	0.0013
MMP14	160020_at	4.8865	0.0019	3.4773	0.0047
FN1	212464_s_at	4.8383	0.0005	3.4132	0.0027
FN1	216442_x_at	4.4944	0.0021	3.0716	0.0102
FN1	210495_x_at	4.2237	0.0019	2.9449	0.0068
CXCL1	204470_at	3.9186	0.0043	3.7274	0.0085
FN1	211719_x_at	3.8019	0.0014	2.6330	0.0031
MMP14	202827_s_at	3.7214	0.0044	2.7331	0.0022
ICAM1	215485_s_at	3.6130	0.0145	3.1697	0.0240
ICAM1	202637_s_at	3.0251	0.0023	3.5331	0.0039
TNFRSF1A	207643_s_at	2.8443	0.0009	3.0650	0.0018
MMP14	217279_x_at	2.8208	0.0040	2.3340	0.0279
MMP14	202828_s_at	2.7547	0.0163	2.2126	0.0054
CCL3	205114_s_at	2.6619	0.0332	1.7348	0.1135
IL6ST	204864_s_at	2.4452	0.0076	2.2657	0.0017
SERPINE1	1568765_at	2.4004	0.0153	1.9428	0.0240
CTSB	200838_at	2.3929	0.0010	2.1928	0.0004
MMP7	204259_at	2.1369	0.0279	2.1674	0.0348
CTSB	213275_x_at	2.0471	0.0048	2.0078	0.0096
TNFRSF11B	204932_at	2.0199	0.0086	1.5166	0.0126
CTSB	200839_s_at	2.0019	0.0042	1.8895	0.0059
ICAM3	204949_at	1.8924	0.0369	2.1128	0.0650
FGF7	1554741_s_at	1.7336	0.0278	1.8370	0.0374
IL6ST	204863_s_at	1.6633	0.0045	1.7249	0.0036
IL6ST	211000_s_at	1.6341	0.0018	1.7239	0.0197

IGFBP5	211959_at	1.6244	0.0103	1.6953	0.0040
CXCL2	1569203_at	1.6225	0.0383	1.6037	0.0330
IGFBP5	203426_s_at	1.5690	0.0402	1.7185	0.0103
MMP12	204580_at	1.5366	0.1178	1.4900	0.1240
FAS	216252_x_at	1.5148	0.2440	1.5735	0.0703
IGFBP5	1555997_s_at	1.4901	0.2125	1.6803	0.1328
MIF	217871_s_at	1.3975	0.0772	1.0902	0.6262
MMP3	205828_at	1.3823	0.1104	1.2495	0.2148
FAS	204780_s_at	1.3788	0.0086	1.7397	0.0206
IL6ST	234474_x_at	1.3703	0.0236	1.2611	0.1752
IL6ST	234967_at	1.3692	0.3254	1.3924	0.2936
IGFBP4	201508_at	1.3427	0.1669	1.2910	0.1657
CCL7	208075_s_at	1.3384	0.1592	1.3257	0.2098
FAS	215719_x_at	1.3358	0.2968	1.5757	0.1113
IL6ST	212196_at	1.2803	0.0488	1.3153	0.0361
IL6ST	212195_at	1.2681	0.0132	1.3519	0.1165
CXCL2	230101_at	1.2345	0.2113	1.0848	0.4705
EGFR	201984_s_at	1.2331	0.5104	1.2819	0.3549
IGFBP5	203424_s_at	1.2260	0.0622	1.2332	0.0992
PIGF	205078_at	1.2177	0.3419	1.2399	0.3467
EGFR	201983_s_at	1.1966	0.1275	1.1880	0.0776
FAS	204781_s_at	1.1928	0.4316	1.3652	0.1670
TNFRSF10C	234644_x_at	1.1868	0.1485	1.0269	0.8248
EGFR	211551_at	1.1852	0.4175	1.1671	0.4360
HGF	209961_s_at	1.1663	0.2695	1.1399	0.3261
CSF3	207442_at	1.1583	0.1488	1.2133	0.1252
CXCL11	210163_at	1.1578	0.2833	1.2260	0.0717
HGF	210998_s_at	1.1387	0.4343	1.0454	0.7946
MIP	220863_at	1.1291	0.4134	1.0434	0.8228
HGF	209960_at	1.1277	0.2589	1.0574	0.6441
IGFBP2	202718_at	1.1242	0.3510	1.0753	0.4799
CXCL11	211122_s_at	1.1141	0.4834	1.1994	0.1518
FGF7	205782_at	1.1044	0.6170	-1.0330	0.7993
FGF7	1555102_at	1.1036	0.7331	1.0975	0.7398
IL6	205207_at	1.0878	0.4145	1.0235	0.6806
CCL13	216714_at	1.0871	0.4884	1.0619	0.6186
MMP13	205959_at	1.0820	0.4368	-1.0573	0.5553
CCL1	207533_at	1.0810	0.6081	-1.0163	0.9579
CCL13	206407_s_at	1.0681	0.2348	-1.0675	0.5791
TNFRSF10C	211163_s_at	1.0649	0.8249	1.1671	0.5337
FGF7	1555103_s_at	1.0471	0.8048	1.0840	0.5901
MMP2	1566678_at	1.0449	0.4842	-1.1098	0.4355
IL13	207844_at	1.0410	0.4712	1.0755	0.3457
IGFBP5	203425_s_at	1.0371	0.6021	-1.0324	0.4760
CCL25	206988_at	1.0294	0.6057	1.0805	0.1872
IL15	217371_s_at	1.0285	0.6654	1.0314	0.4485
MGC31957	210484_s_at	1.0285	0.7939	-1.0031	0.9762
CSF2	210228_at	1.0281	0.8233	-1.2158	0.0869
IFNG	210354_at	1.0269	0.2842	1.0748	0.0930
CCL11	210133_at	1.0267	0.5845	1.0023	0.9757
NGF	206814_at	1.0252	0.8973	1.0327	0.8518
CXCL13	205242_at	1.0252	0.9008	-1.0138	0.9115
CXCL12	203666_at	1.0030	0.9488	-1.0521	0.7262
FGF2	204421_s_at	-1.0006	0.9763	1.0127	0.9401
CXCL12	209687_at	-1.0016	0.9965	-1.1004	0.4117
CCL16	207354_at	-1.0066	0.9734	-1.0001	0.9968
IL15	205992_s_at	-1.0139	0.9955	-1.0066	0.9647
EGFR	211607_x_at	-1.0151	0.9441	-1.0712	0.6927
CCL8	214038_at	-1.0165	0.2637	1.0396	0.6928

EGFR	210984_x_at	-1.0273	0.7900	1.0750	0.1977
MMP9	203936_s_at	-1.0285	0.8642	-1.1353	0.4949
CCL26	223710_at	-1.0301	0.6491	-1.0069	0.7501
EGFR	1565484_x_at	-1.0414	0.1787	1.0302	0.6722
EGF	206254_at	-1.0473	0.6813	-1.0176	0.9889
HGF	210755_at	-1.0548	0.5387	-1.0228	0.9878
HGF	210997_at	-1.0564	0.4660	-1.0662	0.7221
FGF2	204422_s_at	-1.0651	0.5468	-1.0131	0.9996
EGFR	1565483_at	-1.0759	0.4095	-1.0736	0.4237
CSF2	210229_s_at	-1.1108	0.4831	-1.0699	0.5506
IGFBP5	211958_at	-1.1168	0.3038	-1.0560	0.6157
MMP2	1566677_at	-1.1209	0.2171	-1.1891	0.3193
TNFRSF10C	234195_at	-1.1229	0.4629	-1.0089	0.9158
IGFBP7	213910_at	-1.1264	0.5705	1.3832	0.3339
FAS	237522_at	-1.1296	0.1296	1.0139	0.9009
IGFBP7	201162_at	-1.1623	0.0433	1.0118	0.8682
IL7	206693_at	-1.1713	0.5060	-1.1249	0.7206
MGC31957	210483_at	-1.1781	0.0845	-1.3397	0.1355
EGFR	211550_at	-1.1875	0.4728	-1.1076	0.3381
TNFRSF10C	206222_at	-1.2052	0.6116	-1.5212	0.3136
IGFBP6	203851_at	-1.2193	0.3383	-1.3419	0.1717
TIMP2	231579_s_at	-1.3574	0.0046	-1.2565	0.0402
IL1A	208200_at	-1.3592	0.4520	1.2507	0.2593
IGFBP7	201163_s_at	-1.4003	0.0384	-1.3383	0.3381
TIMP2	203167_at	-1.4666	0.0671	-1.7053	0.0325
ANG	205141_at	-1.4766	0.1547	-1.2790	0.3127
TIMP2	224560_at	-1.5040	0.0082	-1.4030	0.0152
CCL2	216598_s_at	-1.6632	0.1510	1.1464	0.5336
PIGF	205077_s_at	-2.0819	0.0009	-2.0770	0.0019
MMP2	201069_at	-9.0031	0.0060	-8.0408	0.0072

Supplementary List 2. SASP genes

Gene list taken from Coppé, J.-P., Desprez, P.-Y., Krtolica, A. & Campisi, J. The senescence-associated secretory phenotype: the dark side of tumor suppression. *Annual review of pathology* **5**, 99-118, doi:10.1146/annurev-pathol-121808-102144 (2010).

Gene symbol	AffyID	Rel to Empty Vector fold change	Rel to Empty Vector BH-fdr	Rel to Uninfected fold change	Rel to Uninfected BH-fdr
TOP2A	201292_at	-44.8859	0.0016	-55.7509	0.0015
TOP2A	201291_s_at	-34.2267	0.0021	-45.2168	0.0020
BUB1	209642_at	-32.2549	0.0009	-53.4989	0.0003
BIRC5	202095_s_at	-30.7667	0.0013	-42.3286	0.0013
MKI67	212022_s_at	-24.0368	0.0043	-37.5308	0.0045
MKI67	212023_s_at	-20.2889	0.0012	-30.3190	0.0013
BUB1	215509_s_at	-19.1853	0.0003	-31.0591	0.0010
MKI67	212021_s_at	-17.9553	0.0024	-35.8066	0.0021
CENPE	205046_at	-16.4139	0.0006	-28.1259	0.0007
TYMS	1554696_s_at	-16.3937	0.0031	-21.4815	0.0035
CENPF	209172_s_at	-16.2523	0.0012	-17.8198	0.0021
CENPF	207828_s_at	-16.2055	0.0024	-20.2671	0.0023
BUB1	216275_at	-15.6598	0.0031	-27.2758	0.0030
CCNA2	203418_at	-15.0083	0.0036	-24.3372	0.0026
MAD2L1	203362_s_at	-12.4805	0.0007	-17.8810	0.0007
CCNB1	228729_at	-12.4024	0.0009	-17.0089	0.0009
DHFR	48808_at	-11.0022	0.0017	-18.2494	0.0013
BIRC5	202094_at	-9.1614	0.0007	-21.2281	0.0002
RRM2	209773_s_at	-8.6989	0.0008	-12.9431	0.0008
TYMS	202589_at	-8.5810	0.0037	-10.2470	0.0034
CDC7	204510_at	-8.2603	0.0031	-8.0243	0.0051
MCM6	201930_at	-7.7811	0.0003	-10.9691	0.0003
CHEK1	238075_at	-7.6500	0.0014	-8.3723	0.0040
RRM2	201890_at	-6.9223	0.0007	-8.8350	0.0017
AURKB	209464_at	-6.8894	0.0117	-12.5745	0.0066
DHFR	202532_s_at	-6.8825	0.0008	-10.0535	0.0005
CCNB1	214710_s_at	-6.6654	0.0023	-8.9851	0.0019
MAD2L1	1554768_a_at	-6.6323	0.0069	-10.5511	0.0006
PRIM1	205053_at	-6.5266	0.0008	-9.1693	0.0008
DHFR	202534_x_at	-6.3652	0.0003	-8.4143	0.0012
MCM6	238977_at	-5.8564	0.0079	-8.1128	0.0026
MKI67	212020_s_at	-5.6633	0.0028	-8.9172	0.0021
CDC6	203968_s_at	-5.5732	0.0005	-11.0302	0.0013
DHFR	202533_s_at	-5.0454	0.0005	-8.5075	0.0005
CCNA2	213226_at	-4.5545	0.0011	-6.0145	0.0020
CKS2	204170_s_at	-4.4439	0.0001	-4.9734	0.0006
MCM3	201555_at	-4.3716	0.0009	-5.3418	0.0012
CHEK1	205394_at	-4.3151	0.0026	-6.9643	0.0016
CDC6	203967_at	-4.2674	0.0037	-9.2174	0.0019
CDC20	202870_s_at	-3.8475	0.0012	-7.2994	0.0008
CHEK1	205393_s_at	-3.8475	0.0040	-6.8540	0.0016
BIRC5	210334_x_at	-3.7875	0.0075	-6.2339	0.0017
FEN1	204768_s_at	-3.7153	0.0008	-6.8893	0.0004
CDC25C	205167_s_at	-3.6609	0.0058	-5.4690	0.0026
DDX11	208159_x_at	-2.9145	0.0073	-2.8059	0.0103
DDX11	208149_x_at	-2.9140	0.0129	-2.2182	0.0252
MCM5	216237_s_at	-2.8935	0.0008	-4.7029	0.0022
UNG	202330_s_at	-2.8530	0.0018	-2.7516	0.0015
BUB1	216277_at	-2.8528	0.0167	-2.7029	0.0293
CDC25C	216914_at	-2.7553	0.0056	-3.7502	0.0102
NASP	201969_at	-2.7213	0.0078	-2.9033	0.0022
MCM4	222037_at	-2.7143	0.0295	-3.7554	0.0190
MYB	204798_at	-2.6925	0.0254	-3.3102	0.0116
PCNA	201202_at	-2.5347	0.0096	-2.8865	0.0128
MCM4	212141_at	-2.5332	0.0153	-4.0600	0.0063
PTTG1	203554_x_at	-2.5295	0.0019	-3.0075	0.0026

DDX11	232816_s_at	-2.5267	0.0946	-2.3352	0.1352
CCNE1	213523_at	-2.4623	0.0129	-2.2788	0.0061
MCM5	201755_at	-2.4538	0.0383	-3.9411	0.0142
MCM4	222036_s_at	-2.4528	0.0035	-3.1417	0.0065
MCM4	212142_at	-2.3492	0.0012	-3.4694	0.0027
CCNF	204827_s_at	-2.3320	0.0028	-3.7308	0.0042
CCNF	204826_at	-2.3098	0.0250	-2.7522	0.0176
DDX11	213378_s_at	-2.1349	0.0241	-2.3947	0.0186
RFC1	209085_x_at	-2.0979	0.0601	-2.2243	0.0468
RFC1	208021_s_at	-2.0454	0.0065	-1.9586	0.0073
RRM1	201476_s_at	-2.0282	0.0014	-3.1355	0.0036
RRM1	201477_s_at	-1.9752	0.0012	-2.6510	0.0052
EXOSC9	205061_s_at	-1.9585	0.0026	-2.4175	0.0013
FEN1	204767_s_at	-1.9471	0.0002	-2.2987	0.0063
CTPS	202613_at	-1.8522	0.0169	-2.1921	0.0137
ORC1L	205085_at	-1.8176	0.0386	-2.6801	0.0037
NASP	201970_s_at	-1.7248	0.0084	-2.1317	0.0030
PLK1	202240_at	-1.6583	0.0227	-2.2607	0.0107
AURKB	239219_at	-1.6327	0.0267	-2.0771	0.0032
CDC25C	217010_s_at	-1.6200	0.0409	-1.8740	0.0402
PKMYT1	204267_x_at	-1.6155	0.0939	-1.9207	0.0467
DNMT1	201697_s_at	-1.3273	0.1126	-1.3683	0.0195
BUB1	215508_at	-1.2773	0.2330	-1.1330	0.4016
TOP2A	237469_at	-1.2330	0.3472	-1.7193	0.0436
E2F3	203693_s_at	-1.2141	0.0739	-1.1565	0.3087
DDX11	210206_s_at	-1.2088	0.2582	-1.4679	0.0929
NASP	242918_at	-1.0974	0.5734	-1.0843	0.6062
RRM1	231028_at	-1.0935	0.3454	-1.0066	0.9738
PCNA	217400_at	-1.0773	0.5234	-1.2496	0.1402
MYB	215152_at	-1.0452	0.8571	-1.1819	0.4529
CCNE1	242105_at	-1.0182	0.9587	-1.1797	0.4511
RFC1	208133_at	1.0295	0.8756	-1.0114	0.9306
NASP	237276_at	1.0331	0.8987	-1.1211	0.4998
TYMS	217684_at	1.0547	0.7721	1.0857	0.6135
E2F3	203692_s_at	1.1500	0.3726	1.1348	0.3665
MAPK13	210059_s_at	1.5277	0.1906	1.2128	0.5592
MAPK13	210058_at	1.8961	0.0266	1.5525	0.0166
TIMP1	201666_at	31.6117	0.0002	20.5237	0.0005

Supplementary List 3. Proliferation Genes
Gene list taken from Whitfield, M. L., George, L. K., Grant, G. D. & Perou, C. M. Common markers of proliferation. *Nature reviews Cancer* **6**, 99-106, doi:10.1038/nrc1802 (2006).

		Rel to Empty Vector		Rel to Uninfected	
Gene symbol	AffyID	fold change	BH-fdr	fold change	BH-fdr
MITF	1554874_at	-12.4571	0.0071	-11.6057	0.0079
MITF	207233_s_at	-8.0532	0.0024	-8.9015	0.0025
MITF	226066_at	-5.4008	0.0012	-5.3919	0.0013
MYC	202431_s_at	-4.6222	0.0024	-3.4764	0.0107
AXIN2	222696_at	-2.3293	0.0055	-1.9772	0.0100
CCND1	208711_s_at	-1.5601	0.0100	-2.3588	0.0216
FZD7	203705_s_at	-1.5588	0.0768	-1.9647	0.0878
FZD7	203706_s_at	-1.5566	0.0481	-2.1452	0.0227
CCND1	208712_at	-1.4086	0.0063	-1.7371	0.0041
TCF4	212386_at	-1.3876	0.3539	-1.3677	0.4023
AXIN2	224176_s_at	-1.2740	0.2376	-1.1914	0.3386
FGF18	211485_s_at	-1.1607	0.1777	-1.0482	0.6759
AXIN2	222695_s_at	-1.1506	0.3926	-1.2601	0.2775
PCBD1	203557_s_at	-1.1313	0.3335	-1.1496	0.3591
TCF4	228837_at	-1.0568	0.7203	-1.0041	0.9912
TCF4	212387_at	-1.0494	0.7771	-1.0684	0.6737
TCF4	212385_at	-1.0465	0.7519	-1.1648	0.1934
FGF18	231382_at	-1.0398	0.6942	1.0830	0.3777
FGF18	206987_x_at	-1.0087	0.9324	1.0141	0.9830
LGR5	210393_at	1.0054	0.7666	1.0805	0.4254
FGF18	206986_at	1.0122	0.9385	-1.0937	0.4133
PPARD	242218_at	1.0146	0.8928	1.1480	0.4524
FGF18	211029_x_at	1.0427	0.8461	1.0225	0.9261
AXIN2	224498_x_at	1.0657	0.3348	-1.3133	0.3999
PITX2	207558_s_at	1.0740	0.7578	1.0639	0.7944
FGF18	214284_s_at	1.1042	0.3364	-1.0250	0.8643
LGR5	213880_at	1.1105	0.4534	1.0428	0.6444
PPARD	208044_s_at	1.1324	0.2009	1.1113	0.3431
PPARD	210636_at	1.2011	0.6176	-1.0011	0.9621
TCF4	213891_s_at	1.2379	0.3622	1.0445	0.7619
TCF4	212382_at	1.2455	0.3594	1.4834	0.2238
TCF4	203753_at	1.2668	0.3153	1.5447	0.2024
TCF4	222146_s_at	1.2923	0.4067	1.3829	0.3459
MYCBP	203359_s_at	1.3042	0.0359	1.3718	0.0569
PPARD	37152_at	1.3233	0.0603	1.1701	0.3063
LEF1	221557_s_at	1.3324	0.0223	1.3541	0.0387
FST	207345_at	1.4197	0.0376	1.4752	0.0521
CTLA4	231794_at	1.4241	0.0881	1.2300	0.2315
CTLA4	221331_x_at	1.4287	0.0545	1.3385	0.0952
JUN	201464_x_at	1.4403	0.0011	1.5761	0.0508
CLDN1	222549_at	1.4541	0.0575	1.8664	0.0427
MYCBP	203361_s_at	1.5649	0.1812	1.7138	0.1742
CTLA4	234895_at	1.5995	0.0620	1.3319	0.1701
JUN	201466_s_at	1.6069	0.0506	2.0416	0.0224
CTLA4	234362_s_at	1.7776	0.0720	1.3971	0.2002
JUN	213281_at	1.7909	0.0023	1.9579	0.0125
CLDN1	218182_s_at	1.9339	0.0848	2.2686	0.0836
MYCBP	203360_s_at	2.0705	0.0074	1.5949	0.0560
MMP7	204259_at	2.1369	0.0279	2.1674	0.0348
ID2 /// ID2B	213931_at	2.6436	0.0241	2.3591	0.0083
JUN	201465_s_at	2.6715	0.0195	2.7391	0.0276
LEF1	221558_s_at	3.5588	0.0016	4.3085	0.0003
ID2	201566_x_at	3.8746	0.0034	2.1236	0.0058
FST	204948_s_at	4.3432	0.0068	4.5846	0.0074
NRCAM	204105_s_at	5.6001	0.0005	8.0074	0.0019

ID2	201565_s_at	5.6182	0.0012	3.8794	0.0021
LEF1	210948_s_at	6.2248	0.0011	7.0645	0.0072
FOSL1	204420_at	7.5031	0.0004	2.6338	0.0018
VCAN	204619_s_at	8.4387	0.0006	8.5447	0.0012
NRCAM	216959_x_at	14.8622	0.0009	15.2476	0.0003
CTLA4	236341_at	24.4499	0.0002	17.4087	0.0005
VEGFA	212171_x_at	25.8076	0.0024	23.3654	0.0023
VCAN	204620_s_at	26.3090	0.0016	28.1722	0.0021
FST	226847_at	39.5068	0.0012	32.4893	0.0015
VCAN	221731_x_at	40.8034	0.0010	43.9661	0.0009
VCAN	211571_s_at	49.6754	0.0014	45.4431	0.0019
VEGFA	210512_s_at	49.9752	0.0011	38.8791	0.0011
VEGFA	210513_s_at	50.7094	0.0004	45.6331	0.0003
VEGFA	211527_x_at	54.5323	0.0001	51.1821	0.0021
VCAN	215646_s_at	96.6196	0.0006	128.8974	0.0002

Supplementary List 4. Direct Wnt Target Genes
Gene list taken from http://www.stanford.edu/group/nusselab/cgi-bin/wnt/target_genes and further refined through primary literature search for those genes with functional TCF/LEF binding sites in gene promoter.

9 References

1 Gray-Schopfer, V. C. *et al*. Cellular senescence in naevi and immortalisation in melanoma: a role for p16? *British Journal of Cancer* **95**, 496-505, doi:10.1038/sj.bjc.6603283 (2006).

2 Michaloglou, C. *et al*. BRAF(E600)-associated senescence-like cell cycle arrest of human naevi. *Nature* **436**, 720-724, doi:10.1038/nature03890 (2005).

3 Pollock, P. M. *et al*. High frequency of BRAF mutations in nevi. *Nature Genetics* **33**, 19-20, doi:10.1038/ng1054 (2002).

4 Gray-Schopfer, V., Wellbrock, C. & Marais, R. Melanoma biology and new targeted therapy. *Nature* **445**, 851-857, doi:10.1038/nature05661 (2007).

5 Elder, D. E., Elenitsas, R., Johnson, B. L., Murphy, G. F. & Xu, X. 1408 (Lippincott Williams & Wilkins, 2008).

6 Bevona, C., Goggins, W., Quinn, T., Fullerton, J. & Tsao, H. Cutaneous melanomas associated with nevi. *Archives of dermatology* **139**, 1620-1624- discussion 1624, doi:10.1001/archderm.139.12.1620 (2003).

7 Smolle, J., Kaddu, S. & Kerl, H. Non-random spatial association of melanoma and naevi--a morphometric analysis. *Melanoma research* **9**, 407-412 (1999).

8 Stolz, W., Schmoeckel, C., Landthaler, M. & Braun-Falco, O. Association of early malignant melanoma with nevocytic nevi. *Cancer* **63**, 550-555 (1989).

9 Robinson, W. A. *et al*. Human acquired naevi are clonal. *Melanoma research* **8**, 499-503 (1998).

10 Smolle, J., Soyer, H. P., Juettner, F. M., Hoedl, S. & Kerl, H. Nuclear parameters in the superficial and deep portion of melanocytic lesions--a morphometrical investigation. *Pathology, research and practice* **183**, 266-270 (1988).

11 Barnhill, R. L. & Piepkorn, M. *Pathology of Melanocytic Nevi and Malignant Melanoma* (2004).

12 HAYFLICK, L. THE LIMITED IN VITRO LIFETIME OF HUMAN DIPLOID CELL STRAINS. *Experimental cell research* **37**, 614-636 (1965).

13 HAYFLICK, L. & MOORHEAD, P. S. The serial cultivation of human diploid cell strains. *Experimental cell research* **25**, 585-621 (1961).

14 Earle, W. R. *et al*. Production of malignancy in vitro. IV. The mouse fibroblast cultures and changes seen in the living cells. *J. Nat. Cancer Inst* **4**, 51 (1943).

15 Herbig, U., Jobling, W. A., Chen, B. P. C., Chen, D. J. & Sedivy, J. M. Telomere shortening triggers senescence of human cells through a pathway involving ATM, p53, and p21(CIP1), but not p16(INK4a). *Molecular cell* **14**, 501-513 (2004).

16 d'Adda di Fagagna, F. *et al*. A DNA damage checkpoint response in telomere-initiated senescence. *Nature* **426**, 194-198, doi:10.1038/nature02118 (2003).

17 d'Adda di Fagagna, F., Teo, S.-H. & Jackson, S. P. Functional links between telomeres and proteins of the DNA-damage response. *Genes & development* **18**, 1781-1799, doi:10.1101/gad.1214504 (2004).

18 Harley, C. B., Futcher, A. B. & Greider, C. W. Telomeres shorten during ageing of human fibroblasts. *Nature* **345**, 458-460, doi:10.1038/345458a0 (1990).
19 Hastie, N. D. *et al*. Telomere reduction in human colorectal carcinoma and with ageing. *Nature* **346**, 866-868, doi:10.1038/346866a0 (1990).
20 Olovnikov, A. M. A theory of marginotomy. The incomplete copying of template margin in enzymic synthesis of polynucleotides and biological significance of the phenomenon. *Journal of theoretical biology* **41**, 181-190 (1973).
21 Watson, J. D. Origin of concatemeric T7 DNA. *Nature: New biology* **239**, 197-201 (1972).
22 Counter, C. M. *et al*. Telomere shortening associated with chromosome instability is arrested in immortal cells which express telomerase activity. *The EMBO journal* **11**, 1921-1929 (1992).
23 Bodnar, A. G. *et al*. Extension of life-span by introduction of telomerase into normal human cells. *Science (New York, NY)* **279**, 349-352 (1998).
24 Blackburn, E. H. Telomere states and cell fates. *Nature* **408**, 53-56 (2000).
25 Di Leonardo, A., Linke, S. P., Clarkin, K. & Wahl, G. M. DNA damage triggers a prolonged p53-dependent G1 arrest and long-term induction of Cip1 in normal human fibroblasts. *Genes & development* **8**, 2540-2551, doi:10.1101/gad.8.21.2540 (1994).
26 Chang, B. D. *et al*. A senescence-like phenotype distinguishes tumor cells that undergo terminal proliferation arrest after exposure to anticancer agents. *Cancer research* **59**, 3761-3767 (1999).
27 Ogryzko, V. V., Hirai, T. H., Russanova, V. R., Barbie, D. A. & Howard, B. H. Human fibroblast commitment to a senescence-like state in response to histone deacetylase inhibitors is cell cycle dependent. *Molecular and Cellular Biology* **16**, 5210-5218 (1996).
28 Munro, J., Barr, N. I., Ireland, H., Morrison, V. & Parkinson, E. K. Histone deacetylase inhibitors induce a senescence-like state in human cells by a p16-dependent mechanism that is independent of a mitotic clock. *Experimental cell research* **295**, 525-538, doi:10.1016/j.yexcr.2004.01.017 (2004).
29 Narita, M. *et al*. Rb-Mediated Heterochromatin Formation and Silencing of E2F Target Genes during Cellular Senescence. *Cell* **113**, 703-716, doi:10.1016/S0092-8674(03)00401-X (2003).
30 Minucci, S. & Pelicci, P. G. Histone deacetylase inhibitors and the promise of epigenetic (and more) treatments for cancer. *Nature reviews Cancer* **6**, 38-51, doi:10.1038/nrc1779 (2006).
31 Fusenig, N. E. & Boukamp, P. Multiple stages and genetic alterations in immortalization, malignant transformation, and tumor progression of human skin keratinocytes. *Molecular Carcinogenesis* **23**, 144-158 (1998).
32 Parrinello, S. *et al*. Oxygen sensitivity severely limits the replicative lifespan of murine fibroblasts. *Nature cell biology* **5**, 741-747, doi:10.1038/ncb1024 (2003).
33 Yaswen, P. & Stampfer, M. R. Molecular changes accompanying senescence and immortalization of cultured human mammary epithelial cells. *The international journal of biochemistry & cell biology* **34**, 1382-1394 (2002).

34 Serrano, M., Lin, A. W., McCurrach, M. E., Beach, D. & Lowe, S. W. Oncogenic ras provokes premature cell senescence associated with accumulation of p53 and p16INK4a. *Cell* **88**, 593-602 (1997).

35 Lin, A. W. *et al.* Premature senescence involving p53 and p16 is activated in response to constitutive MEK/MAPK mitogenic signaling. *Genes & development* **12**, 3008-3019, doi:10.1101/gad.12.19.3008 (1998).

36 Zhu, J., Woods, D., McMahon, M. & Bishop, J. M. Senescence of human fibroblasts induced by oncogenic Raf. *Genes & development* **12**, 2997-3007, doi:10.1101/gad.12.19.2997 (1998).

37 Dimri, G. P., Itahana, K., Acosta, M. & Campisi, J. Regulation of a senescence checkpoint response by the E2F1 transcription factor and p14ARF tumor suppressor. *Molecular and Cellular Biology* **20**, 273-285, doi:10.1128/MCB.20.1.273-285.2000 (2000).

38 Bartkova, J. *et al.* Oncogene-induced senescence is part of the tumorigenesis barrier imposed by DNA damage checkpoints. *Nature* **444**, 633-637, doi:10.1038/nature05268 (2006).

39 Di Micco, R. *et al.* Oncogene-induced senescence is a DNA damage response triggered by DNA hyper-replication. *Nature* **444**, 638-642, doi:10.1038/nature05327 (2006).

40 Mallette, F. A., Gaumont-Leclerc, M.-F. & Ferbeyre, G. The DNA damage signaling pathway is a critical mediator of oncogene-induced senescence. *Genes & development* **21**, 43-48, doi:10.1101/gad.1487307 (2007).

41 Woo, R. A. & Poon, R. Y. C. Activated oncogenes promote and cooperate with chromosomal instability for neoplastic transformation. *Genes & development* **18**, 1317-1330, doi:10.1101/gad.1165204 (2004).

42 Mathon, N. F., Malcolm, D. S., Harrisingh, M. C., Cheng, L. & Lloyd, A. C. Lack of replicative senescence in normal rodent glia. *Science (New York, NY)* **291**, 872-875, doi:10.1126/science.1056782 (2001).

43 Tang, D. G., Tokumoto, Y. M., Apperly, J. A., Lloyd, A. C. & Raff, M. C. Lack of replicative senescence in cultured rat oligodendrocyte precursor cells. *Science (New York, NY)* **291**, 868-871, doi:10.1126/science.1056780 (2001).

44 Buday, L. & Downward, J. Epidermal growth factor regulates p21ras through the formation of a complex of receptor, Grb2 adapter protein, and Sos nucleotide exchange factor. *Cell* **73**, 611-620 (1993).

45 Huang, D. C., Marshall, C. J. & Hancock, J. F. Plasma membrane-targeted ras GTPase-activating protein is a potent suppressor of p21ras function. *Molecular and Cellular Biology* **13**, 2420-2431, doi:10.1128/MCB.13.4.2420 (1993).

46 Malumbres, M. & Barbacid, M. RAS oncogenes: the first 30 years. *Nature reviews Cancer* **3**, 459-465, doi:10.1038/nrc1097 (2003).

47 Boguski, M. S. & McCormick, F. Proteins regulating Ras and its relatives. *Nature* **366**, 643-654, doi:10.1038/366643a0 (1993).

48 Krontiris, T. G. & Cooper, G. M. Transforming activity of human tumor DNAs. *Proceedings of the National Academy of Sciences of the United States of America* **78**, 1181-1184 (1981).

49 Perucho, M. *et al.* Human-tumor-derived cell lines contain common and different transforming genes. *Cell* **27**, 467-476 (1981).

50 Shih, C. & Weinberg, R. A. Isolation of a transforming sequence from a human bladder carcinoma cell line. *Cell* **29**, 161-169 (1982).

51 Sherr, C. J. & McCormick, F. The RB and p53 pathways in cancer. *Cancer Cell* **2**, 103-112 (2002).

52 Brown, J. P., Wei, W. & Sedivy, J. M. Bypass of senescence after disruption of p21CIP1/WAF1 gene in normal diploid human fibroblasts. *Science (New York, NY)* **277**, 831-834, doi:10.1126/science.277.5327.831 (1997).

53 Bulavin, D. V. *et al*. Inactivation of the Wip1 phosphatase inhibits mammary tumorigenesis through p38 MAPK-mediated activation of the p16(Ink4a)-p19(Arf) pathway. *Nature Genetics* **36**, 343-350, doi:10.1038/ng1317 (2004).

54 Deng, Q., Liao, R., Wu, B.-L. & Sun, P. High intensity ras signaling induces premature senescence by activating p38 pathway in primary human fibroblasts. *The Journal of biological chemistry* **279**, 1050-1059, doi:10.1074/jbc.M308644200 (2004).

55 Ito, K. *et al*. Reactive oxygen species act through p38 MAPK to limit the lifespan of hematopoietic stem cells. *Nature medicine* **12**, 446-451, doi:10.1038/nm1388 (2006).

56 Nicke, B. *et al*. Involvement of MINK, a Ste20 family kinase, in Ras oncogene-induced growth arrest in human ovarian surface epithelial cells. *Molecular cell* **20**, 673-685, doi:10.1016/j.molcel.2005.10.038 (2005).

57 Voncken, J. W. *et al*. MAPKAP kinase 3pK phosphorylates and regulates chromatin association of the polycomb group protein Bmi1. *The Journal of biological chemistry* **280**, 5178-5187, doi:10.1074/jbc.M407155200 (2005).

58 Beauséjour, C. M. *et al*. Reversal of human cellular senescence: roles of the p53 and p16 pathways. *The EMBO journal* **22**, 4212-4222, doi:10.1093/emboj/cdg417 (2003).

59 Gire, V., Roux, P., Wynford-Thomas, D., Brondello, J.-M. & Dulic, V. DNA damage checkpoint kinase Chk2 triggers replicative senescence. *The EMBO journal* **23**, 2554-2563, doi:10.1038/sj.emboj.7600259 (2004).

60 Won, J. *et al*. Small molecule-based reversible reprogramming of cellular lifespan. *Nature chemical biology* **2**, 369-374, doi:10.1038/nchembio800 (2006).

61 Olsen, C. L., Gardie, B., Yaswen, P. & Stampfer, M. R. Raf-1-induced growth arrest in human mammary epithelial cells is p16-independent and is overcome in immortal cells during conversion. *Oncogene* **21**, 6328-6339, doi:10.1038/sj.onc.1205780 (2002).

62 Ryan, J. M. & Cristofalo, V. J. Histone acetylation during aging of human cells in culture. *Biochemical and biophysical research communications* **48**, 735-742 (1972).

63 Kennedy, A. L. *et al*. Senescent mouse cells fail to overtly regulate the HIRA histone chaperone and do not form robust Senescence Associated Heterochromatin Foci. *Cell Division* **5**, -, doi:10.1186/1747-1028-5-16 (2010).

64 Dang, W. *et al*. Histone H4 lysine 16 acetylation regulates cellular lifespan. *Nature* **459**, 802-807, doi:10.1038/nature08085 (2009).

65 Ye, X. *et al*. Definition of pRB- and p53-dependent and -independent steps in HIRA/ASF1a-mediated formation of senescence-associated heterochromatin foci. *Molecular and Cellular Biology* **27**, 2452-2465, doi:10.1128/MCB.01592-06 (2007).

66 Chan, H. M., Narita, M., Lowe, S. W. & Livingston, D. M. The p400 E1A-associated protein is a novel component of the p53 --> p21 senescence

pathway. *Genes & development* **19**, 196-201, doi:10.1101/gad.1280205 (2005).

67 Rai, T. S. *et al*. Human CABIN1 is a functional member of the human HIRA/UBN1/ASF1a histone H3.3 chaperone complex. *Molecular and Cellular Biology* **31**, 4107-4118, doi:10.1128/MCB.05546-11 (2011).

68 Zhang, R. *et al*. Formation of MacroH2A-containing senescence-associated heterochromatin foci and senescence driven by ASF1a and HIRA. *Developmental cell* **8**, 19-30, doi:10.1016/j.devcel.2004.10.019 (2005).

69 Kaufman, P. D., Cohen, J. L. & Osley, M. A. Hir proteins are required for position-dependent gene silencing in Saccharomyces cerevisiae in the absence of chromatin assembly factor I. *Molecular and Cellular Biology* **18**, 4793-4806 (1998).

70 Moshkin, Y. M. *et al*. Histone chaperone ASF1 cooperates with the Brahma chromatin-remodelling machinery. *Genes & development* **16**, 2621-2626, doi:10.1101/gad.231202 (2002).

71 Phelps-Durr, T. L., Thomas, J., Vahab, P. & Timmermans, M. C. P. Maize rough sheath2 and its Arabidopsis orthologue ASYMMETRIC LEAVES1 interact with HIRA, a predicted histone chaperone, to maintain knox gene silencing and determinacy during organogenesis. *The Plant cell* **17**, 2886-2898, doi:10.1105/tpc.105.035477 (2005).

72 Sharp, J. A., Franco, A. A., Osley, M. A. & Kaufman, P. D. Chromatin assembly factor I and Hir proteins contribute to building functional kinetochores in S. cerevisiae. *Genes & development* **16**, 85-100, doi:10.1101/gad.925302 (2002).

73 Singer, M. S. *et al*. Identification of high-copy disruptors of telomeric silencing in Saccharomyces cerevisiae. *Genetics* **150**, 613-632 (1998).

74 Wajapeyee, N., Serra, R. W., Zhu, X., Mahalingam, M. & Green, M. R. Oncogenic BRAF induces senescence and apoptosis through pathways mediated by the secreted protein IGFBP7. *Cell* **132**, 363-374, doi:10.1016/j.cell.2007.12.032 (2008).

75 Gazin, C., Wajapeyee, N., Gobeil, S., Virbasius, C.-M. & Green, M. R. An elaborate pathway required for Ras-mediated epigenetic silencing. *Nature* **449**, 1073-1077, doi:10.1038/nature06251 (2007).

76 Loppin, B. *et al*. The histone H3.3 chaperone HIRA is essential for chromatin assembly in the male pronucleus. *Nature* **437**, 1386-1390, doi:10.1038/nature04059 (2005).

77 Zhang, R., Chen, W. & Adams, P. D. Molecular dissection of formation of senescence-associated heterochromatin foci. *Molecular and Cellular Biology* **27**, 2343-2358, doi:10.1128/MCB.02019-06 (2007).

78 Funayama, R., Saito, M., Tanobe, H. & Ishikawa, F. Loss of linker histone H1 in cellular senescence. *The Journal of cell biology* **175**, 869-880, doi:10.1083/jcb.200604005 (2006).

79 Narita, M. *et al*. A novel role for high-mobility group a proteins in cellular senescence and heterochromatin formation. *Cell* **126**, 503-514, doi:10.1016/j.cell.2006.05.052 (2006).

80 Changolkar, L. N., Singh, G. & Pehrson, J. R. macroH2A1-dependent silencing of endogenous murine leukemia viruses. *Molecular and Cellular Biology* **28**, 2059-2065, doi:10.1128/MCB.01362-07 (2008).

81 Costanzi, C. & Pehrson, J. R. Histone macroH2A1 is concentrated in the inactive X chromosome of female mammals. *Nature* **393**, 599-601, doi:10.1038/31275 (1998).

82 Timinszky, G. *et al*. A macrodomain-containing histone rearranges chromatin upon sensing PARP1 activation. *Nature structural & molecular biology* **16**, 923-929, doi:10.1038/nsmb.1664 (2009).

83 Bartel, D. P. MicroRNAs: genomics, biogenesis, mechanism, and function. *Cell* **116**, 281-297 (2004).

84 Davis, B. N. & Hata, A. Regulation of MicroRNA Biogenesis: A miRiad of mechanisms. *Cell communication and signaling : CCS* **7**, 18, doi:10.1186/1478-811X-7-18 (2009).

85 Pfeffer, S. *et al*. Identification of virus-encoded microRNAs. *Science (New York, NY)* **304**, 734-736, doi:10.1126/science.1096781 (2004).

86 Murchison, E. P. & Hannon, G. J. miRNAs on the move: miRNA biogenesis and the RNAi machinery. *Current opinion in cell biology* **16**, 223-229, doi:10.1016/j.ceb.2004.04.003 (2004).

87 Eiring, A. M. *et al*. miR-328 functions as an RNA decoy to modulate hnRNP E2 regulation of mRNA translation in leukemic blasts. *Cell* **140**, 652-665, doi:10.1016/j.cell.2010.01.007 (2010).

88 Lee, I. *et al*. New class of microRNA targets containing simultaneous 5'-UTR and 3'-UTR interaction sites. *Genome research* **19**, 1175-1183, doi:10.1101/gr.089367.108 (2009).

89 Ørom, U. A., Nielsen, F. C. & Lund, A. H. MicroRNA-10a binds the 5'UTR of ribosomal protein mRNAs and enhances their translation. *Molecular cell* **30**, 460-471, doi:10.1016/j.molcel.2008.05.001 (2008).

90 Lewis, B. P., Shih, I.-h., Jones-Rhoades, M. W., Bartel, D. P. & Burge, C. B. Prediction of mammalian microRNA targets. *Cell* **115**, 787-798 (2003).

91 Lafferty-Whyte, K., Cairney, C. J., Jamieson, N. B., Oien, K. A. & Keith, W. N. Pathway analysis of senescence-associated miRNA targets reveals common processes to different senescence induction mechanisms. *Biochimica et biophysica acta* **1792**, 341-352, doi:10.1016/j.bbadis.2009.02.003 (2009).

92 He, L. *et al*. A microRNA component of the p53 tumour suppressor network. *Nature* **447**, 1130-1134, doi:10.1038/nature05939 (2007).

93 Langley, E. *et al*. Human SIR2 deacetylates p53 and antagonizes PML/p53-induced cellular senescence. *The EMBO journal* **21**, 2383-2396, doi:10.1093/emboj/21.10.2383 (2002).

94 Yamakuchi, M. & Lowenstein, C. J. MiR-34, SIRT1 and p53: the feedback loop. *Cell cycle (Georgetown, Tex)* **8**, 712-715 (2009).

95 Christoffersen, N. R. *et al*. p53-independent upregulation of miR-34a during oncogene-induced senescence represses MYC. *Cell death and differentiation* **17**, 236-245, doi:10.1038/cdd.2009.109 (2010).

96 Feliciano, A., Sánchez-Sendra, B., Kondoh, H. & LLeonart, M. E. MicroRNAs Regulate Key Effector Pathways of Senescence. *Journal of aging research* **2011**, 205378, doi:10.4061/2011/205378 (2011).

97 Wirawan, E., Berghe, T. V., Lippens, S., Agostinis, P. & Vandenabeele, P. Autophagy: for better or for worse. *Cell Research*, doi:10.1038/cr.2011.152 (2011).

98 Cuervo, A. M. & Dice, J. F. Age-related decline in chaperone-mediated autophagy. *The Journal of biological chemistry* **275**, 31505, doi:10.1074/jbc.M002102200 (2000).

99 Kang, H. T., Lee, K. B., Kim, S. Y., Choi, H. R. & Park, S. C. Autophagy impairment induces premature senescence in primary human fibroblasts. *PloS one* **6**, e23367, doi:10.1371/journal.pone.0023367 (2011).

100 Young, A. R. J. *et al.* Autophagy mediates the mitotic senescence transition. *Genes & development* **23**, 798-803, doi:10.1101/gad.519709 (2009).
101 Mathew, R., Karantza-Wadsworth, V. & White, E. Role of autophagy in cancer. *Nature reviews Cancer* **7**, 961-967, doi:10.1038/nrc2254 (2007).
102 Dimri, G. P. A Biomarker that Identifies Senescent Human Cells in Culture and in Aging Skin in vivo. *Proceedings of the National Academy of Sciences* **92**, 9363-9367, doi:10.1073/pnas.92.20.9363 (1995).
103 Going, J. J., Stuart, R. C., Downie, M., Fletcher Monaghan, A. J. & Nicol Keith, W. 'Senescence - associated' β - galactosidase activity in the upper gastrointestinal tract. *The Journal of pathology* **196**, 394-400, doi:10.1002/path.1059 (2002).
104 Severino, J., Allen, R., Balin, S., Balin, A. & Cristofalo, V. J. Is [beta]-Galactosidase Staining a Marker of Senescence in Vitro and in Vivo? *Experimental cell research* **257**, 162-171, doi:10.1006/excr.2000.4875 (2000).
105 Yang, N. C. & Hu, M. L. The limitations and validities of senescence associated-ß-galactosidase activity as an aging marker for human foreskin fibroblast Hs68 cells. *Experimental gerontology* **40**, 813-819, doi:10.1016/j.exger.2005.07.011 (2005).
106 d'Adda di Fagagna, F. *et al.* A DNA damage checkpoint response in telomere-initiated senescence. *Nature* **426**, 194-198, doi:10.1038/nature02118 (2003).
107 de Stanchina, E. *et al.* PML is a direct p53 target that modulates p53 effector functions. *Molecular cell* **13**, 523-535 (2004).
108 Ferbeyre, G. *et al.* PML is induced by oncogenic ras and promotes premature senescence. *Genes & development* **14**, 2015-2027 (2000).
109 Pearson, M. *et al.* PML regulates p53 acetylation and premature senescence induced by oncogenic Ras. *Nature* **406**, 207-210, doi:10.1038/35018127 (2000).
110 Alcorta, D. A. Involvement of the cyclin-dependent kinase inhibitor p16 (INK4a) in replicative senescence of normal human fibroblasts. *Proceedings of the National Academy of Sciences* **93**, 13742-13747, doi:10.1073/pnas.93.24.13742 (1996).
111 Malumbres, M. *et al.* Cellular Response to Oncogenic Ras Involves Induction of the Cdk4 and Cdk6 Inhibitor p15INK4b. *Molecular and Cellular Biology* **20**, 2915-2925, doi:10.1128/MCB.20.8.2915-2925.2000 (2000).
112 Afshari, C. Investigation of the Role of G1/S Cell Cycle Mediators in Cellular Senescence. *Experimental cell research* **209**, 231-237, doi:10.1006/excr.1993.1306 (1993).
113 Tahara, H., Sato, E., Noda, A. & Ide, T. Increase in expression level of p21sdi1/cip1/waf1 with increasing division age in both normal and SV40-transformed human fibroblasts. *Oncogene* **10**, 835-840 (1995).
114 Braig, M. *et al.* Oncogene-induced senescence as an initial barrier in lymphoma development. *Nature* **436**, 660-665, doi:10.1038/nature03841 (2005).
115 Chen, Z. *et al.* Crucial role of p53-dependent cellular senescence in suppression of Pten-deficient tumorigenesis. *Nature* **436**, 725-730, doi:10.1038/nature03918 (2005).

116 Collado, M. *et al*. Tumour biology: senescence in premalignant tumours. *Nature* **436**, 642, doi:10.1038/436642a (2005).
117 Shelton, D. N., Chang, E., Whittier, P. S., Choi, D. & Funk, W. D. Microarray analysis of replicative senescence. *Current Biology* **9**, 939-945, doi:10.1016/S0960-9822(99)80420-5 (1999).
118 Campisi, J. Senescent cells, tumor suppression, and organismal aging: good citizens, bad neighbors. *Cell* **120**, 513-522, doi:10.1016/j.cell.2005.02.003 (2005).
119 Kortlever, R. M., Higgins, P. J. & Bernards, R. Plasminogen activator inhibitor-1 is a critical downstream target of p53 in the induction of replicative senescence. *Nature cell biology* **8**, 877-884, doi:10.1038/ncb1448 (2006).
120 Kuilman, T. & Peeper, D. S. Senescence-messaging secretome: SMS-ing cellular stress. *Nature reviews Cancer* **9**, 81-94, doi:10.1038/nrc2560 (2009).
121 Chien, Y. *et al*. Control of the senescence-associated secretory phenotype by NF-κB promotes senescence and enhances chemosensitivity. *Genes & development* **25**, 2125-2136, doi:10.1101/gad.17276711 (2011).
122 Acosta, J. C. *et al*. Chemokine signaling via the CXCR2 receptor reinforces senescence. *Cell* **133**, 1006-1018, doi:10.1016/j.cell.2008.03.038 (2008).
123 Kuilman, T. *et al*. Oncogene-induced senescence relayed by an interleukin-dependent inflammatory network. *Cell* **133**, 1019-1031, doi:10.1016/j.cell.2008.03.039 (2008).
124 Xue, W. *et al*. Senescence and tumour clearance is triggered by p53 restoration in murine liver carcinomas. *Nature* **445**, 656-660, doi:10.1038/nature05529 (2007).
125 Krtolica, A. Senescent fibroblasts promote epithelial cell growth and tumorigenesis: A link between cancer and aging. *Proceedings of the National Academy of Sciences* **98**, 12072-12077, doi:10.1073/pnas.211053698 (2001).
126 Parrinello, S., Coppé, J.-P., Krtolica, A. & Campisi, J. Stromal-epithelial interactions in aging and cancer: senescent fibroblasts alter epithelial cell differentiation. *Journal of cell science* **118**, 485-496, doi:10.1242/jcs.01635 (2005).
127 Hanahan, D. & Weinberg, R. A. The hallmarks of cancer. *Cell* **100**, 57-70 (2000).
128 Jacobs, J. J. L. & de Lange, T. Significant role for p16INK4a in p53-independent telomere-directed senescence. *Current biology : CB* **14**, 2302-2308, doi:10.1016/j.cub.2004.12.025 (2004).
129 Bond, J. A., Wyllie, F. S. & Wynford-Thomas, D. Escape from senescence in human diploid fibroblasts induced directly by mutant p53. *Oncogene* **9**, 1885-1889 (1994).
130 Collins, C. J. & Sedivy, J. M. Involvement of the INK4a/Arf gene locus in senescence. *Aging cell* **2**, 145-150 (2003).
131 Hara, E., Tsurui, H., Shinozaki, A., Nakada, S. & Oda, K. Cooperative effect of antisense-Rb and antisense-p53 oligomers on the extension of life span in human diploid fibroblasts, TIG-1. *Biochemical and biophysical research communications* **179**, 528-534 (1991).
132 Ohtani, N., Yamakoshi, K., Takahashi, A. & Hara, E. The p16INK4a-RB pathway: molecular link between cellular senescence and tumor

suppression. *The journal of medical investigation : JMI* **51**, 146-153 (2004).
133 Schmitt, C. A. *et al.* A senescence program controlled by p53 and p16INK4a contributes to the outcome of cancer therapy. *Cell* **109**, 335-346 (2002).
134 Shay, J. W., Pereira-Smith, O. M. & Wright, W. E. A role for both RB and p53 in the regulation of human cellular senescence. *Experimental cell research* **196**, 33-39 (1991).
135 Sherr, C. J. & DePinho, R. A. Cellular Senescence: Mitotic Clock or Culture Shock? *Cell* **102**, 407-410 (2000).
136 Dhomen, N. *et al.* Oncogenic Braf induces melanocyte senescence and melanoma in mice. *Cancer Cell* **15**, 294-303, doi:10.1016/j.ccr.2009.02.022 (2009).
137 Gurtner, G. C., Werner, S., Barrandon, Y. & Longaker, M. T. Wound repair and regeneration. *Nature* **453**, 314-321, doi:10.1038/nature07039 (2008).
138 Krizhanovsky, V. *et al.* Senescence of activated stellate cells limits liver fibrosis. *Cell* **134**, 657-667, doi:10.1016/j.cell.2008.06.049 (2008).
139 Jun, J.-I. & Lau, L. F. The matricellular protein CCN1 induces fibroblast senescence and restricts fibrosis in cutaneous wound healing. *Nature cell biology* **12**, 676-685, doi:10.1038/ncb2070 (2010).
140 Chen, C.-C. & Lau, L. F. Functions and mechanisms of action of CCN matricellular proteins. *The international journal of biochemistry & cell biology* **41**, 771-783, doi:10.1016/j.biocel.2008.07.025 (2009).
141 Erusalimsky, J. D. & Kurz, D. J. Cellular senescence in vivo: its relevance in ageing and cardiovascular disease. *Experimental gerontology* **40**, 634-642, doi:10.1016/j.exger.2005.04.010 (2005).
142 Jeyapalan, J. C., Ferreira, M., Sedivy, J. M. & Herbig, U. Accumulation of senescent cells in mitotic tissue of aging primates. *Mechanisms of ageing and development* **128**, 36-44, doi:10.1016/j.mad.2006.11.008 (2007).
143 Melk, A. *et al.* Cell senescence in rat kidneys in vivo increases with growth and age despite lack of telomere shortening. *Kidney international* **63**, 2134-2143, doi:10.1046/j.1523-1755.2003.00032.x (2003).
144 Paradis, V. *et al.* Replicative senescence in normal liver, chronic hepatitis C, and hepatocellular carcinomas. *Human Pathology* **32**, 327-332, doi:10.1053/hupa.2001.22747 (2001).
145 Wang, C. *et al.* DNA damage response and cellular senescence in tissues of aging mice. *Aging cell* **8**, 311-323, doi:10.1111/j.1474-9726.2009.00481.x (2009).
146 Sedelnikova, O. A. *et al.* Senescing human cells and ageing mice accumulate DNA lesions with unrepairable double-strand breaks. *Nature* **6**, 168-170, doi:10.1038/ncb1095 (2004).
147 Krishnamurthy, J. *et al.* Ink4a/Arf expression is a biomarker of aging. *The Journal of clinical investigation* **114**, 1299-1307, doi:10.1172/JCI22475 (2004).
148 Herbig, U., Ferreira, M., Condel, L., Carey, D. & Sedivy, J. M. Cellular senescence in aging primates. *Science (New York, NY)* **311**, 1257, doi:10.1126/science.1122446 (2006).
149 Hsieh, C.-C. & Papaconstantinou, J. Thioredoxin-ASK1 complex levels regulate ROS-mediated p38 MAPK pathway activity in livers of aged and long-lived Snell dwarf mice. *FASEB journal : official publication of the*

Federation of American Societies for Experimental Biology **20**, 259-268, doi:10.1096/fj.05-4376com (2006).
150 Minamino, T. & Komuro, I. Vascular cell senescence: contribution to atherosclerosis. *Circulation research* **100**, 15-26, doi:10.1161/01.RES.0000256837.40544.4a (2007).
151 Price, J. S. *et al.* The role of chondrocyte senescence in osteoarthritis. *Aging cell* **1**, 57-65 (2002).
152 Wiemann, S. U. *et al.* Hepatocyte telomere shortening and senescence are general markers of human liver cirrhosis. *FASEB journal : official publication of the Federation of American Societies for Experimental Biology* **16**, 935-942, doi:10.1096/fj.01-0977com (2002).
153 Molofsky, A. V. *et al.* Increasing p16INK4a expression decreases forebrain progenitors and neurogenesis during ageing. *Nature* **443**, 448-452, doi:10.1038/nature05091 (2006).
154 Janzen, V. *et al.* Stem-cell ageing modified by the cyclin-dependent kinase inhibitor p16INK4a. *Nature* **443**, 421-426, doi:10.1038/nature05159 (2006).
155 Krishnamurthy, J. *et al.* p16INK4a induces an age-dependent decline in islet regenerative potential. *Nature* **443**, 453-457, doi:10.1038/nature05092 (2006).
156 Baker, D. J. *et al.* Opposing roles for p16Ink4a and p19Arf in senescence and ageing caused by BubR1 insufficiency. *Nature cell biology* **10**, 825-836, doi:10.1038/ncb1744 (2008).
157 Tomás-Loba, A. *et al.* Telomerase reverse transcriptase delays aging in cancer-resistant mice. *Cell* **135**, 609-622, doi:10.1016/j.cell.2008.09.034 (2008).
158 Maier, B. *et al.* Modulation of mammalian life span by the short isoform of p53. *Genes & development* **18**, 306-319, doi:10.1101/gad.1162404 (2004).
159 Tyner, S. D. *et al.* p53 mutant mice that display early ageing-associated phenotypes. *Nature* **415**, 45-53, doi:10.1038/415045a (2002).
160 Baker, D. J. *et al.* Clearance of p16Ink4a-positive senescent cells delays ageing-associated disorders. *Nature* **479**, 232-236, doi:10.1038/nature10600 (2011).
161 Medawar, P. B. An Unsolved Problem of Biology., H.K. Lewis & Co., London. (1952).
162 Williams, G. C. in *Evolution* 398-411 (1957).
163 Rodier, F. & Campisi, J. Four faces of cellular senescence. *The Journal of cell biology* **192**, 547-556, doi:10.1083/jcb.201009094 (2011).
164 Nishimura, E. K., Granter, S. R. & Fisher, D. E. Mechanisms of hair graying: incomplete melanocyte stem cell maintenance in the niche. *Science (New York, NY)* **307**, 720-724, doi:10.1126/science.1099593 (2005).
165 Chambers, S. M. *et al.* Aging hematopoietic stem cells decline in function and exhibit epigenetic dysregulation. *PLoS biology* **5**, e201, doi:10.1371/journal.pbio.0050201 (2007).
166 Morrison, S. J., Wandycz, A. M., Akashi, K., Globerson, A. & Weissman, I. L. The aging of hematopoietic stem cells. *Nature medicine* **2**, 1011-1016 (1996).
167 Coppé, J.-P., Desprez, P.-Y., Krtolica, A. & Campisi, J. The senescence-associated secretory phenotype: the dark side of tumor suppression.

Annual review of pathology **5**, 99-118, doi:10.1146/annurev-pathol-121808-102144 (2010).

168 Burrage, P. S., Mix, K. S. & Brinckerhoff, C. E. Matrix metalloproteinases: role in arthritis. *Frontiers in bioscience : a journal and virtual library* **11**, 529-543 (2006).

169 Coppé, J.-P., Kauser, K., Campisi, J. & Beauséjour, C. M. Secretion of vascular endothelial growth factor by primary human fibroblasts at senescence. *The Journal of biological chemistry* **281**, 29568-29574, doi:10.1074/jbc.M603307200 (2006).

170 Coppé, J.-P. *et al*. A human-like senescence-associated secretory phenotype is conserved in mouse cells dependent on physiological oxygen. *PloS one* **5**, e9188, doi:10.1371/journal.pone.0009188 (2010).

171 Coppé, J.-P. *et al*. Senescence-associated secretory phenotypes reveal cell-nonautonomous functions of oncogenic RAS and the p53 tumor suppressor. *PLoS biology* **6**, 2853-2868, doi:10.1371/journal.pbio.0060301 (2008).

172 Kang, M. K. *et al*. Senescence-associated genes in normal human oral keratinocytes. *Experimental cell research* **287**, 272-281, doi:10.1016/S0014-4827(03)00061-2 (2003).

173 Ksiazek, K., Jorres, A. & Witowski, J. Senescence induces a proangiogenic switch in human peritoneal mesothelial cells. *Rejuvenation research* **11**, 681-683, doi:10.1089/rej.2008.0736 (2008).

174 Millis, A. J., Hoyle, M., McCue, H. M. & Martini, H. Differential expression of metalloproteinase and tissue inhibitor of metalloproteinase genes in aged human fibroblasts. *Experimental cell research* **201**, 373-379 (1992).

175 Wright, W. E. & Shay, J. W. Telomere dynamics in cancer progression and prevention: fundamental differences in human and mouse telomere biology. *Nature medicine* **6**, 849-851, doi:10.1038/78592 (2000).

176 Chadeneau, C., Siegel, P., Harley, C. B., Muller, W. J. & Bacchetti, S. Telomerase activity in normal and malignant murine tissues. *Oncogene* **11**, 893-898 (1995).

177 Harvey, M. *et al*. In vitro growth characteristics of embryo fibroblasts isolated from p53-deficient mice. *Oncogene* **8**, 2457-2467 (1993).

178 Peeper, D. S., Dannenberg, J. H., Douma, S., te Riele, H. & Bernards, R. Escape from premature senescence is not sufficient for oncogenic transformation by Ras. *Nature cell biology* **3**, 198-203 (2001).

179 Sage, J. *et al*. Targeted disruption of the three Rb-related genes leads to loss of G1 control and immortalization. *Genes & development* **14**, 3037-3050 (2000).

180 Rowland, B. D. *et al*. E2F transcriptional repressor complexes are critical downstream targets of p19ARF/p53-induced proliferative arrest. *Cancer Cell* **2**, 55-65 (2002).

181 Shay, J. W., Wright, W. E. & Werbin, H. Defining the molecular mechanisms of human cell immortalization. *Biochimica et biophysica acta* **1072**, 1-7 (1991).

182 Honda, R., Tanaka, H. & Yasuda, H. Oncoprotein MDM2 is a ubiquitin ligase E3 for tumor suppressor p53. *FEBS letters* **420**, 25-27 (1997).

183 Wei, W., Hemmer, R. M. & Sedivy, J. M. Role of p14ARF in replicative and induced senescence of human fibroblasts. *Molecular and Cellular Biology* **21**, 6748-6757, doi:10.1128/MCB.21.20.6748–6757.2001 (2001).

184 Hahn, W. C. *et al*. Creation of human tumour cells with defined genetic elements. *Nature* **400**, 464-468 (1999).
185 Land, H., Parada, L. F. & Weinberg, R. A. Tumorigenic conversion of primary embryo fibroblasts requires at least two cooperating oncogenes. *Nature* **304**, 596 (1983).
186 Coulombe, P. A. & Omary, M. B. 'Hard' and 'soft' principles defining the structure, function and regulation of keratin intermediate filaments. *Current opinion in cell biology* **14**, 110-122 (2002).
187 Langbein, L., Rogers, M. A., Winter, H., Praetzel, S. & Schweizer, J. The catalog of human hair keratins. II. Expression of the six type II members in the hair follicle and the combined catalog of human type I and II keratins. *The Journal of biological chemistry* **276**, 35123-35132, doi:10.1074/jbc.M103305200 (2001).
188 Marinkovich, M. P., Keene, D. R., Rimberg, C. S. & Burgeson, R. E. Cellular origin of the dermal-epidermal basement membrane. *Developmental Dynamics* **197**, 255-267, doi:10.1002/aja.1001970404 (1993).
189 Szabo, G. The regional anatomy of the human integument with special reference to the distribution of hair follicles, sweat glands and melanocytes. *Philosophical Transactions of the Royal Society of London. Series B, Biological Sciences*, 447-485, doi:10.1098/rstb.1967.0029 (1967).
190 Whiteman, D. C., Parsons, P. G. & Green, A. C. Determinants of melanocyte density in adult human skin. *Archives of dermatological research* **291**, 511-516 (1999).
191 Pieri, L., Domenici, L. & Romagnoli, P. Langerhans cells differentiation: a three-act play. *Italian journal of anatomy and embryology = Archivio italiano di anatomia ed embriologia* **106**, 47-69 (2001).
192 Lacour, J. P., Dubois, D., Pisani, A. & Ortonne, J. P. Anatomical mapping of Merkel cells in normal human adult epidermis. *The British journal of dermatology* **125**, 535-542 (1991).
193 Spetz, A. L., Strominger, J. & Groh-Spies, V. T cell subsets in normal human epidermis. *The American journal of pathology* **149**, 665-674 (1996).
194 Nishimura, E. K. *et al*. Dominant role of the niche in melanocyte stem-cell fate determination. *Nature* **416**, 854-860, doi:10.1038/416854a (2002).
195 Akiyama, M., Dale, B. A., Sun, T. T. & Holbrook, K. A. Characterization of hair follicle bulge in human fetal skin: the human fetal bulge is a pool of undifferentiated keratinocytes. *The journal of investigative dermatology Symposium proceedings / the Society for Investigative Dermatology, Inc [and] European Society for Dermatological Research* **105**, 844-850 (1995).
196 Yu, H. *et al*. Isolation of a novel population of multipotent adult stem cells from human hair follicles. *The American journal of pathology* **168**, 1879-1888, doi:10.2353/ajpath.2006.051170 (2006).
197 Yu, H., Kumar, S. M., Kossenkov, A. V., Showe, L. & Xu, X. Stem cells with neural crest characteristics derived from the bulge region of cultured human hair follicles. *Journal of Investigative Dermatology* **130**, 1227-1236, doi:10.1038/jid.2009.322 (2010).
198 Dintzis, S. M., ACVP, P. M. T. D. M. D., Treuting, P. & PhD, S. M. D. M. *Comparative Anatomy and Histology: A Mouse and Human Atlas*. 1 edn, (Academic Press, 2011).

199 BREATHNACH, A. S. Extra-cutaneous melanin. *Pigment cell research / sponsored by the European Society for Pigment Cell Research and the International Pigment Cell Society* **1**, 234-237 (1988).
200 RAWLES, M. E. Origin of pigment cells from the neural crest in the mouse embryo. *Physiological Zoology* **20**, 248-266 (1947).
201 Dorris, F. The production of pigment in vitro by chick neural crest. *Development Genes and Evolution* **138**, 323-334 (1938).
202 Dorris, F. The production of pigment by chick neural crest in grafts to the 3 – day limb bud. *Journal of Experimental Zoology* **80**, 315-345 (1939).
203 DuShane, G. P. An experimental study of the origin of pigment cells in Amphibia. *Journal of Experimental Zoology* **72**, 1-31 (1935).
204 Erickson, C. A. From the crest to the periphery: control of pigment cell migration and lineage segregation. *Pigment cell research / sponsored by the European Society for Pigment Cell Research and the International Pigment Cell Society* **6**, 336-347 (1993).
205 Ris, H. An experimental study on the origin of melanophores in birds. *Physiological Zoology* **14**, 48-69 (1941).
206 Dunn, K. J. *et al.* WNT1 and WNT3a promote expansion of melanocytes through distinct modes of action. *Pigment cell research / sponsored by the European Society for Pigment Cell Research and the International Pigment Cell Society* **18**, 167-180, doi:10.1111/j.1600-0749.2005.00226.x (2005).
207 Dunn, K. J., Williams, B. O., Li, Y. & Pavan, W. J. Neural crest-directed gene transfer demonstrates Wnt1 role in melanocyte expansion and differentiation during mouse development. *Proceedings of the National Academy of Sciences of the United States of America* **97**, 10050-10055 (2000).
208 Hari, L. *et al.* Lineage-specific requirements of beta-catenin in neural crest development. *The Journal of cell biology* **159**, 867-880, doi:10.1083/jcb.200209039 (2002).
209 Ikeya, M., Lee, S. M., Johnson, J. E., McMahon, A. P. & Takada, S. Wnt signalling required for expansion of neural crest and CNS progenitors. *Nature* **389**, 966-970, doi:10.1038/40146 (1997).
210 Ferguson, C. A. & Kidson, S. H. The regulation of tyrosinase gene transcription. *Pigment cell research / sponsored by the European Society for Pigment Cell Research and the International Pigment Cell Society* **10**, 127-138 (1997).
211 Hirobe, T. Histochemical survey of the distribution of the epidermal melanoblasts and melanocytes in the mouse during fetal and postnatal periods. *The Anatomical record* **208**, 589-594, doi:10.1002/ar.1092080414 (1984).
212 Adameyko, I. *et al.* Schwann cell precursors from nerve innervation are a cellular origin of melanocytes in skin. *Cell* **139**, 366-379, doi:10.1016/j.cell.2009.07.049 (2009).
213 Fitzpatrick, T. B. & BREATHNACH, A. S. Das epidermale melanin-einheit-system. *Dermatologische Wochenschrift* **147**, 481-489 (1963).
214 Jimbow, K., Quevedo, W. C., Fitzpatrick, T. B. & Szabo, G. Some aspects of melanin biology: 1950-1975. *The journal of investigative dermatology Symposium proceedings / the Society for Investigative Dermatology, Inc [and] European Society for Dermatological Research* **67**, 72-89 (1976).

215 Tang, A. *et al*. E-cadherin is the major mediator of human melanocyte adhesion to keratinocytes in vitro. *Journal of cell science* **107 (Pt 4)**, 983-992 (1994).
216 Okazaki, K., Uzuka, M., Morikawa, F., Toda, K. & Seiji, M. Transfer mechanism of melanosomes in epidermal cell culture. *The journal of investigative dermatology Symposium proceedings / the Society for Investigative Dermatology, Inc [and] European Society for Dermatological Research* **67**, 541-547 (1976).
217 Yamamoto, O. & Bhawan, J. Three modes of melanosome transfers in Caucasian facial skin: hypothesis based on an ultrastructural study. *Pigment cell research / sponsored by the European Society for Pigment Cell Research and the International Pigment Cell Society* **7**, 158-169 (1994).
218 Thody, A. J. *et al*. Pheomelanin as well as eumelanin is present in human epidermis. *The journal of investigative dermatology Symposium proceedings / the Society for Investigative Dermatology, Inc [and] European Society for Dermatological Research* **97**, 340-344 (1991).
219 Prota, G. Recent advances in the chemistry of melanogenesis in mammals. *The journal of investigative dermatology Symposium proceedings / the Society for Investigative Dermatology, Inc [and] European Society for Dermatological Research* **75**, 122-127 (1980).
220 Kobayashi, T. *et al*. Tyrosinase related protein 1 (TRP1) functions as a DHICA oxidase in melanin biosynthesis. *The EMBO journal* **13**, 5818-5825 (1994).
221 Price, E. R. *et al*. alpha-Melanocyte-stimulating hormone signaling regulates expression of microphthalmia, a gene deficient in Waardenburg syndrome. *The Journal of biological chemistry* **273**, 33042-33047 (1998).
222 Cui, R. *et al*. Central role of p53 in the suntan response and pathologic hyperpigmentation. *Cell* **128**, 853-864, doi:10.1016/j.cell.2006.12.045 (2007).
223 Smith, A. I. & Funder, J. W. Proopiomelanocortin processing in the pituitary, central nervous system, and peripheral tissues. *Endocrine reviews* **9**, 159-179 (1988).
224 Chakraborty, A. K. *et al*. Production and release of proopiomelanocortin (POMC) derived peptides by human melanocytes and keratinocytes in culture: regulation by ultraviolet B. *Biochimica et biophysica acta* **1313**, 130-138 (1996).
225 Kippenberger, S. *et al*. Transcription of Melanogenesis Enzymes in Melanocytes: Dependence upon Culture Conditions and Co – Cultivation With Keratinocytes. *Pigment cell research* **9**, 179-184 (1996).
226 Lunec, J., Pieron, C., Sherbet, G. V. & Thody, A. J. Alpha-melanocyte-stimulating hormone immunoreactivity in melanoma cells. *Pathobiology : journal of immunopathology, molecular and cellular biology* **58**, 193-197 (1990).
227 Valverde, P., Healy, E., Jackson, I., Rees, J. L. & Thody, A. J. Variants of the melanocyte-stimulating hormone receptor gene are associated with red hair and fair skin in humans. *Nature Genetics* **11**, 328-330, doi:10.1038/ng1195-328 (1995).
228 Gilchrest, B. A. *et al*. Characteristics of cultivated adult human nevocellular nevus cells. *The journal of investigative dermatology*

Symposium proceedings / the Society for Investigative Dermatology, Inc [and] European Society for Dermatological Research **87**, 102-107 (1986).

229 Gottlieb, B., Brown, A. L. & Winkelmann, R. K. Fine structure of the nevus cell. *Archives of dermatology* **92**, 81-87 (1965).

230 MacKie, R. M., English, J., Aitchison, T. C., Fitzsimons, C. P. & Wilson, P. The number and distribution of benign pigmented moles (melanocytic naevi) in a healthy British population. *The British journal of dermatology* **113**, 167-174 (1985).

231 Rampen, F. H. & de Wit, P. E. Racial differences in mole proneness. *Acta dermato-venereologica* **69**, 234-236 (1989).

232 Sigg, C. & Pelloni, F. Frequency of acquired melanonevocytic nevi and their relationship to skin complexion in 939 schoolchildren. *Dermatologica* **179**, 123-128 (1989).

233 Unna, P. *Naevi und naevocarcinome* Vol. 30 (Berl Klin Wochenschr, 1893).

234 Hui, P., Perkins, A. & Glusac, E. Assessment of clonality in melanocytic nevi. *Journal of cutaneous pathology* **28**, 140-144 (2001).

235 Maize, J. C. & Foster, G. Age-related changes in melanocytic naevi. *Clinical and experimental dermatology* **4**, 49-58 (1979).

236 MASSON, P. My conception of cellular nevi. *Cancer* **4**, 9-38 (1951).

237 Niizuma, K. Electron microscopic study of nevic corpuscle. *Acta dermato-venereologica* **55**, 283-289 (1975).

238 Evans, M. J., Sanders, D. S., Grant, J. H. & Blessing, K. Expression of Melan-A in Spitz, pigmented spindle cell nevi, and congenital nevi: comparative immunohistochemical study. *Pediatric and developmental pathology : the official journal of the Society for Pediatric Pathology and the Paediatric Pathology Society* **3**, 36-39, doi:10.1007/s100249910004 (2000).

239 MISHIMA, Y. MACROMOLECULAR CHANGES IN PIGMENTARY DISORDERS. *Archives of dermatology* **91**, 519-557 (1965).

240 Cramer, S. F. The origin of epidermal melanocytes. Implications for the histogenesis of nevi and melanomas. *Archives of pathology & laboratory medicine* **115**, 115-119 (1991).

241 Hayward, N. New developments in melanoma genetics. *Current oncology reports* **2**, 300-306 (2000).

242 Sviderskaya, E. V. *et al.* p16(Ink4a) in melanocyte senescence and differentiation. *Journal of the National Cancer Institute* **94**, 446-454 (2002).

243 Halaban, R., Ghosh, S., Duray, P., Kirkwood, J. M. & Lerner, A. B. Human melanocytes cultured from nevi and melanomas. *The journal of investigative dermatology Symposium proceedings / the Society for Investigative Dermatology, Inc [and] European Society for Dermatological Research* **87**, 95-101 (1986).

244 Herlyn, M. *et al.* Characteristics of cultured human melanocytes isolated from different stages of tumor progression. *Cancer research* **45**, 5670-5676 (1985).

245 Glaessl, A. *et al.* Increase in telomerase activity during progression of melanocytic cells from melanocytic naevi to malignant melanomas. *Archives of dermatological research* **291**, 81-87 (1999).

246 Rudolph, P. *et al.* Telomerase activity in melanocytic lesions: A potential marker of tumor biology. *The American journal of pathology* **156**, 1425-1432, doi:10.1016/S0002-9440(10)65011-0 (2000).

247 Davies, H. *et al*. Mutations of the BRAF gene in human cancer. *Nature* **417**, 949-954, doi:10.1038/nature00766 (2002).
248 Sensi, M. *et al*. Mutually exclusive NRASQ61R and BRAFV600E mutations at the single-cell level in the same human melanoma. *Oncogene* **25**, 3357-3364, doi:10.1038/sj.onc.1209379 (2006).
249 Rajagopalan, H. *et al*. Tumorigenesis: RAF/RAS oncogenes and mismatch-repair status. *Nature* **418**, 934, doi:10.1038/418934a (2002).
250 Omholt, K., Platz, A., Kanter, L., Ringborg, U. & Hansson, J. NRAS and BRAF mutations arise early during melanoma pathogenesis and are preserved throughout tumor progression. *Clinical cancer research : an official journal of the American Association for Cancer Research* **9**, 6483-6488 (2003).
251 Reifenberger, J. *et al*. Frequent alterations of Ras signaling pathway genes in sporadic malignant melanomas. *International journal of cancer Journal international du cancer* **109**, 377-384, doi:10.1002/ijc.11722 (2004).
252 Patton, E. E. *et al*. BRAF mutations are sufficient to promote nevi formation and cooperate with p53 in the genesis of melanoma. *Current biology : CB* **15**, 249-254, doi:10.1016/j.cub.2005.01.031 (2005).
253 Michaloglou, C., Vredeveld, L. C. W., Mooi, W. J. & Peeper, D. S. BRAF(E600) in benign and malignant human tumours. *Oncogene* **27**, 877-895, doi:10.1038/sj.onc.1210704 (2008).
254 CRUK. *Skin Cancer - UK incidence statistics*, <http://info.cancerresearchuk.org/cancerstats/types/skin/incidence/> (2012).
255 CRUK. Skin cancer - UK mortality statistics. (2012).
256 Clark, W. H. J. *et al*. A study of tumor progression: the precursor lesions of superficial spreading and nodular melanoma. *Human Pathology* **15**, 1147-1165 (1984).
257 Lee, J. Y. *et al*. Genetic alterations of p16INK4a and p53 genes in sporadic dysplastic nevus. *Biochemical and biophysical research communications* **237**, 667-672, doi:10.1006/bbrc.1997.7212 (1997).
258 Guldberg, P., Birck, A., Ahrenkiel, V., Kirkin, A. F. & Zeuthen, J. Disruption of the MMAC1/PTEN gene by deletion or mutation is a frequent event in malignant melanoma. *Cancer research* **57**, 3660 (1997).
259 Vredeveld, L. C. W. *et al*. Abrogation of BRAFV600E-induced senescence by PI3K pathway activation contributes to melanomagenesis. *Genes & development* **26**, 1055-1069, doi:10.1101/gad.187252.112 (2012).
260 Bennett, D. C. How to make a melanoma: what do we know of the primary clonal events? *Pigment Cell & Melanoma Research* **21**, 27-38, doi:10.1111/j.1755-148X.2007.00433.x (2008).
261 Bennett, D. C. Human melanocyte senescence and melanoma susceptibility genes. *Oncogene* **22**, 3063-3069, doi:10.1038/sj.onc.1206446 (2003).
262 Tsao, H., Zhang, X., Fowlkes, K. & Haluska, F. G. Relative reciprocity of NRAS and PTEN/MMAC1 alterations in cutaneous melanoma cell lines. *Cancer research* **60**, 1800-1804 (2000).
263 Halachmi, S. & Gilchrest, B. A. Update on genetic events in the pathogenesis of melanoma. *Current opinion in oncology* **13**, 129-136 (2001).

264 Patel, J. K., Didolkar, M. S., Pickren, J. W. & Moore, R. H. Metastatic pattern of malignant melanoma. A study of 216 autopsy cases. *American journal of surgery* **135**, 807-810 (1978).

265 Chin, L., Merlino, G. & DePinho, R. A. Malignant melanoma: modern black plague and genetic black box. *Genes & development* **12**, 3467-3481 (1998).

266 Yang, A. S. & Chapman, P. B. The history and future of chemotherapy for melanoma. *Hematology/oncology clinics of North America* **23**, 583-597- x, doi:10.1016/j.hoc.2009.03.006 (2009).

267 Atkins, M. B. *et al*. High-dose recombinant interleukin 2 therapy for patients with metastatic melanoma: analysis of 270 patients treated between 1985 and 1993. *Journal of clinical oncology : official journal of the American Society of Clinical Oncology* **17**, 2105-2116 (1999).

268 Sondak, V. K., Smalley, K. S. M., Kudchadkar, R., Grippon, S. & Kirkpatrick, P. in *Nature reviews. Drug discovery* Vol. 10 411-412 (2011).

269 Bollag, G. *et al*. Clinical efficacy of a RAF inhibitor needs broad target blockade in BRAF-mutant melanoma. *Nature* **467**, 596-599, doi:10.1038/nature09454 (2010).

270 Hodi, F. S. *et al*. Improved survival with ipilimumab in patients with metastatic melanoma. *The New England journal of medicine* **363**, 711-723, doi:10.1056/NEJMoa1003466 (2010).

271 Chapman, P. B. *et al*. Improved survival with vemurafenib in melanoma with BRAF V600E mutation. *The New England journal of medicine* **364**, 2507-2516, doi:10.1056/NEJMoa1103782 (2011).

272 Fedorenko, I. V., Paraiso, K. H. T. & Smalley, K. S. M. Acquired and intrinsic BRAF inhibitor resistance in BRAF V600E mutant melanoma. *Biochemical pharmacology* **82**, 201-209, doi:10.1016/j.bcp.2011.05.015 (2011).

273 Nazarian, R. *et al*. Melanomas acquire resistance to B-RAF(V600E) inhibition by RTK or N-RAS upregulation. *Nature* **468**, 973-977, doi:10.1038/nature09626 (2010).

274 Poulikakos, P. I. *et al*. RAF inhibitor resistance is mediated by dimerization of aberrantly spliced BRAF(V600E). *Nature* **480**, 387-390, doi:10.1038/nature10662 (2011).

275 Whittaker, S. *et al*. Gatekeeper mutations mediate resistance to BRAF-targeted therapies. *Science translational medicine* **2**, 35ra41, doi:10.1126/scitranslmed.3000758 (2010).

276 Wagle, N. *et al*. Dissecting therapeutic resistance to RAF inhibition in melanoma by tumor genomic profiling. *Journal of clinical oncology : official journal of the American Society of Clinical Oncology* **29**, 3085-3096, doi:10.1200/JCO.2010.33.2312 (2011).

277 Nusse, R. & Varmus, H. E. Many tumors induced by the mouse mammary tumor virus contain a provirus integrated in the same region of the host genome. *Cell* **31**, 99-109 (1982).

278 Kusserow, A. *et al*. Unexpected complexity of the Wnt gene family in a sea anemone. *Nature* **433**, 156-160, doi:10.1038/nature03158 (2005).

279 Nichols, S. A., Dirks, W., Pearse, J. S. & King, N. Early evolution of animal cell signaling and adhesion genes. *Proceedings of the National Academy of Sciences of the United States of America* **103**, 12451-12456, doi:10.1073/pnas.0604065103 (2006).

280 Srivastava, M. *et al*. The Trichoplax genome and the nature of placozoans. *Nature* **454**, 955-960, doi:10.1038/nature07191 (2008).
281 Gordon, M. D. & Nusse, R. Wnt signaling: multiple pathways, multiple receptors, and multiple transcription factors. *The Journal of biological chemistry* **281**, 22429-22433, doi:10.1074/jbc.R600015200 (2006).
282 Dann, C. E. *et al*. Insights into Wnt binding and signalling from the structures of two Frizzled cysteine-rich domains. *Nature* **412**, 86-90 (2001).
283 He, X., Semenov, M., Tamai, K. & Zeng, X. LDL receptor-related proteins 5 and 6 in Wnt/beta-catenin signaling: arrows point the way. *Development (Cambridge, England)* **131**, 1663-1677, doi:10.1242/dev.01117 (2004).
284 Mao, J. *et al*. Low-density lipoprotein receptor-related protein-5 binds to Axin and regulates the canonical Wnt signaling pathway. *Molecular cell* **7**, 801-809 (2001).
285 Zeng, X. *et al*. Initiation of Wnt signaling: control of Wnt coreceptor Lrp6 phosphorylation/activation via frizzled, dishevelled and axin functions. *Development (Cambridge, England)* **135**, 367-375, doi:10.1242/dev.013540 (2008).
286 Wallingford, J. B. & Habas, R. The developmental biology of Dishevelled: an enigmatic protein governing cell fate and cell polarity. *Development (Cambridge, England)* **132**, 4421-4436, doi:10.1242/dev.02068 (2005).
287 Sugioka, K., Mizumoto, K. & Sawa, H. Wnt regulates spindle asymmetry to generate asymmetric nuclear β-catenin in C. elegans. *Cell* **146**, 942-954, doi:10.1016/j.cell.2011.07.043 (2011).
288 Klaus, A. & Birchmeier, W. Wnt signalling and its impact on development and cancer. *Nature reviews Cancer* **8**, 387-398, doi:10.1038/nrc2389 (2008).
289 He, T. C. *et al*. Identification of c-MYC as a target of the APC pathway. *Science (New York, NY)* **281**, 1509-1512 (1998).
290 He, T. C., Chan, T. A., Vogelstein, B. & Kinzler, K. W. PPARdelta is an APC-regulated target of nonsteroidal anti-inflammatory drugs. *Cell* **99**, 335-345 (1999).
291 Tetsu, O. & McCormick, F. Beta-catenin regulates expression of cyclin D1 in colon carcinoma cells. *Nature* **398**, 422-426, doi:10.1038/18884 (1999).
292 Brabletz, T., Jung, A., Dag, S., Hlubek, F. & Kirchner, T. beta-catenin regulates the expression of the matrix metalloproteinase-7 in human colorectal cancer. *The American journal of pathology* **155**, 1033-1038 (1999).
293 Takeda, K. *et al*. Induction of melanocyte-specific microphthalmia-associated transcription factor by Wnt-3a. *The Journal of biological chemistry* **275**, 14013-14016 (2000).
294 MANN, B. *et al*. Target genes of beta-catenin-T cell-factor/lymphoid-enhancer-factor signaling in human colorectal carcinomas. *Proceedings of the National Academy of Sciences of the United States of America* **96**, 1603-1608 (1999).
295 Jho, E.-h. *et al*. Wnt/beta-catenin/Tcf signaling induces the transcription of Axin2, a negative regulator of the signaling pathway. *Molecular and Cellular Biology* **22**, 1172-1183 (2002).

296 Dorsky, R. I., Moon, R. T. & Raible, D. W. Control of neural crest cell fate by the Wnt signalling pathway. *Nature* **396**, 370-373, doi:10.1038/24620 (1998).
297 Kageshita, T. *et al*. Loss of beta-catenin expression associated with disease progression in malignant melanoma. *The British journal of dermatology* **145**, 210-216 (2001).
298 Chien, A. J. *et al*. Activated Wnt/beta-catenin signaling in melanoma is associated with decreased proliferation in patient tumors and a murine melanoma model. *Proceedings of the National Academy of Sciences of the United States of America* **106**, 1193-1198, doi:10.1073/pnas.0811902106 (2009).
299 Murakami, T. *et al*. Constitutive activation of Wnt/beta-catenin signaling pathway in migration-active melanoma cells: role of LEF-1 in melanoma with increased metastatic potential. *Biochemical and biophysical research communications* **288**, 8-15, doi:10.1006/bbrc.2001.5719 (2001).
300 Schmidt, C., McGonnell, I., Allen, S. & Patel, K. The role of Wnt signalling in the development of somites and neural crest. *Advances in anatomy, embryology, and cell biology* **195**, 1-64 (2008).
301 Luciani, F. *et al*. Biological and mathematical modeling of melanocyte development. *Development (Cambridge, England)* **138**, 3943-3954, doi:10.1242/dev.067447 (2011).
302 Yamaguchi, Y., Morita, A., Maeda, A. & Hearing, V. J. Regulation of skin pigmentation and thickness by Dickkopf 1 (DKK1). *The journal of investigative dermatology Symposium proceedings / the Society for Investigative Dermatology, Inc [and] European Society for Dermatological Research* **14**, 73-75, doi:10.1038/jidsymp.2009.4 (2009).
303 Van Mater, D., Kolligs, F. T., Dlugosz, A. A. & Fearon, E. R. Transient activation of beta -catenin signaling in cutaneous keratinocytes is sufficient to trigger the active growth phase of the hair cycle in mice. *Genes & development* **17**, 1219-1224, doi:10.1101/gad.1076103 (2003).
304 Närhi, K. *et al*. Sustained epithelial beta-catenin activity induces precocious hair development but disrupts hair follicle down-growth and hair shaft formation. *Development (Cambridge, England)* **135**, 1019-1028, doi:10.1242/dev.016550 (2008).
305 Ito, M. *et al*. Wnt-dependent de novo hair follicle regeneration in adult mouse skin after wounding. *Nature* **447**, 316-320, doi:10.1038/nature05766 (2007).
306 Andl, T., Reddy, S. T., Gaddapara, T. & Millar, S. E. WNT signals are required for the initiation of hair follicle development. *Developmental cell* **2**, 643-653 (2002).
307 Chan, E. F., Gat, U., McNiff, J. M. & Fuchs, E. A common human skin tumour is caused by activating mutations in beta-catenin. *Nature Genetics* **21**, 410-413, doi:10.1038/7747 (1999).
308 Levy, C., Khaled, M. & Fisher, D. E. MITF: master regulator of melanocyte development and melanoma oncogene. *Trends in molecular medicine* **12**, 406-414, doi:10.1016/j.molmed.2006.07.008 (2006).
309 Lang, D. *et al*. Pax3 functions at a nodal point in melanocyte stem cell differentiation. *Nature* **433**, 884-887, doi:10.1038/nature03292 (2005).
310 Fang, D. *et al*. Defining the conditions for the generation of melanocytes from human embryonic stem cells. *Stem cells (Dayton, Ohio)* **24**, 1668-1677, doi:10.1634/stemcells.2005-0414 (2006).

311 Yamaguchi, Y. *et al.* Dickkopf 1 (DKK1) regulates skin pigmentation and thickness by affecting Wnt/beta-catenin signaling in keratinocytes. *FASEB journal : official publication of the Federation of American Societies for Experimental Biology* **22**, 1009-1020, doi:10.1096/fj.07-9475com (2008).
312 Dissanayake, S. K. *et al.* Wnt5A regulates expression of tumor-associated antigens in melanoma via changes in signal transducers and activators of transcription 3 phosphorylation. *Cancer Research* **68**, 10205-10214, doi:10.1158/0008-5472.CAN-08-2149 (2008).
313 Westfall, T. A. *et al.* Wnt-5/pipetail functions in vertebrate axis formation as a negative regulator of Wnt/beta-catenin activity. *The Journal of cell biology* **162**, 889-898, doi:10.1083/jcb.200303107 (2003).
314 Topol, L. *et al.* Wnt-5a inhibits the canonical Wnt pathway by promoting GSK-3-independent beta-catenin degradation. *The Journal of cell biology* **162**, 899-908, doi:10.1083/jcb.200303158 (2003).
315 Dissanayake, S. K. *et al.* The Wnt5A/protein kinase C pathway mediates motility in melanoma cells via the inhibition of metastasis suppressors and initiation of an epithelial to mesenchymal transition. *The Journal of biological chemistry* **282**, 17259-17271, doi:10.1074/jbc.M700075200 (2007).
316 Da Forno, P. D. *et al.* WNT5A expression increases during melanoma progression and correlates with outcome. *Clinical cancer research : an official journal of the American Association for Cancer Research* **14**, 5825-5832, doi:10.1158/1078-0432.CCR-07-5104 (2008).
317 Ramirez, J. A., Guitart, J., Rao, M. S. & Diaz, L. K. Cyclin D1 expression in melanocytic lesions of the skin. *Annals of diagnostic pathology* **9**, 185-188, doi:10.1016/j.anndiagpath.2005.04.018 (2005).
318 Bergman, R., Lurie, M., Kerner, H., Kilim, S. & Friedman-Birnbaum, R. Mode of c-myc protein expression in Spitz nevi, common melanocytic nevi and malignant melanomas. *Journal of cutaneous pathology* **24**, 219-222 (1997).
319 King, R., Googe, P. B., Weilbaecher, K. N., Mihm, M. C. & Fisher, D. E. Microphthalmia transcription factor expression in cutaneous benign, malignant melanocytic, and nonmelanocytic tumors. *The American journal of surgical pathology* **25**, 51-57 (2001).
320 Ying, J. *et al.* WNT5A exhibits tumor-suppressive activity through antagonizing the Wnt/beta-catenin signaling, and is frequently methylated in colorectal cancer. *Clinical cancer research : an official journal of the American Association for Cancer Research* **14**, 55-61, doi:10.1158/1078-0432.CCR-07-1644 (2008).
321 Roman-Gomez, J. *et al.* WNT5A, a putative tumour suppressor of lymphoid malignancies, is inactivated by aberrant methylation in acute lymphoblastic leukaemia. *European journal of cancer (Oxford, England : 1990)* **43**, 2736-2746, doi:10.1016/j.ejca.2007.10.004 (2007).
322 Liang, H. *et al.* Wnt5a inhibits B cell proliferation and functions as a tumor suppressor in hematopoietic tissue. *Cancer Cell* **4**, 349-360 (2003).
323 Clevers, H. & Nusse, R. Wnt/ß-Catenin Signaling and Disease. *Cell* **149**, 1192-1205, doi:10.1016/j.cell.2012.05.012 (2012).
324 Polakis, P. Wnt signaling in cancer. *Cold Spring Harbor perspectives in biology* **4**, doi:10.1101/cshperspect.a008052 (2012).

325 Schneikert, J. & Behrens, J. The canonical Wnt signalling pathway and its APC partner in colon cancer development. *Gut* **56**, 417-425, doi:10.1136/gut.2006.093310 (2007).
326 Horst, D. *et al*. The intratumoral distribution of nuclear β-catenin is a prognostic marker in colon cancer. *Cancer* **115**, 2063-2070 (2009).
327 Rimm, D. L., Caca, K., Hu, G., Harrison, F. B. & Fearon, E. R. Frequent nuclear/cytoplasmic localization of beta-catenin without exon 3 mutations in malignant melanoma. *The American journal of pathology* **154**, 325-329 (1999).
328 Omholt, K., Platz, A., Ringborg, U. & Hansson, J. Cytoplasmic and nuclear accumulation of beta-catenin is rarely caused by CTNNB1 exon 3 mutations in cutaneous malignant melanoma. *International journal of cancer Journal international du cancer* **92**, 839-842, doi:10.1002/ijc.1270 (2001).
329 Reifenberger, J. *et al*. Molecular genetic analysis of malignant melanomas for aberrations of the WNT signaling pathway genes CTNNB1, APC, ICAT and BTRC. *International journal of cancer Journal international du cancer* **100**, 549-556, doi:10.1002/ijc.10512 (2002).
330 Chen, D. *et al*. SKI activates Wnt/beta-catenin signaling in human melanoma. *Cancer Research* **63**, 6626-6634 (2003).
331 Delmas, V. *et al*. Beta-catenin induces immortalization of melanocytes by suppressing p16INK4a expression and cooperates with N-Ras in melanoma development. *Genes & development* **21**, 2923-2935, doi:10.1101/gad.450107 (2007).
332 Ye, X. *et al*. Downregulation of Wnt signaling is a trigger for formation of facultative heterochromatin and onset of cell senescence in primary human cells. *Molecular cell* **27**, 183-196, doi:10.1016/j.molcel.2007.05.034 (2007).
333 Goodall, J. *et al*. Brn-2 expression controls melanoma proliferation and is directly regulated by beta-catenin. *Molecular and Cellular Biology* **24**, 2915-2922 (2004).
334 Nakai, S. *et al*. The POU domain transcription factor Brn-2 is required for the determination of specific neuronal lineages in the hypothalamus of the mouse. *Genes & development* **9**, 3109-3121 (1995).
335 Thomson, J. A. *et al*. The brn-2 gene regulates the melanocytic phenotype and tumorigenic potential of human melanoma cells. *Oncogene* **11**, 691-700 (1995).
336 Goodall, J. *et al*. The Brn-2 transcription factor links activated BRAF to melanoma proliferation. *Molecular and Cellular Biology* **24**, 2923-2931, doi:10.1128/MCB.24.7.2923–2931.2004 (2004).
337 Garraway, L. A. *et al*. Integrative genomic analyses identify MITF as a lineage survival oncogene amplified in malignant melanoma. *Nature* **436**, 117-122, doi:10.1038/nature03664 (2005).
338 Cronin, J. C. *et al*. Frequent mutations in the MITF pathway in melanoma. *Pigment Cell & Melanoma Research* **22**, 435-444, doi:10.1111/j.1755-148X.2009.00578.x (2009).
339 Murakami, H. & Arnheiter, H. Sumoylation modulates transcriptional activity of MITF in a promoter-specific manner. *Pigment cell research / sponsored by the European Society for Pigment Cell Research and the International Pigment Cell Society* **18**, 265-277, doi:10.1111/j.1600-0749.2005.00234.x (2005).

340 Miller, A. J., Levy, C., Davis, I. J., Razin, E. & Fisher, D. E. Sumoylation of MITF and its related family members TFE3 and TFEB. *The Journal of biological chemistry* **280**, 146-155, doi:10.1074/jbc.M411757200 (2005).
341 McGill, G. G. *et al*. Bcl2 regulation by the melanocyte master regulator Mitf modulates lineage survival and melanoma cell viability. *Cell* **109**, 707-718 (2002).
342 King, R. *et al*. Microphthalmia transcription factor. A sensitive and specific melanocyte marker for MelanomaDiagnosis. *The American journal of pathology* **155**, 731-738, doi:10.1016/S0002-9440(10)65172-3 (1999).
343 Salti, G. I. *et al*. Micropthalmia transcription factor: a new prognostic marker in intermediate-thickness cutaneous malignant melanoma. *Cancer research* **60**, 5012-5016 (2000).
344 Lucero, O. M., Dawson, D. W., Moon, R. T. & Chien, A. J. A Re-evaluation of the "Oncogenic" Nature of Wnt/β-catenin Signaling in Melanoma and Other Cancers. *Current Oncology Reports* **12**, 314-318, doi:10.1007/s11912-010-0114-3 (2010).
345 Weeraratna, A. T. A Wnt-er wonderland--the complexity of Wnt signaling in melanoma. *Cancer metastasis reviews* **24**, 237-250, doi:10.1007/s10555-005-1574-z (2005).
346 Ackermann, J. *et al*. Metastasizing melanoma formation caused by expression of activated N-RasQ61K on an INK4a-deficient background. *Cancer Research* **65**, 4005-4011, doi:10.1158/0008-5472.CAN-04-2970 (2005).
347 Delmas, V., Martinozzi, S., Bourgeois, Y., Holzenberger, M. & Larue, L. Cre-mediated recombination in the skin melanocyte lineage. *Genesis (New York, NY : 2000)* **36**, 73-80, doi:10.1002/gene.10197 (2003).
348 Shibata, H. *et al*. Rapid colorectal adenoma formation initiated by conditional targeting of the Apc gene. *Science (New York, NY)* **278**, 120-123 (1997).
349 Tuveson, D. A. *et al*. Endogenous oncogenic K-rasG12D stimulates proliferation and widespread neoplastic and developmental defects. *Cancer Cell* **5**, 375-387, doi:10.1016/S1535-6108(04)00085-6 (2004).
350 Sarkisian, C. J. *et al*. Dose-dependent oncogene-induced senescence in vivo and its evasion during mammary tumorigenesis. *Nature cell biology* **9**, 493-505, doi:10.1038/ncb1567 (2007).
351 Serrano, M. *et al*. Role of the INK4a locus in tumor suppression and cell mortality. *Cell* **85**, 27-37 (1996).
352 Roe, T., Reynolds, T. C., Yu, G. & Brown, P. O. Integration of murine leukemia virus DNA depends on mitosis. *The EMBO journal* **12**, 2099-2108 (1993).
353 TEMIN, H. M. & RUBIN, H. Characteristics of an assay for Rous sarcoma virus and Rous sarcoma cells in tissue culture. *Virology* **6**, 669-688 (1958).
354 Lewis, P., Hensel, M. & Emerman, M. Human immunodeficiency virus infection of cells arrested in the cell cycle. *The EMBO journal* **11**, 3053-3058 (1992).
355 Denoyelle, C. *et al*. Anti-oncogenic role of the endoplasmic reticulum differentially activated by mutations in the MAPK pathway. *Nature cell biology* **8**, 1053-1063, doi:10.1038/ncb1471 (2006).
356 Qian, Y., Zhang, J., Yan, B. & Chen, X. DEC1, a Basic Helix-Loop-Helix Transcription Factor and a Novel Target Gene of the p53 Family, Mediates

p53-dependent Premature Senescence. *The Journal of biological chemistry* **283**, 2896-2905, doi:10.1074/jbc.M708624200 (2007).

357 Fang, X. *et al*. Expression of p16 induces transcriptional downregulation of the RB gene. *Oncogene* **16**, 1-8, doi:10.1038/sj.onc.1201525 (1998).

358 Schroeder, A. *et al*. The RIN: an RNA integrity number for assigning integrity values to RNA measurements. *BMC molecular biology* **7**, 3, doi:10.1186/1471-2199-7-3 (2006).

359 Irizarry, R. A. *et al*. Summaries of Affymetrix GeneChip probe level data. *Nucleic acids research* **31**, e15, doi:10.1093/nar/gng015 (2003).

360 Whitfield, M. L., George, L. K., Grant, G. D. & Perou, C. M. Common markers of proliferation. *Nature reviews Cancer* **6**, 99-106, doi:10.1038/nrc1802 (2006).

361 Salzman, J., Jiang, H. & Wong, W. H. Statistical modeling of RNA-Seq data. *Statistical Science* **26**, 62-83 (2011).

362 Choi, J. *et al*. Expression of senescence-associated beta-galactosidase in enlarged prostates from men with benign prostatic hyperplasia. *Urology* **56**, 160-166 (2000).

363 Sun, P. *et al*. PRAK Is Essential for ras-Induced Senescence and Tumor Suppression. *Cell* **128**, 295-308, doi:10.1016/j.cell.2006.11.050 (2007).

364 Liu, D. & Hornsby, P. J. Senescent human fibroblasts increase the early growth of xenograft tumors via matrix metalloproteinase secretion. *Cancer research* **67**, 3117-3126, doi:10.1158/0008-5472.CAN-06-3452 (2007).

365 Ohuchida, K. *et al*. Radiation to stromal fibroblasts increases invasiveness of pancreatic cancer cells through tumor-stromal interactions. *Cancer research* **64**, 3215-3222 (2004).

366 Tsai, K. K. C., Chuang, E. Y.-Y., Little, J. B. & Yuan, Z.-M. Cellular mechanisms for low-dose ionizing radiation-induced perturbation of the breast tissue microenvironment. *Cancer research* **65**, 6734-6744, doi:10.1158/0008-5472.CAN-05-0703 (2005).

367 Norgauer, J., Metzner, B. & Schraufstätter, I. Expression and growth-promoting function of the IL-8 receptor beta in human melanoma cells. *The Journal of Immunology* **156**, 1132-1137 (1996).

368 Schadendorf, D. *et al*. IL-8 produced by human malignant melanoma cells in vitro is an essential autocrine growth factor *The Journal of Immunology* **151**, 2667-2675 (1993).

369 Wang, D. *et al*. MGSA/GRO-mediated melanocyte transformation involves induction of Ras expression. *Oncogene* **19**, 4647-4659, doi:10.1038/sj.onc.1203820 (2000).

370 Bertolotto, C. *et al*. A SUMOylation-defective MITF germline mutation predisposes to melanoma and renal carcinoma. *Nature* **480**, 94-98, doi:10.1038/nature10539 (2011).

371 Yokoyama, S. *et al*. A novel recurrent mutation in MITF predisposes to familial and sporadic melanoma. *Nature* **480**, 99-103, doi:10.1038/nature10630 (2011).

372 Fuerer, C. & Nusse, R. Lentiviral vectors to probe and manipulate the Wnt signaling pathway. *PloS one* **5**, e9370, doi:10.1371/journal.pone.0009370 (2010).

373 van de Wetering, M. *et al*. The ß-catenin/TCF-4 complex imposes a crypt progenitor phenotype on colorectal cancer cells. *Cell* **111**, 241-250 (2002).

374 Zalaudek, I. *et al*. Frequency of dermoscopic nevus subtypes by age and body site: a cross-sectional study. *Archives of dermatology* **147**, 663-670, doi:10.1001/archdermatol.2011.149 (2011).
375 Glatz, K., Hartmann, C., Antic, M. & Kutzner, H. Frequent Mitotic Activity in Banal Melanocytic Nevi Uncovered by Immunohistochemical Analysis. *The American Journal of dermatopathology* **32**, 643-649, doi:10.1097/DAD.0b013e3181d7ce6f (2010).
376 Ruhoy, S. M., Kolker, S. E. & Murry, T. C. Mitotic activity within dermal melanocytes of benign melanocytic nevi: a study of 100 cases with clinical follow-up. *The American Journal of dermatopathology* **33**, 167-172, doi:10.1097/DAD.0b013e3181f3dba3 (2011).
377 Eng, A. M. Solitary small active junctional nevi in juvenile patients. *Archives of dermatology* **119**, 35 (1983).
378 Foucar, E., Bentley, T. J., Laube, D. W. & Rosai, J. A histopathologic evaluation of nevocellular nevi in pregnancy. *Archives of dermatology* **121**, 350 (1985).
379 Tran, S. L. *et al*. Absence of Distinguishing Senescence Traits in Human Melanocytic Nevi. *Journal of Investigative Dermatology*, doi:10.1038/jid.2012.126 (2012).
380 Alison, M. R. Assessing cellular proliferation: what's worth measuring? *Human & experimental toxicology* **14**, 935-944 (1995).
381 Klaes, R. *et al*. Overexpression of p16INK4a as a specific marker for dysplastic and neoplastic epithelial cells of the cervix uteri. *International Journal of Cancer* **92**, 276-284 (2001).
382 Sawicka, M. *et al*. The Specificity and Patterns of Staining in Human Cells and Tissues of p16INK4a Antibodies Demonstrate Variant Antigen Binding. *PloS one* **Submitted** (2012).
383 Nilsson, K. & Landberg, G. Subcellular localization, modification and protein complex formation of the cdk-inhibitor p16 in Rb-functional and Rb-inactivated tumor cells. *International journal of cancer Journal international du cancer* **118**, 1120-1125, doi:10.1002/ijc.21466 (2006).
384 Gerace, L. & Huber, M. D. Nuclear lamina at the crossroads of the cytoplasm and nucleus. *Journal of structural biology* **177**, 24-31, doi:10.1016/j.jsb.2011.11.007 (2012).
385 Shimi, T. *et al*. The role of nuclear lamin B1 in cell proliferation and senescence. *Genes & development* **25**, 2579-2593, doi:10.1101/gad.179515.111 (2011).
386 Freund, A., Laberge, R.-M., Demaria, M. & Campisi, J. Lamin B1 loss is a senescence-associated biomarker. *Molecular biology of the cell* **23**, 2066-2075, doi:10.1091/mbc.E11-10-0884 (2012).
387 Feser, J. *et al*. Elevated histone expression promotes life span extension. *Molecular cell* **39**, 724-735, doi:10.1016/j.molcel.2010.08.015 (2010).
388 O'Sullivan, R. J., Kubicek, S., Schreiber, S. L. & Karlseder, J. Reduced histone biosynthesis and chromatin changes arising from a damage signal at telomeres. *Nature structural & molecular biology* **17**, 1218-1225, doi:10.1038/nsmb.1897 (2010).
389 Kobayashi, M. *et al*. Nuclear translocation of beta-catenin in colorectal cancer. *British Journal of Cancer* **82**, 1689-1693, doi:10.1054/bjoc.1999.1112 (2000).

390 Whimster, I. Recurrent pigment cell naevi and their significance in the problem of endogenous carcinogenesis. *Ann Ital Dermatol Clin Sper* **19**, 168-191 (1965).
391 Damsky, W. E. *et al.* β-Catenin Signaling Controls Metastasis in Braf-Activated Pten-Deficient Melanomas. *Cancer Cell* **20**, 741-754, doi:10.1016/j.ccr.2011.10.030 (2011).
392 Dankort, D. *et al.* Braf(V600E) cooperates with Pten loss to induce metastatic melanoma. *Nature Genetics* **41**, 544-552, doi:10.1038/ng.356 (2009).
393 Bataille, V. *et al.* Nevus size and number are associated with telomere length and represent potential markers of a decreased senescence in vivo. *Cancer epidemiology, biomarkers & prevention : a publication of the American Association for Cancer Research, cosponsored by the American Society of Preventive Oncology* **16**, 1499-1502, doi:10.1158/1055-9965.EPI-07-0152 (2007).
394 Giles, R. H., van Es, J. H. & Clevers, H. Caught up in a Wnt storm: Wnt signaling in cancer. *Biochimica et biophysica acta* **1653**, 1-24 (2003).
395 Ettenberg, S. A. *et al.* Inhibition of tumorigenesis driven by different Wnt proteins requires blockade of distinct ligand-binding regions by LRP6 antibodies. *Proceedings of the National Academy of Sciences* **107**, 15473-15478, doi:10.1073/pnas.1007428107 (2010).